UNIVERSITÀ DEGLI STUDI DI NAPOLI FEDERICO II

SCUOLA POLITECNICA E DELLE SCIENZE DI BASE

DIPARTIMENTO DI INGEGNERIA CHIMICA, DEI MATERIALI E DELLA PRODUZIONE INDUSTRIALE - DICMAPI

PhD Program in INDUSTRIAL PRODUCT AND PROCESS ENGINEERING

Ph.D THESIS

"Combustion kinetic characteristics of Smart Energy Carriers in model reactors"

by

Marco Lubrano Lavadera

TUTOR
Professor Antonio Cavaliere

COTUTOR
Dr. Mara de Joannon
Dr. Raffaele Ragucci
Dr. Pino Sabia

2017

TABLE OF CONTENTS

The results presented in the current thesis have been published in the following journal papers:

1) Sabia, P, de Joannon, M, Lubrano Lavadera, M, Giudicianni, P & Ragucci, R 2014, "Autoignition delay times of propane mixtures under MILD conditions at atmospheric pressure", *Combustion and Flame*, vol. 161, pp. 3022-3030.

2) Sabia, P, Lubrano Lavadera, M, Giudicianni, P, Sorrentino, G, Ragucci, R & de Joannon, M 2015, "CO_2 and H_2O effect on propane auto-ignition delay times under mild combustion operative conditions", *Combustion and Flame*, vol. 162, pp. 533-543.

3) Sabia, P, Lubrano Lavadera, M, Sorrentino, G, Giudicianni, P, Ragucci, R & de Joannon, M 2016, "H_2O and CO_2 Dilution in MILD Combustion of Simple Hydrocarbons", *Flow, Turbulence and Combustion*, vol. 96, no. 2, pp. 433-448.

4) Lubrano Lavadera, M, Sabia, P, Sorrentino, G, Ragucci, R & de Joannon, M 2016, "Experimental study of the effect of CO_2 on propane oxidation in a Jet Stirred Flow Reactor", *Fuel*, vol. 184, pp. 876-888.

ABSTRACT

The use of advanced combustion technologies is among the most promising methods to reduce emission of pollutants. For such technologies, working temperatures are enough low to boost the formation of several classes of pollutants, such as NO_x and soot. To access this temperature range, a significant dilution as well as preheating of reactants is required. Such conditions are usually achieved by a strong recirculation of exhaust gases that simultaneously dilute and pre-heat the fresh reactants. These peculiar operative conditions also imply strong fuel flexibility, thus allowing the use of low calorific values (LCV) energy carriers with high efficiency.
Coupling these innovative combustion technologies with the energy carriers, define the Smart Energy Carriers.
The intersection of low combustion temperatures and highly diluted mixtures with intense pre-heating alters the evolution of the combustion process with respect to traditional flames, thereby affecting the kinetics involved during fuel ignition and oxidation. Furthermore, the high content of diluent species, namely CO_2 and H_2O, deriving either from the presence of diluent in LCV fuels or from the recirculation of flue gases, makes the role of these species relevant in the oxidation chemistry in such a non-standard condition. Such issues are currently largely unexplored.
The effects of high dilution and pre-heating levels, along with the significant presence of non-conventional diluents on the ignition and oxidation kinetics were studied in two model reactors. More specifically, ignition delay times have been experimentally evaluated in a Plug Flow Reactor using propane and a model gas surrogating the gaseous fraction of biomass pyrolysis products containing C1-C2 species, CO and CO_2. Experimental tests have also been carried out in a Jet Stirred Flow Reactor, using methane, propane and n-pentane as reference fuels. The experimental analysis has been carried out at atmospheric pressure, in a wide range of inlet temperatures and equivalence ratios, for mixtures highly diluted in He, N_2, CO_2, H_2O, or mixtures of them.
Temperature and species concentration measurements obtained in the Jet Stirred Flow Reactor, along with the ignition delay times obtained in the Plug Flow Reactor, suggest that the ignition and oxidation processes of simple fuels are significantly altered by CO_2 and H_2O in dependence of mixture inlet temperatures and equivalence ratios. Furthermore, the exploitation of the ignition and oxidation processes under diluted conditions leads to the identification of peculiar phenomena and combustion regimes, such as the existence of an NTC-like behaviour for propane mixtures at intermediate temperature, strong and weak ignitions, and oscillatory regimes for all the tested fuel mixtures.
Numerical simulations for studying the ignition and oxidation processes in the same working conditions of experimental tests have been carried out by means of twelve kinetic models available in the literature. It has been shown that kinetic models are not always able to correctly reproduce the experimental results, particularly when CO_2 and H_2O are used as diluents. In addition, large variations can be observed among models themselves.
Further analysis were performed to identify the controlling reaction pathways in these non-standard conditions and to explore the interaction of CO_2 and H_2O with the ignition and oxidation processes. Results suggested that, for diluted conditions and lower adiabatic flame temperatures, the competition among several pathways, i.e. intermediate- and high-temperature branching, branching and recombination channels, oxidation and recombination/pyrolysis pathways, is enhanced, thus permitting the onset of phenomena that are generally hidden during conventional combustion processes.
Moreover, CO_2 and H_2O participate in this competition, influencing termolecular reactions as third body species with high collisional efficiencies, or directly participating in bimolecular reactions.

LIST OF ABBRVIATIONS

GHG GreenHouse Gas
VOC Volatile Organic Compounds
PM Particulate Matter
UHC Unburned HydroCarbons
PAH Polycyclic Aromatic Hydrocarbons
LHV Lower Heating Value
LCV Low Calorific Value
DME DiMethyl Ether
SNG Synthetic Natural Gas
MILD Moderate or Intense Low-oxygen Dilution
ΔT Temperature increase
T_{si} Self-Ignition Temperature
T_{in} Inlet Temperature
FLOX Flameless Oxidation
CDC Colourless Distributed Combustion
HiTAC High Temperature Air Combustion
LTC Low Temperature Combustion
HCCI Homogeneous Charge Compression Ignition
MGT Micro Gas Turbine
CCS/U Carbon Capture and Storage/Utilization
SECs Smart Energy Carriers
JHC Jet in Hot Co-flow
Da Damköhler number
τ_{turb} Turbulent mixing time
τ_{chem} Chemical kinetic time
$C_{\varepsilon 1}$ k-ε modified constant
RNG ReNormalization Group
RKE Realizable k-ε
SKE Standard k-ε
ξ/PDF Mixture fraction/Probability Density Function
EDC Eddy Dissipation Concept
CFD Computational Fluid Dynamics
DMF 2,5-DiMethylFuran
NTC Negative Temperature Coefficient
MIE Minimum Ignition Energy
CRGT Chemical Recuperation Gas Turbine
IC Internal Combustion
X Molar fraction
Φ Equivalence ratio
TFR Tubular Flow Reactor
JSFR Jet Stirred Flow Reactor
LPG Liquefied Petroleum Gas
PFR Plug Flow Reactor
PSR Perfectly Stirred Reactor
d Dilution
t Ignition delay time
v Flow velocity
SSR Solid State Relay
PID Proportional Integral Derivative
Ω Oxygen ratio
τ Residence time
TCD Thermal Conductivity Detector
FID Flame Ionization Detector
C/O Carbon to Oxygen ratio
x_{ig} Ignition location in the PFR
x axial coordinate in the PFR
RR Reaction Rates
K Rate constant
A Pre-exponential factor
E Activation energy
R Universal gas constant
ST Shock Tube
RCM Rapid Compression Machine
Re Reynolds number
D Diameter of the PFR
ν Kinematic viscosity
V Volume
Q Volume flow rate
E (t) Residence time distribution
WSR Well Stirred Reactor
J Ratio of momentum of flows
CEM Controlled Evaporator Mixer
S Sensitivity coefficient
M Third body species
U Heat transfer coefficient
T_{ad} Adiabatic Flame Temperature
Y Fictitious species
ROP Rate of Production
S Sensitivity Coefficient
F_c Center broadening factor

LIST OF FIGURES

LIST OF TABLES

CHAPTER 1 – INTRODUCTION

1.1 The need for new and smarter fuels

Presently, more than 85% of primary world energy consumption remains to be based on fossil fuels combustion. However, continuous fluctuating oil prices and the insecurity over possible future supply associated with finite fossil fuel reserves are among the highest concerns of contemporary society. Furthermore, fossil fuels combustion leads to emission of carbon dioxide (CO_2), which is the key greenhouse gas (GHG) responsible for environmental issues of climate change (Agarwal 2007). Moreover, combustion processes produce several (regulated and unregulated) pollutants, which are the main causes of local and global environmental impact. These pollutants include nitrogen, sulphur and carbon oxides (NO_x, SO_x, CO), volatile organic compounds (VOC), particulate matter (PM), unburned hydrocarbons (UHC), polycyclic aromatic hydrocarbons (PAH), etc.
All these aspects have led to the definition of the main priorities that a contemporary energy supply system should satisfy, i.e.:

1) **security**: the effectiveness of management of primary energy supply;
2) **equity**: the accessibility and affordability of energy supply across the population;
3) **sustainability**: the utilization of efficient and from renewable (low-carbon) energy sources.

The conjunction of these three principles is what is known as “energy trilemma” (World Energy Council 2012).
Renewable energy is one of the most efficient ways to achieve sustainable development. Harnessing hydro, solar, wind and geothermal can, at least in principle, completely eliminate fossil fuels from electricity production. More difficult, however, is to replace the other essential roles of fossil fuels, including their use as energy-trading commodities and transportation fuels. Indeed, even if electricity is produced with clean energy sources it cannot be stored, which would enable the separation of the primary energy production and end-use consumption in both space and time (Bergthorson et al. 2015). For this reason, it is expected that in the future the combustion processes still play a key role regarding the energy production.
Nowadays, improvement of combustion-based energy systems focuses on reducing emissions, increasing efficiency and lowering costs without sacrificing reliability. Advances are occurring on all three fronts, but progress is usually achieved on a single-composition fuel. Employing other secondary fuels normally results in greatly reduced efficiency, reliability and operating range. As a matter of fact, when a power system is designed for peak efficiency at the lowest lifetime cost, trade-offs are usually encountered that force the system to operate in a rather narrow parameter space and only one fuel can be used to achieve this peak efficiency. A completely new design of the combustion system is necessary if the fuel characteristics are very different to that of the designated fuel (Ren et al. 2001; Zornek et al. 2015). However, in order to ensure equity and security, it should be considered locally available fuels, which may strongly vary with each other. Furthermore, in order to avoid transportation, energy production plants using local fuels should be located close to energy consumption centres, especially for remote areas (Gupta et al. 2010; Sims et al. 2010). Thus, there is a need to consider fuel composition and fuel property variables on advanced/distributed power generation systems, maintaining the traditional processes configurations (Richards et al. 2001).
To date, the handful of solutions that have been proposed, in most cases, do not simultaneously meet the aforementioned three principles. This represents a great challenge and places indeed the contemporary energy society being in a “trilemma”.

Given this background, the three principles of the "energy trilemma" may become requirements for combustion technologies. Therefore, the greatest challenge that the combustion-based energy industry has to face in the next few years is the urgent need for:

1) adjustment of **distributed energy production**;
2) maximization of **fuel flexibility** of combustion technologies;
3) minimization of **GHG emissions** (de Joannon 2014).

1) The realization of a new energy production and distribution system based on smart grid concepts is often seen as a possible straightforward option for developing countries. Also, the ecology movement would be more prone to accept the build-up of a strongly delocalized energy system as an alternative and a more eco-compatible development model (de Joannon 2014).
2) Fuel flexibility is a prerequisite to face a fast changing fuel market and an increasing number of energy carriers available in the local market, mainly due to the increased penetration of renewable and unconventional energy sources (de Joannon 2014).
3) Mitigation of GHG emissions to the atmosphere is a central priority of the EU Horizon 2020 research-funding programme. To mitigate global climate change, current energy and transportation systems must transition away from fossil fuel sources to CO_2-neutral clean and renewable energy sources. It currently appears that a multifaceted approach, encompassing highly efficient low-carbon technologies coupled with medium-term emission containment (e.g. Carbon Capture and Storage/Utilization (CCS/U)), will have to be pursued in order to avoid potentially catastrophic climate consequences (Gupta et al. 2010; de Joannon 2014).

All these factors call for the characterization, specification and proper utilization of new and smarter fuels.
The term fuel refers to any reduced solid, liquid, or gaseous material that can be oxidized, typically by oxygen in the air, to produce energy, but any such fuel produced from low-carbon primary energy is, in reality, a secondary energy vector or energy carrier (Bergthorson et al. 2015).
A secondary energy carrier may include a wide range of compounds like aliphatics, oxygenates (alcohols, esters, ethers) as well as olefins, naphthenes and their mixtures with diluents (N_2, CO_2 and H_2O), as in the case of syngas, biogas, landfill gas, pyrolysis oil, etc. As a consequence, energy conversion systems have to face an increasing variety of solid, liquid and gaseous energy carriers that change their characteristics (composition, lower heating value (LHV), physical properties, etc.) depending on the available source and production process. Consequently, how to utilize these energy carriers economically, efficiently, and eco-friendly is always a "hot" topic.

1.2 Innovative combustion technologies for smart fuels and energy carriers

In principle, the burning mode of these variable energy carriers is similar to that of conventional fossil fuels, therefore, a way to use them could be the direct combustion in conventional technologies. However, even though tailor-made fuel technologies are under development, feedstock and fuel processing variability influences fuel properties in a complex and sometimes unpredictable way, so that for this kind of energy carriers the conventional combustion mode generally suffers from a number of serious problems (Liu et al. 2015). For example, important combustion characteristics like flame speeds, ignition delay times, flammability limits, ignition temperatures, and adiabatic flame temperatures depend on the fuel composition. As a consequence, some complications such as flame flashback, blowout, incomplete fuel conversion with CO and UHC emissions are to be handled properly, especially when engine loads are modulated, which could be the case of distributed energy conversion systems (Ren et al. 2001; Zornek et al. 2015).

Within certain limits, the flame surface can shrink or grow to accommodate changes in the flow rate, or changes in the flame speed due to differences in fuel type, fuel concentration or temperature. If the flow rate is too high relative to the flame speed, the flame will be blown-off. In aero-engines, the concept of flame blowout is well appreciated and must be avoided during conditions of rapid power changes. In stationary engines, blowout has traditionally been less of concern because earlier diffusion-style combustors were fairly forgiving in the comparatively modest operating regime of stationary engines. However, the current trend to operate stationary engine combustors very close to the lean-blowout limit has raised the status of this issue. For fuels with variable composition, the control may require modification to accommodate the different fuel properties at different sites, because the actual blowout limit may change with the fuel properties (Richards et al. 2001). At the other extreme, if the flame speed is large compared to the local gas velocity, the flame will propagate into the approach flow (i.e. flashback). For example this can happen with syngas, since hydrogen contained in syngas (in variable quantities) has a much greater flame speed compared to hydrocarbon fuels (around 240 vs. 40 cm/s at standard conditions) (Richards et al. 2001). This led to the production of countless experimental and numerical studies on the hydrogen and syngas flame speed, which are summarized in the work of Varga et al. (2016). Furthermore, commercially available burners are designed for conventional fuels (such as natural gas or diesel fuel), which have a high LHV. If fuels with lower LHVs are used, the fuel mass flow rate increases respectively. Enlarging the fuel mass flow rate affects the aerodynamics inside the combustion chamber and as a consequence the stoichiometry. Near the lean combustion limit, even minor changes in reaction stoichiometry can lead to significant variations in heat release. If these variations are synchronized with the resonant pressure field, oscillating combustion can be sustained with a frequency from tens to thousands of cycles per second. It has been shown that the timing also depends on the specific fuel chemical reaction time scale, demonstrating that changes in fuel type can be expected to change dynamics. With sufficient amplitude, the vibration and enhanced heat transfer that accompany these oscillations can lead to fatigue failure of the combustor liner in a matter of hours. A universal solution to this problem has not yet been proven. At the present time, “mapping” dynamic regimes, may provide some insurance that a given engine design is operating well inside the stable operating regimes, so that minor changes in fuel type do not produce oscillations (Richards et al. 2001). Another important consideration in premixed combustion is auto-ignition. At sufficiently high ambient temperatures, flame propagation is not needed to initiate combustion reaction. Instead, the reactions can occur spontaneously throughout the premixed gases. The time needed for initiating spontaneous combustion is known as the auto-ignition time. In reciprocating engines, and in premixed gas turbine combustors, the auto-ignition time is recognized as a critical design parameter. The auto-ignition time depends critically on the ambient pressure, temperature, mixture type and composition. Low Calorific Value (LCV) fuels (mixtures of fuels with diluents) tend to have very higher auto-ignition times respect to long-chain hydrocarbons, making these fuels difficult to use in conventional combustion systems (Richards et al. 2001). Furthermore, in industrial burners, changing fuel types can affect the length of the flame reaction zone and completing oxidation becomes a matter of providing enough residence time at high temperature. This becomes more difficult with fuels that produce a relatively low flame temperature. Attempts to use particularly LCV fuels require extended residence time to complete oxidation (Richards et al. 2001). Furthermore, in diffusion flames, usually combustion reaction is very rapid, and therefore the process is essentially controlled by species diffusion, and the impact of fuel can be related to the physical properties, which can strongly vary with the fuel type. Again, compatibility of different fuels with conventional burners liquid fuel delivery/injection systems is primarily a function of fuel viscosity and volatility, but not all the alternative fuels fall within the max allowable range for a conventional combustion system. This leads to problems related to pumping, atomization and spray processes. In fact, if larger size fuel droplets are injected from injector nozzle instead of a spray of fine droplets, an inefficient mixing of fuel with air occurs. This

involves incomplete combustion and an increment in particulate emissions, combustion chamber deposits and gum formations (Gupta et al. 2010).
Thus, the fuel type, concentration, or temperature, determine many of the significant features of how combustion occurs. This introduces design challenges for non-conventional fuels.
In order to remedy these shortcomings, it becomes necessary a fuel upgrading through some physical, chemical, and biochemical processes in order to bring the combustion properties of alternative fuels closer to those of conventional fuels or to obtain pure fuels as the final product (e.g. hydrogen, methane, methanol, ethanol, dimethyl ether (DME), synthetic natural gas (SNG), etc.) (Gupta et al. 2010). Although through such treatment the quality of energy carriers can be upgraded significantly, unfortunately this way increases the cost of processing and does not meet the requirements of efficiency, energy distribution and fuel flexibility. Therefore, to meet the aforementioned needs, innovative combustion technologies for power generation in the industrial, domestic, and transport sectors are required. Such technologies have to be fuel-flexible and able to achieve high efficiencies, assuring stable combustion and low pollutant emissions for a wide range of operative conditions. Therefore, it is necessary that combustion systems operate under conditions (in terms of temperature, pressure and mixture composition) that are significantly different from those of conventional combustion modes (de Joannon 2014; Liu et al. 2015).
In this framework, MILD (Moderate or Intense Low-oxygen Dilution) combustion constitutes a promising option, avoiding drastic changes in the configuration of traditional plants. A combustion process is named MILD when the inlet temperature of the reactant mixture is higher than mixture self-ignition temperature whereas the maximum allowable temperature increase with respect to inlet temperature during combustion is lower than self-ignition temperature (in Kelvin) (Cavaliere & de Joannon 2004).
The usefulness of the MILD combustion definition may be appreciated by some considerations in relation to the map shown in Fig. 1.1 numerically obtained for a $CH_4/O_2/N_2$ mixture with 0.1/0.05/0.85 molar fractions (Cavaliere & de Joannon 2004). It defines all possible inlet temperatures (abscissa) and temperature increases (ordinate) for a residence time of 1 s and atmospheric pressure. In this case the self-ignition temperature of reactant mixture is 1000 K, but in general different self-ignition temperatures may be obtained for different compositions, pressures and residence times of reactants. The map of Fig. 1.1 is divided in three regions by the straight lines intercepting the self-ignition temperature on both axes. These regions are named Feedback, High Temperature and MILD Combustion respectively. The two combustion modes placed in the upper part of the map where the condition $\Delta T > T_{si}$ is satisfied, so that Feedback and High Temperature Combustion, satisfy the necessary condition for which a traditional combustion process may occur, namely the heat release is sufficient to sustain the minimum temperature required for process evolution.
On the contrary, according to the definition given by Cavaliere and de Joannon (2004) (i.e. $\Delta T < T_{si} < T_{in}$) MILD Combustion is placed in the lower-right quadrant. To access this temperature range, in comparison to the other two fields, significant dilution as well as preheating of the reactant mixtures is required. In practical systems, dilution and preheating are usually achieved through internal or external exhaust gas recirculation.
The low combustion temperature enables low hazardous pollutant emissions like NO_x and soot without gas after-treatment, which avoids adding costs, complexity and space. Moreover, the requirement of inlet temperature higher than the self-ignition one adds a further obvious advantage of these systems, namely the stable burning of alternative fuels, in particular LCV fuels, because flame stabilization is not needed. In situation where fuel variability can be a problem, exhaust gas recirculation represents a very effective control variable, since it allows to easily tuning the level of dilution, and thus the temperature (Dally et al. 2004). Furthermore, the relatively high temperatures of inlet streams leads to a faster heating of the liquid fuel and therefore to better atomization and evaporation processes (Cavaliere & de Joannon 2004).

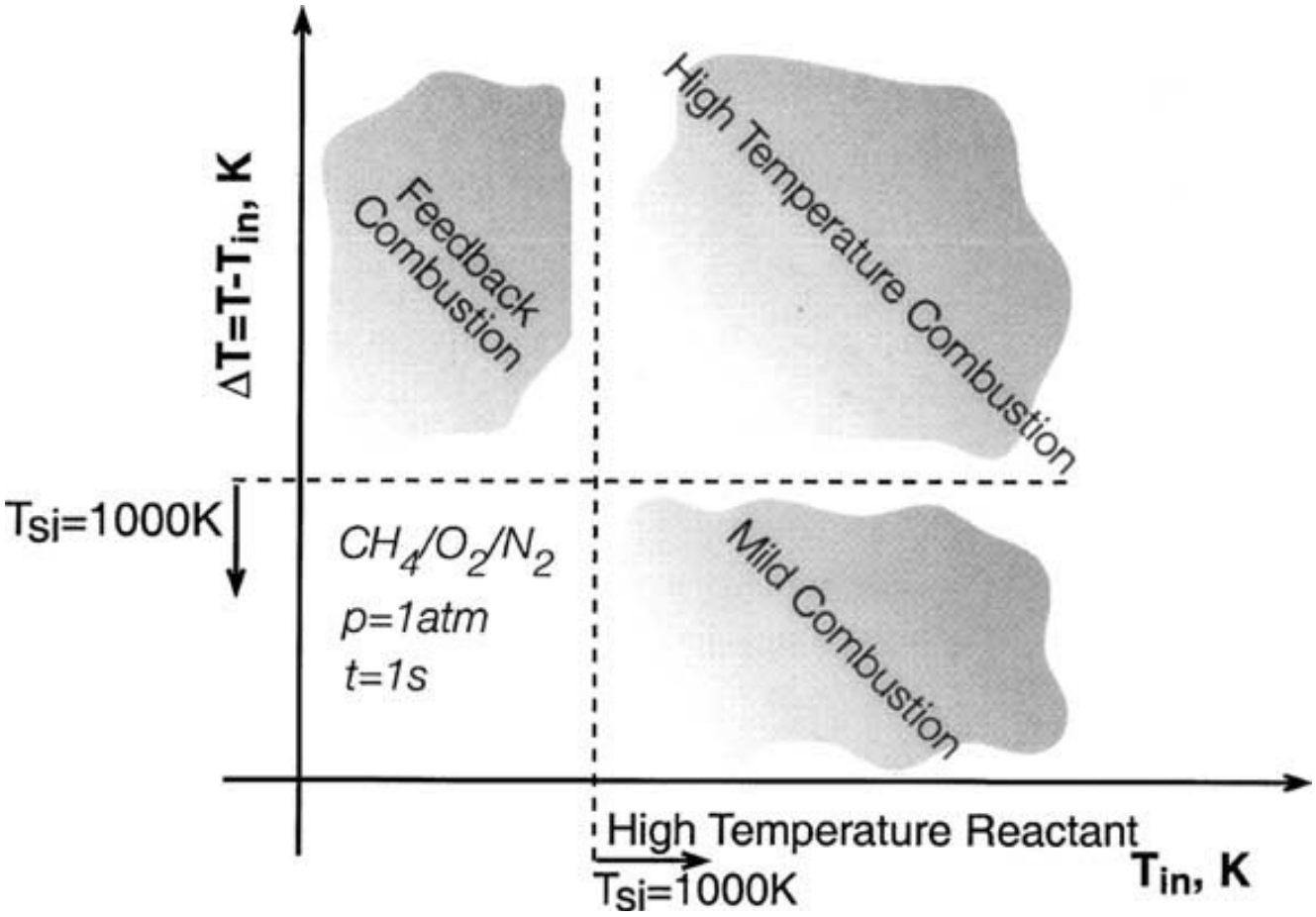

Fig. 1.1 T_{in}-ΔT locus of different combustion modes for a methane/oxygen/nitrogen mixture (adapted from Cavaliere & de Joannon 2004).

Until now, several studies on MILD combustion of LCV fuels have been published. Effuggi et al. (2008) perhaps are the pioneers in this field. The authors experimentally investigated the products of biogas MILD combustion. They found that biogas MILD combustion has great capability to reduce pollutant emissions, especially soot formation. In succession, the successfully performance of LCV fuels under diluted combustion conditions was reported by Colorado et al. (2010), and Hosseini and Wahid (2013).

Flameless Oxidation (FLOX®) (Wünning & Wünning 1997), colourless distributed combustion (CDC) or High Temperature Air Combustion (HiTAC) (Tsuji et al. 2002), Low Temperature Combustion (LTC) (Jacobs & Assanis 2007) and Homogeneous Charge Compression Ignition (HCCI) engines (Yao et al. 2009) are similar approaches, which can be used for industrial purposes, power generation and transportation. These advanced combustion strategies have the common feature of operating at low combustion temperatures, high dilution levels and high preheating temperatures. In addition to low NO_x and soot emissions and fuel flexibility, these flames have other attractive features such as highly distributed reaction zone, uniform temperature field, low luminescence, low noise, and higher radiation flux.

Therefore, harnessing these innovative combustion technologies, the development of a reliable, fuel flexible system can be accomplished with relatively little effort during the design stage. As low temperature/diluted combustion systems are considered to be fuel-flexible, there is a growing interest to use them for decentralized/integrated high-efficiency energy production systems. Distributed power may be expected to increase demand for very small generators (less than 1 MW). This demand may be filled by reciprocating engines, or micro-turbines (Richards et al. 2001).

Zornek et al. (2015) demonstrated the stability and fuel-flexibility of a FLOX-combustion chamber in a Micro Gas Turbine (MGT), which assured stable and complete combustion. The results proved the feasibility to operate the turbine with LCV fuels, meeting emission limits over the whole

operating range, i.e. from 80% to 100% turbine speed. de Joannon et al. (2016) tested the sustainability of the MILD combustion process, depending on inlet mixture pre-heating and dilution level, in a laboratory cyclonic burner. They showed that a small size cyclonic burner is stable in a range of parameters very wide with respect to the one of a standard burner, with reduced combustion peak temperatures and thereby very low NO_x and CO emissions.
An innovative process similar to those mentioned, which is widely applied in coal-combustion technologies, is oxy-fuel combustion (Buhre et al. 2005). This process uses pure oxygen instead of air and recycles most of the flue gas (basically CO_2), exhausting only a small fraction of the total flue gas. The flue gases recirculation is necessary to restrain the adiabatic flame temperatures to values that are compatible with the material thermal resistance and not critical for pollutants formation. The resulting flue gas is composed primarily of carbon dioxide and water vapour along with some N_2, O_2, and trace gases such as SO_2 and NO_x. The flue gas can be processed through rectification or distillation to enrich the CO_2 content in the product gas up to 95%, thus making possible an easy CO_2 recovery in CCS/U technologies. Furthermore, with respect to a conventional combustion, O_2/CO_2 combustion reduces NO_x emissions, improves fuel flexibility and combustion efficiency, widens load change range, and facilitates stable combustion even at low O_2 concentration (Liu & Okazaki 2003; Toporov et al. 2008).

1.3 The Smart Energy Carrier concept

The energy carriers, coupled with these innovative combustion technologies, define the "**Smart Energy Carriers**" (**SECs**). This category, thus, includes conventional and novel energetic molecules from alternative or conventional (re)sources, selected on the basis of their best available production and/or utilization technologies. Accordingly, to be considered "smart", an energy carrier and related technologies must be energetically and CO_2 efficient and able to provide the most suitable energy mix to meet the intermittency of renewable energies, to exploit varying and locally diverse sources and to satisfy the requirements for eco-compatibility and sustainability. SECs are strong candidates as possible solutions for energy storage, transfer and transformation from renewable (wind, solar, biomass, wastes) and unconventional sources (e.g. shale gas) (de Joannon 2014).
A new knowledge has to be built to make SECs and new combustion technologies usable in efficient and sustainable way.

1.4 Challenges

Despite much progress in the application of new combustion concepts to practical systems, there remain unresolved issues on the stabilization, auto-ignition, and structure of the reaction zone. In particular, the influence of fuel type on the fundamental aspects of the combustion remains poorly understood. For this reason, large-scale implementation of SECs combustion processes is hampered by the risks associated with adopting relatively unknown new techniques.
Moreover, all the abovementioned advantages should not obscure potential counter indications and fundamental problems associated with SECs operation. For example, a problem of homogeneous low-temperature combustion is the susceptibility to oscillations (as will be discussed hereinafter, conceptually and phenomenologically different from the thermo-acoustic oscillations mentioned above), which are undesirable during combustion, and such instability hampers the application of these technologies in many areas such as one in the HCCI engines (de Joannon et al. 2005). Moreover, it is important to understand that, given the low temperature and high dilution, SECs combustion will require combustors with higher residence time to achieve oxygenated compounds oxidation (Richards et al. 2001). Furthermore, SECs combustion may not only present a challenge for combustor and engine design; it may also lead to a different species pool from that in conventional combustion situations. Therefore, detailed information on combustion chemistry is of

pre-eminent importance for the assessment of pollutant formation when using novel fuels and fuel combinations. For example, combustion of oxygenate fuels in premixed flames has been found to decrease typical soot precursor concentrations, potentially at the cost of increasing aldehyde formation (Kohse-Höinghaus & Brockhinke 2009). Furthermore, the preceding discussion on NO_x formation has assumed that the fuel does not contain nitrogen species. However, alternative feedstocks such as landfill gas or gasified biomass, add the fuel nitrogen to the reactant mixture, typically found in the form of ammonia. In these situations, the most common proposal for achieving low NO_x is rich-quench-lean combustion. Air and fuel are burned at overall rich conditions in the first stage of the combustor. By maintaining the ammonia in a high-temperature reducing environment, much of the ammonia is reduced to N_2. Rapid mixing with air in the second-stage combustor completes oxidation of the first-stage products (Richards et al. 2001).
All these aspects are to be handled properly in order to use SECs in an efficient and eco-friendly way.
Usually, the proper design and operation of practical combustors requires that key flame properties, such as laminar flame speed, ignition delay times, extinction characteristics, etc. are well known under the pertinent combustion conditions. This is even more obvious when considering that the unusual operating conditions make the innovative combustion modes completely different from conventional combustion systems. However, all the just mentioned aspects imply that many parameters, such as temperature, pressure, dilution, equivalence ratio, residence time, diluent nature, fuel type and composition, are involved in the SECs combustion processes. Thus, the SECs pertinent combustion conditions are countless. Therefore, in this context, rather than the knowledge of the fundamental combustion properties under certain operating conditions, there is a need for fundamental understanding on which is the impact of critical parameters on combustion properties in order to make SECs and new combustion technologies usable in efficient and sustainable way.
As a matter of fact, under preheated and diluted combustion conditions, the combustion process is expected to have different features with respect to conventional combustion.
In particular, the intermediate species profiles exhibit a distribution different than that observed in a conventional diffusion flame. The latter is typically characterized by a thin symmetrical profile (indicating a narrow reaction zone) slightly shifted toward the fuel-lean side of stoichiometry. In a diluted and preheated regime, however, the species concentrations are lower than that under traditional combustion condition and are homogeneously distributed to a relatively larger region (Christo and Dally 2005; Dally et al. 2002; Plessing et al. 1998). Simultaneously and remarkably, the typical pyrolytic region in the reactive structure disappears and the position of the oxidative structure in mixture fraction space is no longer correlated to the location of the stoichiometric mixture fraction (de Joannon et al. 2007, 2009, 2012). Using a fuel jet in hot low-oxygen co-flow (JHC) device, Dally et al. (2002) emulated the MILD combustion and deduced that there would be difference of the chemical pathways between the highly-diluted and non-diluted JHC flames. Also, interactions of reaction zones are observed for the conditions of MILD combustion and the frequency and extent of this interaction seem to increase with dilution (Minamoto et al. 2014).
Therefore, in order to aid the design and prediction of performance of innovative combustion devices, robust fluid dynamic as well as chemical kinetic modelling tools are sought. However, given the SECs combustion conditions, events such as autoignition, reaction of mixtures containing reactants and hot products with radicals and intermediates, and interaction of these phenomena are entangled in space and time and separating them for modelling purposes may not be easy.
In conventional flames, where the chemical reactions take place in a well-defined thin flame front, combustion models are based on the notion that for fast burning fuels, the overall rate of reaction is controlled by turbulent mixing (mixing-limited), and therefore, it would be a reasonable approximation to neglect chemical kinetic effects on the overall rate of reaction. In particular, reaction rate is fast compared with the mixing rate, giving a high Damköhler number ($Da = \tau_{turb} / \tau_{chem}$) (Christo & Dally 2005). However, to prevent reactions from occurring before the flame is stabilized, a finite-rate chemistry term with three or fewer reactions is included in the model

formulation. Another hypothesis generally assumed considers that reactions occur in a thin sheet with inner structure generally defined as laminar flamelet, decoupling fluid dynamic and chemical problems.
The hypotheses considered for these models could be no longer valid with MILD or other diluted/low temperature combustion processes, where the conditions of low and uniform temperature distribution and high dilution levels (thus low oxygen concentrations) lead to chemical reactions rates comparable to the reactants turbulent mixing rates (enhanced by recirculation) and enhance the influence of molecular diffusion on flame characteristics. These two effects, in particular, challenge the applicability of combustion models that assume fast chemistry and neglect the effects of differential diffusion, taking into account only turbulent diffusion. In diluted combustion the extended reactive region is characterized by Da numbers lower than those observed in the flame front of a burner operating in conventional mode. So diluted combustion is primarily kinetics-controlled (Christo & Dally 2005).
Under these non-conventional conditions, the accuracy of the numerical solution is found to be highly sensitive to boundary conditions, especially turbulence quantities. Therefore special attention should be paid to ensuring accurate definition of these parameters. Christo and Dally (2005) found that the standard k-ε turbulence model with a modified constant ($C_{\varepsilon 1}$) was in excellent agreement with experiment. Other variants of the k-ε model, including the renormalization group (RNG) and realizable k-ε (RKE) models, however, did not perform as well as the modified standard k-ε (SKE) model. Also conventional combustion models, such as conserved scalar-based approaches, including the mixture fraction/probability density function (ξ/PDF) and flamelet models, could not be performing for modelling MILD flames. The volumetric reaction approach, in particular the eddy dissipation concept (EDC), however yielded reasonable results. Moreover, differential diffusion effects play an important role in determining the accuracy of the predictions and need to be included in the computational fluid dynamics (CFD) model, as well as thermal radiation (Galletti et al. 2007). The representation of the chemistry in the model also plays an important role in the accurate prediction of flame characteristics. Incorporating detailed chemical kinetics into the EDC solver (Parente et al. 2008), instead of a global or skeletal mechanism, is found to improve accuracy significantly, albeit at computational cost. An attractive strategy for including detailed chemistry effects using moderate CPU resources are tabulated chemistry techniques (Lamoroux et al. 2014). Lamoroux et al. (2014) demonstrated that chemistry is affected by dilution, impacting fundamental flame properties, including flame structure, species composition, and pollutant emission. This result is shown only from detailed chemistry and not from infinitely fast chemistry approximation, or one-step irreversible chemistry. Furthermore, the authors found that also heat losses are of paramount importance in affecting the flame behaviour (Lamoroux et al. 2014).
Given the large number of processes influencing the combustion behaviour, this makes the isolation and investigation of a single aspect troublesome. Therefore, advanced turbulence, chemical kinetics and turbulence-chemistry interaction models are required. In particular, the present work is focused on the kinetic aspects.
With regard to chemical kinetics, a major issue in the modelling of these advanced conversion technologies is the pronounced sensitivity of the flame structure to the reaction chemistry compared to conventional engines. The difficulty is exacerbated by the fact that advanced engines operate at pressure and temperature conditions that are especially challenging to study experimentally (Burke et al. 2015). As a result, there are not many quantities to be used for validation. Consequently, given that the reaction pathways and the accentuated portion of their associated rates within temperature, pressure and mixture composition space vary strongly with the exact local thermodynamic conditions, extrapolation of kinetic models, particularly to the operating conditions relevant to advanced engines, is often problematic, as illustrated by recent examples for even relatively simple combustion systems where the reaction proceeds through only 20-30 reactions (Burke et al. 2010). The ultimate goal of these modelling efforts is to achieve accurate predictive behaviour of combustor features necessary for reliable operation. Such requirements, combined with observed

deficiencies of model predictions involving extrapolation (Burke et al. 2015), emphasize the need for experiments spanning an as wide as possible range of operating conditions.

CHAPTER 2 – COMBUSTION KINETICS OF SMART ENERGY CARRIERS

2.1 State of the art

Since about fifty years, great efforts have been devoted to the understanding of fossil fuel combustion mechanisms at molecular level, from simple to more complex systems. Countless experimental data have been collected on reference experiments on molecules that represent standard fossil fuels and numerous comprehensive chemical kinetic mechanisms describing the reaction process in detail have been developed and proposed (Westbrook & Dryer 1984).
In general, the chemical processes that occur in combustion are highly complex and highly condition-dependent. Namely, the overall conversion of fuel and oxygen to carbon dioxide and water in fact proceeds through numerous (sometimes reaching thousands, depending upon the complexity of the fuel) of intermediate species, all of which undergo simultaneous sequential and parallel reactions, each of which occurs at rates that can be temperature, pressure, and mixture-composition dependent (Burke et al. 2010).
Continued extension of kinetic modelling to hydrocarbon fuels of increasing size led to kinetic mechanisms of even greater size. While early methane kinetic models included fewer than 20 chemical species, later models for propane and n-butane reached about 100 chemical species, and later models for isomers of heptane and octane reached about 1000 chemical species (Westbrook et al. 2005). The validation of these kinetic models requires experimental data and in order to obtain it, different experimental techniques have been used: flames supported by burners, static reactors, plug flow reactors, shock tubes, rapid compression machines and continuous-flow stirred reactors (Griffiths 1995). The availability of these experiments, along with the increasing computer power, enabled very substantial and important progress in the construction of comprehensive kinetic models for hydrocarbons oxidation. These models currently include a great level of complexity and realism, attaining a certain level of reliability (Westbrook et al. 2005).
However, several basic issues intersect with the combustion of SECs. On the one hand there is the fuel variability. SECs can range from simple molecules or mixtures of simple molecules, up to complex molecules or mixtures of complex molecules, which can be different respect to molecules representative of standard fossil fuels. On the other hand the additional challenge arise from advanced combustion technologies operating conditions that, as noted before, are completely different respect to that of conventional combustion systems; mainly low combustion temperature (< 1800 K), high pressure (up to 30 bar), high preheating temperature ($T_{in} > T_{si}$), high dilution and significant concentrations of non-conventional diluents (such as CO_2 and H_2O) due to both the use of LCV fuels, and to exhaust gas recirculation. Under these conditions very few experimental data are available and the combustion is currently only insufficiently understood, also for very simple fuels (Ihme 2012; Ren et al. 2001).
Therefore, although advanced combustion technologies allows for real fuel flexibility, an effective use of such technologies for SECs requires a thorough analysis of the combustion characteristics in order to identify optimal operating conditions and control strategies with high efficiency and low pollutant emissions. First, it is required a clear understanding of the role that the fuel type will play. With regard to fuel composition, it may seem interesting that the combustion chemistry of oxygenated fuels (alcohols, ethers, esters and aldehydes) has not been studied with equal intensity and similarly long tradition as pure hydrocarbons combustion (Kohse-Höinghaus & Brockhinke 2009). While combustion devices are being designed to tolerate fuel flexibility, including novel fuel mixtures, chemical pathways in the decomposition and oxidation of such fuels must be studied to assess their emissions. For example, large amount of data in the literature concerns linear and branched C_1-C_5 alcohols (Sarathy et al. 2014), a class of molecules candidates for building SECs (de Joannon 2014). Combustion of oxygenate fuels in premixed flames has been found to decrease

typical soot precursor concentrations, potentially at the cost of increasing aldehyde formation (Sarathy et al. 2014). Such fuels exhibit a molecular structure with a backbone of several carbon atoms and associated functional groups; they present a significant challenge for detailed chemical analysis and kinetic modelling studies since a large number of isomers may be involved. Detailed chemical mechanisms related to oxygenate fuels are still in the early stages of their development and more accurate kinetic parameters and experimental results are desired for engine conditions, including higher more energy-dense alcohols. Particular attention has been devoted to 2,5-dimethylfuran (DMF), a promising second-generation biofuel candidate with a high octane number. Based on quantum chemical calculations, a mechanism has been developed that represent the initial DMF consumption and reproduce only the main features of its oxidation (Togbé et al. 2014).
Furthermore, while there is a significant amount of data and models on single components (at least fossil fuels), experiments and detailed kinetic models for multi-component fuels (as SECs can be) are very few and mainly related to binary mixtures (Cancino et al. 2011). In particular, most of these studies are related to syngas combustion under gas-turbine-relevant operating conditions (Varga et al. 2016). In principle, the comprehensive kinetic models could be used to predict the behaviour of any mixture of alkanes or isomers within the range of structures that are represented in the schemes. In practice, when different fuel components are mixed, the possibility of cross-reactions among the different intermediates typically requires including additional chemical species and reactions (Cancino et al. 2011). Therefore, there remains a need for carefully controlled experiments on fuel mixtures that provide data against which the models may be validated.
Furthermore, the most of the experiments have been obtained under standard conditions, thus high temperature and low dilution, while advanced combustion technologies, as repeatedly stressed, operate under conditions that are completely different respect to that of conventional combustion systems. Under highly diluted conditions with intense pre-heating, that feature a low combustion temperature, the combustion process is expected to have different characteristics (i.e. structure of the reactive region, the ignition and oxidation chemistry, the laminar burning velocities).
Focusing the attention only on the chemical kinetics, the exponential dependence of the temperature indicates that temperature is by far the most dominant parameter on the rate of reaction.
High-temperature combustion of hydrocarbons is driven by reactions of atoms and small radicals. In this temperature range, while the heat release and the temperature of the flame are governed by the thermodynamics of the hydrocarbon, its kinetics and their dependence on its detailed structure are less important. The combustion is more complex at lower temperatures. The generation of radicals is more closely dependent on the chemical structure of the hydrocarbon (Miller et al. 2005).
N-heptane has been the subject of many studies that try to elucidate the ignition characteristics of high molecular weight aliphatic fuels. A particular and well-established striking feature of large hydrocarbon molecules in the low-temperature region ($T < 800$ K) is two-stage ignition, which is also related to cool flame phenomena and the negative temperature coefficient (NTC) of the ignition delay time. Under low-temperature conditions the fuel type can be significantly much important than high temperatures. For example, aromatics and alcohols present a single-stage auto-ignition, differently from n-paraffins, iso-paraffins, and cyclo-paraffins that show a two-stage auto-ignition (Fieweger et al. 1997).
Scientific interpretations of these phenomena date back several decades because modelling of the low temperature oxidation of hydrocarbons is relevant to the onset of “knock” in spark-ignition (SI) engines, or to the initiation of diesel fuels (Griffiths, 1995). The work of Benson (1981) provided a basis for the current understanding of alkyl/alkylperoxy radical chemistry that drives the low-temperature oxidation of large hydrocarbon molecules. Among the major points of his analysis, Benson (1981) suggested that the competition between the highly reversible oxygen addition reaction $R + O_2 = RO_2$ and the reaction $R + O_2 \rightarrow$ olefin + HO_2 (where R represents an alkyl radical) provides the switch from branching to non-branching behaviour as temperature increases. The second reaction is effectively terminating because HO_2 is largely non-reactive at low to moderate temperatures. On the other hand, for large hydrocarbon molecules, internal isomerization

of alkylperoxy (RO_2) species leads to an intramolecular branching sequence at low temperatures through hydroperoxyalkyl radical (QOOH), a second O_2 addition, followed by another isomerization and decomposition of the formed ketoalkylperoxide. Isomerization depends sensitively on the size and structure of the original fuel molecule and the site in that fuel where the O_2 group is located, because the species forms a ring-like transition state where the terminal O atom approaches an extractable H atom within the RO_2 species. Detailed information about this kinetic mechanism can be found in the topical review of Westbrook (2000).

Detailed as well as reduced reaction mechanisms of various levels of predictive ability describing low-temperature oxidation of large hydrocarbons started to appear in the late 1980s and are still under heavy development at present. Despite the availability of such reaction schemes capable of quantitative predictions of various experimental observations related to two-stage ignition phenomena, the detailed prediction of the low-temperature ignition and oxidation of practical fuels and fuel blends is a challenging task, discussed in a recent review (Battin-Leclerc 2008).

The emerging demands for smart energy carriers and technologies have strengthened the need to better understand the fundamental chemistry leading two-stage ignition. For example, it has been found that fuels with two-stage ignition offer significant advantages in controlling combustion phasing and extending the HCCI operating range. Consequently, it is essential to better understand the phenomena associated with the first-stage ignition delay so that better control strategies can be developed for optimal fuel economy and lower pollutant emissions (Zhang et al. 2016).

As introduced in the chapter 1, a problem of homogeneous low-temperature combustion is the susceptibility to oscillations, which are undesirable during combustion. In MILD combustion, the requirement of inlet temperature higher than the auto-ignition one definitely improves stability by eliminating the possibility of thermo-acoustic fluctuations, briefly described in chapter 1. On the other hand, the same operating conditions that eliminate the onset of thermo-acoustic oscillations may lead to chemical oscillations, which can be observed even in well-stirred reactors (de Joannon et al. 2005).

It is well known (Griffiths & Scott 1987) that central to oscillatory regimes is a negative feedback mechanism (by feedback is meant that the products of the mechanism influence the rates of earlier steps in the mechanism) that checks the runaway acceleration of an intermediate concentration and differentiates the oscillatory reaction from an explosion, where the feedback is always positive. Negative feedback can be caused by a number of different phenomena, some purely physical, others of a more chemical nature.

It has been previously mentioned the role of the equilibrium $R + O_2 = RO_2$ on establishing, for heavy hydrocarbons, the competition between branching and termination, which can be accompanied by oscillations. The forward reaction has, in general, only a slight activation energy. In contrast the reverse reaction, the dissociation of the peroxy compound, involves the breaking of a C-O bond and is therefore strongly temperature dependent. In cool flame oscillations it is the rise in temperature and the effect that it has on the equilibrium that provides the negative feedback. As the temperature rises, the equilibrium shifts to reactants, $R + O_2$ and the source of chain branching reagents is terminated. This shift with hydrocarbon fuels occurs at temperatures near 850 K. The temperature above which these equilibria favour dissociation has been termed the “ceiling temperature” by Benson (1981). The cumulative effect is the NTC regime, where the ignition delay actually increases with increasing temperature. With a marked decrease in chain branching, the rate of reaction, and hence heat evolution, decreases. The reaction mixture cools, eventually reaching a point at which the $R + O_2$ equilibrium has a significant RO_2 component and the process can begin again (Griffiths & Scott 1987).

The complete mechanism of cool flame oscillations is more complex than this brief outline. Further details may be found in the work of Griffiths and Scott (1987).

In the past, several experimental (de Joannon et al. 2005; Sabia et al. 2013) and numerical (Dally & Peters 2007; Wada et al. 2009) studies have focused on methane ignition and oxidation under MILD combustion operative conditions in flow reactors at atmospheric pressure. These studies

highlighted the onset of oscillatory regimes for a variety of equivalence ratios and residence times also for a simple fuel, but at higher temperatures (1000-1300 K). Sabia et al. (2007) extended the study of de Joannon et al. (2005) by adding H_2 to the mixtures and quantitatively examining the effects. Their work reported a more detailed classification of the relationship of oscillation behaviour to temperature and a reduction of oscillating conditions compared to those found without addition of H_2.

At temperatures above about 850 K but below 1200 K, OH radicals are formed from HO_2 through the sequence $HO_2 + HO_2 = O_2 + H_2O_2$ and H_2O_2 (+M) = 2OH (+M), where the second reaction corresponds to branching. At even higher temperatures, reaction acceleration proceeds primarily via the branching step $H + O_2 = OH + O$. Therefore, in order to interpret this oscillatory behaviour, a different mechanism is required which cannot, now, involve the peroxy radical, which is unstable under these temperature conditions. Furthermore, higher hydrocarbon oxidation pathways differ from methane pathways. de Joannon et al. (2005) and Sabia et al. (2013) identified different kinetic routes promoted by high inlet temperatures and highly diluted mixtures with respect to conventional flames. In particular they pointed out that the competition between termolecular recombination reactions and branching reactions is crucial for the insurgence of these regimes. Wada et al. (2009) added that a key reaction path at low-intermediate temperatures is between CH_3 and CH_2O. At intermediate temperatures, CH_3 leads to CH_3O and CH_3O_2 instead of CH_2O, and these intermediates lead to CH_2O. Sabia et al. (2007, 2013), Dally and Peters (2007), and Wada et al. (2009) confirmed the findings of de Joannon et al. (2005) so that this chemically induced oscillation is caused by a balance between the heat released by chemical reactions and the heat loss.

In the works cited above, simulations with a variety of chemical kinetic models have been employed to predict oscillation behaviour. However, the mechanism of the oscillations has not been clarified, and an understanding of combustion instabilities at intermediate-temperatures has yet to be demonstrated.

In addition, recent high dilution investigations have revealed considerable discrepancies between experimental data and model predictions, which cannot be only attribute to the effects of non-idealities. Several reasons have been proposed to explain these discrepancies, including the sensitivity of rate coefficients at high-pressure/low-temperature/diluted conditions.

For instance, Natarajan et al. (2008) determined flame speeds of highly diluted $H_2/O_2/N_2$ mixtures preheated up to 700 K. They identified significant disagreements between kinetic model predictions and their flame speed measurements for preheated and highly diluted flames. They cited the temperature dependence of one or more reaction rates as the likely source of disagreement.

Qiao et al. (2007) investigated the effects of He, Ar, N_2, and CO_2 diluents on the near-limit properties of microgravity hydrogen flames using a short-drop free-fall laboratory facility. The measured and computed values of the laminar burning velocity were close when diluent concentrations were low. The agreement was less satisfactory for the near-limit mixtures with low laminar burning velocity and high diluent concentrations. The discrepancies increased with the diluent concentration. They discussed that the near-limit discrepancy could arise from uncertainties in chemical reaction rates and transport properties used in the calculations. Zhang et al. (2012) realized numerical simulations of the minimum ignition energies (MIE) for different H_2/air/diluent (He, Ar, N_2, and CO_2) mixtures using four kinetic mechanisms for hydrogen oxidation available in the literature. The dependence of the MIE on the kinetic mechanisms was shown to be noticeable only when the dilution ratio was close to the dilution limit. Qiao et al. (2007) and Zhang et al. (2012) indicated that the three-body recombination reaction $H + O_2 + M = HO_2 + M$ is extremely important for highly diluted near-limit mixtures. As noticed by the authors, this is due to the competition between chain-branching and chain-terminating reactions near the dilution limits. Temperature and pressure dependence of this recombination reaction is a focus of several recent experimental and theoretical studies aiming at improved accuracy in interpretation of available experimental data, however, different rate constant are still in use in different models (Alekseev et al. 2015). Alekseev et al. (2015) studied the effect of temperature on the laminar burning velocities

of $H_2/O_2/N_2$ flames in a wide range of equivalence ratios and dilution levels. In particular they quantified the power exponent α value that describes the dependence of the burning velocity on temperature. They showed that for undiluted stoichiometric mixtures α is almost constant and close to 1.5, however, for highly diluted and preheated mixtures, a rapid increase of α was observed, especially for fuel lean and rich mixtures. The authors suggested reconsidering the burning velocity correlation for highly diluted and preheated mixtures.

Burke et al. (2010) measured the burning rates for $H_2/CO/O_2$/diluent flames spanning a wide range of conditions in terms of equivalence ratio, flame temperature, pressure, CO fuel fraction, and dilution concentrations of He, Ar and CO_2. They found similar discrepancies between the experimental data and model predictions. However, their analyses indicated that the problem could be considerably more complicated by large uncertainties in the temperature and pressure dependences of several key reactions and perhaps even deficiencies in the common H_2/O_2 mechanism reaction set. For example, the reaction $O + OH + M = HO_2 + M$ is not included in nearly all H_2 models but shows strong sensitivity at high pressure, lean conditions.

In addition, the alteration of the combustion properties in diluted systems is stressed by the presence of great amounts of carbon dioxide and steam, induced both by the strong recirculation of exhausted gases towards the fresh reactants and by the use of LCV fuels. As matter of fact, such species may (1) vary the transport and thermal properties of the mixture, (2) enhance the radiation heat transfer and (3) chemically interact with the oxidation kinetics. These effects occur simultaneously and are intimately coupled (Liu et al. 2001).

Recently, mixtures of fuels with CO_2 and H_2O have received attention. In the scientific literature, a lot of works have been reported on the study of laminar flame speeds and extinction strain rates (Burke et al. 2010; Liu et al. 2003; Mazas et al. 2011; Natarajan et al. 2007, 2009; Prathap et al. 2012; Qiao et al. 2010; Ratna Kishore et al. 2011; Ren et al. 2001; Santner et al. 2013) for CH_4 and/or H_2/CO mixtures partially diluted in CO_2 or H_2O, because of the increasing interest in landfill gas, biogas, syngas and chemical recuperation gas turbine (CRGT) cycle. The common statement is that the CO_2 and H_2O significantly reduce the burning velocities and the extinction strain rates of these mixtures. Indeed, CO_2 and H_2O decrease the flame temperature, thus the fuel oxidation reaction rate. For systems working at high temperatures, it has also been pointed out that CO_2 and H_2O are not inert but directly participate in chemical reactions. CO_2 participates primarily through the reaction $CO_2 + H = CO + OH$ (Barbas et al. 2015; Glarborg & Bentzen 2008; Gonzalo-Tirado & Jiménez 2015; Liu et al. 2003; Mendiara & Glarborg 2009a, 2009b; Qiao et al. 2010 Watanabe et al. 2011, 2013). Such a reaction consumes H radicals thus inhibits the radical high temperature chain branching reaction $H + O_2 = OH + O$, and alters the concentrations of H, O, and OH radicals, so that leads to significant reduction of the overall rate of combustion. On the other hand, water addition was found to dramatically reduce H and O mole fractions but increase OH, mainly due to $H_2O + O = 2OH$ (Santner et al. 2013). However, most of these studies were limited to room temperature of reactants, standard oxygen levels and limited CO_2 and H_2O concentrations. In combustion systems that operate with higher dilution and strong pre-heating levels, along with higher concentrations of CO_2 and H_2O, it is expected that such species can affect the oxidation process in a marked or in different ways.

Giménez-López et al. (2010) studied experimentally the emissions of CO, NO, N_2, N_2O and HNCO in oxy-fuel combustion of HCN in a flow reactor examining the influence of different parameters of the combustion process. Their results indicated that NO and N_2O emissions decreased in a CO_2 atmosphere compared to air combustion. They made some modifications in the starting mechanism to take into account the effect of the presence of high CO_2 concentration levels. Therefore, they have included different reactions involving CO_2, which did not appear in the initial mechanism. Moreover, they have further made a number of modifications of the most sensitive reactions in the mechanism under the conditions studied based on their experimental results.

Anderlhor et al. (2010) numerically investigated the thermal and kinetic impact of the residual species CO, CO_2 and H_2O on the oxidation chemistry of n-heptane/iso-octane/toluene blends at

high dilution ratio (97%) from low to medium temperatures (650-1100 K) at atmospheric pressure. These operative conditions are relevant for the post-oxidation zone in IC engines. They found that the CO_2 and H_2O thermal effects inhibited the oxidation process instead of the kinetic one mainly because of the third-body reactions. They showed the importance of H_2O_2 dissociation at low and intermediate temperatures. The authors suggested revising the efficiencies of the potential collision partners.

Abián et al. (2011) investigated the oxidation of CO in a quartz flow reactor that operated at atmospheric pressure over the temperature range of 700-1800 K from fuel-rich to fuel-lean conditions in the presence of various amounts of CO_2 and H_2O, representing different exhaust-gas recirculation conditions. They found that CO_2 inhibits the CO oxidation not only by the reaction $CO_2 + H = CO + OH$, but also by the reaction $H + O_2 + M = HO_2 + M$ because of the high CO_2 three-body collisional efficiency. Both reactions compete with the reaction $H + O_2 = OH + O$, diminishing the system reactivity. The authors changed the CO_2 three-body efficiency in the model that they used.

Schönborn et al. (2013) experimentally investigated the influence of CO_2 on the propane ignition delay times for the mole fractions of $0 < X_{CO2} < 0.1$ at 870 K, 0.5 MPa and $\Phi = 0.4$. They showed that the auto-ignition delay increased when the mole fraction of CO_2 increased. The chemical kinetic computation failed to accurately predict this behaviour. They suggested that such discrepancy mainly occurred because of the high collisional efficiency of CO_2 in third-body reactions.

Di et al. (2014) presented experimental data to consider the effects of diluents, including Ar, N_2, and CO_2, on the low temperature ignition processes of iso-octane and n-heptane, using a rapid compression machine. The experimental and modelling results confirmed that buffer gas composition has significant impact on ignition at conditions exhibiting two-stage ignition within the NTC region. However, the authors claimed that the buffer gas composition has little impact on the first-stage ignition at any of the conditions studied. For temperatures below 800 K, the major impact of the buffer gas composition was due to thermal effects. The chemical effect increased with increasing temperature.

In all the cited papers, the authors recommended further investigation of the effect of higher concentrations of CO_2 and H_2O in the reactive mixture, as models need further validation in this parameter space.

These combustion conditions stress a region of parameter space where combustion properties are strongly sensitive to a number of reactions that have large uncertainties in their temperature and pressure dependence (Konnov 2008). As matter of fact, the higher dilution, lower flame temperatures, and high three-body collisional efficiencies of diluents such as CO_2 and H_2O produce a kinetic regime, which is largely controlled by HO_2 and H_2O_2 pathways (Burke et al. 2010). Detailed mechanisms for low-temperature combustion are challenging to assemble because significantly more species and reactions must be considered than for high-temperature conditions, and large uncertainties remain regarding reactions and rate coefficients (Struckmeier et al. 2010). There are two major distinctions about the low temperature reactions when compared with the higher temperature classifications. The degradation of the hydrocarbons (involving both abstraction and addition processes) tends to follow a sequential breakdown of the carbon backbone (such as $C_4 \rightarrow C_3 \rightarrow C_2 \rightarrow C_1$) rather than the easy fragmentation into smaller carbon-containing units that may occur at higher temperatures ($C_4 \rightarrow 2C_2$, for example). Thus, simplifications of the kind that are employed at higher temperatures, as a result of common structures within certain classes of reactions, are not so readily applicable. Also, the selectivity of reaction of different propagating free radicals (especially OH, HO_2, RO_2 or RO) is so much more marked, and also the reactivity at particular C-H bonds of the alkane or its molecular derivatives may differ appreciably. These kinetic aspects have an increased importance at low temperatures because the relative magnitudes of rate constants for individual reactions are so much dependent on the activation energies in the Arrhenius expression at lower temperatures (Griffiths, 1994). Kinetic models require reaction rate,

thermochemical, and transport data for the rapidly growing number of species and reactions present. Unfortunately, only a relatively small proportion of reactions now included in comprehensive kinetic schemes actually have been studied directly by experiment. Theoretical methods for calculating reaction pathways and rates of reaction have been developed, many of which now require supercomputer resources to solve the complex quantum mechanical systems involved. Thus, there is considerable recourse to estimation techniques for reaction rates and thermochemical quantities required by models (Westbrook et al. 2005).
To sum up, fundamental study is necessary to understand the mechanisms of SECs combustion phenomena. The understanding of such phenomena must rely on validated detailed reaction models established for non-conventional conditions than those conventionally addressed. To assist the development and validation of more reliable chemistry models for SECs combustion, new experiments are required, spanning as many different types of practical systems and as wide a range of conditions as possible.

2.2 Scope of the work

From the literature survey, it is evident that disagreement exists in model predictions for SECs combustion conditions and it should be assessed by further systematic studies whether these non-conventional conditions contribute to these disagreement. For these reasons, the understanding of each aspect of the SECs combustion and the development of a correct mechanism that can simulate experimental data are of the highest importance. Since most chemical kinetic models have been validated at higher temperatures and low dilution, there is a need of optimal experiments in order to restrict uncertainties for low temperatures and high dilution conditions. These targets become fundamental because of the inability of the kinetic models available in the literature to reproduce the oxidation behaviour even of standard fuels in the presence of high dilution levels with particular regard to cases where significant amounts of CO_2 and H_2O are present.
Flow reactors are well-established configurations to study chemical reaction pathways in combustion.
In particular, the study of the characteristic ignition and oxidation times is mandatory to develop reliable tools for designing industrial appliances. The ignition delays provide valuable data in the low-to-intermediate-temperature regime. As a matter of fact, they are widely used parameters against which numerical models are tested. The auto-ignition time has practical relevance because it is one of the parameters essential for combustion design, in particular for advanced combustion technologies for which $T_{in} > T_{si}$. Therefore, it is important to determine the dependence of the ignition delay on pressure, temperature and mixture composition for new fuels in order to be able to predict the start and the control of combustion. Furthermore, an understanding of the kinetics routes established during auto-ignition is relevant because reaction rates are relatively slow and very sensitive to temperature and mixture composition. In this thesis, the ignition delay times have been studied using a Tubular Flow Reactor (TFR).
In addition, quantitative concentrations of all major and minor species and their variation with important parameters are desirable for a comparison of experimental data with modelling results. These measurements have been obtained in a Jet Stirred Flow Reactor (JSFR). Kinetic measurements, such as ignition delay and species concentrations, are important targets for the validation and optimization of chemical kinetic mechanisms.
On light of the impact of the different constituents forming a fuel mixture, namely fuel and diluent, it is better to characterize the combustion kinetics starting from mixtures for which the models still reproduce the behaviour of the individual constituents (at least in standard combustion conditions).
Table 2.1 summarizes the different types of fuel mixtures studied in this work, along with the experimental system adopted for the study.

	Diluents						
Fuels	Fuel mixtures	He	N_2	CO_2	H_2O	N_2/CO_2	N_2/H_2O	CO_2/H_2O
	CH_4	JSFR	JSFR	JSFR			JSFR	
	$CO/CH_4/C_2H_4/C_2H_6$			TFR		TFR		TFR
	C_3H_8		TFR/JSFR	TFR/JSFR	TFR	JSFR	JSFR	
	$N\text{-}C_5H_{12}$			JSFR				

Table 2.1 – List of fuel mixtures studied along with the experimental system adopted.

Four reference fuels were studied: CH_4, C_3H_8, n-C_5H_{12}, and a mixture of $CO/CH_4/C_2H_4/C_2H_6$. This provides a sort of "longitudinal" comparison of fuels whose structure (i.e., n-alkane) is the same, but the length of the straight chain is increasing. This approach may aid in the development of a hierarchical kinetic model that can be validated with hypothetical SECs conditions. The C_1C_3 molecules chosen here form the base of hierarchical combustion chemistry. Their chemical kinetics is fundamentally important for all combustion processes of hydrocarbons, is well known, and is sufficiently simple. The elementary reactions of the combustion of these C_1C_3 molecules and their intermediate oxidation species are a central part of the mechanisms that describe the combustion of any hydrocarbon or oxygenated fuel. Furthermore, the C_1C_3 molecules that were chosen as the reference fuels are important fuels for practical applications (predominantly methane in natural gas and propane in LPG). Moreover, propane reflects the thermochemical and combustion properties of larger hydrocarbons. Because of these properties, it is a key fuel in experiments aimed at characterizing the ignition and oxidation kinetics of light to heavy hydrocarbons. As a matter of fact, n-propyl resulting from H-abstraction from propane is the smallest alkyl radical that has the key six-member ring transition state (i.e. to form the γ-QOOH, 3-hydroperoxypropyl from n-propylperoxy). As a result the n-propyl radical exhibits all the key features of ignition of larger alkyl radicals, such as second O_2 addition. Thus propane is considered as a combustion archetype.
After that, to bridge the gap to more complex fuels, n-pentane was investigated.
On the other hand it has been just mentioned the important role of diluents. Therefore, good understanding of combustion kinetics of simple hydrocarbons with diluents at high dilution is central to developing robust computational tools for optimizing the design of advanced combustion technologies for any more complex fuels.
Several diluent gases were used in this work: He, N_2, CO_2, H_2O. First, understanding the effect of each diluent in isolation serves to advance our understanding of SECs. Then, mixtures of N_2/CO_2, N_2/H_2O and CO_2/H_2O in different proportions were investigated.
The attention has been focused on ignition and oxidation characteristics and their dependences on the environmental parameters, such as temperature, dilution and equivalence ratio. Following the above discussion, it is aware that these parameters are relevant in the transition between different combustion regimes. The difference in the chemical paths for these fuel mixtures provides a way of assessing the sensitivity of the diluted combustion regime to fuel mixture type. It has been chosen to exclude the pressure from the investigated parameters because the literature survey has evidenced that this parameter has an effect similar to the dilution on the kinetics characteristics, in particular the pressure and the dilution have both an influence on termolecular reactions. Therefore, keeping the pressure to a constant value aids to better clarify the effect of dilution on the kinetics characteristics.

Specific objectives
Given this background, the objectives of the current thesis were to investigate the effect of mixture composition (in terms of fuel and diluent type) on the ignition delay times and concentration

profiles of chemical species, including data obtained in a TFR and a JSFR, at conditions relevant to diluted combustion using the mixtures of Table 2.1 as reference fuel mixtures. The experiments were carried out for lean, stoichiometric, and rich mixtures, at atmospheric pressure. The study focused on low-intermediate temperature conditions of practical interest to diluted combustion applications. In the Appendix, it is provided a detailed list of the operating conditions for each investigated case.

Obtaining such measurements was the primary objective of the present study. They provide validation targets for SECs kinetic mechanism development.

In addition, the performance of updated kinetic models in predicting the experimental data was tested. The experiments do not only provide data for models validation, but also contain information in itself. Therefore, numerical analyses were performed to gain an understanding of the contribution of these non-conventional conditions on the combustion chemical kinetics. This part of the thesis, rather than merely catalogue all the reactions, aimed at simplifying the process by identifying the most important reactions and by quantifying the effects of these reactions on the combustion characteristics. Finally, possible sources of disagreement between the model predictions and experimental data were outlined.

CHAPTER 3 – EXPERIMENTAL AND NUMERICAL TOOLS

3.1 Model reactors: suitability, selection and accuracy in non-conventional combustion conditions

In a practical combustion system, in general, several processes occur simultaneously. A general modelling approach can be called "full-system modelling" in which as many as possible processes in the combustor being modelled are included. In order to do it, usually the degree of complexity is reduced by making simplifying assumptions. Two- and three-dimensional CFD engine simulations usually include simplified chemical kinetics sub-models, simplified turbulence models, little or no radiation sub-model, and other engine simulations greatly simplify the problem geometry by assuming the combustion has two-dimensional symmetry (Westbrook et al. 2005). As stressed in the chapter 1, in the case of SECs combustion, usually this kind of simplifications could not be possible.

As extensively discussed above, the present experimental combustion study is intended to focus on the chemical kinetics. In this context, model reactors are very useful tools. Model reactors have the advantage of highlighting on one specific process (the chemical kinetics) that we can study experimentally and computationally under controlled conditions and in considerable detail, separated from other factors that might also be occurring (in particular the fluid-dynamics).

The model reactors that have been used in this study are the Plug Flow Reactor (PFR) and the Perfectly Stirred Reactor (PSR). These systems have found widespread application in combustion chemistry studies because the combustion characteristics can be measured as a function of a single coordinate (time or space). Correspondingly, zero- or one-dimensional combustion models with detailed mechanisms can be employed in the respective computer simulations.

It should be underlined that also shock tubes and static reactors have the advantage of being free from transport effects (in the appropriate conditions), which simplifies the modelling procedure.

In particular, it is possible to consider PSR and PFR as two opposite paradigms. In the PFR, chemical reactions are carried along with the flow, and there is no back-mixing of products species. While a PSR represents an idealization where combustion products are back-mixed with reactants so quickly that the reaction zone is distributed uniformly in space. Therefore, in a PSR, no gradients in temperature or species exist and the combustion region can be characterized by a single value for temperature and all species. Because all the reaction products are back-mixed with the reactants, the chemical pathways for combustion and pollutant formation can be different than in purely premixed or diffusion flames (Richards et al. 2001). Differently from these latter experimental techniques, PSR and PFR enable to systematically study the dependence of the combustion kinetics characteristics (in this case ignition delay times and chemical species distribution) as a function of a range of combustion parameters, such as fuel mixture composition, temperature, and fuel/air equivalence ratio. Controlling the temperature of the test mixtures allows the effects of mixture composition to be more easily and independently studied using these fundamental facilities. Furthermore, CO_2 and H_2O can be added in controlled amounts while maintaining the same O_2 concentration.

It has to be pointed out that in non-conventional practical combustors, intense turbulent mixing of reaction zones, together with the slow combustion chemical kinetics, can produce back-mixing conditions that approach the perfectly stirred reactor idealization, whereas the PFR condition corresponds approximately to what happens to the slower chemical reactions which occur downstream of the main heat release zone in turbine combustors. As a matter of fact, early models of combustion system have used combinations of PSR and PFR to represent the combined effect of back-mixing and plug-flow aerodynamics (Richards et al. 2001).

3.2 Plug Flow Reactor

Ignition delay measurements are commonly conducted in shock tubes (STs), rapid compression machines (RCMs), and continuous tubular flow reactors (TFRs). Flow reactors are of particular interest for ignition studies at SECs combustion operating conditions, since these facilities provide access to extended test-times (from about 1 ms to about 1 s). Currently employed TFR-facilities share a similar setup. In its simplest form, a flow reactor consists of a long pipe that is separated by a fuel injector module into a flow conditioner and a test section. Oxidant (air or a mixture of oxygen and diluent) is supplied through the flow conditioner in which the oxidant is preheated. The fuel is subsequently injected via a mixing module, and different mixing strategies are utilized to achieve an approximately homogeneous mixture prior to ignition. Following the mixing, the test gas mixture passes down the test section in which autoignition takes place. To minimize heat losses and other secondary effects (for example a non-flat temperature profile in non-reactive conditions), the test section is commonly heated and thermally insulated. Thermocouples, photo-diodes, and pressure sensors are employed to detect the ignition location, using several criteria. The ignition location, x_{ig}, is then related to an ignition delay time, t, using the theoretical bulk flow velocity v:

$t = x_{ig}/v$

To guarantee that the mixture ignites within the finite-length test section, mass flow rates, and thus bulk velocities, are adjusted, depending on the pressure and temperature conditions of the test gas mixture.

The ignition can be most-likely dependent on facility-specific non-idealities that are present in the flow reactor. In particular, Beerer & McDonell (2011) pointed out that the sources for sporadic ignition events could be linked to incomplete mixing between fuel and oxidizer, temperature variations in the preheater, turbulent mixing in the test section, and the influence of the boundary layer in affecting the induction time and the ignition process. In this case the ignition event occurs earlier than predicted from homogeneous isobaric reactor simulations. Therefore, a better understanding of the effects of inhomogeneities in temperature and mixture composition, and the role of the aerodynamics in affecting the ignition process is crucial towards the characterization of ignition properties of SEC fuels. Below it is provided an explanation on how these non-idealities have been addressed.

3.2.1 Experimental setup

A continuous TFR is used in the current study. This type of a device has the following features: isobaric, turbulent, and subsonic.

This continuous flow ignition test apparatus was designed by Sabia (2006) in order to study the autoignition characteristics of a wide variety of fuels and diluents, at atmospheric pressure, under a variety of experimental conditions such as T_{in}, equivalence ratio and diluent concentrations. These main parameters controlling the chemical processes can be varied independently.

The device used in the current study is a laboratory-scale stainless steel flow reactor like the one used by Freeman & Lefebvre (1984), Peschke & Spadaccini (1985), Beerer & McDonell (2011).

The experimental setup can be schematically divided into three main sections: a feeding section, a flow heating system and the TFR.

An overview of the experimental set-up used for the study of SECs ignition is schematically represented in Fig. 3.1.

Two gas feed lines are shown in the scheme: the main gas flow line, composed of a diluent species (i.e., N_2 in the figure) and oxygen, and a secondary fuel line, composed of fuel and diluent (i.e., N_2 in the figure).

Gases are stored in cylinders and supplied to the system by means of calibrated thermal mass flow controllers (BronkHorst High-Tech) connected to a PC and interfaced by sub-routines developed in Labview. The precision of the mass flow rates corresponds to ± 0.5% of the set operating conditions. Gases are provided with high purities: > 99.99% for nitrogen and oxygen, 99.5% for carbon dioxide and fuels.

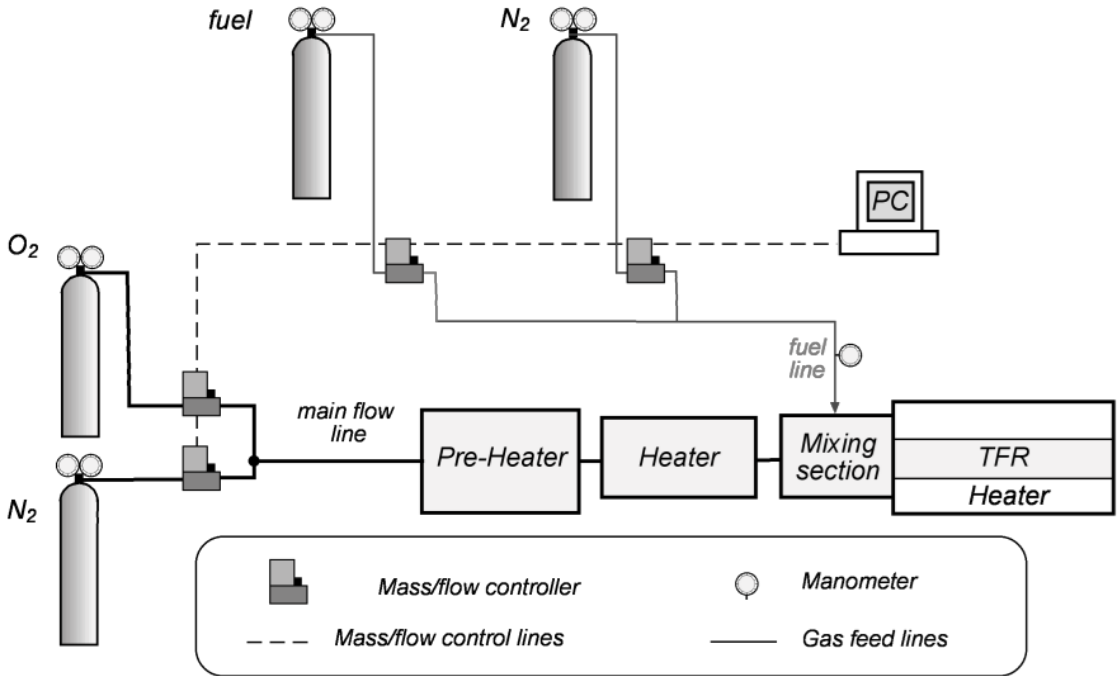

Fig. 3.1 – Sketch of the experimental facility (example with a generic fuel and nitrogen as diluent).

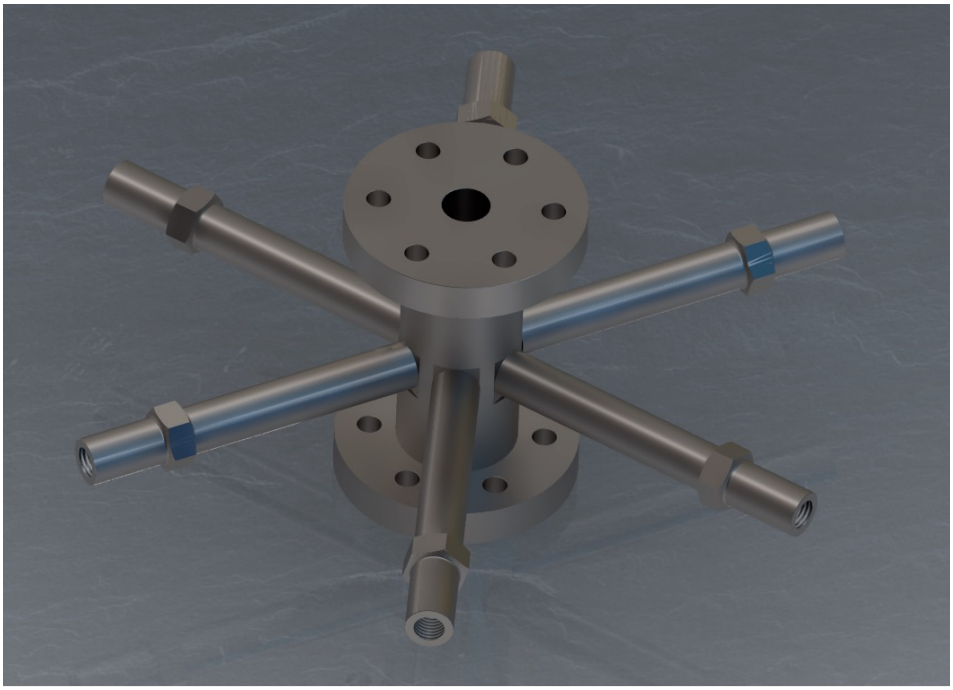

Fig. 3.2 – Detail of the mixing section of the reactor.

Water vapour is produced with a steam generator. The flow rate is controlled with a solenoid valve and measured with a calibrated rotameter.

The main gas flow passes through two stainless steel AISI 310S coils placed inside high-temperature electrically heated ceramic fiber modules supplied by Watlow Srl, which are controlled by Solid State Relay (SSR) actuators and PID controllers. These modules can achieve temperatures of approximately 1400 K. AISI 310S stainless steel was selected as the manufacturing material because it can withstand high operating temperatures without corrosion. The heat exchangers were designed and dimensioned to maximize the heat exchange efficiency.

Fig. 3.3 – Picture of the test section.

The first oven (pre-heater) (15 kW) pre-heats the main flow to 1000-1100 K, while the second oven (5 kW) finely regulates the temperature to the desired value.
The heated main flow then mixes with the fuel flow by means of a "jets in cross flow" configuration. The geometry of the mixing section along with the number, position and dimension of the injectors were optimized based on previous studies, experimental tests and CFD calculations, as reported in Sabia (2006). A detailed view of the premixer is shown in Fig. 3.2.
After that, the pre-mixed charge flows through the reactor where the auto-ignition and oxidation processes take place.
The reactor (Fig. 3.3) is manufactured with AISI 310S stainless steel and it is composed of four 35 cm-long flanged segments bolted together with 10 mm constant inner diameters and it is equipped with one thick quartz window at the end. The total axial dimension of the reactor is 140 cm. As can

be seen from Fig. 3.3, the flow reactor test section begins a short distance downstream of the fuel injector. The TFR reactor is placed in a thermal insulated electrical ceramic oven with two individually controlled zones to minimize heat loss to the surroundings. This allows temperature of up to 1400 K, with a uniform non-reactive temperature profile throughout the reaction zone within ± 10 K. The reactor walls are maintained at the same temperature as the flowing gases (in non-reactive conditions).

3.2.2 Measurement methodology

In each test the total flow was set to a specified velocity (thus a specified residence time), inlet temperature, and mixture composition (the pressure is always atmospheric). The mixture velocity is defined as v = volume flow rate/reactor cross-area. Therefore the flow velocity is dependent on the flow rate that depends on the mixture temperature and the static pressure. Since the pressure is atmospheric, the temperature is the only property that was recorded to calculate the right flow rates. The temperature measured 5 cm downstream of the fuel injectors was reported as the T_{in}. It is useful to remember that the axial temperature profile is uniform throughout the reaction zone within ± 10 K.

After the fuel injection, a period of time (few seconds) was allowed to obtain a steady state. This eliminates any uncertainties in measuring the time at which fuel injection takes place. Inconel shielded thermocouples (type N) were mounted in the walls of the test section at 5 cm intervals along the axis (Fig. 3.3) and permitted the recording of axial temperature profiles, which were used to evaluate oxidation regimes and to measure ignition delay times (t).

In some cases, a full ignition was observed while others only showed a small temperature rise or no rise at all, as it will be shown in the next chapter. In particular, t was defined on the basis of axial steady temperature profiles. Once oxidation reactions occurred, the temperature profile stabilized after a transient period. Once an autoignition condition was established, the mixture velocity and the test section length where autoignition occurred were all that were needed to determine the delay time. The ignition time was then computed: the axial distance (where the zero distance is the beginning of the reactor) over which a temperature increase of 10 K (de Joannon et al. 2002) was measured was divided by the flow velocity.

All these temperatures were controlled with a precision of ± 2 K. Thermocouples were located every 5 cm along the axial direction. This thermocouple spacing led an error in the determination of the ignition location. By changing the flow velocity, the measurement uncertainty was approximately ± 8 x 10^{-4} s for a flow velocity of 30 m/s, and ± 3 x 10^{-4} s for 100 m/s flow velocity. Thus the error varies from 2% for t of about 10^{-2} s to 10% for t of about 10^{-3} s. In the next chapter, experimental results are always presented for different flow velocities giving a clear indication of the uncertainty in the ignition delay times determination with the present methodology.

Thermal gas expansion effects were neglected. This appears to be an appropriate assumption since this investigation is concerned with studying the ignition onset for which density changes and heat-release remain small. The error that is introduced by neglecting these effects can be estimated by considering a control volume over which the temperature increases linearly from T_{in} to $T = T_{in} + 10$. By assuming homogeneous species composition, the difference between the velocity at the ignition location and the inlet flow velocity can then be evaluated as less than 1%, and then it can be assumed that the constant-density approximation has no effect on the ignition delay.

The flow velocity was changed from 30 m/s up to 100 m/s moving from low to high inlet temperatures. The agreement between the different datasets confirmed the good reproducibility of the experiments.

Analysis of measurement reliability

Before presenting the experimental results, discussions related to perturbations or effects of non-idealities on measurements are mandatory. Uncertainty of ignition delay time measurements using

TFRs can come from various sources. In order to obtain useful kinetics data from TFR experiments, many of the secondary effects such as mixing times, fluid-dynamics perturbations, mass and heat thermal diffusion, and wall heterogeneous reactions must be rendered negligible in order to model the experiment as a PFR.

Mixing:

The common problem of flow reactors is the inability to convert experimental profiles as a function of axial distance into time profiles. This problem is usually overcome by shifting the experimental data to match the calculated data at a reference point of 50% consumption of the major reactant. This is not strictly necessary if the mixing configuration allows for characteristic times very shorter than the minimum ignition time when analysing the oxidation process of premixed charges. The mixing section of the current TFR was designed under this constraint (Sabia 2006). In a first phase, a literature survey was made in order to compare different mixing configurations. Then, further studies were made in the evaluation of several parameters such as shape, number and position of the injectors, along with protrusion of the injection orifices into the main channel. The configuration selected for an optimal mixing of fuel and oxidizer/diluent streams consisted of cross-flow jets. The main parameter that influences the efficiency of mixing for a system with cross-flow jets is the ratio of momentum of flows J, defined as:

$$J = \frac{\rho_j v_j^2}{\rho_s v_s^2}$$

where ρ_j and v_j are respectively the density and velocity of incoming flow injected, and ρ_s and v_s are the density and velocity of the main flow.

The optimization procedure was performed by means of CFD calculations and acetone PLIF-measurements for different fuel-oxygen-diluent momentum ratios, number and radial position of the injectors and convergent variations. These analyses showed a nearly homogeneous mixture composition in the TFR-core with six injection nozzles of 0.8 mm diameter located along the walls and a convergent linear with a slope angle of 26 degrees. In particular, this configuration allows for a characteristic mixing time shorter than 10^{-4} s when J = 11. It is possible to adjust the value of J and thus the penetration of the jet, by varying the composition of the side flow adding a diluent to the fuel flow (as shown in Fig. 3.1). This is important because this configuration was used under different operating conditions. Therefore the addition of a diluent to the fuel flow makes the present mixing section very flexible. Actually it allows for a characteristic mixing time shorter than 10^{-4} s, so at least one order of magnitude shorter than measured ignition delay times. Thus no shift is needed. The effect of mixing on ignition delay times was also investigated. In particular a number of ignition experiments were performed with different bath gases in the fuel flow, i.e. N_2, Ar and He that have different densities and then they produce different J, so that different mixing. The results obtained in case of N_2 fuel-dilution are similar to those of Ar fuel-dilution. However, a slight difference is observed in case of He fuel-dilution (with respect to Ar and N_2 cases), confirming the importance of keeping a quite constant J.

It was found (Wu & Ihme 2014) that the ignition delay exhibits a stronger dependence on initial temperature fluctuation than mixture inhomogeneities. Therefore it is necessary to experimentally quantify the magnitude and distribution of the temperature fluctuations in flow reactors. In fact, the mixing section was equipped with a thermocouple to monitor the temperature during flow mixing. When a temperature increase was detected by this thermocouple, indicating the onset of ignition/oxidation reactions during the mixing process, the experimental conditions were not considered. In such cases, the flow velocity was increased to increase the local flow strain rate and shifting the ignition process further downstream in the TFR. In this case, the initial temperature inhomogeneities decayed due to the enhanced turbulent mixing.

Furthermore, intense air-cooling of the fuel injectors in this system prevented the thermal cracking of the fuel prior to ignition. The flow of diluent through the injector, beyond assuring constant

momentum, lowers the fuel concentration and residence time inside the injector. This further reduces the possibility of fuel decomposition inside the injectors. Anyway, for each tested fuel mixture, by means of gas chromatography, it was evaluated the critical temperature that caused fuel decomposition inside the injector. The injector system temperature, monitored with a K-type thermocouple, was always kept at a value lower than this critical temperature (for example 370° C for propane mixtures).

Fluid-dynamics:

Apart from few exceptions, flow reactors are commonly operated in a turbulent flow-regime with Reynolds numbers (Re) on the order of $O(10^3\text{-}10^5)$. Here, Re is defined with respect to the diameter and bulk-velocity: Re = vD/ν. The current flow reactor produces a turbulent regime of a preheated flow (3000 < Re 10000 in all the analysed conditions) in which the fuel is injected. The ignition is fairly insensitive to the flow-field. Under these conditions the ignition location can directly be related to the residence time, and is therefore only dependent on the velocity.

Radial temperatures profiles measurements obtained with movable thermocouples for different inlet flow velocities showed that temperature profiles could be assumed to be flat starting from a radial position of 1 mm. Figure 3.4 shows that the velocity profile remains flat over 80% of the reactor diameter.

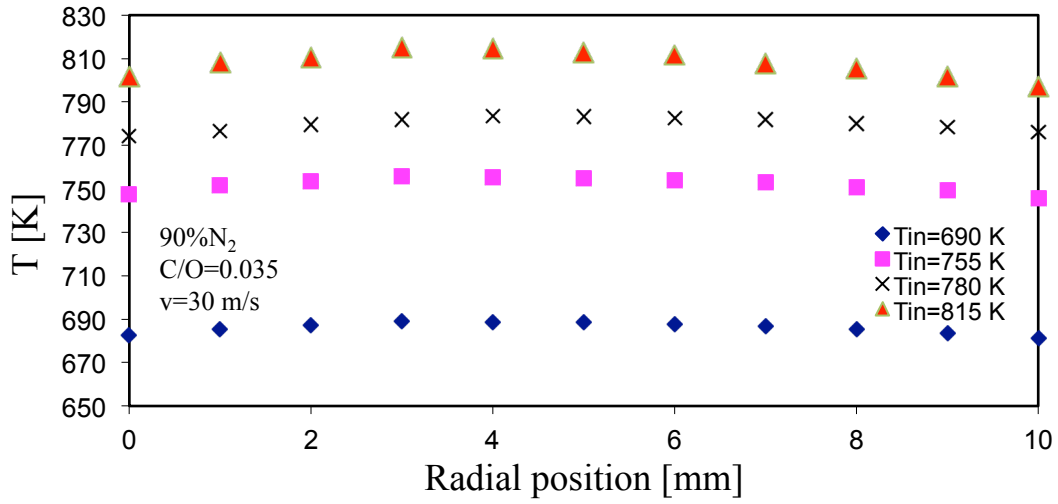

Fig. 3.4 – Radial temperature profiles measured for $C_3H_8/O_2/N_2$ mixtures (d = 90%, Φ = 0.12, v = 30 m/s), obtained for several T_{in}.

The diameter of thermocouples was 1.5 mm. They were inserted in the reactor orthogonally to the flow. To minimize the interference of thermocouples on fluid flow dynamics, the tips of the thermocouples penetrated into the gas stream by 2 mm thereby reducing the perturbation to the flow and yet provided reasonably reliable internal temperatures. The invariance of the measured ignition delays for a range of flow velocities suggested that the thermocouples had no significant effects on the fluid flow.

In an ideal plug flow, the dispersion terms are negligible and hence mass transport is solely due to the bulk flow down the flow reactor. However in any reactor (including current flow reactor) dispersion effects may become non-negligible in certain regions of the flow and their relative importance to the flow chemistry may be significant. A study on the design of the reactor can be found in Sabia (2006). The radial and/or axial mass and heat thermal dispersion, estimated by means of classical methods of chemical engineering (Levenspiel 1958), supported the approximation to plug flow conditions under the investigated operating conditions.

Wall effects:

Another issue to address in flow systems is the effect of heterogeneous reactions at walls. This aspect was thoroughly addressed in several ways:

(1) Tests with mixtures of methane or propane with oxygen diluted in nitrogen were repeated after wall treatments in H_2O or CO_2 flows for hours. Furthermore, experimental tests were conducted in two tubes made from different types of stainless steel, namely AISI 316 and AISI 310S. Negligible differences in the ignition delay times were observed.
(2) The literature suggests that catalytic effects can occur at low temperatures (thus, homogeneous characteristic times are long) and long residence times (i.e., on the order of seconds). Because the current TFR typically operates at intermediate temperatures and low residence times, it is reasonable to infer that catalytic effects are not present or at least heterogeneous combustion times are significantly longer than homogenous times. Indirect evidences of such a statement is given by the similar values of ignition delay times obtained at different flow rates and thus at different residence times.

Heat exchange:

Finally, heat exchange mechanisms with the surroundings can also affect the reliability of measurements. In the experimental tests, heat transfer did not significantly influence the ignition delay times for the considered operation conditions. By varying the inlet flux velocity, and thus the heat exchange coefficient, the change in the ignition time was lower than the uncertainty error induced by thermocouple distance. It should be stressed that this does not mean that the reactor is adiabatic, but only that any variation in the heat exchange coefficient does not alter the measured ignition delay times.

Validation of the experimental methodology

Experimental tests were repeated different times to ensure the measurement reproducibility and the ignition delay times were calculated at several flow velocities to reduce the uncertainty of calculated values.

Tests were conducted over a series of several weeks. The results of each test are shown in the Appendix.

The experimental methodology is first validated with well-documented ignition delay times. The points where ignition occurred are plotted in Fig. 3.5 against previous studies and their derived correlations. It is common to represent the chemistry of combustion systems in the form of a global (or quasi-global) reaction rate. Commonly, the quantitative expressions are derived from the temperature and concentration dependences of measured ignition delays in shock tubes or other experimental systems. Usually the application of global rate equations is associated with high temperature combustion and the major use is to predict combustion rates associated with flame propagation. Therefore, in order to validate the present methodology, only the data obtained at temperatures higher than 1000 K are plotted in Fig. 3.5. The major factor to be considered is the validity of such equations outside the range of conditions in which they were derived (Griffiths 1995). This aspect will be discussed in the next chapter.

Current ignition delay times reported in Fig. 3.5 are measured for $C_3H_8/O_2/N_2$ mixtures with equivalence ratios varying from 0.33 to 1.33 and d = 90%, at atmospheric pressure. As expected, the ignition delay time decreases for higher temperatures. In the high temperature regime (above 1000 K) the ignition delay time plotted versus temperature can be expressed using the correlation of Burcat et al. (1971), who studied propane/oxygen ignition in a wide range of temperatures, pressures and equivalence ratios behind the reflected shock waves. They proposed an empirical correlation from their measurements by following both pressure and heat-flux. Using this correlation, present atmospheric pressure/high dilution results can be compared to the higher pressure/low dilution data reported in the literature. Therefore in Fig. 3.5, the present results are compared with reference measurements of propane ignition delay times obtained with various experimental configurations (Lezberg 1957; Burcat et al. 1971; Herzler et al. 2004; Penyazkov et al. 2005) from 1 to 30 atm, equivalence ratios from 0.5 to 1, and d = 76%. Note that all the experimental data presented in the figure were obtained under conditions that are within the range that was used to develop the correlation. The results presented in Fig. 3.5 validate the experimental

methodology developed for ignition delay times in diluted conditions. This methodology yields results in good agreement with the reference measurements obtained with different experimental techniques within the experimental uncertainty. For inlet temperatures lower than 1100 K, the data scattering increases slightly. This effect will be discussed in the next chapter.

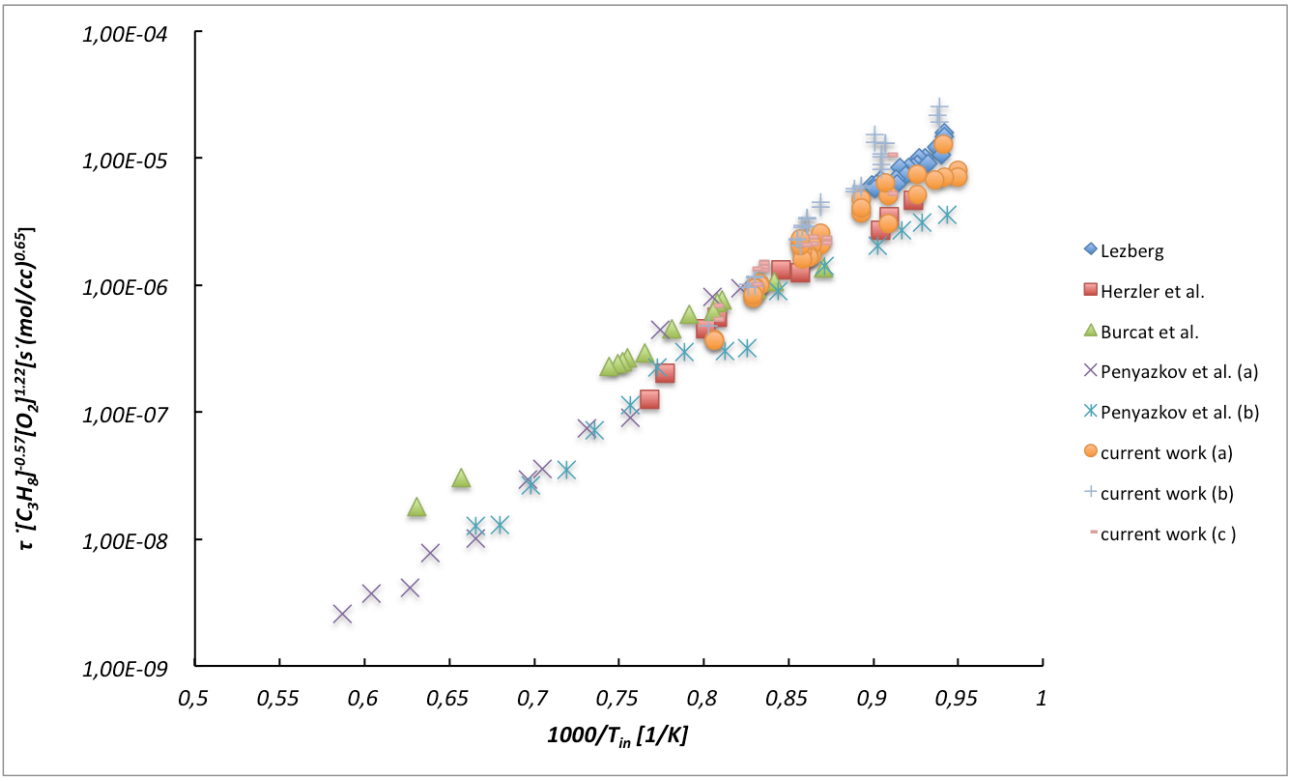

Fig. 3.5 – Comparison of propane ignition delay times obtained in different studies.

3.3 Perfectly Stirred Reactor

Gas phase kinetic studies are mostly performed using closed vessels, burners and PSRs. The PSR, or Well Stirred Reactor (WSR), is an ideal reactor widely used in combustion and chemical engineering studies. In its modelling, instantaneous and homogeneous mixing of reactants and products, and constant temperature, pressure and concentration species profiles inside the reactor is assumed. Furthermore, the steady state operation means no time dependence, and the equations describing the reactor are a set of coupled nonlinear algebraic equations.
Among PSRs is the JSFR; it approaches the behaviour of an ideal PSR.
The JSFR is a continuous-flow stirred reactor and an important experimental tool in kinetic studies because it allows accurate monitoring of the extent of reaction by residence time control, focusing only on chemical kinetics phenomena. The JSFR has often been used to study the gas phase oxidation and thermal decomposition of fuels. These studies consist in measuring the evolution of the mole fractions of species at the outlet of the reactor as a function of different parameters such as reaction temperature, residence time, pressure and composition of the inlet gas (Herbinet & Dayma 2013).
In the literature, some realizations of this reactor were proposed and employed. The principle of the device was to direct inject turbulent premixed jets of fuel and oxidant (air or a mixture of oxygen and diluent) into a chamber designed to maximize stirring by jets interaction, swirl flow and turbulence intensity. The entrainment of the burning mixture causes sufficient recirculation to establish a uniform concentration and temperature throughout the reactor.

The residence time of the gas in the reactor is actually a mean residence time (or space time), which is defined as the ratio of the volume of the reactor, V, and of the volume flow rate of the gas flowing through the reactor, Q, which is also the volume flow rate at the outlet of the reactor (Herbinet & Dayma 2013).
To verify that the reactor can be considered as a PSR, one can measure the residence time distribution E (t) (Levenspiel 1958). The reactor is an ideal PSR if the E (t) can be represented by the following expression:
$E(t) = (1/\tau)\exp(-t/\tau)$
The basis for the design of spherical jet-stirred reactors was proposed by Villermaux in Nancy (David & Matras 1975; Matras & Villermaux 1973) and it has been subsequently employed by Caprio et al. (1981) in Napoli and Dagaut et al. (1986) in Orléans. These reactors were later improved in the same laboratories by D'Anna et al. (1992) and de Joannon et al. (2005) in Napoli, and Herbinet et al. (2007) in Nancy.
The JSFR designed by Villermaux is composed of a sphere in which the reaction takes place. The fresh gases enter the reactor through an injection cross located at the center of the sphere and composed of four nozzles providing jets ensuring the mixing of the gas phase (Herbinet & Dayma 2013).
In this work two JSFRs were used: the one of Napoli (de Joannon et al. 2005) and the one of Nancy (Herbinet et al. 2007). Both the reactors were developed from the rules of construction proposed by the team of Villermaux. In particular the rules of construction of a JSFR rely on the theory of the free jet: the jet from a nozzle leads to the motion of the gas phase in which it flows and this motion results in the distribution of the initial kinetic energy in small turbulent pieces of gas phase. It is assumed that a jet provided by a nozzle in the reactor widens in form of a cone, which bends along a circumference between two nozzles. A detailed description of this type of reactor, along with the construction criteria can be found in the work of Herbinet & Dayma (2013).

3.3.1 Experimental setup

The oxidation of the fuel mixtures reported in Table 2.1 was studied in two JSFRs (Napoli and Nancy), which are shown in Fig. 3.6. Combining the two reactors, a large parameter field with variations of stoichiometry, residence time, and dilution would be accessible that can be used in model validation.
The apparatuses consist basically of a gas feeding system, a reaction system, and a gas analysis system.

Napoli JSFR
The reactor consists of a sphere of 113 cm^3. The reactor is made in quartz to prevent catalytic reactions. The main flow is composed by oxygen and diluent. It passes through a quartz tube located within two cylindrical electrically heated ceramic fiber ovens. The main flow residence time within the quartz tube and the installed electric power are designed to reach pre-heating temperatures up to 1250 K. It subsequently mixes with the secondary flow, composed by fuel and diluent, in a premixing chamber. Then the pre-mixed mixture enters the reactor through four nozzles of 1 mm diameter located at its center. Figure 3.7 shows the detail of the injectors. The well-mixing of the reactor was verified in the past by means of a pulse tracer experiment following a procedure described by Levenspiel (1958).
The results suggested that the reactor behaves as a PSR for residence times lower than 0.6 s. The residence time used in the present experiments was thus fixed to 0.5 s. A further computational residence time distribution showed that, under these conditions, the mean residence time differs from the ideal PSR residence time of 3%. The residence time of the fuel mixture in the injector is more than 100 times lower than the mean residence time in the reactor. Thus, oxidation of the fuel inside the injector is prevented. The products of combustion were exhausted through a 3 mm diameter tube arranged in the wall of the reactor. The reactor is located within other two electrical

fiber ovens to minimize heat loss to the surroundings. A recirculation air system (Fig. 3.6) provides a homogeneous temperature distribution in the oven. The homogeneity of the wall temperature field is monitored with movable thermocouples. The temperatures of the reactor wall and of the gases upstream are measured by type N thermocouples and regulated by PID controllers.

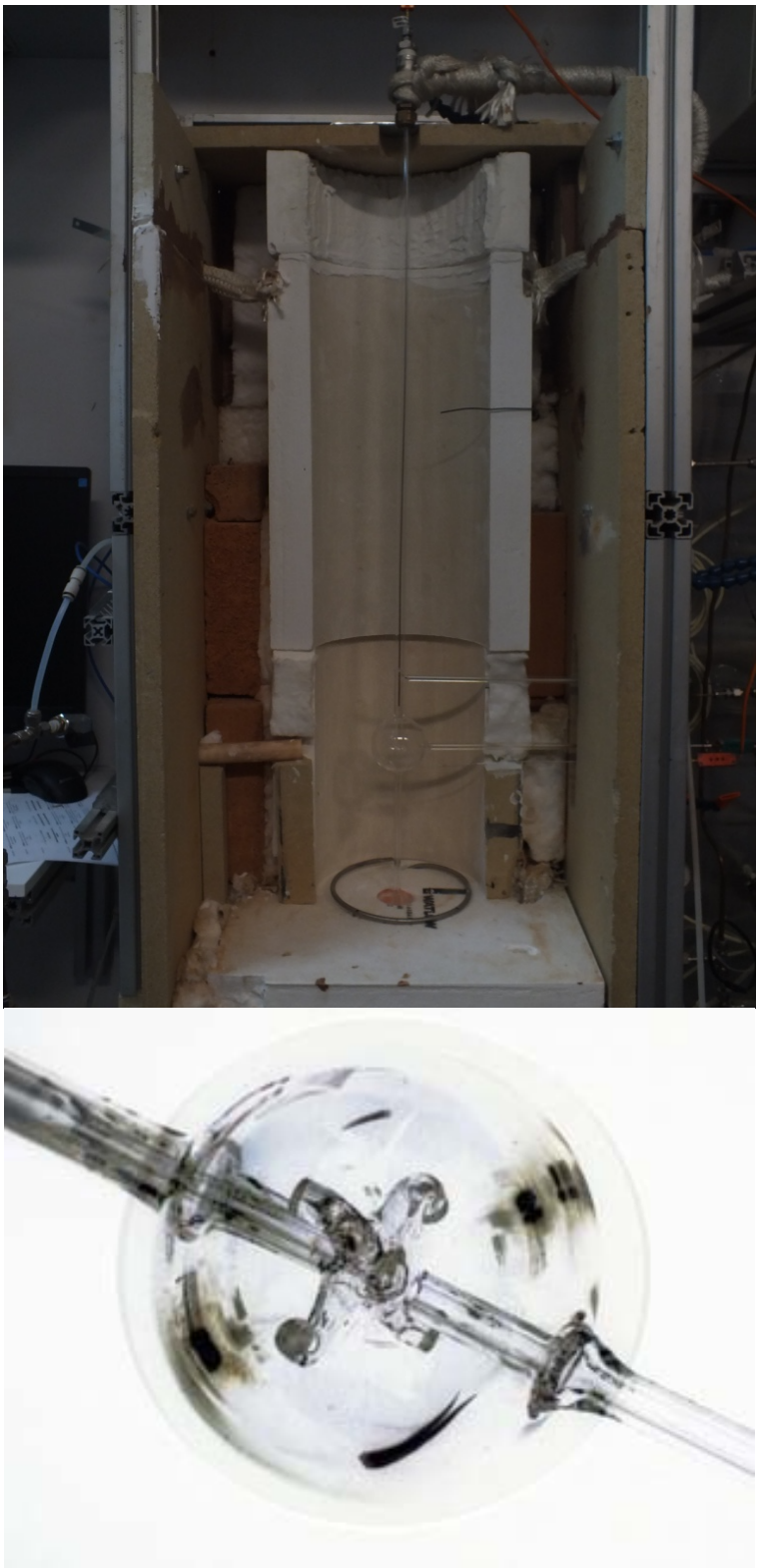

Fig. 3.6 – Picture of the JSFR used in Napoli (top) and the JSFR used in Nancy (down).

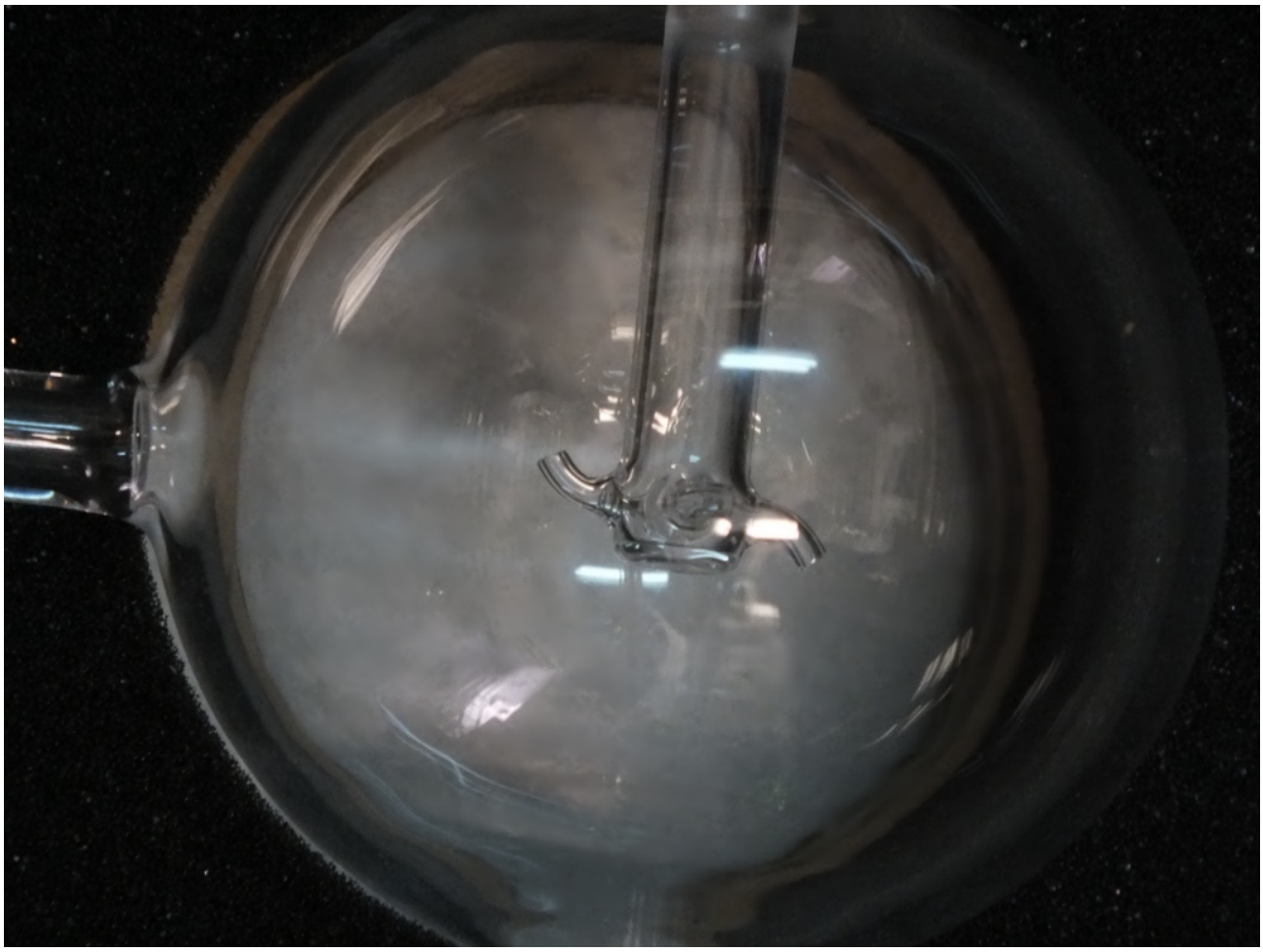

Fig. 3.7 – Detail of the injectors

The flow rates of gases from cylinders are measured and regulated by digital thermal mass flow controllers supplied by BronkHorst High-Tech with a high accuracy (± 0.5%). The controllers are connected to a PC and managed by sub-routines developed in Labview. The pressure is kept constant at 1.1 atm in the apparatus by means of a needle valve on the exhaust line.
Gases were provided with high purities: > 99.99% for nitrogen, oxygen, and helium, 99.5% for carbon dioxide, methane, and propane.
The water feeding system consisted of a stainless steel cylinder, which was pressurized with dry nitrogen in order to feed the distilled water through a calibrated liquid mass flow meter into a Controlled Evaporator Mixer (CEM) provided by BronkHorst High-Tech. It consisted of a control valve, a mixing device and a heat exchanger, the temperature of which is controlled by a temperature controller that is part of the system. The required flow rate is controlled to the set-point value by a control valve that forms an integral part of the CEM system. A carrier gas (nitrogen) controlled by a mass flow controller is used to stimulate the evaporation process as a mixing component, and furthermore to transport the vapour. The process is highly repeatable and efficient.
The temperature of all the components downstream the evaporator is controlled and set at the temperature needed to prevent water condensation (depending on the fed water concentration). This temperature is regulated with electrical coils. The flow system and all the temperatures were controlled automatically by a PC system that also was used for data acquisition.

Nancy JSFR
The reactor consists of a sphere of 85 cm^3 made in quartz to prevent catalytic reactions. The reactor was preceded by an annular preheating zone in which the temperature of the gases was increased up to the reaction temperature before entering inside the reactor. Both the spherical reactor and the

annular preheating zone were heated by Thermocoax heating resistances rolled up around their walls. The advantages of using heating wires are that there is very little thermal inertia and that it is possible to coil them directly around the different parts of the reactor and to heat the zones at different temperatures. Thus the preheating is divided in two zones to obtain progressive heating of the fresh gases before they enter the reactor. This preheating system allows reaching inlet temperatures up to 1250 K. The measure of the inlet temperature is performed by means of a thermocouple, which is slipped in the intra-annular part of the preheater with the extremity of the thermocouple located in the center of the sphere. Then the pre-mixed mixture enters the reactor through four nozzles of 0.3 mm diameter located at its center. The residence time used in the present experiments was fixed to 2 s and the gas mixture residence time inside the annular preheating was only a small percentage compared to the residence time inside the reactor. The pressure is kept constant at 1.05 atm by means of a needle valve on the exhaust line.
The combustion products were exhausted through a tube arranged in the center of the reactor (Fig. 3.6). Due to high heat losses produced by the wires heating system, the Nancy JSFR can be considered as isothermal, with temperature gradients in the reactor below 5 K. From the point of view of chemical analysis, data derived from isothermal reactors under highly diluted conditions are relevant. The significance is that only small or negligible extents of self-heating accompany the exothermic oxidation and thus the temperature at which chemical analyses are made is very well defined. Furthermore, low gradients of transported properties inside the reactor allow focusing only on chemical kinetics.
The flow rates of gases are measured and regulated by digital thermal mass flow controllers supplied by BronkHorst High-Tech with a high accuracy (± 0.5%).
The n-pentane feeding system consisted of a stainless steel cylinder, which was pressurized with dry helium in order to feed the fuel through a coriolis flow controller into a CEM system provided by BronkHorst High-Tech, with the same specifications of that described above. The fuel was provided with a purity > 99%. A CG analysis of the fuel revealed a composition of 99.3% n-pentane, 0.6% 2-methylbutane, and 0.04% cyclopentane.
The temperature of all the components downstream the evaporator is controlled and set at the temperature needed to prevent fuel condensation (depending on the fed fuel concentration). This temperature is regulated with electrical coils.

3.3.2 Measurement methodology

Napoli
To provide a detailed chemical analysis, the outlet stable species were analysed by gas chromatography. A period of time (about 5 min) was allowed to stabilize the flow after the fuel injection and before the chemical analyses. The exit gases were cooled down efficiently by means of a heat exchanger installed at the reactor outlet to quench the oxidation reactions in the sampling line. Then, gases passed through a silica gel trap to eliminate the moisture content before gas analyses. Therefore all the results in the next chapter, obtained with the Napoli JSFR, will be reported on a dry basis. The outlet was connected to two gas chromatographs that were used for the quantification of different species. The former (Agilent 3000) was equipped with two specific capillary columns: a column Plot U to detect online carbon dioxide, ethylene, ethane and acetylene and a column Molsieve 5A equipped with a pre-column Plot U to separate hydrogen, nitrogen, oxygen, methane and carbon monoxide. Species concentrations were quantified by means of a Thermal Conductivity Detector (TCD). The latter (Agilent 7820 A) was equipped with a Caboxen 1010 Plot capillary column and two different detectors, a TCD and a Flame Ionization Detector (FID). It allowed to measure carbon monoxide, carbon dioxide, methane, acetylene, ethylene, ethane, methyl acetylene, propylene and propane. Stable species were identified by the determination of their individual retention times and calibrations were made directly using cold-gas mixtures. Maximum relative errors in mole fractions are estimated to be ± 10% when the

concentrations approach the detection threshold, which is about 1 ppm for species analysed using FID and 100 ppm for species analysed using the TCD. The O_2 concentration was also analysed by means of a continuous O_2 analyser equipped with electrochemical cells that measured the O_2 concentration from 0.05 ppm up to 100%, with an uncertainty of ± 1%. O_2 molar fractions detected by the GC and by the oxygen analyser have shown no significant differences.
It should be stated that, in the case of mixture diluted in water vapour, since water is condensed prior to analysis, the measured concentrations are higher than the real ones. Therefore, in order to compare the results obtained in the case of mixtures diluted in water with the other cases (in which, in turn, concentrations are reported on a dry basis), the species concentrations are recalculated on the basis of the nitrogen concentration, in the following way:

$$X_{real}^{species} = \frac{X_{measured}^{species}}{100 + \left(X_{measured}^{N_2} \left(\frac{X_{in}^{H_2O}}{X_{in}^{N_2}} \right) \right)}$$

where the subscripts "in", "measured" and "real" refer to the molar fractions fed, measured and calculated, while the superscript "species" refers to any measured species. Then, the term in brackets at the denominator is the condensed water, without however taking into account the water produced by the reaction, which is also condensed using the other diluents. This allows comparing the results obtained with different diluents, but adds a higher uncertainty in the data relating to H_2O-diluted mixtures due to the uncertainty of the measured nitrogen concentration.
Experiments were performed at least twice under all test conditions to ensure measurement reproducibility. In particular the measured concentrations were the result of measurements obtained in different days, with different sequences of measurements. The test repeatability was excellent under all conditions with differences among the various tests well within the reported experimental uncertainties. The mean value for each measurement was calculated and evaluated by variance analysis.
In such a system, it is also possible to realize and study stabilized oscillatory oxidation regimes under definite conditions of T_{in} and mixture composition.
To detect and follow accurately the temperature changes during gaseous reactions, the measuring device must have a fast response, a very small thermal capacity, low thermal conductivity, adequate sensitivity, and it must be of robust construction. Our homemade type R unshielded thermocouple gas welded from a very fine Pt-Pt 13% Rh wire (40 μm bead size) comes close to satisfying these criteria. Its response time was less than 20 ms in moving gas and so it was able to give faithful record of all behaviour, with a precision of ± 2 K. Each joint of the thermocouple was housed in thin-wall double-core covers made from pure Al_2O_3 in order to prevent catalytic reactions on the platinum wire. The temperature was acquired on a high-speed multi-channel module National Instruments.

Nancy
Also in this case, the online sampling consisted in sending the gas exiting from the reactor directly through the loop of the injection valve of a gas chromatograph. However, since in these experiments also the products that are liquid under standard conditions were measured, the tube used for connecting the outlet of the reactor to the injection system was heated to avoid condensation of some species and it was used a tube with inert wall in order to avoid adsorption phenomena and reactions at the wall of these species. The temperature of the transfer line was set at 200°C, sufficiently low to avoid thermal reaction in the line and high enough to keep all the reaction products in the gas phase. Two gas chromatographs were used for the quantification of the different species. The first chromatograph, equipped with a Carbosphere-packed column and a TCD was used for the quantification of O_2, CO, CO_2, and CH_4. The second one was fitted with a PlotQ

capillary column and a FID, preceded by a methanizer. It was used for the quantification of molecules from methane to reaction products with up to 5 carbon atoms and 1 or 2 oxygen atoms maximum. The methanizer converted species like CO and CO_2 to methane, and then they were detected by FID, which is more sensitive (by a factor of 100) than TCD. Stable species were identified by the determination of their individual retention times and calibrations were made directly using cold-gas mixtures. For species for which a direct calibration procedure was not applicable the calibration factors were estimated using the effective carbon number method. Maximum relative errors in mole fractions are estimated to ± 10%, with the exception of formaldehyde, for which the error can be higher due to a larger peak. The limit of detection for species is about 1 ppm for species analysed using FID and 100 ppm for species analysed using TCD.

3.4 Computational approach

3.4.1 Chemical Kinetics Solvers: potentialities and limitations

It is evident that realistic computational simulation of combustion phenomena must necessarily require equally realistic input of the laws governing fluid flows and chemistry, as well as realistic characterization of the physical and chemical properties of the gas mixtures involved.
In recent years the importance of chemical kinetics in reacting flows, beyond the simplistic descriptions assuming either equilibrium chemistry or one-step overall reaction, has been recognized, and there has been increasing effort to incorporate more complex reaction mechanisms in simulation studies (Lu & Law 2009).
Simulation of the chemical reactions that release heat and drive the combustion flows is frequently the most computationally demanding part of a full combustion model. In the most common formulation, a time-dependent differential equation is written for the concentration or mole fraction of each chemical species in the system being studied. These coupled equations frequently have widely disparate characteristic time scales, referred to as “stiffness”, and common techniques for their solution are, in general, ineffective. It is no coincidence that kinetic modelling suddenly moved forward once the stiff equation solvers were available. This is one of the sudden advances in capabilities that had enormous impact on computational combustion (Westbrook et al. 2005). This in turn has led to the development of reaction mechanisms at various levels of detail and comprehensiveness.
A key event in combustion modelling was the development of the kinetic mechanism for natural gas oxidation, GRI-Mech. Specifically designed to describe methane and ethane combustion, and limited to high temperature phenomena including particularly flame propagation and shock tube ignition. An essential feature of this mechanism, which is presented in a format compatible to Chemkin codes, was that it was freely available to anyone and that the developer has tested the mechanism more thoroughly than any other mechanism in combustion history (Westbrook et al. 2005). It has since become very widely used and is now a standard for research community (Westbrook et al. 2005). Of course, this mechanism has suffered, like others by usage under conditions where it has not been tested and was never intended to be used, such as very high pressures or temperatures below about 1000 K.
As a matter of fact, while such a development is welcomed, there is the concern that many mechanisms have been developed with severely restricted applicability (in terms of temperature, pressure and mixture composition), and there is also considerable casualness in the selection of mechanisms for simulation. It is evident that the use of inappropriate or inadequate mechanisms could yield inaccurate or even erroneous results that, if adopted indiscriminately, could subsequently generate a ripple effect of efforts of futility and error (Lu & Law 2009).
Therefore, after that we have said in the previous chapters about SECs combustion, the development of detailed mechanisms that are comprehensive is without a question an important and challenging component in the simulation of chemically reacting flows. It is important because the

fidelity of all subsequent steps of mechanism reduction depends on the fidelity of the detailed mechanism. In terms of combustion phenomena, comprehensiveness would require considerations of homogeneous and diffusive ignition, which cover low-, intermediate-, and high-temperature chemistry; steady burning and extinction, which cover high-temperature chemistry; and premixed and non-premixed flames, which cover the relative concentrations of fuel and oxidizer. The global combustion parameters of interest include the system parameters of pressure, equivalence ratio, and reactant concentrations; or the global responses such as ignition delay times, chemical species concentrations, laminar flame speeds, extinction strain rates, etc.
Detailed chemical kinetics models are composed of individual reaction steps. Each reaction step has a prescribed rate law, which is characterized by a set of parameters. Such parameters were primarily based on experimentation with homogeneous systems such as STs. However, recently there has been increasing reliance on quantum mechanical calculations. If these parameters were known or could be known exactly, without any uncertainties, then the construction of a reaction model would entail selecting all pertinent reactions and evaluating their individual roles through such techniques as reaction-path and sensitivity analyses. Unfortunately, whether the rate parameters are determined experimentally or computed theoretically they always have a measurable level of uncertainty, and the process of reaching conclusions on the adequacy of the reaction mechanism is thus coupled to parameter identification (Frenklach 2007).
Recently, there has been increasing use of optimization using experimental flame parameters such as laminar flame speeds and extinction strain rates as targets. It is clear that when experimental flame parameters are used in the optimization, the data should be free from spurious experimental effects. Furthermore, any proposed detailed mechanism must be validated for comprehensiveness or restricted comprehensiveness against data from well-controlled experiments.
However, in the past, Griffiths (1995) pointed out that it is desirable for the experimentalist to provide information under well-defined conditions as possible. In addition to chemical information or physicochemical data, such as ignition delays, aspects of the experimental system itself may have to be quantified. For example, most experimental systems are non-adiabatic. Thus, heat-loss rates from the system must be characterized in some way. Thus the experimentalist and the modeller must come to an accord as to what constitutes a satisfactory "validation" of a model based on the available information. For example, oscillatory cool flames only occur in non-adiabatic reaction systems. Thus their successful modelling relies not only on a quantitative understanding of the underlying kinetics and exothermicity, but also on the heat loss rates from the reactor.

3.4.2 Smart Energy Carriers chemical kinetics mechanisms evaluation and selection

In this work, twelve detailed kinetic mechanisms, which have been validated for a wide range of conditions, were initially tested to check their validity against experimental data obtained in this work. All-important simple hydrocarbons reaction mechanisms published in the last decade were considered.
The characteristics of each mechanism are summarized in Table 3.1. A mechanism identifier is used, which combines the name of the first author or the research group, and the year of publication. Also the size of the mechanism is reported along with the corresponding reference. The GRI_3.0-1999 is commonly used for modelling the combustion of methane and natural gas. All the other mechanisms are more recent and can also be used to simulate the combustion of C_3 species.
These kinetic models are continually being refined. In particular several detailed kinetic sub-mechanisms of hydrogen combustion have been developed recently. These efforts were motivated by the substantial progress made in accurate measurement of the elementary reaction rates and thermodynamic properties as well as in measurement of the integral combustion characteristics such as burning velocities, ignition delays, and product formation during slow oxidation (Konnov 2008). Therefore, multiple mechanisms from the same research group were tested, but only if the older

mechanism is conceptually different from the newer one. Otherwise, only the latest mechanism was considered. The thermochemical data were used as published online and/or provided by the authors directly.

Kinetic mechanism	Species	Reactions	Reference
AramcoMech_1.3-2013	253	1542	Metcalfe et al. 2013
AramcoMech_2.0-2016	493	2716	Zhou et al. 2016
Dagaut-2010	99	743	Le Cong et al. 2010
Konnov_0.6-2009	127	1207	Konnov 2009
LLNL-2004	155	689	Marinov et al. 1998
Merchant-2015	110	631	Merchant et al. 2015
NUIGalway-2010	293	1593	Healy et al. 2010
CRECK-2012	82	1485	Ranzi et al. 2012
CRECK-2014	107	2642	Ranzi et al. 2014
USC_2.0-2007	111	784	Wang et al. 2007
Zhukov-2005	209	1260	Zhukov et al. 2005
GRI_3.0-1999	54	325	Smith et al. 1999

Table 3.1 Detailed kinetic schemes used in simulations.

Comparing model predictions to experimental observations would then assess discrimination among several models. Comparison of kinetic mechanisms often served to prove that one or another model is the best in predicting new experimental data. An extensive comparison of the hydrogen combustion mechanisms has been performed by Olm et al. (2014), mostly to illustrate that under some experimental conditions they give very close results, while under others the difference is notable.

The simulations were then extended using a kinetic mechanism to highlight crucial aspects of auto-ignition and oxidation as a function of the temperature for mixtures with different dilution levels and compositions.

Numerical simulations of the evolution of the fuels oxidation process under diluted and highly preheated conditions in the TFR were carried out using the PLUG code of ChemKin PRO (Reaction Design 2013) and OpenSMOKE++ (Cuoci et al. 2015). Flow reactors are not completely adiabatic, and heat losses may significantly complicate modelling, especially under diluted conditions. The reactor overall heat transfer coefficient was calculated using the thermal resistances in series concept on the basis of system boundary conditions, namely the oven temperature, in which the TFR is inserted to minimize heat exchange to the surroundings, and the inlet flow temperature and velocity, considering a non reactive case. Heat transfer coefficient was calculated by means of empirical correlations for flow in ducts (Kreith & Bohn 2001). The calculated value is 2.4×10^{-3} cal/cm^2 s K.

Furthermore, several simulations were performed over a wide range of values for the global heat exchange coefficient. No significant variations of the ignition delay time were identified for the temperatures considered in the experimental tests (but significant variations can be found respect to the adiabatic case).

The experimental results obtained in the JSFR were simulated using the AURORA code of the Chemkin PRO package (Reaction Design 2013) and the PSR code of the OpenSMOKE++ software (Cuoci et al. 2015). It is an ideal model, where reactants can be mixed perfectly before reactions take place. It predicts the time-dependent and the steady-state properties (only in Chemkin) of an open well-mixed reactor. This zero dimensional model also allows for heat loss from the reactor. Specifications of the reactor were the same as those of the experimental apparatuses, i.e., a volume of 113 cm^3 and an internal surface area of 113 cm^2 for the Napoli reactor. The wall of the reactor is assumed to be infinitely thin, and there is no temperature gradient in the wall. The linear heat convection equation was used, with constant coefficient, to calculate the heat loss term in the gas

energy equation. The wall temperature was set to the same temperature as the inlet. A heat loss occurs only with a temperature increase caused by chemical reactions. There is no additional heat flux from the wall.
The reactor overall heat transfer coefficient in the JSFR was calculated by means of empirical correlations. It was fixed at 1.3×10^{-3} cal/cm^2 s K.
Also in this case several simulations were performed over a wide range of values for the global heat exchange coefficient and no significant variations of the chemical species concentrations were identified for the temperatures considered in the experimental tests (but significant variations can be found respect to the adiabatic case).
In order to simulate the Nancy experiments, simulations were carried out under isothermal conditions, given the characteristics of the reactor.
In addition, the experiments were also simulated in non-isothermal conditions with a high heat exchange coefficient and no differences were found compared with the isothermal case.

CHAPTER 4 – RESULTS

A large set of experimental data related to the combustion of SECs is presented in this chapter. All the inlet operative conditions experimentally explored in the work are related to advanced combustion technologies. In fact, reactants were highly diluted, while inlet temperatures were higher than the nominal auto-ignition temperature. The fuel mixtures used are those presented in Table 2.1.
The experiments were carried out from lean to rich mixtures, in a wide range of inlet temperatures, at atmospheric pressure. The data include 1449 ignition measurements in the PFR and 771 measurements in the JSFR.
The experimental conditions will be presented from time to time for each dataset. Furthermore, all the experimental conditions together with the data collected for each dataset were stored in tables in the Appendix. The stored data provide all the information required for the simulation of experiments, i.e. T_{in}, dilution (d), mixture equivalence ratio (Φ), reactants molar fraction, residence time, and pressure.
In particular, d is the overall percentage molar fraction of the diluent species in the mixture and Φ is defined as:

$$\Phi = \frac{C/O}{C/O_{stoichiometric}}$$

where in this expression C/O indicates the ratio between the molar fraction of carbon atoms in fuel and the molar fraction of oxygen atoms in the oxidant flow, taking into account only the O_2 species, whereas $C/O_{stroichiometric}$ represents the stoichiometric carbon to oxygen ratio. When CO_2 and/or H_2O are present in the reactant mixture, given the definition of C/O, carbon atoms in the CO_2 and oxygen atoms in the CO_2 or H_2O are not included in the C/O ratio calculation.
This section of the thesis begins with the presentation of the results obtained in the PFR, followed by the JSFR results.

4.1 PFR Results

Results are presented for each of the fuels studied to show the effect of temperature, equivalence ratio, dilution, and diluent on ignition delay time.

Characteristic temperature profiles
The evaluation of system behaviour was carried out on the systematic analysis of axial temperature profiles as a function of inlet parameters (inlet pre-heating temperatures, mixture compositions and dilution levels). Fundamental information on chemical evolution of the system came from the analysis of the shapes and trends of the axial temperature profiles measured in the different experimental conditions. More specifically, several main typologies of temperature profiles were recognized and associated to characteristic system behaviours. The temperature profiles reported in Fig. 4.1 are exemplifications of the several reaction modes experimentally detected. In particular Fig. 4.1 reports the temperature increase ($\Delta T = T - T_{in}$) measured in the reactor as a function of the axial coordinate (x) in cm.
The first (starting from the bottom of Fig. 4.1) profile showed no temperature increase and temperature remained equal to the inlet isothermal condition over time. In this case no combustion process takes place. Such a profile identifies the “no combustion” regime.
The second profile is relative to a “pyrolysis” condition. In such a case, the recorded ΔT values were lower than the isothermal inlet profiles, suggesting that endothermic/pyrolytic reactions occurred.

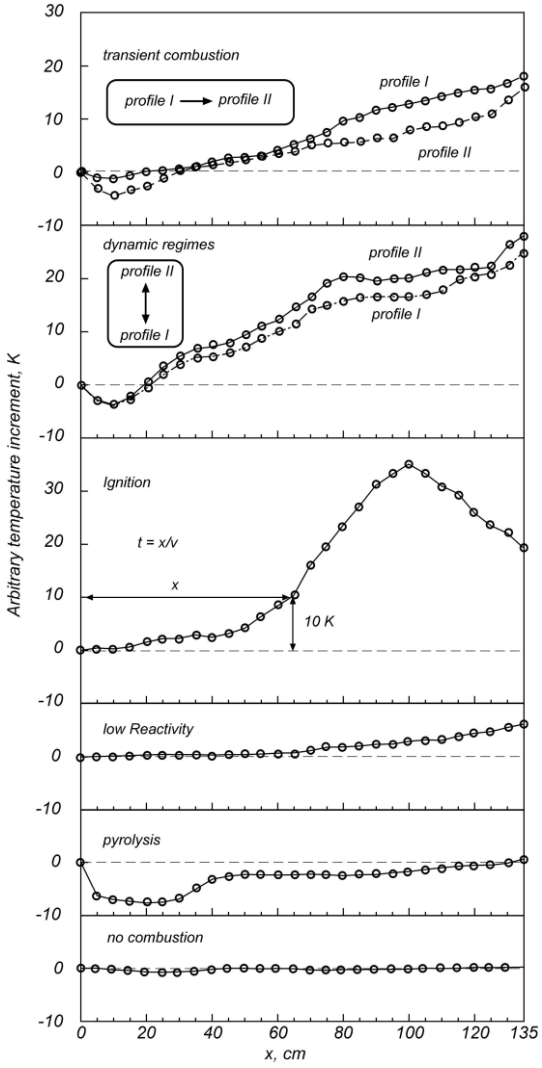

Fig. 4.1 Characteristic axial temperature profiles and combustion regimes (the temperature profiles have been reported on an arbitrary scale to identify the characteristic behaviours).

The third profile refers to a condition where the reactivity of the system is slow and the temperature increase along the reactor axis was lower than 10 K. Thus, in such a condition, the ignition criterion was not satisfied even though a certain amount of fuel was converted. Such behaviour was associated to a "low reactivity" condition. It should be stated that in the latter case, as well as in the previous pyrolytic condition, the occurrence of mixture reactivity was verified through gas chromatographic analyses. In particular, in the "pyrolysis" and "low reactivity" regimes, the presence of intermediate species was identified at the outlet of the reactor, whereas in the "no combustion" condition the composition of the outlet gas was found to be exactly the same of the fed mixture.

The fourth temperature profile shows that ΔT was almost constant up to a certain x value and then it sharply increased reaching a maximum value, followed by a decrease because of the heat exchange to the surroundings. This profile corresponds to an "ignition" condition and allowed for the evaluation of the ignition delay time. The ignition criterion is also shown in the inset.

The fifth profile shows two temperature profiles for the same initial condition. They are representative of the two measured states of the system that, downstream a steady ignition point, periodically switched from one to the other (with frequency of about 1 Hz). These profiles were generally associated to a "dynamic" regime. These fluctuations are not attributed to irregularities in velocity, temperature, or fuel concentration. The "dynamic" regime was identified when only two unique temperature profiles were recorded for the same inlet conditions downstream of a steady ignition point. In this case, two different ignition delay times were reported for the same inlet

condition on the basis of the two temperature profiles. Similarly to the cool flames, they were characterized by a faint luminosity and relatively low temperature rise.
Two temperature profiles for the same inlet condition are reported also in the sixth frame. The mixture ignited temporarily leading to the working condition identified with profile I. Afterwards, the temperature profile spontaneously shifted to a second and final state II. Such a case is referred as "transient combustion". Profiles relative to condition I, always showed a $\Delta T > 10$ K, whilst profiles related to condition II could reach a temperature increase lower or higher than 10 K. When both the first and the second temperature profiles reached $\Delta T > 10$ K, two different auto-ignition times were obtained on the basis of the temperature profiles I and II, respectively.

4.1.1 Propane mixtures

PFR experiments for propane mixtures have been realized for different operating conditions. The parameters examined here are 1) the inlet temperature (T_{in}), 2) the mixture equivalence ratio (Φ), 3) the percentage of diluent in the reactive mixture (d) and 4) the diluent type (N_2, CO_2, H_2O). All experiments are conducted for a constant pressure (P = 1 atm).
The experimental tests have been carried out with C/O ratios from 0.025 (Φ = 0.083) to 1 (Φ = 3.33), T_{in} from 850 to 1250 K and dilution from 90% to 97%.
The experimental conditions are summarized in Table 4.1. Furthermore, the measured ignition delay times, along with all the operative conditions in which experiments with propane mixtures in the PFR have been carried on, are listed in the Appendix.
All results that will be presented in this section, obtained with propane mixtures in the PFR, have been published in the following journal papers:

1) Sabia, P, de Joannon, M, Lubrano Lavadera, M, Giudicianni, P & Ragucci, R 2014, "Autoignition delay times of propane mixtures under MILD conditions at atmospheric pressure", *Combustion and Flame*, vol. 161, pp. 3022-3030.
2) Sabia, P, Lubrano Lavadera, M, Giudicianni, P, Sorrentino, G, Ragucci, R & de Joannon, M 2015, "CO_2 and H_2O effect on propane auto-ignition delay times under mild combustion operative conditions", *Combustion and Flame*, vol. 162, pp. 533-543.

However, in this work, these results will be presented depending on the effect of the individual investigated parameters.

d (%)	Φ	C_3H_8 (vol%)	O_2 (vol%)	N_2 (vol%)	CO_2 (vol%)	H_2O (vol%)	Number of experiments
90	0.083	0.16	9.84	90	0	0	1
90	0.092	0.18	9.82	90	0	0	2
90	0.1	0.20	9.80	90	0	0	20
90	0.11	0.21	9.79	90	0	0	1
90	0.12	0.23	9.77	90	0	0	33
90	0.12	0.23	9.77	0	90	0	21
90	0.12	0.23	9.77	0	0	90	9
90	0.13	0.26	9.74	0	90	0	6
90	0.13	0.26	9.74	0	0	90	3
90	0.17	0.32	9.68	90	0	0	35
90	0.17	0.32	9.68	0	90	0	29
90	0.17	0.32	9.68	0	0	90	14
90	0.25	0.48	9.52	90	0	0	37
90	0.25	0.48	9.52	0	90	0	26
90	0.25	0.48	9.52	0	0	90	14
90	0.33	0.62	9.38	90	0	0	45
90	0.33	0.62	9.38	0	90	0	27

90	0.33	0.62	9.38	0	0	90	14
90	0.4	0.74	9.26	90	0	0	5
90	0.43	0.80	9.20	90	0	0	4
90	0.5	0.91	9.09	90	0	0	48
90	0.5	0.91	9.09	0	90	0	5
90	0.67	1.18	8.82	90	0	0	55
90	0.67	1.18	8.82	0	90	0	24
90	0.67	1.18	8.82	0	0	90	14
90	0.83	1.43	8.57	90	0	0	34
90	1	1.67	8.33	90	0	0	53
90	1	1.67	8.33	0	90	0	23
90	1	1.67	8.33	0	0	90	14
90	1.17	1.89	8.11	90	0	0	1
90	1.25	2	8	90	0	0	1
90	1.33	2.11	7.89	90	0	0	39
90	1.33	2.11	7.89	0	90	0	22
90	1.33	2.11	7.89	0	0	90	14
90	1.67	2.5	7.5	90	0	0	11
90	1.67	2.5	7.5	0	90	0	3
90	2	2.86	7.14	90	0	0	21
90	2	2.86	7.14	0	90	0	17
90	2	2.86	7.14	0	0	90	14
90	2.67	3.48	6.52	90	0	0	20
90	2.67	3.48	6.52	0	90	0	14
90	2.67	3.48	6.52	0	0	90	14
90	3.33	4	6	90	0	0	24
90	3.33	4	6	0	90	0	14
90	3.33	4	6	0	0	90	3
95	0.2	0.19	4.81	95	0	0	1
95	0.25	0.24	4.76	95	0	0	6
95	0.27	0.25	4.75	95	0	0	2
95	0.27	0.25	4.75	0	95	0	1
95	0.33	0.31	4.69	95	0	0	9
95	0.33	0.31	4.69	0	95	0	4
95	0.5	0.45	4.55	95	0	0	3
95	0.5	0.45	4.55	0	95	0	1
95	0.67	0.59	4.41	95	0	0	9
95	0.67	0.59	4.41	0	95	0	4
95	0.83	0.71	4.29	95	0	0	2
95	1	0.83	4.17	95	0	0	9
95	1	0.83	4.17	0	95	0	3
95	1.33	1.05	3.95	95	0	0	7
95	1.33	1.05	3.95	0	95	0	2
95	1.67	1.25	3.75	95	0	0	1
95	1.67	1.25	3.75	0	95	0	1
95	2	1.43	3.57	95	0	0	5
95	2	1.43	3.57	0	95	0	1
95	2.67	1.74	3.26	95	0	0	4
95	2.67	1.74	3.26	0	95	0	1

95	3.33	2	3	95	0	0	4
95	3.33	2	3	0	95	0	1
97	0.5	0.27	2.73	97	0	0	2
97	0.5	0.27	2.73	0	97	0	2
97	0.67	0.35	2.65	97	0	0	3
97	0.67	0.35	2.65	0	97	0	2
97	0.83	0.43	2.57	97	0	0	2
97	1	0.5	2.5	97	0	0	2
97	1	0.5	2.5	0	97	0	2
97	1.33	0.63	2.37	97	0	0	2
97	1.33	0.63	2.37	0	97	0	2
97	2	0.86	2.14	0	97	0	1

Table 4.1 – Experimental conditions studied in the TFR for propane mixtures. P = 1 atm, 850 K < T_{in} < 1250 K, 0.021 s < τ < 0.048 s.

Influence of temperature

In order to show the influence of temperature on the propane ignition delay times, the stoichiometric mixture diluted in N_2 is used as reference case, followed by a comparison between the results of this study and those of previous workers.

A common approach is to use a simple global reaction rate of the form: fuel + air → products, to describe rates of autoignition (Burcat et al. 1971; Horning 2001). Reaction rates (RR) typically obey the Arrhenius rate form:

$$RR = K\,[fuel]^m[oxidizer]^n$$

where K is the rate constant which is function of an activation energy and temperature:

$$K = A \exp(-E/RT)$$

where A is the pre-exponential factor, R is the universal gas constant, E is the activation energy of the overall process. Since the ignition delay time is inversely proportional to the reaction rate, plots of ignition delay data of the form (log t) vs. (1/T) will yield a straight line whose slope is proportional to the activation energy and the intercept of the line with the ordinate axis can be used to determine the pre-exponential factor. The main advantage of this method is its simplicity and that it works successfully for a determined fuel at a given range of pressure and temperature, in which A, n, m, and E parameters are obtained with the ignition delay expression. However, a deviation from a straight line may be observed when a change in the dominant elementary reactions occurs from one temperature to another. This especially concerns the low temperatures oxidation chemistry, which has a very complicated network of temperature and pressure dependent reaction pathways, as discussed in the chapter 2. For those reactions this method does not consider the slow pre-reactions, which produce the cool flames, nor the two-step ignition and the NTC of some fuels.

Figure 4.2 compares the present results with those reported in the literature, obtained for propane mixtures with various experimental configurations and operating conditions (temperature, pressure, equivalence ratio), summarized in Table 4.2. In particular, Fig. 4.2 (top) shows the ignition delay data divided by the concentration of propane and oxygen to the power of the exponents given in the ignition correlation of Burcat et al. (1971), which is the same correlation used in Fig. 3.5, proposed for high temperature propane ignition delay times. On the other hand, Fig. 4.2 (down) shows the same ignition delay data divided by the concentration of propane and oxygen to their exponent from the correlation of Schönborn et al. (2013), which has been proposed in order to compare low temperature propane ignition delay data.

Authors	Facility	P, atm	T, K	Diluent	$X_{Diluent}$	Φ
Holton et al. (2010)	TFR	1	960-1135	N_2	0.76	1
Brokaw & Jackson (1955)	TFR	1	810-1025	N_2	0.76	1
Chang et al. (1958)	TFR	1	1000-1120	N_2	0.76	1
Freeman & Lefebvre (1984)	TFR	1	955-1050	N_2	0.76	1
Lezberg (1957)	TFR	1	1030-1100	N_2	0.76	1
Basevich et al. (2006)	TFR	2	900-980	N_2	0.76	1
Beerer & McDonell (2011)	TFR	9	820-860	N_2	0.76	1
Cowell & Lefebvre (1986)	TFR	10	830-980	N_2	0.76	1
Herzler et al. (2004)	ST	30	835-1300	N_2	0.77	0.5
Burcat et al. (1971)	ST	7	1150-1585	Ar	0.76	1
Penyazkov et al. (2005) (a)	ST	2	1220-1705	N_2	0.76	1
Penyazkov et al. (2005) (b)	ST	15	1020-1500	N_2	0.76	1
Cadman et al. (2000)	ST	5	845-1280	Ar	0.76	1
Gallagher et al. (2008)	RCM	30	705-955	N_2	0.76	1
Schönborn et al. (2013) (a)	TFR	5	860-900	N_2	0.78	0.2
Schönborn et al. (2013) (b)	TFR	5	825-880	N_2	0.78	0.4
Schönborn et al. (2013) (c)	TFR	5	810-875	N_2	0.77	0.6
Current work	TFR	1	995-1240	N_2	0.9	1

Table 4.2 – Literature propane auto-ignition studies from several facilities at different operating conditions.

The temperature that will be seen in practical advanced diluted combustion systems typically lies in the intermediate range, which is not considered in any correlation.

Although the figure does not show all available auto-ignition delay data on propane mixtures, it highlights the temperature dependence of various ignition delay times obtained in several experimental configurations under different operating conditions. The ignition delay times are relative to low diluted propane mixtures (between 76% and 78% of diluent), except the current data where the dilution is 90% in N_2, resembling MILD combustion conditions.

Figure 4.2 shows that both the correlation equations give ignition delay times extremely close to the present experimental data at high temperatures (above 1000 K) but a great deal of scatter can be seen at lower temperatures both within the same system, and between different systems.

In all ignition time experiments, the results show different dependences of ignition delay times on temperature. Auto-ignition delay data in a RCM facility (Gallagher et al. 2008) show the typical NTC behaviour of propane/air mixtures at low temperatures. At higher inlet temperatures, data are generally obtained in TFRs. Under such operating conditions data obtained in TFRs show a linear trend with T_{in}, except the data by Brokaw & Jackson (1955), Holton et al. (2010), and the current data. In such cases, the auto-ignition delay time curve shows two different slopes. However, it should be noted that for the Brokaw & Jackson (1955) experiments, ignition delay data are totally uncorrelated from all others, while in the case of Holton et al. (2010) only two points deviate from the clear Arrhenius behaviour. With regard to present experiments, the deviation from the Arrhenius trend seems to be much more pronounced. In particular, the current data showed that for $T_{in} < 1100$ K t is almost independent on T_{in}, whereas for $T_{in} > 1100$ K it diminishes linearly (on a log scale) with temperature. A similar behaviour was reported for the data obtained in shock tube facilities.

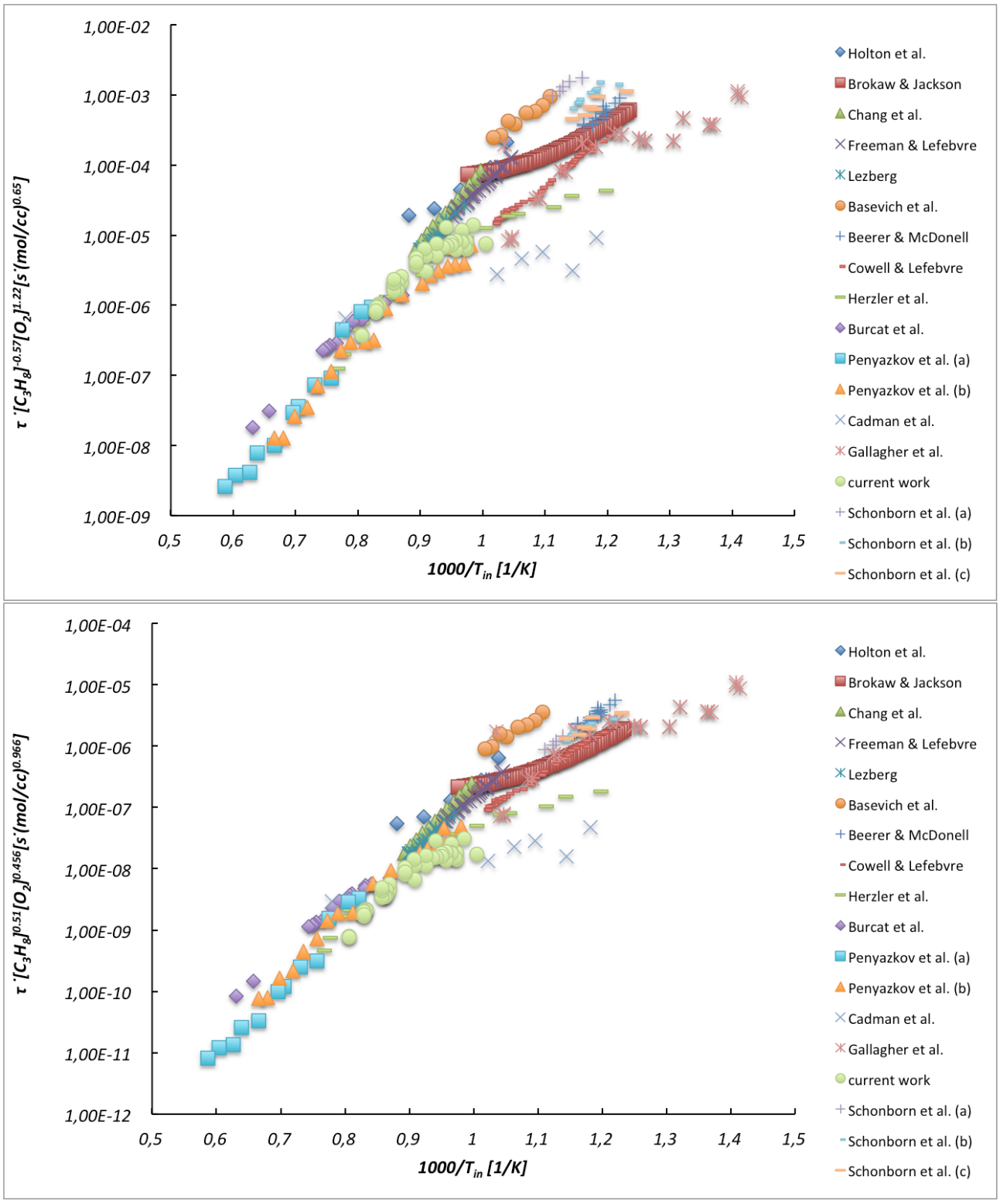

Fig. 4.2 – Comparison of literature data and current results using the correlation of Burcat et al. (1971) (top) and the correlation of Schönborn et al. (2013) (down).

It is interesting to note that the current atmospheric pressure data appear closer to the high-pressure data, rather than the other atmospheric pressure data. At the same time, it is also true that the current data are the only data obtained under highly diluted conditions. This result indicated that highly diluted mixtures are more prone to show a change in slope between low and higher temperatures than undiluted conditions at low pressures. These results supports the idea that mixture dilution

level also may play a role in the onset of different ignition regimes passing from low to intermediate and high temperatures along with the fact that high dilution and high pressure have similar effects on the chemical kinetics, as discussed in the chapter 2. Therefore, in order to understand the dilution effects on the SECs combustion kinetic characteristics, it is an advantage to perform the experiments at atmospheric pressure.
Additionally, experiments conducted outside the validation range will allow estimating the accuracies of the correlations when extrapolated out to new temperatures, pressures, equivalence ratios, and dilution levels. Indeed, significant errors might occur when low dilution data are extrapolated to higher dilution since dilution effects are still not well understood, even for conventional fuels. As a matter of fact, while the propane auto-ignition process has been widely characterized under "air" conditions, there have been no experimental studies under diluted conditions at atmospheric pressure.
Although it is to be expected that differences will arise in measurements from different laboratories due to facility-dependent perturbations, which are unpredictably present in reality and cannot be eliminated, any non-ideality cannot justify the scatter observed. Furthermore, Chaos & Dryer (2010) emphasized that the high sensitivity of induction chemistry to any type of experimental perturbations or nonidealities principally led to similarities in observations among the various experimental venues, instead of differences.
However, there has been an emerging concern about the interpretation of these shock tube data. Ignition delay measurements from various shock tube observations were noted to differ considerably from kinetic model predictions generated using homogeneous, zero-dimensional, isochoric modelling assumptions typically employed by kineticists. In considering these observations, Chaos & Dryer (2010) argued that disparities in observations and kinetic predictions were a result of the ideal modelling assumptions applied and their inability to represent experimental conditions appropriately. In the particular case of shock tube observations, the authors noted the multidimensional nature of the ignition event in the weak ignition regime where characteristic kinetic times are strongly influenced by induction chemistry involving HO_2 and H_2O_2 reactions, and they hypothesized a number of potential perturbing phenomena that would not be captured by modelling approaches that assume uniform, constant internal energy and volume conditions in the reflected sock gases. These revelations had significant impact on the arguments made with regard to kinetic model validation based upon shock tube data presently in the literature.
Consequently, Heufer et al. (2011) included in the simulation the pressure and temperature gradients assuming isentropic compression. In this case the simulation results show the same behaviour as the experiments, e.g. the ignition delay time data deviate from the Arrhenius behaviour for temperatures below 1000 K. Nevertheless, the ignition delay times predicted from simulation are longer than in experiment. This effect becomes more distinct for higher pressures. Therefore they conclude that the discrepancies between simulation and experiment at high pressures likely result from the reaction mechanism employed.
Anyway, the results obtained in the present work, as we will see, even though are similar to the ST results, are well predicted by some detailed kinetic models.
Therefore, while Fig. 4.2, along with Fig. 3.5 may imply that correlations developed for high temperatures and/or low dilution may be sufficient to describe the observed ignition delay times, at low temperatures and high dilution the ignition can not be described by a simple Arrhenius approach, due to a change in the controlling chemistry. Thus, the available prediction tools are highly localized and caution should be exercised in extending it for different conditions. A plausible alternative explanation of the observed behaviour could be a change in the chemistry of propane mixtures leading to the ignition process. These aspects will be analysed in detail in the next chapter.
For this reason, under non-conventional combustion conditions, detailed kinetic models become mandatory, and their reliability is crucial.
In the following a comparison of numerical and the same current experimental results is shown (Fig. 4.3).

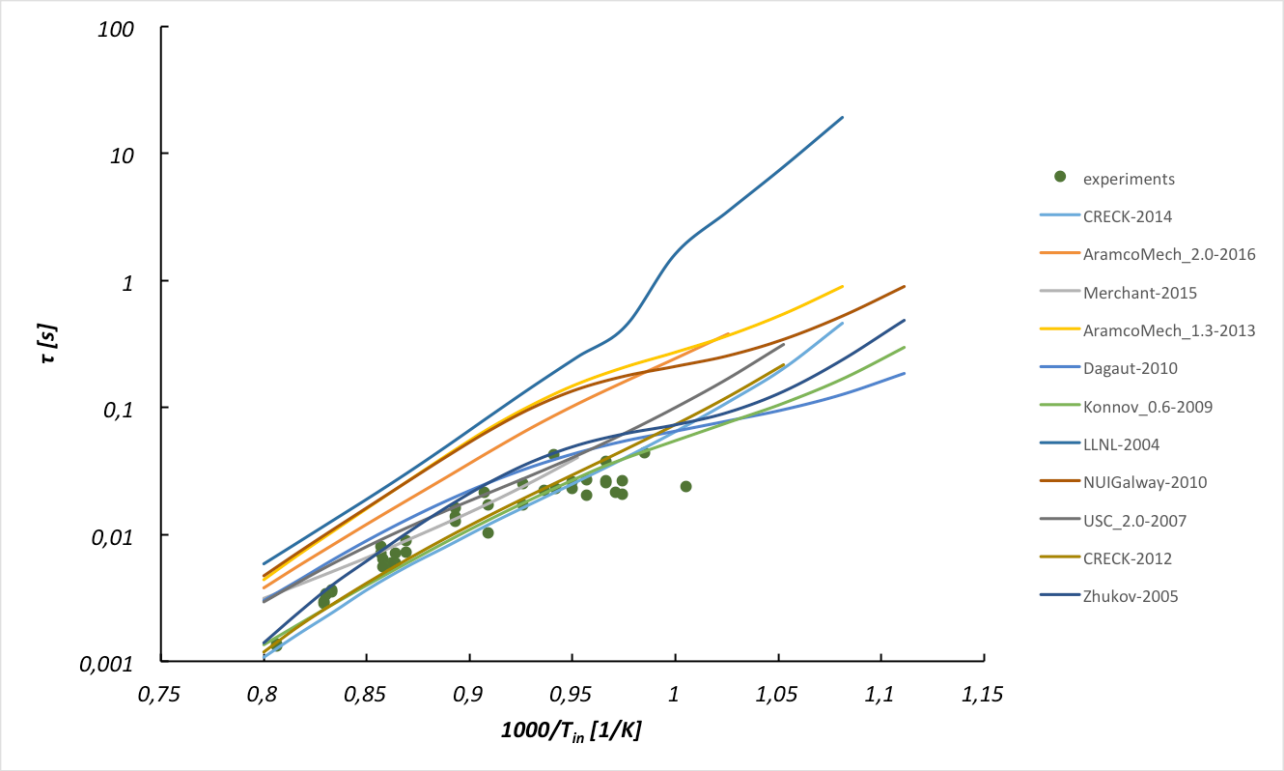

Fig. 4.3 – Comparison between experimental and numerical auto-ignition delay times for a stoichiometric C_3H_8/O_2 mixture diluted in N_2 to 90%.

Simulations were run using the PLUG application of the commercial software ChemKin PRO (Reaction Design 2013) and OpenSMOKE++ (Cuoci et al. 2015). All the detailed kinetic mechanisms listed in Table 3.1, except for the GRI_3.0-1999 (GRI_3.0 was not developed for the combustion of propane, but only natural gas) were evaluated for their ability to accurately predict the experimental data obtained in this work.

There is general confidence in the combustion community in the C_1-C_3 mechanisms and a perception among some that all C_1-C_3 models are essentially the same in terms of their prediction characteristics. One might conclude that in terms of combustion properties predictions, kinetic uncertainties are sufficiently small as to now be of little importance, though there has been a scarcity of high dilution data particularly at low flame temperature conditions. It is interesting to discuss the suitability of current models to address the high-dilution intermediate-temperature combustion in the conditions studied here.

Figure 4.3 shows comparisons between the present experimental results and numerical results using the kinetic mechanisms of Table 3.1. The ignition delay times are given in an Arrhenius diagram as a function of the inverse of the initial temperature T_{in} for a stoichiometric propane/oxygen mixture diluted in nitrogen ($X_{N2} = 0.9$).

First of all, it is possible to notice that the numerical ignition delay times, obtained with the different mechanisms, do not all start at the same T_{in}. There is always a minimum temperature below which ignition is not observed. The existence of a limiting temperature is an inevitability of the non-adiabaticity of the system and the manifestation is that an infinite ignition delay is approached asymptotically as the inlet temperature is decreased (Griffiths, 1995). It can be observed from Fig. 4.3 that this minimum temperature varies from model to model.

Then, the predicted ignition delay times differ substantially from model to model and with experimental data. Much larger disparities are apparent among model predictions themselves at lower temperatures, with variations of nearly two orders of magnitude at 950 K. It needs to be kept in mind that, for the LLNL-2004 and NUIGalway-2010, the validation conditions generally included high-pressure results. Therefore, quantitative agreement between experiment and

simulation cannot be expected with these two mechanisms. It appeared worthwhile, however, to examine the predictions with regard to potential differences of established models. Below 1100 K the experimental results deviate from the Arrhenius behaviour, which is not described by all the mechanisms. In particular, the LLNL-2004, AramcoMech_2.0-2016, Merchant-2015, and USC_2.0-2007 mechanisms cannot reproduce the change of the effective activation energy at temperatures below 1100 K. Results of the calculations using the other seven mechanisms are in good qualitative agreement with the experiments. However, although these seven mechanisms predict changes in the slope of the auto-ignition delay time curve in the Arrhenius diagram in the intermediate temperature range, the predicted auto-ignition delay times for each kinetic scheme differ over all temperature ranges considered up to one order of magnitude. In particular, among these seven mechanisms, while predictions of the Dagaut-2010, Konnov_0.6-2009, CRECK-2012, CRECK-2014, and Zhukov-2005 mechanisms are very close to the experiments, the AramcoMech_1.3-2013 and the NUIGalway-2010 mechanisms significantly overpredict ignition delays. The quality of the agreement of the mechanisms with the propane ignition experiments in highly diluted mixtures from 1100 K up to 1250 K is about the same. In particular, at temperatures above 1100 K, predictions of the Konnov_0.6-2009, CRECK-2012, and CRECK-2014 models are almost indistinguishable from each other and are also very close to the measurements. A slight difference is found with the Zhukov mechanism, yet is within the scattering of the measurements. However, predictive capabilities of these models toward lower temperatures are not the same.

It is interesting to note that the updated mechanism AramcoMech_2.0-2016 is worse than the previous version AramcoMech_1.3-2013 in predicting the present ignition data. In particular, the numerical ignition delay values predicted with the updated version are closer to the experimental ones, but the model does not predict the deviation from the Arrhenius behaviour in the intermediate temperature range. On the other hand, no appreciable difference can be observed between the results from the CRECK-2012 and the CRECK-2014 mechanism.

Note that the tested mechanisms do not contain the rate parameters recommended by Baulch et al. (2005). This shows that although the evaluated rate parameter values of Baulch et al. (2005) are widely used in the creation of combustion mechanisms, further tuning is needed for a good description of ignition delay times.

Given that the kinetic models investigated here were all validated against a wide range of (and frequently the same) data from numerous experimental apparatuses, the disparities noted amongst the predictions and with the present experimental results are noteworthy. A possible reason for the discrepancy has been discussed in the following chapter. Clearly, new experimental data are required to validate these models at intermediate temperatures between typical combustion and slow oxidation.

Furthermore, the performance of the mechanisms compared to ignition delay measurements was tested according to interval ranges of equivalence ratio, diluent concentration, and diluent type respectively (not shown here). In all the ignition delay related plots, LLNL-2004 mechanism can be identified as the worst performing one, while CRECK mechanisms give a slight better agreement with current experiments. This will be also shown later.

Therefore, the CRECK-2014 mechanism was chosen after the evaluation of its performance in predicting main features of the oxidation process under the investigated conditions and the next propane-related ignition data will be compared only with the simulations carried out using this kinetic model.

Influence of equivalence ratio

An overview of several regimes that can be established in the ranges considered is provided by the analyses of axial temperature profiles collected at different inlet pre-heating temperatures, mixture compositions and dilution levels. Typical temperature profiles and the identification of combustion regimes were summarized in Fig. 4.1.

Based on these classifications, a behaviour map in a C/O-T_{in} plane was drawn up and is shown in Fig. 4.4 for an N_2 dilution of 90%. In particular, the map focuses on a temperature range between 850 K and 1150 K and C/O ratios from 0.025 (Φ = 0.083) to 1 (Φ = 3.33) for a 30 m/s inlet flow velocity.

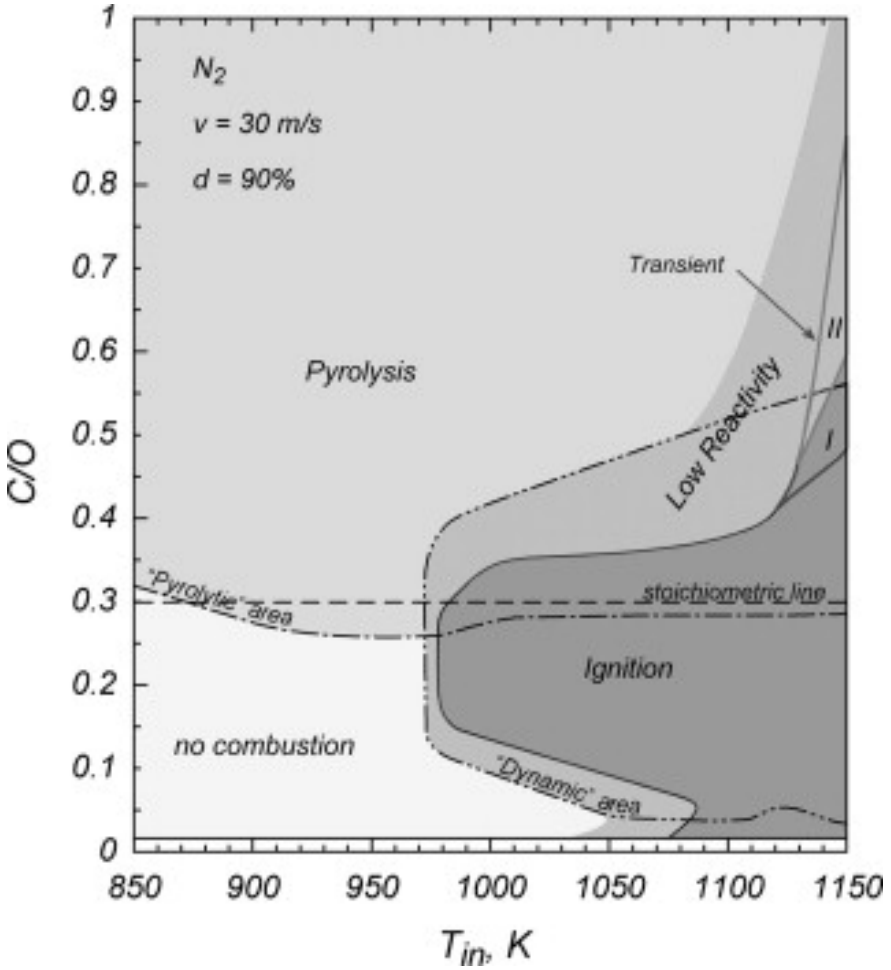

Fig. 4.4 – Map of behaviours of C_3H_8/O_2 mixtures diluted in N_2 up to 90% and for v = 30 m/s.

It is possible to distinguish several areas represented by different grey scale levels corresponding to unique axial profiles.

At low temperatures (i.e., from 850 K to approximately 975 K) and C/O values lower than the stoichiometric ratio no ignition was observed within the test time of the experiment (0.047 s for a velocity of 30 m/s). The area is indicated as "no combustion".

For the stoichiometric (C/O = 0.3) and fuel-rich mixtures, over the same temperature range, a "pyrolytic" behaviour was observed.

As the temperature increased, for C/O values in the neighbourhood of the stoichiometric mixture, the operating conditions led to ignition. For fuel-rich mixtures, the upper limit of the "ignition" region extends up to C/O = 0.35 (Φ = 1.17) and remains constant up to 1125 K, where it increases up to C/O = 0.5 (Φ = 1.67) at T_{in} = 1150 K.

The lower limit of this area slightly extends towards lower C/O feed ratios as T_{in} increases. When the inlet temperature increased up to 1080 K, the "ignition" region extended to fuel ultra-lean conditions.

Between the "ignition" and the "pyrolysis" regions, and between the "ignition" and the "no combustion" regions, the "low reactivity" behaviour occurs.

The pyrolyitc line (dashed-dot) and the dynamic line (double dotted) are also shown in the map. All operating conditions above the pyrolytic line show a temperature decrease relative to the first

thermocouples, indicating the onset of pyrolytic reactions. The operating conditions included in the "dynamic" line show oscillatory behaviours.
The last region in the map is relative to the "transient" behaviour. When both the first and the second temperature profiles reach a $\Delta T > 10$ K corresponding to operating conditions within their ignition regions on the map, two auto-ignition times were obtained as indicated by grey level intensities (transient I). In this case, the second steady state can exhibit a greater or lesser temperature increase than the first steady state. When the second steady profile did not satisfy the "ignition" criterion, the relative transient operating condition decreased into the low reactivity region (transient II).

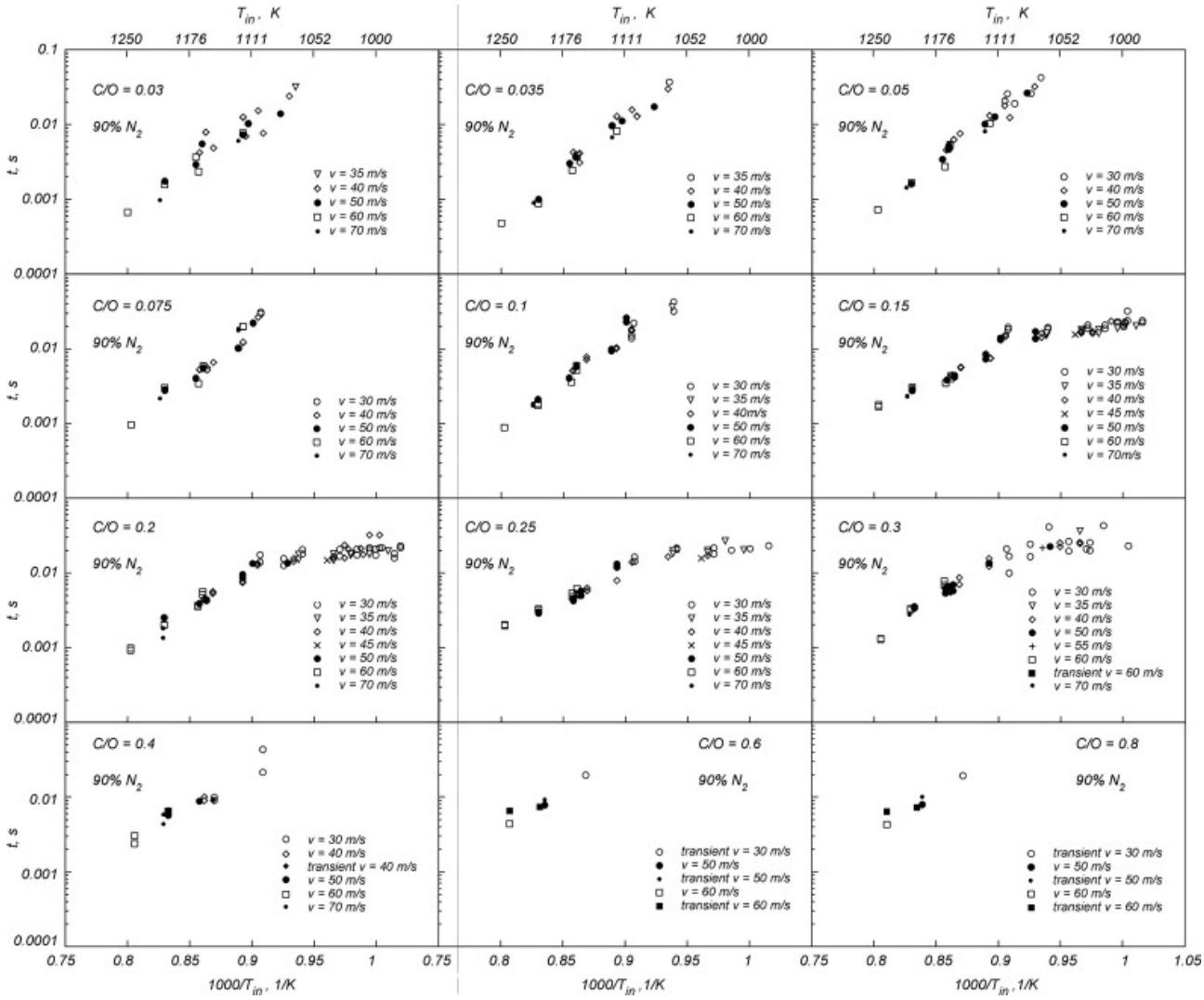

Fig. 4.5 – Auto-ignition delay times for C_3H_8/O_2 mixtures from lean to rich conditions diluted in N_2 to 90%.

The "transient" region incorporates and shifts between the behaviours of several different kinetic controlling routes.
The reactivity maps for other flow inlet velocities were also studied but are not reported here. They show that when the velocity is increased, the combustion regimes are still recognizable but are shifted to higher temperatures.
Based on the temperature profiles used for the map in Fig. 4.4, the auto-ignition times (t) were evaluated for mixtures with 10 K temperature increases.

Here the ignition delay times obtained in the manner described in the previous chapter are presented. The temperature dependence is expressed graphically as the delay time versus the reciprocal of mixture temperature for different mixture compositions.
The results are shown in Fig. 4.5 on a typical Arrhenius plot at 90% dilution and for several C/O ratios and flow velocities (i.e., from 30 to 70 m/s).
For C/O < 0.1 (Φ = 0.33), t shows a linear trend when plotted against temperature in the Arrhenius plot diagram. For 0.15 (Φ = 0.5) < C/O < 0.3 (Φ = 1), the auto-ignition delay time curves show two different slopes. In particular, for temperatures lower than approximately 1100 K, t is nearly independent on T_{in}. For higher temperatures, t linearly diminishes with temperature.
For fuel-rich mixtures (C/O > 0.3), auto-ignition delay times vary linearly with temperature. Similarly, as with the reactivity maps, the ignition area for fuel-rich mixtures is narrow with respect to the inlet temperature parameter and mostly exhibits pyrolytic or transient behaviour. The auto-ignition process is relatively slow with respect to lean/stoichiometric conditions; because of this, few data points were recorded at high temperatures. For transient conditions, two auto-ignition delay times are shown in Fig. 4.5.
In Fig. 4.1, in presenting the different types of observed axial temperature profiles, only one characteristic ignition profile has been shown. Actually, it should be stated that in the region of no dependence of the ignition delay time on temperature, it is observed a weaker temperature increase as a function of the axial coordinate.

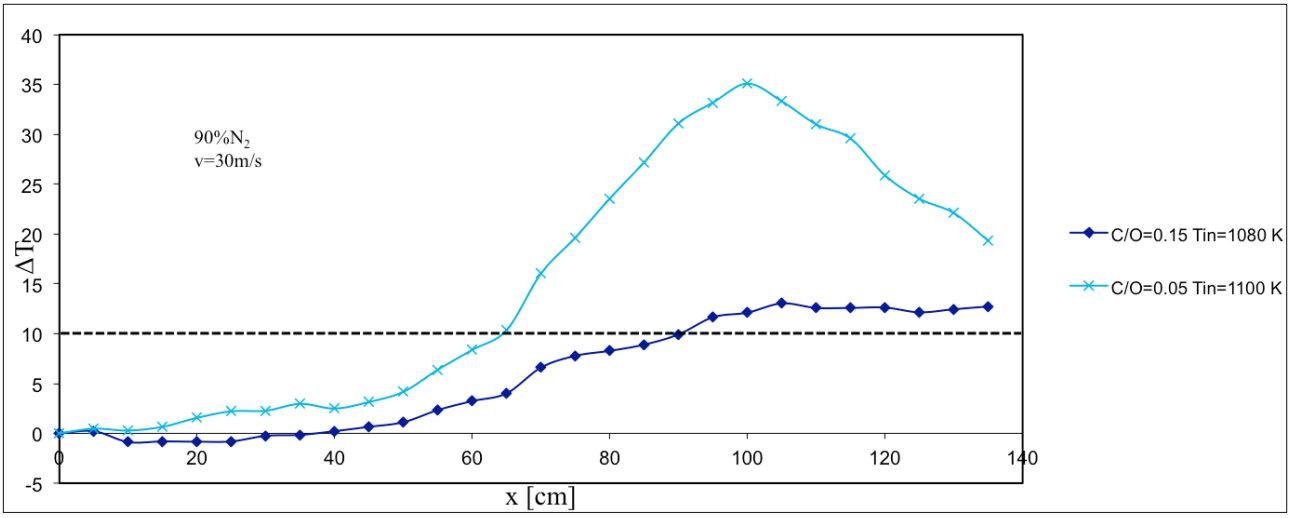

Fig. 4.6 – Characteristic experimental axial temperature profiles representative of two different types of ignition obtained under the condition of T_{in} = 1100 K and C/O = 0.05 (light blue line), T_{in} = 1080 K and C/O = 0.15 (blue line).

Figure 4.6 compares the experimental temperature history obtained under the condition of T_{in} = 1100 K and C/O = 0.05 (light blue line) with the temperature history obtained under the condition of T_{in} = 1080 K and C/O = 0.15 (blue line). A weak ignition phenomenon was observed under the second condition. This difference of behaviour will be analysed and discussed in detail in the next chapter.
Figure 4.7 shows the experimental and numerical ignition delay times for fuel-lean (C/O = 0.05 or Φ = 0.17), fuel-rich (C/O = 0.6 or Φ = 2) and stoichiometric mixtures (C/O = 0.3) in the Arrhenius diagram. The dilution level was kept constant (90%).
For the lean and stoichiometric conditions, the detailed kinetics model seems to agree with the experimental data. For the fuel-rich condition, the model underpredicts the experimental ignition delay times of about a factor of two. In particular, the greater the C/O ratio (i.e., the richer the mixture), the greater the discrepancy between numerical simulations and experimental data.
For inlet temperatures lower than approximately 1100 K, the numerical auto-ignition delay times were shortest for fuel-rich conditions and longest for fuel-lean mixtures. The stoichiometric mixture

ignition time was between these values. As the inlet temperature increased above 1100 K, the fuel-rich mixture exhibited the slowest ignition time, whereas the fuel-lean mixture exhibited the most rapid time.

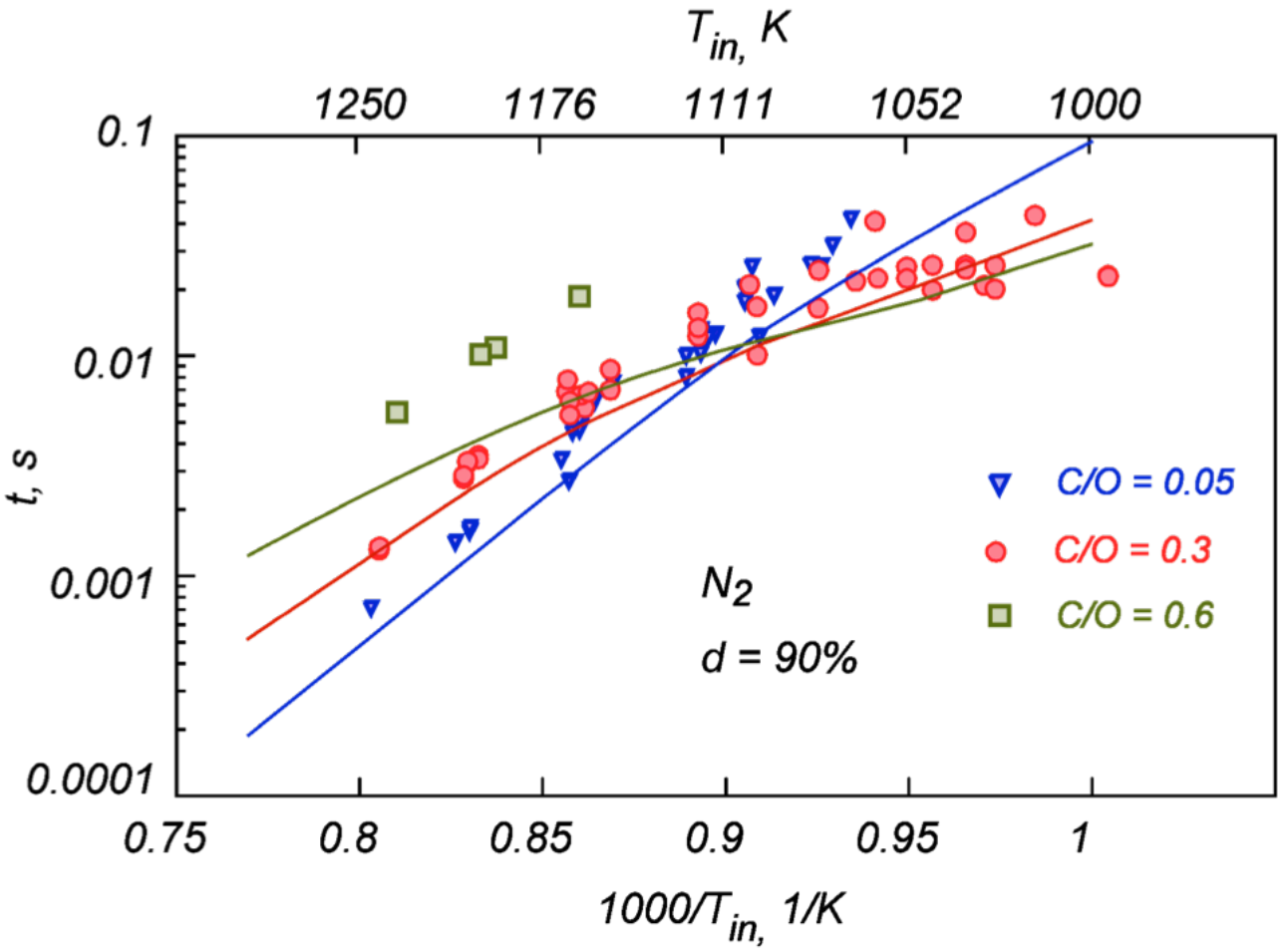

Fig. 4.7 - Experimental and numerical auto-ignition delay times for C_3H_8/O_2 mixtures diluted in N_2 to 90%. Φ = 0.17 (blue), Φ = 1 (red), Φ = 2 (green)

The experimental data confirm that at approximately 1100 K, the lean mixture ignition values were lower than the stoichiometric ignition values.

Influence of dilution

Figure 4.8 shows the experimental measurements and predicted numerical results of stoichiometric propane/oxygen mixtures diluted in nitrogen to several levels (90%, 95% and 97%). There is good agreement between the experimental data and numerical predictions for the 90% dilution level. However, as the dilution level is increased to 95% and 97%, the prediction fails; specifically, the experimental data are longer than the predicted numerical results.

Therefore, although the proposed kinetic mechanism is able to predict auto-ignition times for a few operating conditions, its ability to predict system behaviour in diluted combustion processes is unreliable for fuel-rich mixtures and highly diluted mixtures.

Influence of diluent: N_2, CO_2 and H_2O

As in the case of mixtures diluted in nitrogen, each acquired temperature profile corresponds to a point on a map of behaviour in the C/O-T_{in} plane, as reported in Fig. 4.4. For mixtures diluted in CO_2, experimental tests were carried out by varying the inlet temperature stepwise any 20 K, for thirteen C/O ratios, keeping constant the CO_2 concentration and the inlet flow velocity. For the T_{in}-

C/O values for which transitions among regimes were observed, the step was tightened. The map reported in Fig. 4.9 was drawn up on the basis of about 200 experimental tests. Figure 4.9 allows identifying the combustion regimes in the C/O-T_{in} plane. The T_{in} (850-1170 K) and C/O (0.035-1) ranges in Fig. 4.9 identify the analysed conditions for a flow velocity of 30 m/s and a mixture dilution level of 90% in CO_2. The experimental analysis covers both fuel-lean (C/O < 0.3) and fuel-rich (C/O > 0.3) mixtures (C/O = 0.3 is the stoichiometric condition).

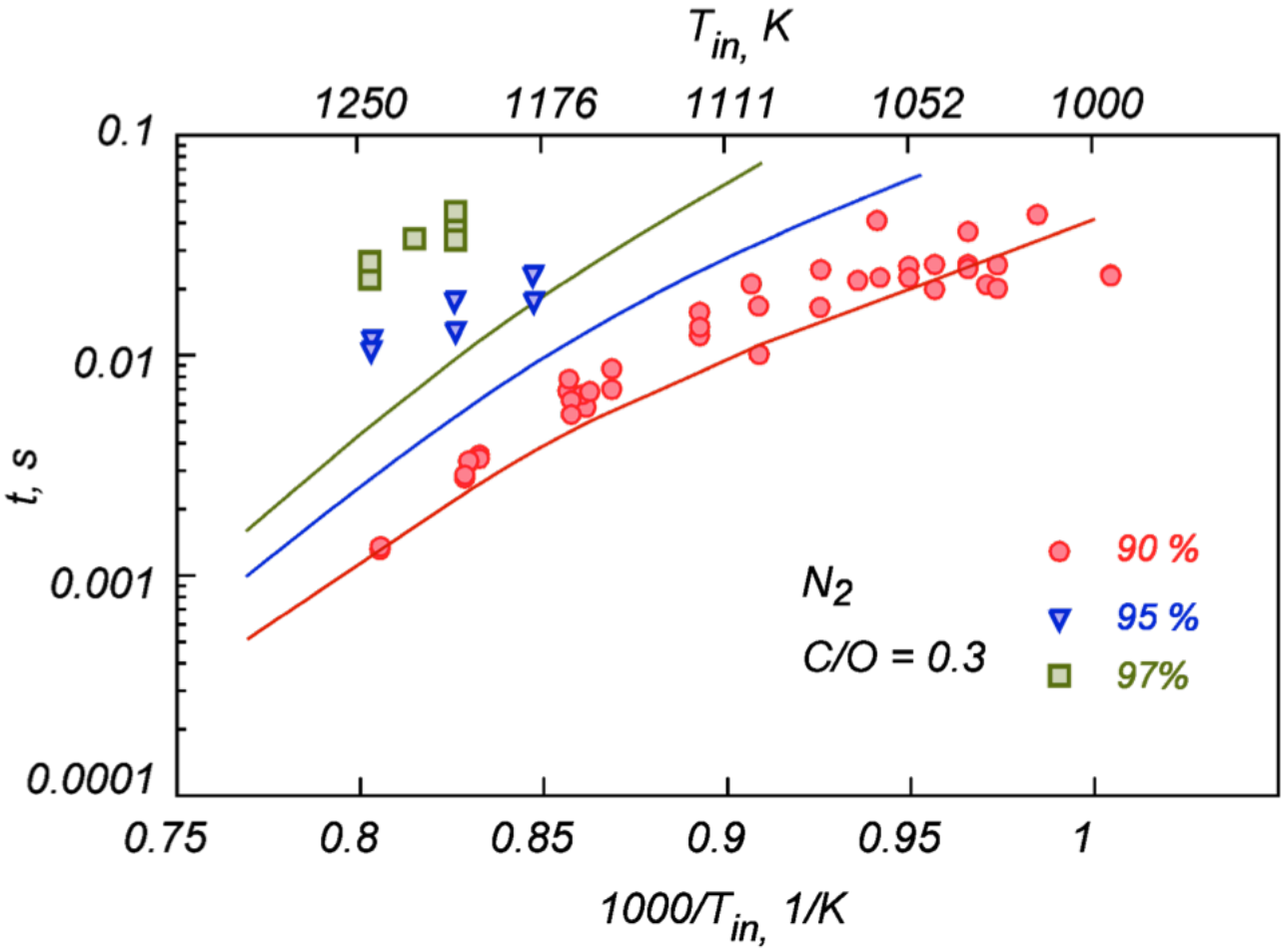

Fig. 4.8 – Experimental and numerical auto-ignition delay times for a stoichiometric C_3H_8/O_2 mixture diluted in N_2 to 90%, 95% and 97%.

For temperatures below 1030 K and ultra-lean/lean conditions, the "no combustion" regime is identified. As soon as the fuel molar fraction is increased, this area extends to slightly higher temperatures. The "no combustion" regime converts into the "pyrolytic regime" when the C/O ratio becomes higher than 0.3. A richer mixture corresponds to a wider "pyrolytic" temperature range in the map.

Both "pyrolytic" and "no combustion" behaviors border with the "low reactivity" region. For mixtures that are characterized by a C/O feed ratio of 0.035 (Φ = 0.12), this region extends from 1040 K to 1090 K. As soon as the C/O feed ratio is increased, the "low reactivity" area borders move towards higher temperatures, which slightly reduces the difference between their edge temperatures.

For T_{in} above 1090 K and ultra-lean conditions, the ignition process occurs. When the C/O ratio is increased, the ignition temperature increases.

In the map, the "pyrolytic" (dashed dot) and the "dynamic" lines (double dotted) are drawn. All operative conditions on the map above the "pyrolytic line" show a temperature decrease relative to the first thermocouples, which indicates the onset of pyrolytic reactions, whereas the ones included

in the “dynamic” line show an oscillating behaviour. The latter develops for T_{in} above 1120 K and C/O near the stoichiometric ratio.

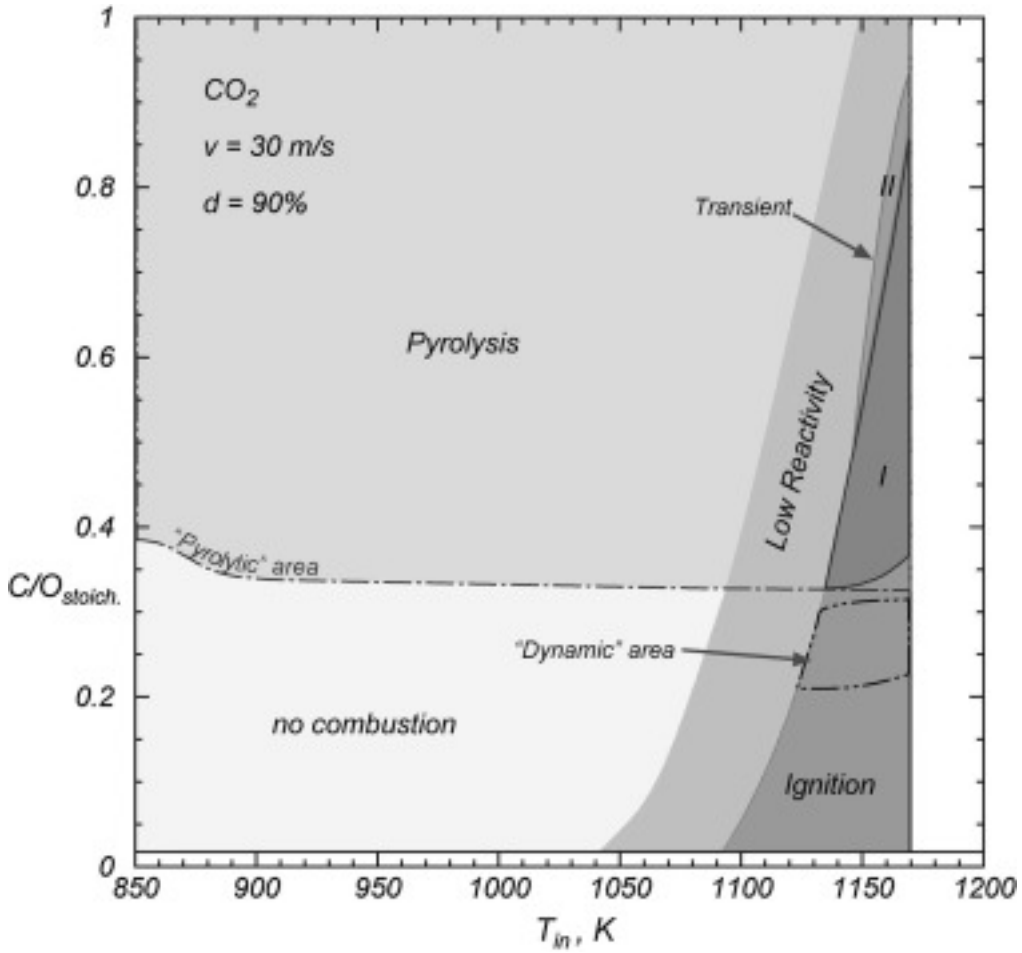

Fig. 4.9 – Map of behaviour for C_3H_8/O_2 mixtures that were diluted to 90% in CO_2 at v = 30 m/s.

For rich conditions, the ignition process occurs throughout a transient behaviour. In particular, in the map, the “transient” area is labelled with I and II. The transient condition that is identified by I is relative to the case where both steady states exceed 10 K, whereas the second temperature profile in case II does not reach the ignition condition ($\Delta T = T - T_{in} < 10$ K).

It is worth noting that when the temperature increases and/or the mixture composition changes, the shift among “no combustion/pyrolytic” and “ignition” regimes occur under the “low reactivity” and/or “transient” conditions, which identifies a gradual change of the system behaviour.

In general, it is worth noting that lean mixtures at high temperatures ignite and reach a steady condition, whereas in the neighbourhood of the stoichiometric condition, the operative conditions give rise to temperature-oscillating behaviours, which suggests that the kinetic pathways compete among themselves. In rich conditions, the system reactivity is damped by pyrolytic reactions. Therefore, such results indicate that the dynamic behaviour is established for the competition between oxidative and pyrolytic reactions. A detailed analysis on the dynamic of these systems will be provided in the next chapter.

Experimental measurements were performed at higher velocities and temperatures (up to 70 m/s and 1250 K), but the maps do not show substantial differences from the reported result in Fig. 4.9; thus, for the sake of brevity, they are not displayed.

Applying the same regime classification that was used to comment on the obtained results for C_3H_8/O_2 mixtures diluted in CO_2, the map was drawn relative to the mixtures diluted in H_2O. For a dilution level of 90% and a flow velocity of 30 m/s, the explored temperature range was 850-1180 K, whereas the C/O feed ratio range was 0.035-1. The map is shown in Fig. 4.10.

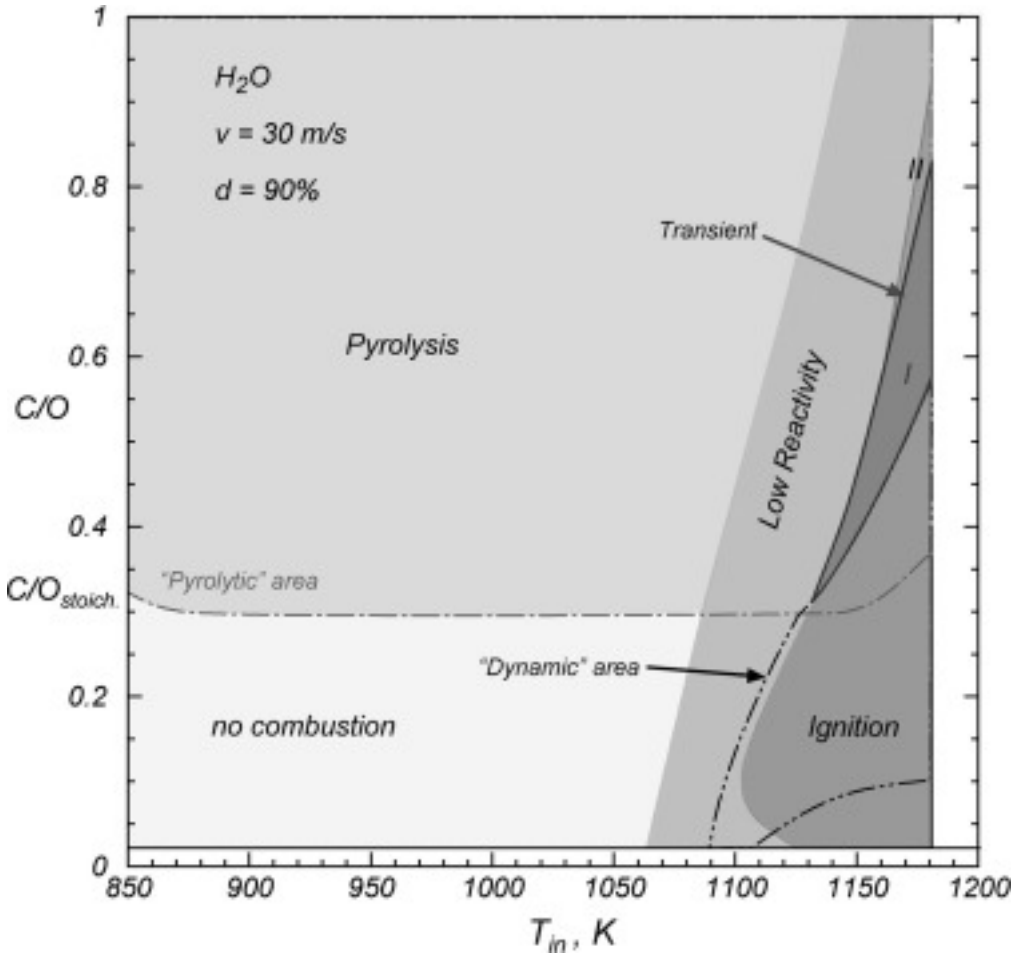

Fig. 4.10 – Map of behaviour for C_3H_8/O_2 mixtures that were diluted to 90% in H_2O at v = 30 m/s.

The "no combustion" region extends from 850 K to 1060 K for C/O = 0.025 (Φ = 0.083). This area slightly widens in the inlet temperature range when C/O increases toward the stoichiometric condition. For C/O above 0.3, the temperature profiles show the typical trend of the "pyrolytic" case. The "pyrolytic" and "no combustion" behaviours change to the "low reactivity" case, which increases the inlet temperature. This region extends from 1060 K to 1130 K for C/O = 0.025 (Φ = 0.083) and from 1140 K to 1180 K for C/O = 1 (Φ = 3.33).

A further increase of the temperature makes the system move to reactive conditions. In particular, for C/O = 0.1 (Φ = 0.33) and 0.025 (Φ = 0.083), the "ignition" case is recognizable at approximately 1100 K and 1130 K, respectively. This region extends to 0.55 (Φ = 1.83) for T_{in} = 1170 K.

In addition, in this map, as illustrated in Figs. 4.4 and 4.9, the "pyrolytic" and "dynamic" lines were shown. In particular, the dynamic behaviour region in the map is more extended than that in the case of mixtures that were diluted in CO_2, and it includes the "low reactivity" conditions. It extends for T_{in} higher than 1090 K and C/O lean conditions; then, when the temperature increases, it is also established for richer conditions. In case of fuel-rich mixtures, the propane oxidation evolves through the "transient" regimes. For T_{in} = 1180 K, it is recognized up to C/O = 0.85-0.9 (Φ = 2.83-3). This region is subdivided into "transient I" and "transient II" areas following the previously reported classification.

In this case, experimental measurements were also performed at higher velocities and temperatures (up to 50 m/s and 1235 K), but the maps do not show substantial differences compared to the one in Fig. 4.10.

Based on the temperature profiles that are used to build the maps, the auto-ignition times were evaluated according to the criterion of 10 K temperature increment. They were reported in Fig. 4.11

for several C/O feed ratios and inlet temperatures for a dilution level of 90% in CO_2 in a typical Arrhenius plot at several flow velocities (30-70 m/s).

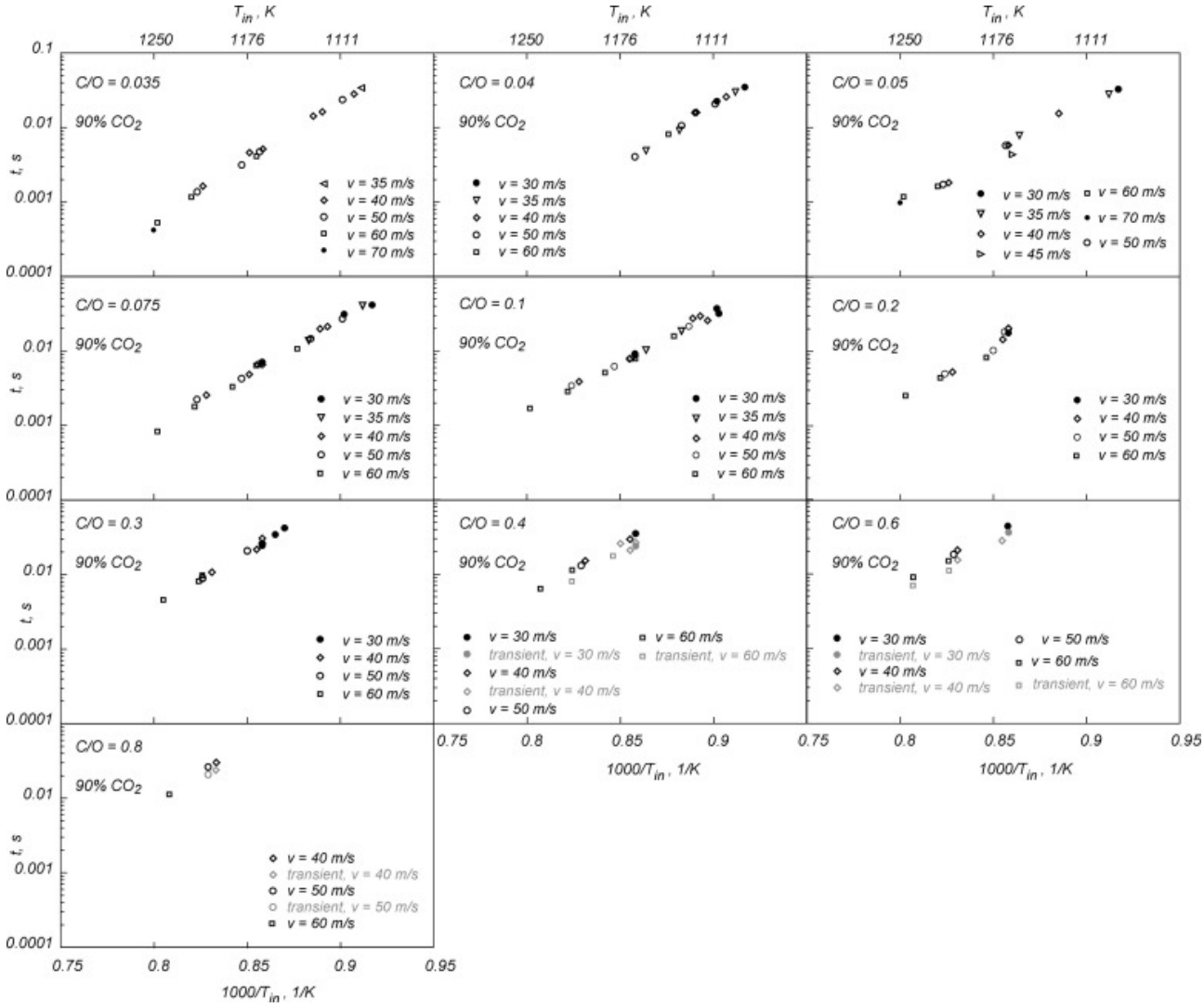

Fig. 4.11 – Auto-ignition delay times for C_3H_8/O_2 mixtures from lean to rich conditions, which were diluted to 90% in CO_2.

It is worth noting that the auto-ignition values are slightly influenced by the flow velocity. Furthermore, when the velocity is increased, the resolution time of the ignition process increases because the flow covers the distance between two thermocouples in less time, which makes the temperature profile measurements more accurate.

When the transitional regimes occur, two ignition delay values are reported (case I in the map).

For any C/O feed ratio, the auto-ignition delay times exhibit a linear trend as a function of the inlet temperature on an Arrhenius diagram. For the fuel-rich mixtures, fewer points are reported because the required temperatures to achieve ignition are higher, as shown in Fig. 4.9.

Numerical simulations were performed using the PLUG application of the ChemKin PRO with the "CRECK-2014" kinetic mechanism.

Figure 4.12 shows the ignition delay times for propane/oxygen mixtures that were diluted up to 90% in CO_2 for fuel-lean (C/O = 0.05 or Φ = 0.17), stoichiometric (C/O = 0.3) and fuel-rich (C/O = 0.6 or Φ = 2) conditions.

It is evident that in the high temperature range, the kinetic mechanism well predicts the increase of the delay times with increasing C/O, but the experimental and numerical results are only consistent

for the lean conditions. Under rich and stoichiometric conditions, the model underestimates the experimental data.

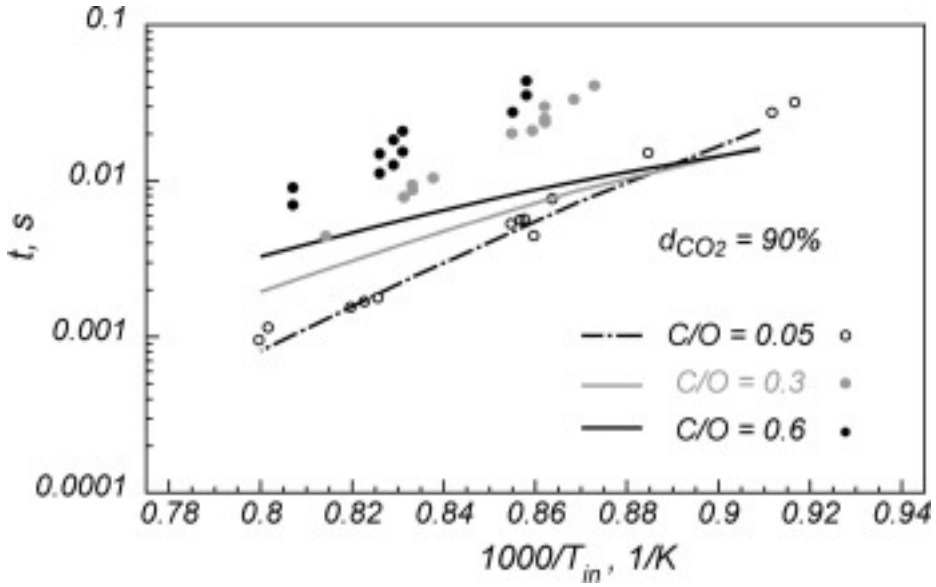

Fig. 4.12 – Experimental and numerical auto-ignition delay times for C_3H_8/O_2 mixtures that were diluted to 90% in CO_2 for fuel-lean (C/O = 0.05 or Φ = 0.17), stoichiometric (C/O = 0.3) and fuel-rich (C/O = 0.6 or Φ = 2).

Also in the case of mixtures diluted in H_2O, it was possible to evaluate the auto-ignition times for all analysed operative conditions that satisfied the criterion of ignition. Figure 4.13 shows the ignition delay times for several C/O values from lean to rich reactive conditions on a typical Arrhenius plot. The mixtures were diluted to 90 % in H_2O, and the flow velocity was changed from 30 to 50 m/s.

When the transitional regimes occur, two ignition delay values are reported for the C/O-T_{in} values in the "transient I" case. In any case, the auto-ignition delay times show a linear trend as a function of the inlet temperature on the Arrhenius diagram.

For rich mixtures, fewer points are reported because the required temperatures to achieve ignition are higher, as shown in Fig. 4.10.

Figure 4.14 shows the same comparison reported in Fig. 4.12, for propane/oxygen mixtures that were diluted to 90% in H_2O. The disagreement between experimental and numerical data is even more pronounced in this case, and the kinetic mechanism cannot predict the experimental results. It should be noted that for any C/O feed ratio, the experimental ignition delay times are notably close to each other in the entire exploited range of T_{in}. The kinetic mechanism properly reproduces this behaviour, but the predicted values are lower than the test data by almost one order of magnitude.

Further experimental tests were realized for mixtures that were diluted at 95% and 97% in CO_2 to evaluate the influence of the dilution degree on the process features. The results suggested that higher dilution levels imply the achievement of lower temperature increase inside the reactor, but the oxidation regimes were identical; therefore, the C/O-T_{in} maps are omitted. Nevertheless, a comparison among the ignition delay times at different dilution degrees is provided. For H_2O diluted mixtures it was not possible to collect sufficient data to build C/O-T_{in} maps for dilution levels above 90% because the system reactivity was low.

In Fig. 4.15, the ignition delay times for a stoichiometric propane/oxygen mixture that was diluted to 90%, 95% and 97% in CO_2 are compared. The figure shows a clear slowing of the ignition process when the dilution level of the mixture increases. The disagreement between experimental and numerical results increases with the dilution degree.

To evaluate the effect of CO_2 and H_2O on the propane ignition process, it is useful to compare the obtained results (experimental and numerical) with those of mixtures that were diluted in inert environments.

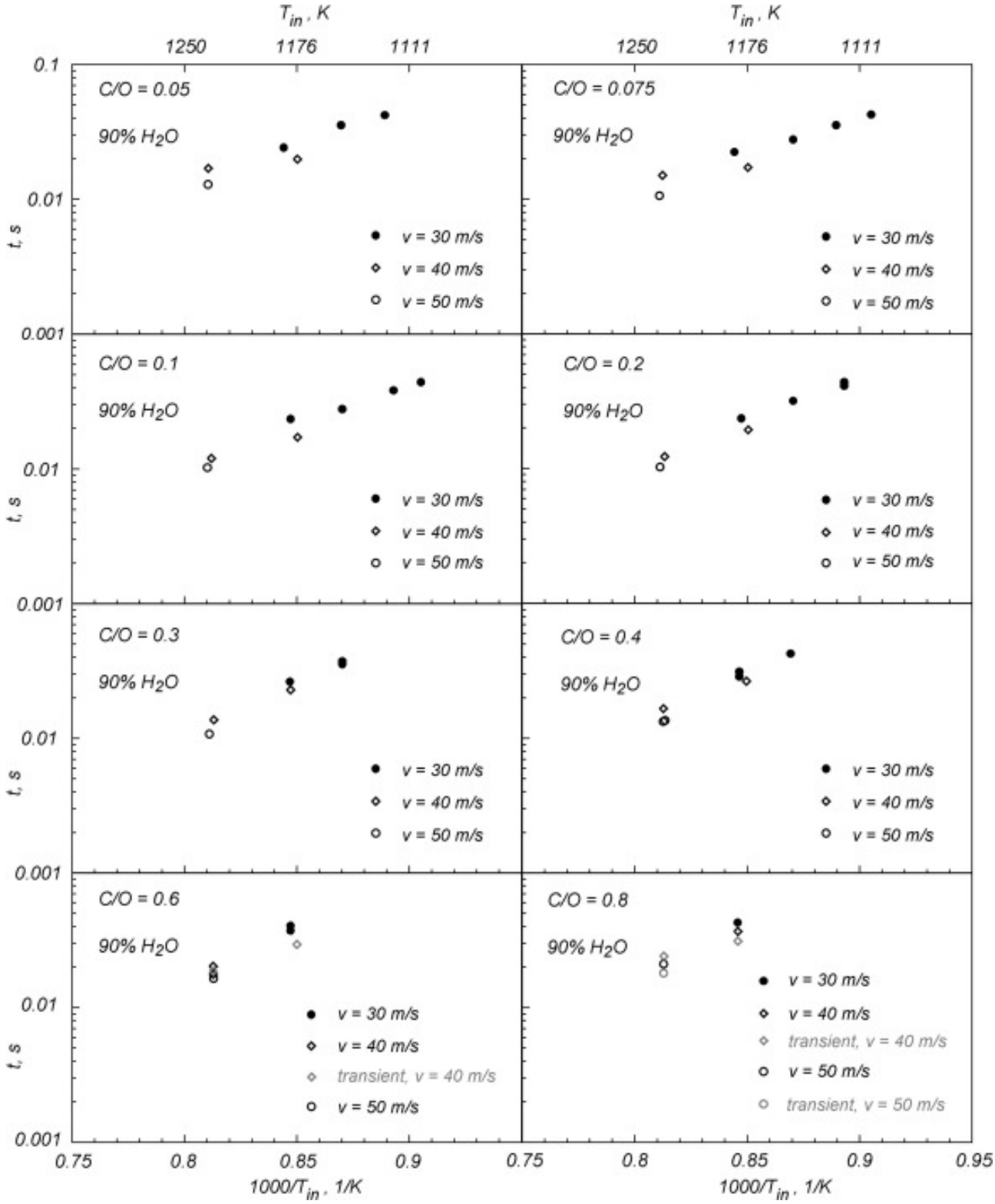

Fig. 4.13 – Auto-ignition delay times for C_3H_8 mixtures from lean to rich conditions, which were diluted to 90% in H_2O.

Figure 4.16 shows the auto-ignition delay times for a stoichiometric propane/oxygen mixture that was diluted up to 90% in N_2, CO_2 and H_2O. The numerical predictions are reported with lines.

Experimental data show that the ignition occurs for lower inlet temperatures in the case of N_2, whereas for CO_2 and H_2O it starts at nearly the same high T_{in}. In both cases, the ignition times are longer by almost one order of magnitude than those obtained for the mixture diluted in nitrogen. All three sets of data show an Arrhenius trend in the range of high temperature, whereas for lower temperatures, the obtained data for nitrogen show a change in activation energy of the ignition process that passes from intermediate to high inlet temperature, as widely discussed before.

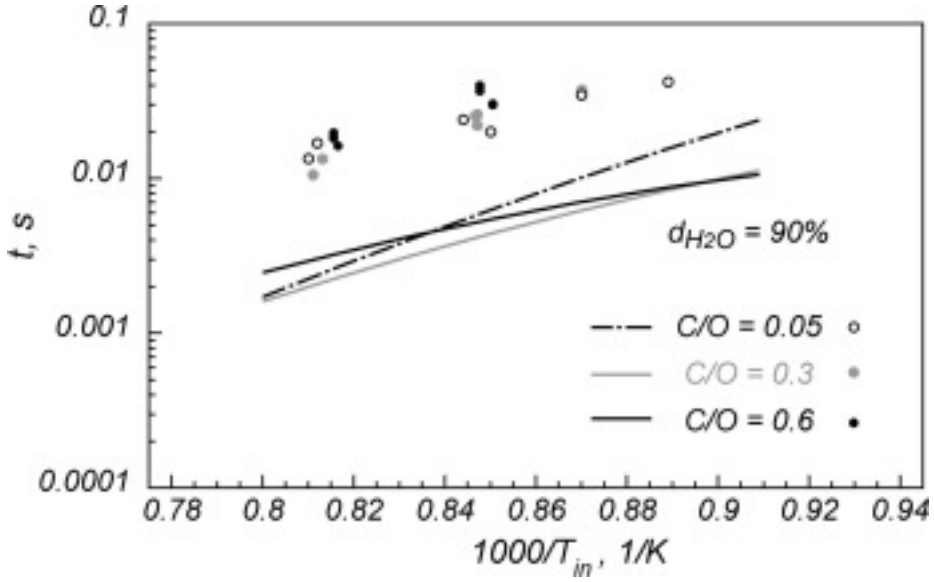

Fig. 4.14 – Experimental and numerical auto-ignition delay times for C_3H_8/O_2 mixtures that were diluted to 90% in H_2O for fuel-lean (C/O = 0.05 or Φ = 0.17), stoichiometric (C/O = 0.3) and fuel-rich (C/O = 0.6 or Φ = 2).

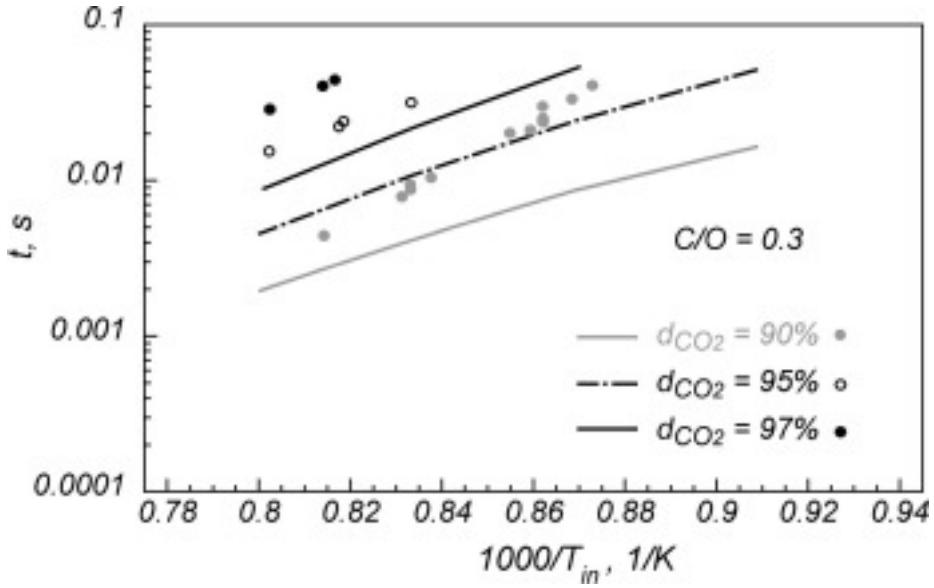

Fig. 4.15 – Experimental and numerical auto-ignition delay times for a stoichiometric C_3H_8/O_2 mixture that was diluted to 90%, 95% and 97% in CO_2.

It is possible to note that although the auto-ignition data obtained for N_2 are predicted with a good approximation using the chosen kinetic mechanism, the consistency was not good for the other two diluent species. Furthermore, in contrast to the experimental data, the numerical predictions suggest that in the considered temperature range, carbon dioxide is the most effective in delaying the auto-ignition times.

Figure 4.17 shows the experimental ignition delay times for an ultra-lean (C/O = 0.05 or Φ = 0.17) mixture and a rich mixture (C/O = 0.6 or Φ = 2) and the numerical predictions. The experimental auto-ignition data for CO_2-diluted mixtures are near the nitrogen values for fuel ultra-lean (Fig. 4.17a), whereas the ignition delay times of the H_2O-diluted system are longer and show a different slope in the Arrhenius plot with respect to the N_2 and CO_2 times.
Numerical simulations perform well in predicting N_2 and CO_2 test data, but a significant discrepancy occurs between the experimental and the numerical data for H_2O.

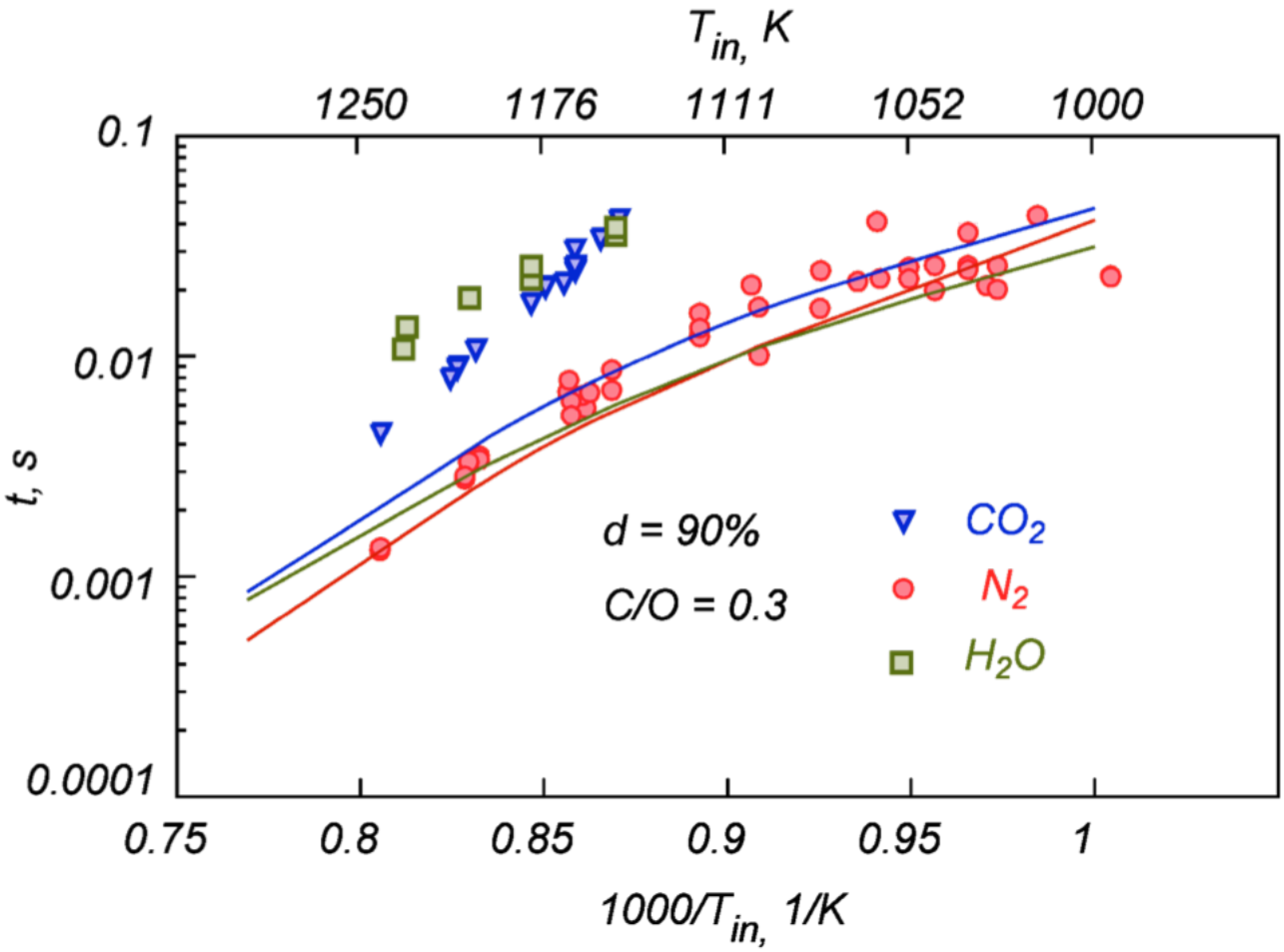

Fig. 4.16 – Experimental and numerical auto-ignition delay times for stoichiometric C_3H_8/O_2 mixtures that were diluted to 90% in N_2 (red), H_2O (green) and CO_2 (blue).

For fuel-rich mixtures (Fig. 4.17b), the difference among the obtained experimental data for the three reference fuels becomes less pronounced, and noticeable differences occur between numerical and experimental results, particularly for H_2O.
It should be clarified that, when the models are not able to correctly reproduce the experimental ignition delay times, the numerical predictions are lower than the experimental observations, while Chaos & Dryer (2010) emphasized that one or more perturbations substantially reduce chemical induction times and hence observed ignition delays.

4.1.2 C_1-C_2 mixtures

In addition to the pure fuels, the self-ignition of their mixtures is of basic importance. Therefore, in this part of work, the ignition process of a model gas surrogate for the gaseous fraction of biomass pyrolysis products was investigated, with a typical composition of low temperature pyrolysis processes. The reference gas was a mixture of 1% C_2H_4, 2% C_2H_6, 10% CH_4, 25% CO and 62% CO_2. Such values are representative of the main species mean concentrations reported in the review

of Di Blasi (2009). The ignition and oxidation processes of this model gas were experimentally and numerically studied over a wide range of temperatures and overall compositions, in the presence of different diluent species (namely, N_2, CO_2, and H_2O).

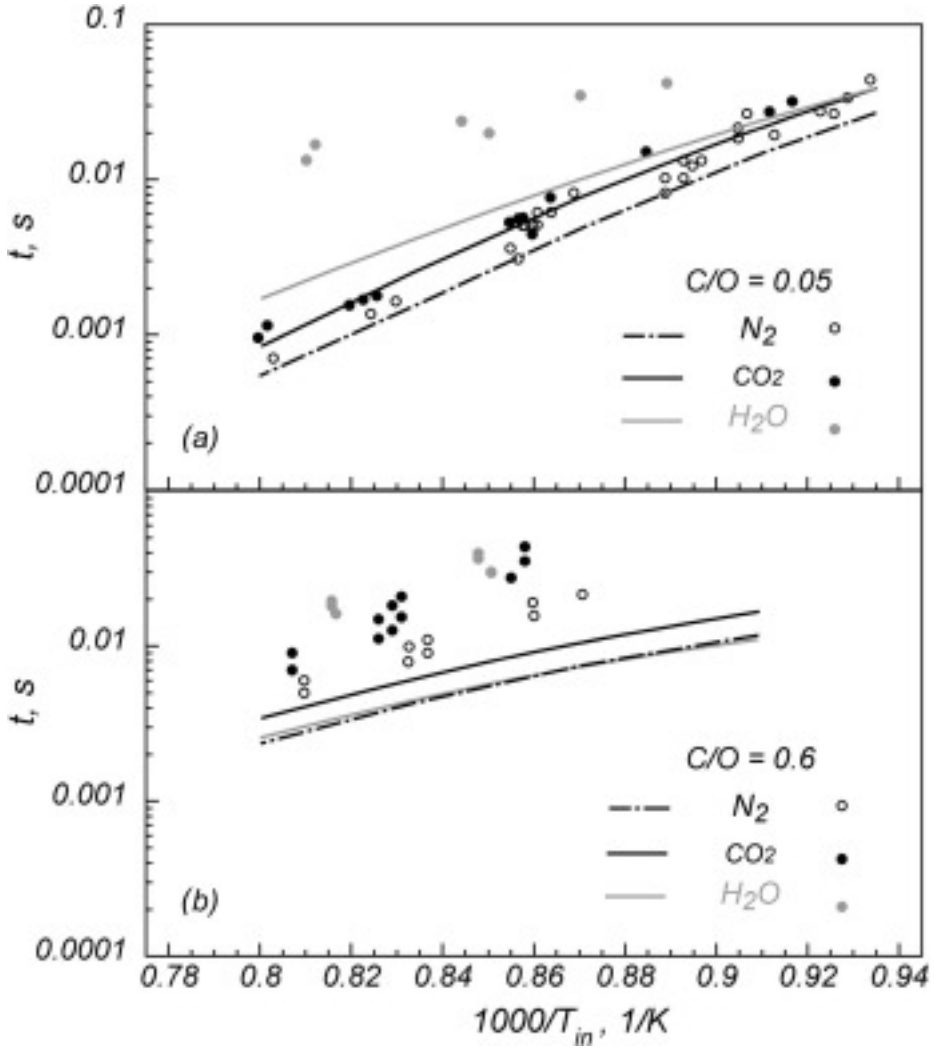

Fig. 4.17 – Experimental and numerical auto-ignition delay times for fuel-lean (a) (C/O = 0.05 or Φ = 0.17) to fuel-rich (b) (C/O = 0.6 or Φ = 2) C_3H_8/O_2 mixtures that were diluted to 90% in N_2, H_2O, and CO_2.

Due to the presence of partially oxidized compounds in the reactive species, namely CO, the carbon to oxygen content in the mixture was expressed in terms of the oxygen ratio (Ω) (Mueller et al. 2003). Ω parameter is defined as "the amount of oxygen in the mixture divided by the amount of oxygen required for stoichiometric combustion of the same quantity of fuel, where atoms bound in stable species are neglected". In this case, a stable species is defined as a species that is neither a fuel nor an oxidizer. The general formula of the model fuel mixture has the form:

$$\sum_i a_i C_{n_{C,i}} H_{n_{H,i}} O_{n_{O,i}}$$

where a_i is the number of moles of the i^{th} species and $n_{[element],I}$ is the number of atoms of [element] in the i^{th} species. Thus Ω is calculated by means of the following equation:

$$\Omega = \frac{\sum_k a_k n_{O,k} + \sum_m a_m n_{O,m}}{\sum_r a_r (2n_{C,r} + \frac{n_{H,r}}{2})}$$

where k, m, and r are indices of, respectively, fuel, oxidizer, and fuel-plus-oxidizer reactant species. In mathematical terms, if each species in the reactants has a unique index, then indices k and m have no intersection, and their union is the set of indices r. On the basis of this definition, Ω = 1 represents a stoichiometric mixture, while Ω > 1 identifies fuel lean cases.
In this case d takes also into account the amount of CO_2 present in the pyrolysis gas, which has a fixed composition.
The evaluation of system behaviour was carried out by the systematic analysis of temperature profiles as a function of inlet pre-heating temperature, Ω ratios and diluent composition, both for the quantification of ignition delay and for identification of established regimes from the shapes and trends of the axial temperature profiles measured under the different experimental conditions. As already described in the previous paragraph, five main typologies of temperature profiles were recognized and associated with characteristic system behaviours.
The experimental tests were carried out at atmospheric pressure, varying Ω from 0.7 to 10, in a T_{in} range from 1000 K to 1300 K. The effect of diluent on the ignition delay and oxidation regimes was evaluated. Thus N_2, CO_2 and H_2O were alternatively used as diluent species such that d ranged from 90% to 97%.
The experimental conditions are summarized in Table 4.3. Furthermore, the measured ignition delay times, along with all the operative conditions in which experiments with C_1C_2 mixtures in the PFR have been carried on, are listed in the Appendix.
All results that will be presented in this section, obtained with C_1C_2 mixtures in the PFR, have been published in the following journal paper:
Sabia, P, Lubrano Lavadera, M, Sorrentino, G, Giudicianni, P, Ragucci, R & de Joannon, M 2016, "H_2O and CO_2 Dilution in MILD Combustion of Simple Hydrocarbons", *Flow, Turbulence and Combustion*, vol. 96, no. 2, pp. 433-448.

d (%)	Ω	Pyrolysis gas (vol%)	O_2 (vol%)	N_2 (vol%)	Added CO_2 (vol%)	H_2O (vol%)	Number of experiments
90	0.34	22.60	1.40	0	76	0	1
90	0.5	18.87	2.83	78.30	0	0	7
90	0.5	18.87	2.83	0	78.30	0	1
90	0.7	15.63	4.06	80.31	0	0	14
90	0.7	15.63	4.06	0	80.31	0	2
90	0.7	15.63	4.06	0	0	80.31	2
90	0.75	14.98	4.31	0	80.71	0	1
90	0.8	14.39	4.53	81.08	0	0	5
90	0.8	14.39	4.53	0	81.08	0	1
90	0.8	14.39	4.53	0	0	81.08	5
90	0.85	13.84	4.74	81.42	0	0	6
90	0.85	13.84	4.74	0	81.42	0	3
90	0.9	13.33	4.93	81.73	0	0	10
90	0.9	13.33	4.93	0	81.73	0	3
90	0.9	13.33	4.93	0	0	81.73	9
90	0.91	13.24	4.97	81.79	0	0	2
90	0.91	13.24	4.97	0	81.79	0	1
90	0.95	12.86	5.11	82.03	0	0	2
90	0.95	12.86	5.11	0	82.03	0	1
90	1	12.42	5.28	82.30	0	0	19

90	1	12.42	5.28	0	82.30	0	11
90	1	12.42	5.28	0	0	82.30	9
90	1.25	10.61	5.97	83.42	0	0	9
90	1.25	10.61	5.97	0	83.42	0	6
90	1.25	10.61	5.97	0	0	83.42	6
90	1.5	9.26	6.48	84.26	0	0	11
90	1.5	9.26	6.48	0	84.26	0	6
90	1.5	9.26	6.48	0	0	84.26	7
90	1.67	8.52	6.76	84.72	0	0	26
90	1.67	8.52	6.76	0	84.72	0	10
90	1.67	8.52	6.76	0	0	84.72	8
90	2	7.20	7.38	85.42	0	0	9
90	2	7.20	7.38	0	85.42	0	12
90	2	7.20	7.38	0	0	85.42	10
90	2.25	6.70	7.45	0	0	85.85	1
90	2.5	6.13	7.67	86.20	0	0	5
90	2.5	6.13	7.67	0	86.20	0	9
90	2.5	6.13	7.67	0	0	86.20	10
90	3	5.25	8.01	86.75	0	0	4
90	3	5.25	8.01	0	86.75	0	15
90	3	5.25	8.01	0	0	86.75	7
90	3.33	4.79	8.18	87.03	0	0	22
90	3.33	4.79	8.18	0	87.03	0	11
90	3.33	4.79	8.18	0	0	87.03	10
90	4	4.07	8.45	0	87.47	0	3
90	5	3.33	8.74	87.94	0	0	20
90	5	3.33	8.74	0	87.94	0	11
90	5	3.33	8.74	0	0	87.94	10
90	7	2.44	9.07	88.49	0	0	19
90	7	2.44	9.07	0	88.49	0	10
90	7	2.44	9.07	0	0	88.49	10
90	10	1.74	9.34	88.92	0	0	19
90	10	1.74	9.34	0	88.92	0	8
90	10	1.74	9.34	0	0	88.92	8
95	0.8	7.19	2.27	90.54	0	0	1
95	0.9	6.67	2.47	90.87	0	0	3
95	1	6.21	2.64	91.15	0	0	3
95	1	6.21	2.64	0	91.15	0	2
95	1.25	5.31	2.98	91.71	0	0	3
95	1.5	4.63	3.24	92.13	0	0	3
95	1.67	4.26	3.38	92.36	0	0	3
95	1.67	4.26	3.38	0	92.36	0	2
95	2	3.69	3.60	0	92.71	0	1
95	3.33	2.40	4.09	93.51	0	0	3
95	3.33	2.40	4.09	0	93.51	0	2
95	5	1.66	4.37	93.97	0	0	3
95	5	1.66	4.37	0	93.97	0	2
95	7	1.22	4.54	94.24	0	0	1
95	7	1.22	4.54	0	94.24	0	2

95	10	0.87	4.67	94.46	0	0	1
95	10	0.87	4.67	0	94.46	0	2
97	0.9	4.00	1.48	94.52	0	0	2
97	1	3.73	1.58	94.69	0	0	2
97	1.25	3.18	1.79	95.03	0	0	2
97	1.5	2.78	1.94	95.28	0	0	2
97	1.67	2.56	2.03	95.41	0	0	2
97	2	2.21	2.16	95.63	0	0	2
97	3.33	1.44	2.45	96.11	0	0	2
97	5	1.00	2.62	96.38	0	0	2

Table 4.3 – Experimental conditions studied in the TFR for C_1-C_2 mixtures. P = 1 atm, 1000 K < T_{in} < 1300 K, 0.015 s < τ < 0.048 s.

Influence of temperature and equivalence ratio

Experimental ignition delay times for the pyrolysis gas/oxygen mixtures diluted in N_2 up to 90% for Ω equal 0.9, 1 and 1.67 for fuel rich, stoichiometric and lean conditions, respectively, are reported with symbols in Fig. 4.18 in the Arrhenius diagram. In the considered T_{in} range, the autoignition delay times change linearly with T_{in} in the Arrhenius diagram plot. In particular, for Ω = 1.67, t goes down from 4 x 10^{-2} s at T_{in} = 1090 K (1000/T_{in} = 0.92) to 2.3 x 10^{-3} s at T_{in} = 1285 K (1000/T_{in} = 0.78). For the stoichiometric condition (Ω = 1), t = 0.025 s at T_{in} = 1165 K, while it is 8.6 x 10^{-3} s at T_{in} = 1285 K and, for the fuel rich mixture, from 1.9 x 10^{-2} s at T_{in} = 1200 K to 1.1 x 10^{-2} s at T_{in} = 1285 K.

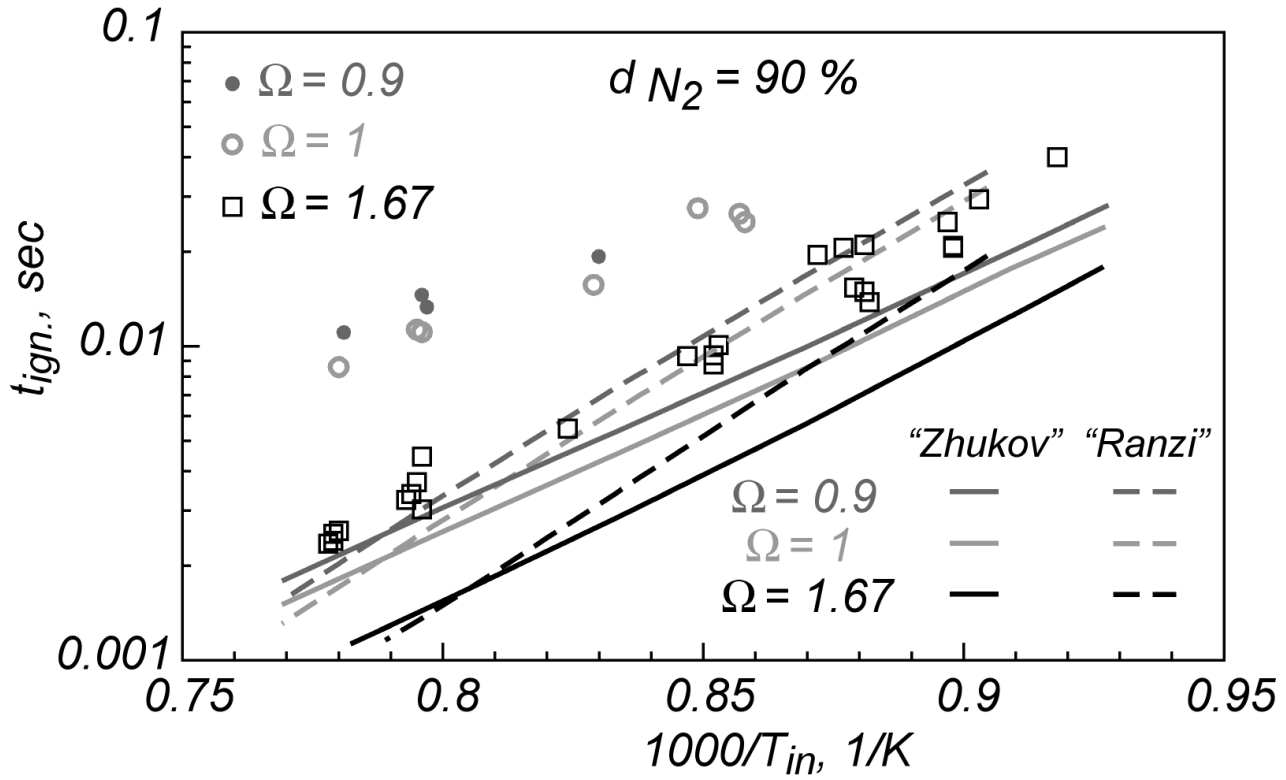

Fig. 4.18 – Experimental (symbols) and numerical (lines) ignition delay times at atmospheric pressure for three pyrolysis gas/oxygen mixtures (Ω = 0.9, 1 and 1.67) diluted in nitrogen at 90%.

Figure 4.18 also reports the numerical predictions obtained by the Zhukov-2005 and the CRECK-2014 ("Ranzi" in the figure) mechanisms, which resulted to be the most suitable schemes to

simulate the ignition process for propane mixtures. It must be said that in these dataset also the GRI_3.0-1999 was tested. The temperature dependence of the ignition delay times predicted by the GRI_3.0-1999 is the same as that predicted by Zhukov-2005, however the latter predicted ignition times closer to those experimentally observed.
In general, the measured t are longer with respect to the computed t.
Although experimental values were not well reproduced by any tested mechanisms, the Zhukov-2005 scheme was able to reproduce the slope of the autoignition delay curves in the Arrhenius diagram. As such, from a kinetic point of view, the mechanism can be supposed to predict the relative weight of the different kinetic paths well with changing working conditions. Therefore, the Zhukov-2005 mechanism has been chosen to gain deep insight into the chemistry involved in the ignition process that will be discussed in the next chapter.
A complete list of the entire measured ignition delay times as a function of temperature and equivalence ratio is provided in the Appendix.

Influence of diluent: N_2, CO_2 and H_2O
Figure 4.19 shows the T_{in}-C/O maps for the systems diluted in N_2 (a), CO_2 (b), H_2O (c). Any map was built performing experiments each 25 K in the T_{in} range considered, and changing the Ω ratios for fifteen values. The tests were tightened in correspondence of the change of the system behaviours, in order to better draw the characteristic areas up.

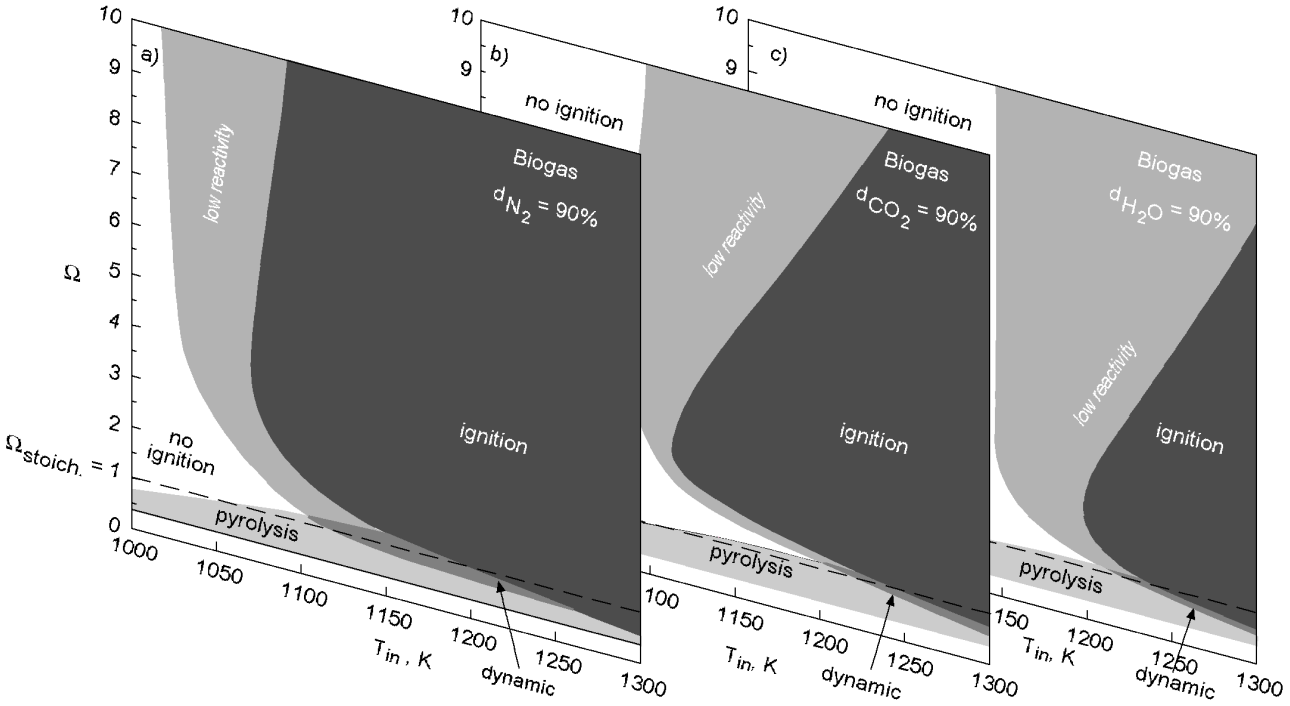

Fig. 4.19 – Map of behaviours for pyrolysis gas/oxygen mixtures diluted at 90% in N_2 (a), CO_2 (b), H_2O (c).

Figure 4.19a identifies such regimes in the T_{in}-C/O plane for a N_2 dilution level of 90%.
The "no ignition" region was associated with low inlet temperatures and lean Ω ratios. The "low reactivity region" is present on the left side on the map for lean conditions, covering a temperature range of approximately 70 K at the leanest condition. Under rich conditions, profiles characterized by a negative temperature increase ("pyrolysis" region) were detected in the whole temperature range considered.
The widest region on the map is relative to the "ignition" case. For such system inlet conditions, collected temperature profiles show $\Delta T \geq 10$ K, so the threshold criterion for ignition delay (t) is

satisfied. This region covers a temperature range from approximately 1070 K up to 1300 K for Ω from approximately 0.5 up to the maximum value considered.
The widest region on the map is relative to the "ignition" case. For such system inlet conditions, collected temperature profiles show $\Delta T \geq 10$ K, so the threshold criterion for ignition delay (t) is satisfied. This region covers a temperature range from approximately 1070 K up to 1300 K for Ω from approximately 0.5 up to the maximum value considered.
The "dynamic regime" area, ranging from T_{in} = 1100 K up to 1250 K, straddles the stoichiometric condition.
An analogous identification of regimes can also be made when CO_2 or H_2O instead of N_2 is used as the diluent species.
Figure 4.19b is relative to mixtures diluted in CO_2. All the regions are evidently shifted toward higher initial temperatures. More specifically, the combustion does not occur for temperature below 1100 K, whereas the slow combustion region extends up to approximately 1240 K under very lean conditions. The combustion region shrinks, especially in the lean region of the map, to cover a temperature range from 1240 K to 1300 K for Ω = 10. The same path is followed by the dynamic region that straddles the stoichiometric condition from 1200 K to below 1300 K. In the same way, the presence of H_2O (Fig. 4.19c) as diluent stresses the variations described for the CO_2 dilution with respect to N_2 dilution. Thus, the reactivity of the mixture is not appreciable up to 1140 K, where the low reactivity region ranges from Ω = 3 up to Ω = 10. The ignition region extends from 1180 K for Ω = 3 up to 1300 K for Ω in the range 0.75-8.5.
The change in mixture reactivity observed using different diluents is also evident in the comparison of t evaluated from the temperature profiles.
Figure 4.20 shows experimental and numerical ignition values for pyrolysis gas/oxygen mixtures at 90% of the dilution for the three diluents and ultra-lean conditions.

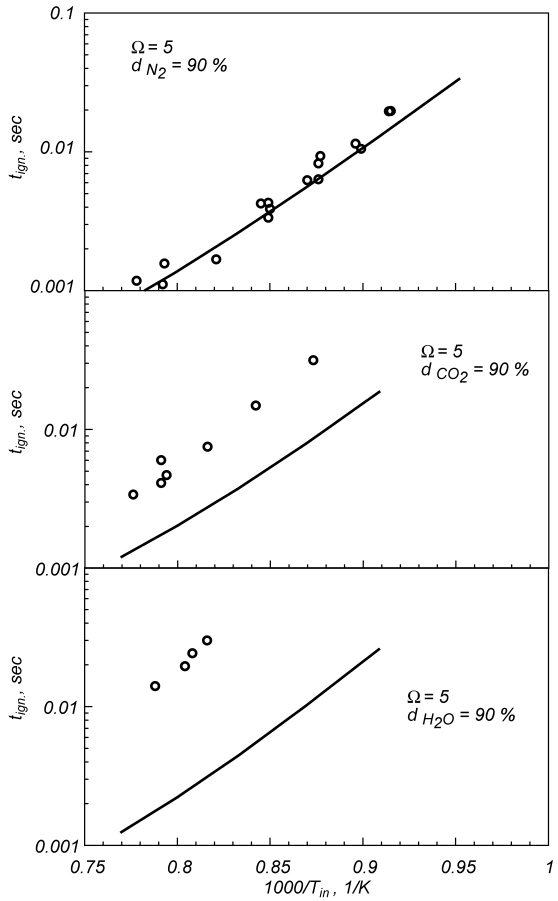

Fig. 4.20 – Experimental and numerical $t_{N2,\ CO2,\ H2O}$ for pyrolysis gas/oxygen mixtures at Ω = 5.

For ultra-lean conditions (Ω =5), the experimental auto-ignition delay times are quite well reproduced by the numerical simulations for the system diluted in N_2. In case of systems diluted with CO_2 and H_2O, the agreement is not so good as in case of the mixtures diluted in N_2. To quantify at a glance such discrepancies, a parameter $K_{diluent}$ was introduced. It was defined as the ratio between experimental and numerical ignition times.
The $K_{diluent}$ factor is 2 for the system diluted in CO_2, while it is 10 for the systems diluted in H_2O, confirming the inadequacy of the kinetic mechanisms to predict the auto-ignition delay times when CO_2 and H_2O dilute the mixture.
Figure 4.21 shows experimental and numerical ignition values for pyrolysis gas/oxygen mixtures at 90% of the dilution, for several oxygen feed ratios Ω (1.67, 1, 0.9) and for the three diluents.

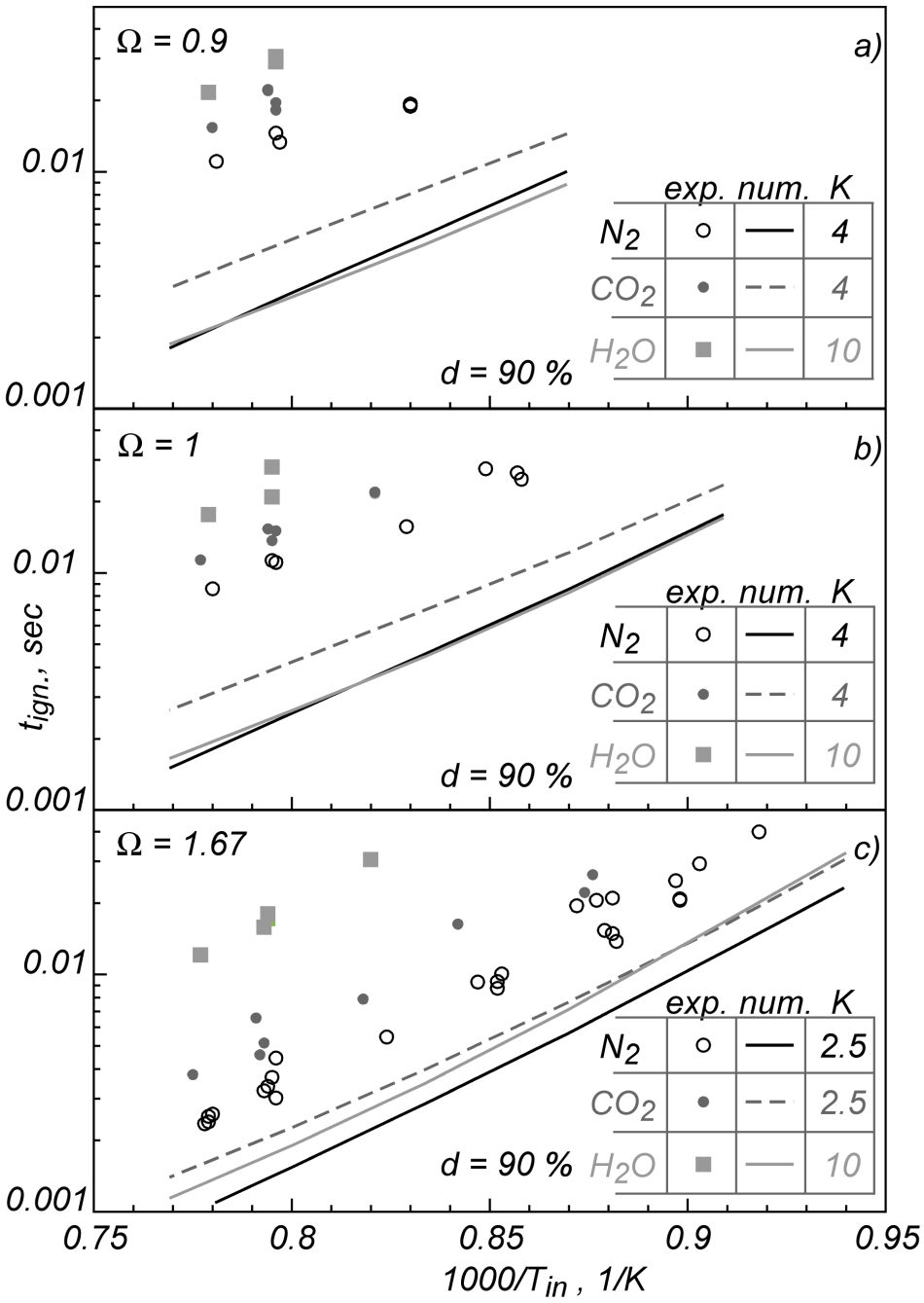

Fig. 4.21 – Experimental (symbols) and numerical (lines) ignition delay times (t) at atmospheric pressure for pyrolysis gas/oxygen mixtures diluted at 90% in $N_2/CO_2/H_2O$ at Ω = 0.9 (a), 1 (b), 1.67 (c).

Some noticeable discrepancies between experimental and numerical data occurred. In the system diluted with N_2, for $\Omega = 1.67$, $K_{N2} = 2.5$, while for the stoichiometric and the fuel rich conditions, $K_{N2} = 4$. In general, the parameter K_{N2} increases passing from fuel lean to rich mixtures and this had also been seen previously in the case of propane mixtures. Such trends again suggest a net dependence of the ignition process on mixture composition.
In the case relative to pyrolysis gas/oxygen mixtures diluted with CO_2 and H_2O, for any considered Ω, the experimental t_{H2O} are always longer than t related to the other diluents, while t_{N2} are the shortest ones. The parameter t_{CO2} always lies between t_{N2} and t_{H2O}.
Numerical results show that the values of t_{CO2} are always longer than the values of t_{N2} and t_{H2O}, depicting a dependence of autoignition delay times on the diluent species that is relatively different with respect to the experimental autoignition delay. In particular, for $\Omega = 0.9$ (Fig. 4.21a) and 1 (Fig. 4.21b), the numerical t_{CO2} is longer than both t_{N2} and t_{H2O}, that result to be close to each other. For $\Omega = 1.67$ (Fig. 4.21c), t_{CO2} and t_{H2O} are very similar at low temperatures, while for $1000/T_{in} < 0.9$, t_{H2O} becomes shorter than t_{CO2}. For this mixture composition, the numerical t_{N2} are always shorter than the ones relative to the other diluents.
In general, numerical predictions significantly underestimate the experimental data. For $\Omega = 0.9$ and 1, $K_{N2} = K_{CO2} = 4$, while $K_{H2O} = 10$. In the case of lean mixtures, $K_{N2} = K_{CO2} = 2.5$ and $K_{H2O} = 10$. Also this is in perfect agreement with what observed in the case of propane mixtures. However, it should be emphasized that increasing the fuel complexity, that is, moving from propane mixtures to pyrolysis gas mixtures, the disagreement between experimental and numerical results increases.

4.2 Jet Stirred Flow Reactor results

With regard to the experiments realized in the two JSFRs (Napoli and Nancy), the parameters that have been varied are the fuel type, the diluent type, the inlet temperature, and the equivalence ratio. The influence of these parameters has been studied by measuring the outlet concentrations of chemical species. In addition, in the Napoli JSFR also the temperature inside the reactor has been measured. Experiments are performed at a constant pressure (1.1 bar for the Napoli reactor and 1.05 bar for the Nancy reactor) and at a fixed residence time (τ) (0.5 s in the Napoli reactor and 2 s in the Nancy reactor). The behaviours of various results are considered by assuming one parameter varying while the others are fixed.
The measured concentration species, along with all the operative conditions in which experiments in the JSFR have been carried on, are listed in the Appendix.

4.2.1 Methane mixtures

All experiments (in both reactors) were conducted maintaining the molar fraction of diluent at 0.9.
The experimental conditions are summarized in Table 4.4.

d (%)	Φ	τ (s)	CH_4 (vol%)	O_2 (vol%)	He (vol%)	N_2 (vol%)	CO_2 (vol%)	H_2O (vol%)	Number of experiments
90	0.5	0.5	2.00	8.00	0	90	0	0	22
90	0.5	0.5	2.00	8.00	0	0	90	0	15
90	0.5	0.5	2.00	8.00	0	81	9	0	1
90	0.5	0.5	2.00	8.00	0	72	18	0	1
90	0.5	0.5	2.00	8.00	0	63	27	0	1
90	0.5	0.5	2.00	8.00	0	49.5	40.5	0	1
90	0.5	0.5	2.00	8.00	0	22.5	67.5	0	1
90	0.5	0.5	2.00	8.00	0	81	0	9	1
90	0.5	0.5	2.00	8.00	0	72	0	18	1
90	0.5	0.5	2.00	8.00	0	63	0	27	1

90	0.5	0.5	2.00	8.00	0	49.5	0	40.5	20
90	0.5	2	2.00	8.00	90	0	0	0	14
90	0.5	2	2.00	8.00	0	90	0	0	13
90	0.5	2	2.00	8.00	0	0	90	0	14
90	1	0.5	3.33	6.67	0	90	0	0	24
90	1	0.5	3.33	6.67	0	0	90	0	15
90	1	0.5	3.33	6.67	0	49.5	0	40.5	22
90	1	2	3.33	6.67	90	0	0	0	20
90	1	2	3.33	6.67	0	90	0	0	15
90	1	2	3.33	6.67	0	0	90	0	15
90	1.5	0.5	4.29	5.71	0	90	0	0	25
90	1.5	0.5	4.29	5.71	0	0	90	0	17
90	1.5	0.5	4.29	5.71	0	49.5	0	40.5	23
90	2	2	5.00	5.00	90	0	0	0	15
90	2	2	5.00	5.00	0	90	0	0	15
90	2	2	5.00	5.00	0	0	90	0	15

Table 4.4 – Experimental conditions studied in the JSFRs for CH_4 mixtures. 795 K < T_{in} < 1225 K, P = 1.1 atm when τ = 0.5 s and P = 1.05 atm when τ = 2 s.

Influence of temperature

In order to show the influence of temperature on the methane mixtures results, the stoichiometric mixture diluted in N_2 is used as a reference case.

As for the PFR results, also in this case in order to value the mechanisms performance and to elucidate some peculiar features of the oxidation process of methane under diluted conditions, a preliminary analysis was performed comparing the experimental and numerical species profiles as a function of T_{in} along with the ΔT. Results for ΔT, CH_4 and O_2 conversions of stoichiometric $CH_4/O_2/N_2$ mixtures at 90% of dilution, inlet temperatures from 795 K to 1210 K and τ = 0.5 s are plotted in Fig. 4.22, together with the calculated data only from the CRECK-2014 and the AramcoMech_1.3-2016 models, which were found to be the best performing among the tested models. It should be stated that under these conditions also the Dagaut-2010 mechanism was found to be performing. However, the aim of this comparison, in addition to test the available mechanisms, is to choose the best model in order to analyse the effect of the different parameters on the oxidation characteristics. One of these investigated parameters is the effect of the bath gas. Since in this dataset also helium was used as diluent, which is not included among the species in the Dagaut-2010 model, it has been preferred to exclude such a mechanism from the comparison.

In Fig. 4.22 symbols represent experimental results while the predictions are reported with lines.

The oxidation onset is experimentally identifiable for T_{in} = 1070 K, as the reactor temperature starts increasing, while methane and oxygen concentrations slightly diminish.

The system temperature increases up to T_{in} = 1100 K. For higher T_{in}, the methane oxidation occurs throughout a periodic oscillatory regime characterized by temperature oscillations. Oscillations were observed as the temperature changes in time. For this oxidation regime, two ΔT are reported for the same T_{in} in Fig. 4.22. They correspond to the maximum and minimum values detected during the oscillatory behaviour. Different types of oscillatory behaviour are observed depending on the inlet temperature and mixture composition. Figure 4.23 shows examples of the type of behaviour that can be observed, by varying the inlet conditions. It should be stressed that both the type of oscillations observed, and the operating conditions for which they occur, are in excellent agreement with the results of de Joannon et al. (2005) and Sabia et al. (2007), obtained in a different reactor than that used in this work. For this reason, the same classification of the type of oscillations made in the just cited papers has been used, i.e. bell-shape, double, cusp-shape, triangular, irregular, and damped. These oscillations are similar to those observed in the PFR.

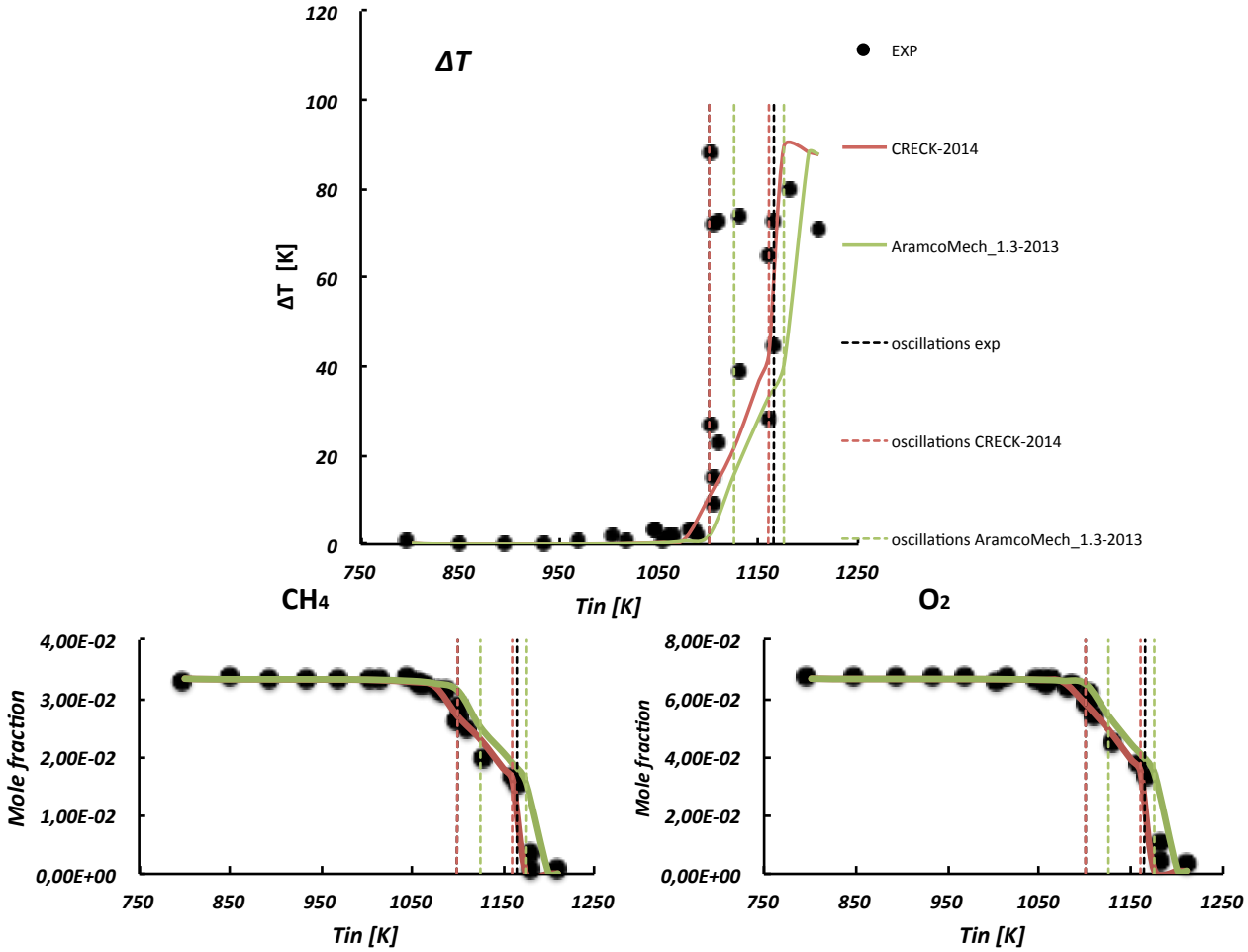

Fig. 4.22 – Experimental (symbols) and numerical (lines) ΔT and concentration profiles versus inlet temperature. Φ = 1, τ = 0.5 s, p = 1.1 atm, d = 90% N_2.

In particular, similarly to the PFR, they are characterized by a faint pulsing blue luminosity. Also in this case, as in the PFR, it is possible to say that these fluctuations are not attributed to irregularities in velocity, temperature, or fuel concentration, but, as can be seen from Fig. 4.23, they are periodic, with a frequency of about 1 Hz. In addition, previous studies (Sabia 2006) had shown that the temperature inside the reactor is essential uniform (in space), also during the oscillations. In particular, in order to collect the spontaneous light emitted from the reacting volume, an intensified CCD camera, sensible in a wide spectral range, was used. An example of images collected during oscillations obtained for an inlet temperature of 1125 K and a Φ of 1.2 were reported in Fig. 4.24, where Fig. 4.24a represents an image of reactor detected in correspondence of the minimum temperature acquired during the oscillation of 1135 K, i.e. 10 degrees higher than T_{in}. It shows that, in this condition, no luminous signal can be detected in the wavelength range here considered. The reactor image detected in correspondence of the maximum oscillation temperature of 1458 K was reported in Fig. 4.24b. It shows that the luminous signal can be detected from the whole reactor volume and it is uniformly distributed. The same results were obtained in the most of the experimental conditions, thus testifying that the system works in well-mixed conditions.

In such a case, the measured concentration values are averaged over time because of the time that elapses for the gas sampling before the chemical analyses, thus only one value is reported in Fig. 4.22. It should be underlined that the sampling time is about 20 s, then about 20 times greater than one cycle time. Therefore, the error committed in considering an averaged value is inside the measurement uncertainty.

For T_{in} > 1180 K the periodic regime is interrupted and the system becomes stable again.

The O_2 profile is very similar to the methane one. Actually its concentration monotonically diminishes with T_{in}.

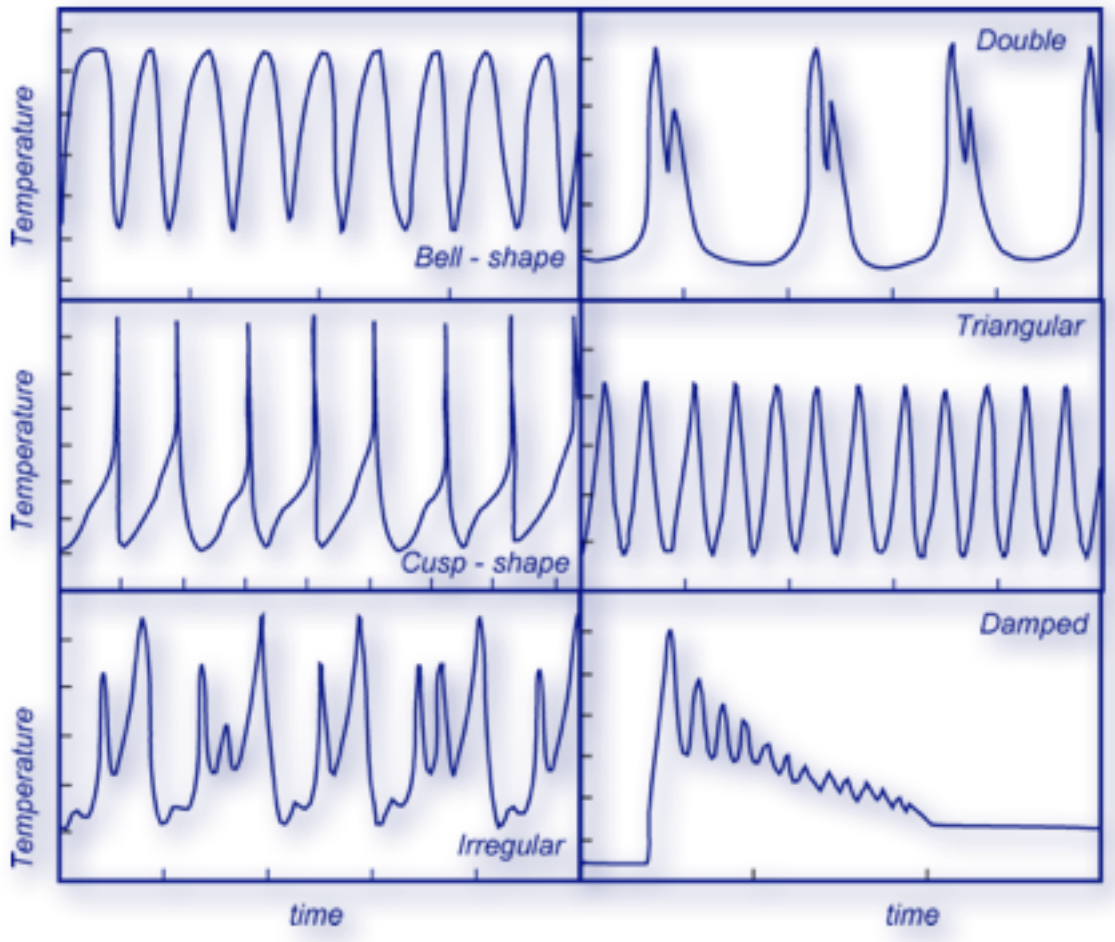

Fig. 4.23 - Characteristic temporal temperature profiles during periodic regimes (the temperature profiles as a function of time have been reported on arbitrary scales to identify the characteristic behaviours).

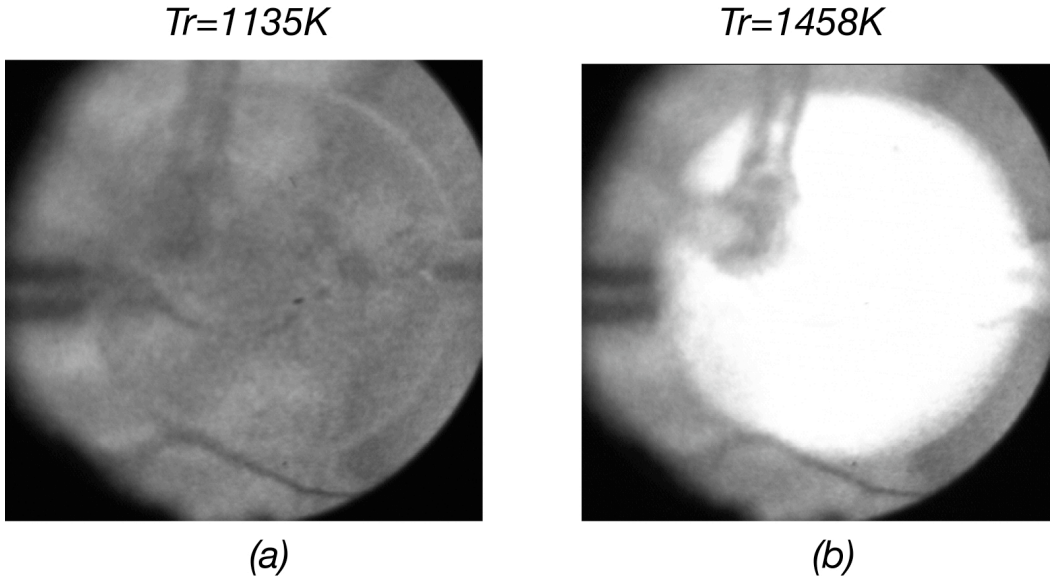

Fig. 4.24 – JSFR images at $\Phi = 1.2$ and d = 90% (adapted from Sabia 2006).

Along with the experimental data, Fig. 4.22 also reports the numerical simulations obtained with the two chosen kinetic mechanisms. The CRECK-2014 scheme well predicts the onset of the oxidation reactions (around 1070 K), whereas for the AramcoMech_1.3-2016 this onset is slightly shifted to higher inlet temperatures. For T_{in} = 1100 K, both the kinetic mechanisms predict the insurgence of temperature oscillations in time that persist up to T_{in} = 1175 K. The operating conditions for which the oscillatory behaviours were experimentally and numerically detected are identified on Fig. 4.22 with vertical dashed lines. It can be seen that both the mechanisms are capable of predicting the oscillatory behaviour with an excellent accuracy. In the case of oscillations, the temperatures reported in Fig. 4.22 are reported as time averaged values considering an oscillation period. Such a choice comes from the consideration that the numerical temperature oscillation amplitudes are considerably higher than the experimental ones. Thus, for the sake of clearness of the figure, just the averaged values are reported. With both the kinetic mechanisms, numerical working temperatures are slightly lower than the experimental ones, while a good agreement between numerical and experimental CH_4 and O_2 concentrations is observable. Overall, both mechanisms show a very similar performance. The results for the CRECK-2014 are slightly better than those of the AramcoMech_1.3-2016. Based on this comparison, the CRECK-2014 mechanism was selected to simulate the JSFR experimental data.
Figure 4.25 shows the performance of the CRECK-2014 mechanism in reproducing outlet concentrations for various species measured in the JSFR as a function of T_{in}.

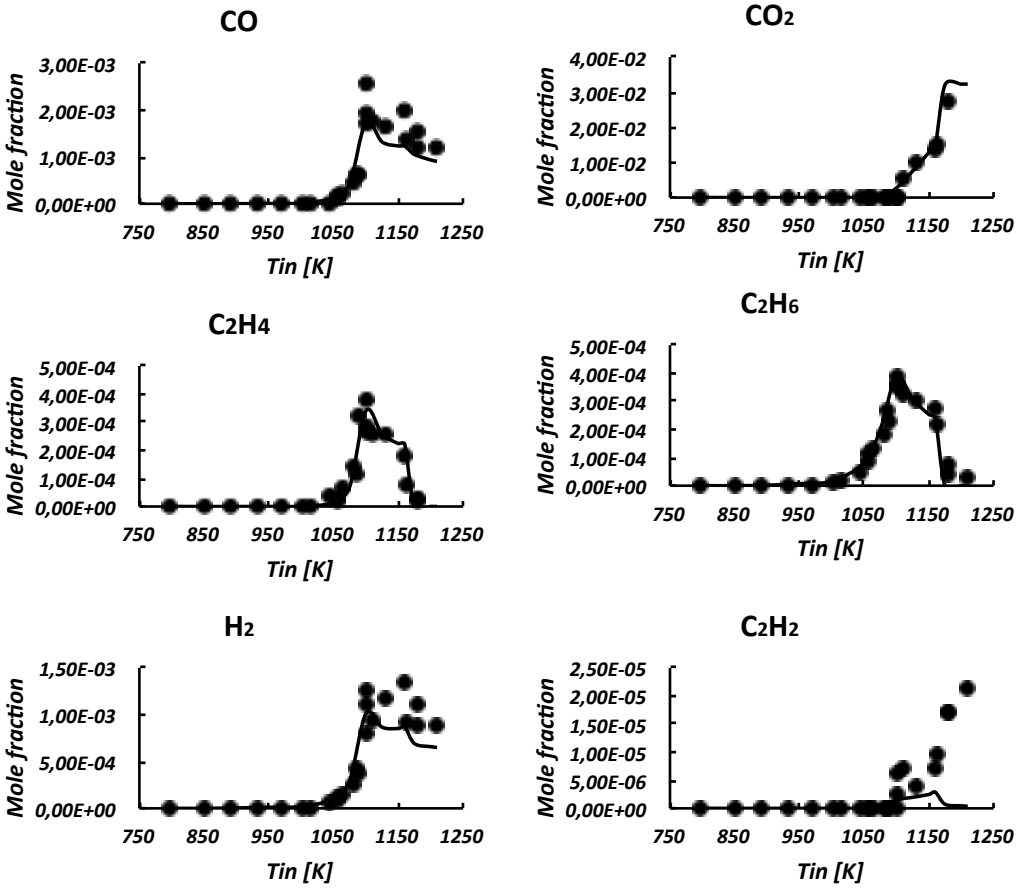

Fig. 4.25 - Experimental (symbols) and numerical (lines) concentration profiles versus inlet temperature. Φ = 1, τ = 0.5 s, p = 1.1 atm, d = 90% N_2.

As can be seen from Fig. 4.25, all the experimental intermediate species start to form in correspondence of methane and oxygen consumption. The predictions are also in very good

agreement with the experimental data for major and minor species shown in Fig. 4.25. However, the comparison of simulated C_2H_2 profiles with the experimental data shows some differences. In particular, C_2H_2 concentration is consistently underestimated.
Figure 4.26 depicts the experimental and numerical concentrations of chemical species as a function of T_{in} for stoichiometric methane/oxygen mixtures diluted at 90% in N_2 obtained in the Nancy JSFR at $\tau = 2$ s.

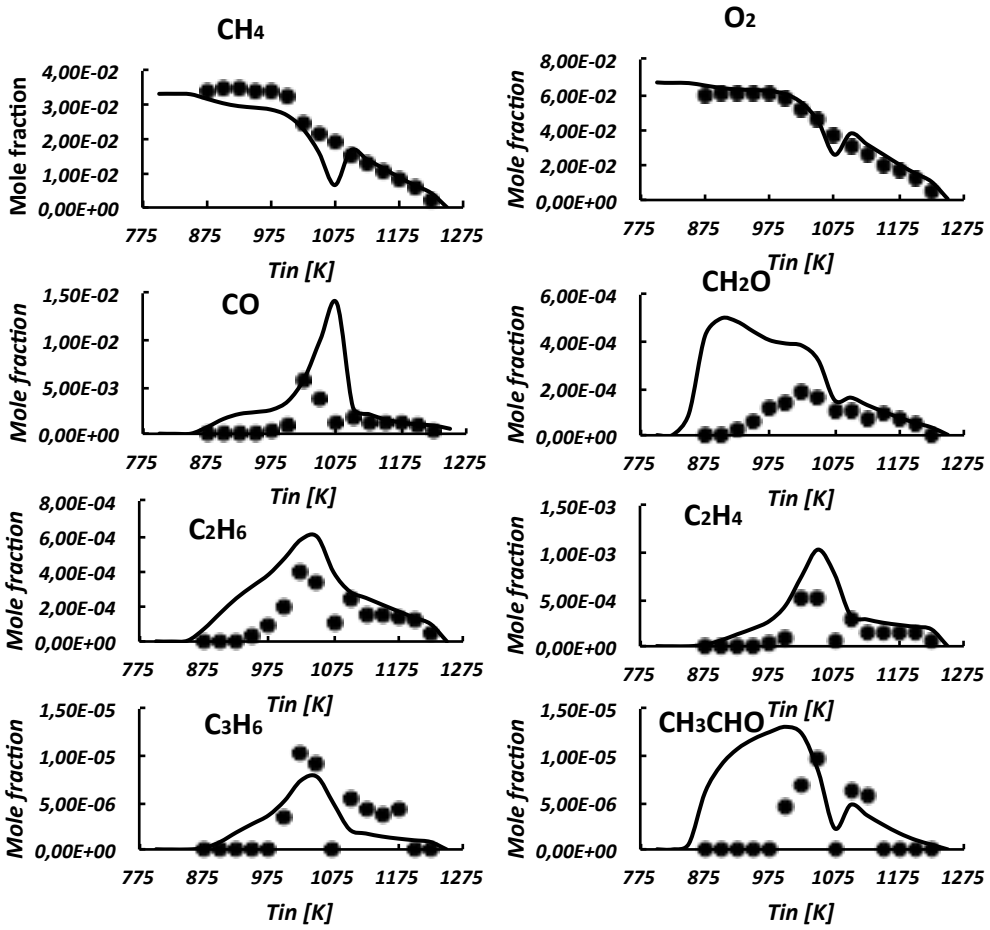

Fig. 4.26 – Experimental (symbols) and numerical (lines) concentration profiles versus inlet temperature. $\Phi = 1$, $\tau = 2$ s, p = 1.05 atm, d = 90% N_2.

The methane and the oxygen profiles with T_{in} for the mixture at $\tau = 2$ s are similar to the ones obtained with a residence time of 0.5 s. Nonetheless, Fig. 4.26 shows that for such a mixture the oxidation onset occurs for $T_{in} = 1000$ K, thus slightly anticipating the reactivity with respect to the system at $\tau = 0.5$ s, as it is expected from a system with a higher residence time. For 1050 K < T_{in} < 1200 K, the periodic dynamic behaviour is also experimentally detected for the system with a higher residence time. The dynamic behaviour occurs for a slightly wider T_{in} range in the case of mixture with a $\tau = 2$ s. It should be pointed out that in the Napoli JSFR the temperature fluctuations are measured with a thermocouple, whereas in the Nancy JSFR there are no thermocouples inserted into the reactor, but pressure excursions are followed by a pressure transducer. Thus, it is possible to detect this type of behaviour, but it is not possible to compare in detail the oscillations observed in the two systems. However, a rough comparison between the temperature fluctuations detected in the Napoli JSFR and the pressure fluctuations observed in the Nancy JSFR suggests that the oscillations observed in the two different systems are characterized by the same frequencies.
Intermediate species detection showed signals of C_1, C_2 and C_3 compounds. Mole fraction maxima are in the range of 10^{-2} to 10^{-6}. Species with more than three carbon atoms were not detected within

the detection limit (about 1 ppm). C_2H_6, C_2H_4 and C_2H_2 are formed, involving CH_3 recombination, and their maxima appear sequentially shifted to slightly higher temperatures, consistent with detailed methane oxidation schemes. However, the kinetic mechanism anticipates the consumption of the reactants with respect to test results. For $T_{in} > 1100$ K, a good agreement between numerical and experimental data is observable. For $T_{in} = 1100$ K, also in this case the kinetic mechanism predicts the insurgence of oscillations in time that persists up to $T_{in} = 1200$ K. It should be recalled that in this case, the simulations were made under isothermal conditions. Nonetheless, the model predicts oscillatory behaviours. This confirms the purely chemical nature of this phenomenology, which will be addressed in the next chapter.
In correspondence of the onset of the oscillatory behaviour, both the measured and the simulated concentrations show a discontinuity with an abrupt decrease of concentration. With increasing the inlet temperature, the concentrations again increase, or at least reach a plateau level. Such a trend is well predicted by the mechanism.

Influence of equivalence ratio and diluent: He, N_2, CO_2 and H_2O
In this section, the results for methane/oxygen mixtures diluted at 90% in nitrogen, carbon dioxide and 49.5% nitrogen-40.5% water are reported for the Napoli experiments, from lean to rich conditions at $\tau = 0.5$ s, while the results for mixtures diluted at 90% in helium, nitrogen and carbon dioxide are reported for the Nancy experiments, from lean to rich conditions at $\tau = 2$ s.
It must be underlined that, for the mixture diluted in water the dilution is still 90%, but it was not possible to fully dilute the mixture in water because, as explained in the previous chapter, the CEM system works with a carrier gas.
In order to elucidate some peculiar features of the methane oxidation process under diluted conditions, for different equivalence ratios and diluents, and to value the mechanisms performance in predicting these features, only the concentrations of some main species as a function of T_{in} are presented. In particular for the Napoli experiments, the concentrations of CH_4, O_2, CO and H_2 are shown, while for the Nancy experiments, since for the detection of chemical species through gas chromatography it was always used helium as carrier gas, it was not possible to detect hydrogen. Therefore, instead of hydrogen, the concentration of formaldehyde is presented, which was not detected in the Napoli experiments.
All the other measured concentration species, along with all the operative conditions in which experiments in the JSFR have been carried on, are available upon request.
The simulated concentrations were obtained using the CRECK-2014 mechanism. A preliminary analysis (not reported here) showed that CRECK-2014 model is appropriate for most types of bath gases, while other mechanisms perform well for one type of bath gas and poorly for another.
Experimental and numerical results obtained in stoichiometric conditions for CH_4/O_2 diluted in N_2, CO_2, and N_2-H_2O are shown in Fig. 4.27. Black circles symbols represent experimental results for the N_2-diluted system, blue square symbols represent experimental results for the N_2-H_2O-diluted system, while green triangles are relative to the CO_2-diluted system. The predictions are reported with black lines for N_2, blue lines for N_2-H_2O and green lines for CO_2. The N_2 results are the same presented in Figs. 4.24 and 4.25. The experimental CH_4 and O_2 profiles with T_{in} for the mixtures diluted in CO_2 or N_2-H_2O are similar to the ones relative to the N_2-diluted mixture. Nonetheless, Fig. 4.27 shows that for CO_2 and N_2-H_2O mixtures the reactants concentrations are slightly higher than the ones detected for the N_2 mixture and the difference among the different diluted mixtures is higher for higher temperatures, in particular for the CO_2-diluted mixture.
The effect of diluent is higher for the intermediate species. For example, in stoichiometric conditions, the relative difference of CO concentration between CO_2-diluted system and N_2 diluted system is about 0.45 for $T_{in} = 1115$ K. This value is the same obtained for the N_2-H_2O-diluted system. At $T_{in} = 1210$ K the relative difference of CO concentration between CO_2 and N_2 dilution reaches about 0.8. This value is twice that obtained for the mixture diluted simultaneously in N_2 and H_2O for the same inlet temperature. Furthermore, starting from $T_{in} = 1100$ K, while in N_2- and N_2-

H_2O-diluted systems the CO concentration decreases with increasing temperature, in CO_2 dilution the trend is the opposite, i.e. the CO concentration increases with temperature. This may indicate that chemical effects of steam addition on CO concentration are reduced for high temperatures compared to CO_2.

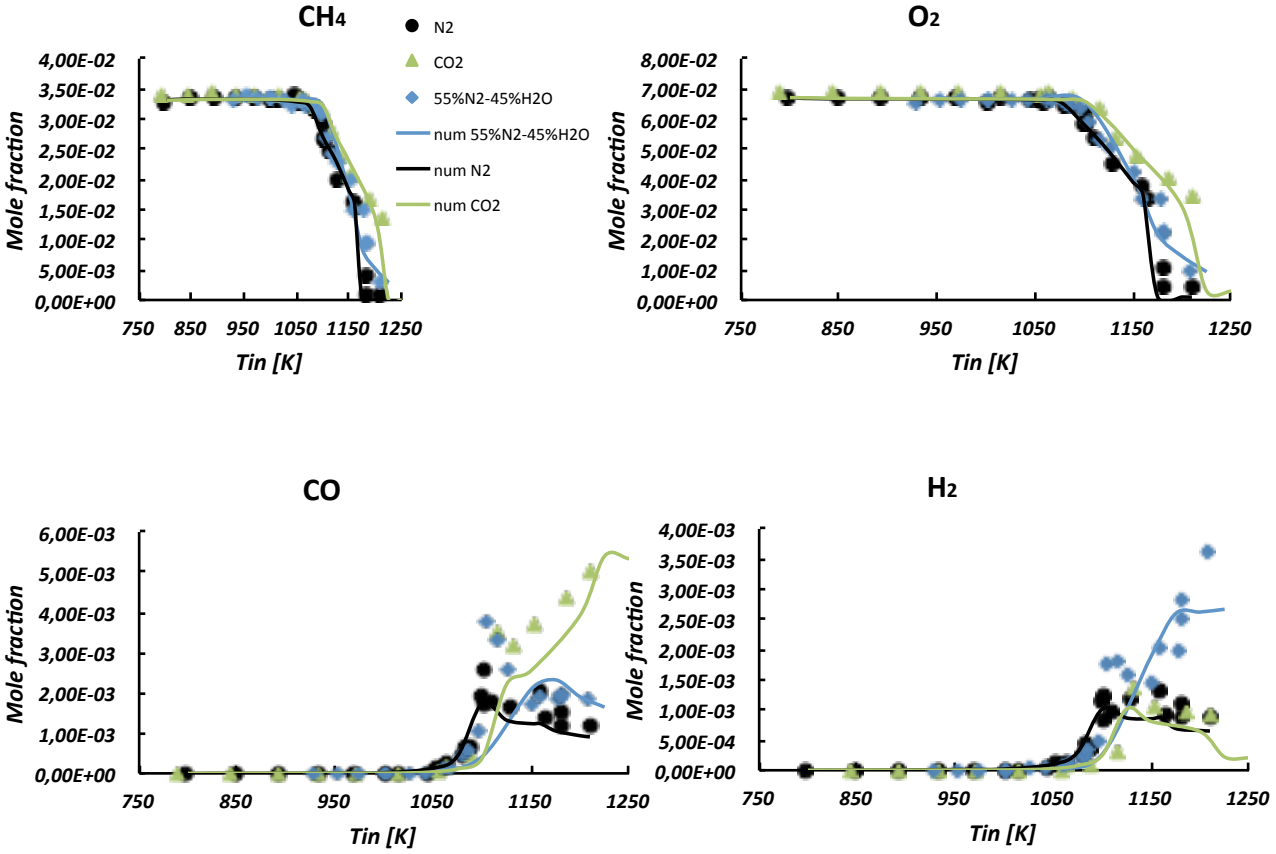

Fig. 4.27 - Experimental (symbols) and numerical (lines) concentration profiles versus inlet temperature. $\Phi = 1$, $\tau = 0.5$ s, p = 1.1 atm, d = 90%, N_2 (circle symbols), CO_2 (triangle symbols), N_2-H_2O (square symbols).

A similar trend is observable for the H_2. In particular, the relative difference of H_2 concentration between CO_2-diluted system and N_2-diluted system is negligible, while it is about 0.8 for the N_2-H_2O-diluted system at 1210 K. Furthermore, similarly to CO, starting from T_{in} = 1100 K, while in N_2- and CO_2-diluted systems the H_2 concentration decreases with increasing temperature, in N_2-H_2O dilution the trend is the opposite, i.e. the H_2 concentration increases with temperature. Therefore, chemical effects of water addition have an impact on H_2 concentration, rather than CO concentration, as in the case of CO_2 addition.

The periodic dynamic behaviour is also experimentally detected for the system diluted in CO_2, for $T_{in} > 1130$ K, and for the system diluted in N_2-H_2O, for $1115 < T_{in} < 1180$ K. Therefore, the dynamic behaviour occurs for higher T_{in} in the case of mixtures diluted in CO_2 and N_2-H_2O, compared to N_2-dilution.

Figure 4.27 also investigates the performance of the CRECK-2014 mechanism to predict species concentrations measurements according to the type of the bath gas or diluent mixture. The predictions are in good agreement with the experimental data. Furthermore, the model well predicts the retarding effect of H_2O and CO_2 on the temperature onset of the dynamic behaviour with respect

to the mixture inlet temperatures. However, for the majority of the species, experiments using N_2-containing mixtures tend to be better predicted than those with CO_2- or H_2O-containing mixtures. Results are now presented in Fig. 4.28 for CH_4/O_2 mixtures diluted in helium, nitrogen, and CO_2, for stoichiometric mixtures, at $\tau = 2$ s.

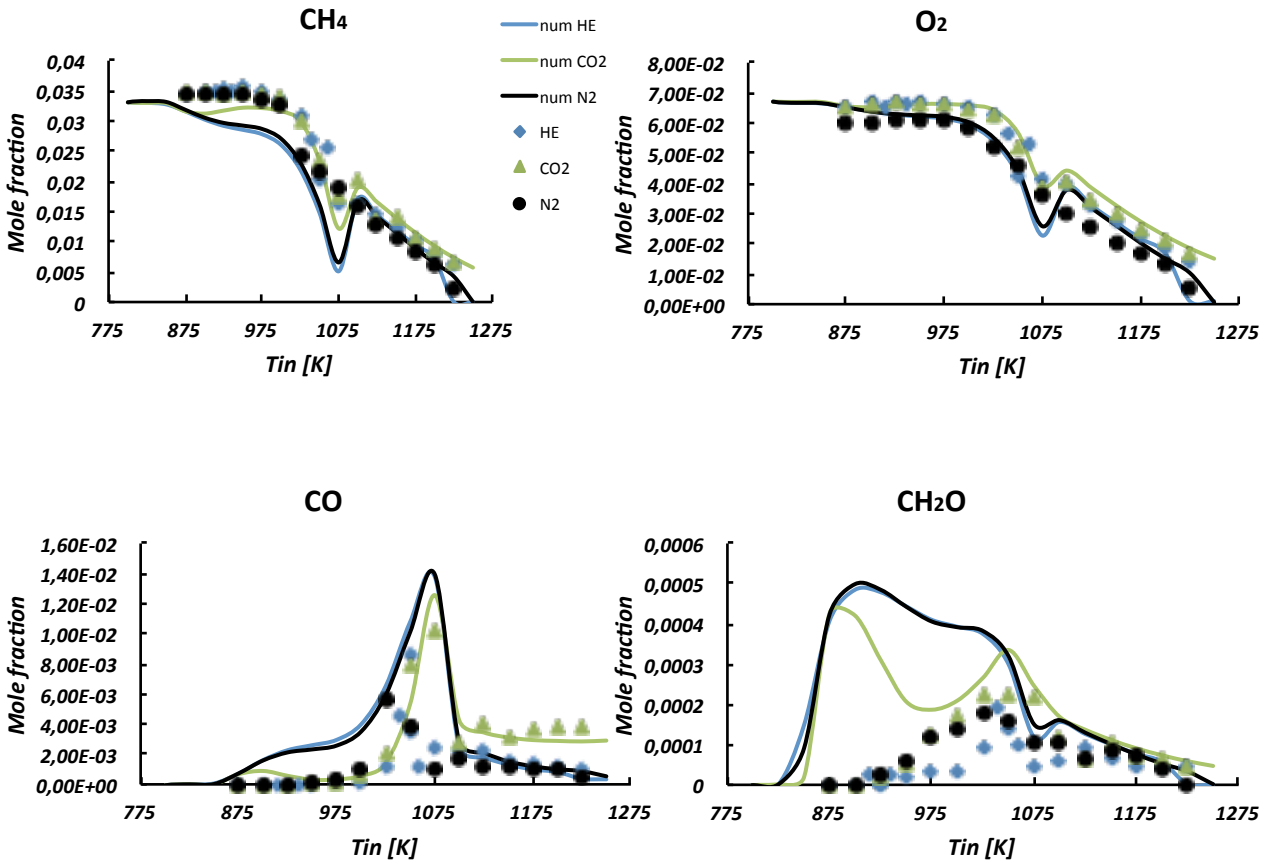

Fig. 4.28 - Experimental (symbols) and numerical (lines) concentration profiles versus inlet temperature. $\Phi = 1$, $\tau = 2$ s, p = 1.05 atm, d = 90%, N_2 (circle symbols), CO_2 (triangle symbols), He (square symbols).

Black circles symbols represent experimental results for the N_2-diluted system, blue square symbols represent experimental results for the He-diluted system, while green triangles are relative to the CO_2-diluted system. The predictions are reported with black lines for N_2, blue lines for He and green lines for CO_2. The N_2 results are the same presented in Figs. 4.26. It should be stated that the oxygen concentration in the system diluted in nitrogen is affected by a higher error, given the co-elution of these two species on the Carboshpere column because of the closeness of the retention times.

The experimental profiles with T_{in} for the mixtures diluted in He or CO_2 are similar to the ones relative to the N_2-diluted mixture. Nonetheless, it is worth emphasizing that at low temperatures (T_{in} < 1100 K) there is an unexpected difference between the data obtained in nitrogen and the data obtained in He. This suggests that there may be an impact of nitrogen on the chemical species profiles that reduces with increasing inlet temperature.

Furthermore, Fig. 4.28 shows that, contrary to what observed in Fig. 4.27 ($\tau = 0.5$ s), the difference among the different diluted mixtures is higher for lower temperatures, while it is negligible for higher temperatures. This implies that also the residence time plays a fundamental role in the evolution of the oxidation process.

However, at high temperature, a CO_2 effect is still encountered in the CO concentration. In particular, the relative difference of CO concentration between CO_2-diluted system and N_2-diluted system increases with increasing temperature and reaches about 0.8 for T_{in} = 1225 K, that is almost the same value obtained for a residence time of 0.5 s, for the same inlet temperatures. Furthermore, starting from T_{in} = 1100 K, while in N_2- and He-diluted systems the CO concentration decreases with increasing temperature, in CO_2 dilution the trend is the opposite, i.e. the CO concentration increases with temperature, or at least reaches a plateau level. The T_{in} value for which this behaviour is observed (1100 K), is the same as in the case of τ = 0.5 s (Fig. 4.27).
The periodic dynamic behaviour is also experimentally detected for the system diluted in CO_2, for T_{in} > 1100 K, and for the system diluted in He, for T_{in} > 1060 K. Therefore, compared to N_2 dilution, the dynamic behaviour occurs for higher T_{in} in the case of mixtures diluted in CO_2, and about the same temperature in the case of mixtures diluted in He.
Figure 4.28 also investigates the performance of the CRECK-2014 mechanism to predict species concentrations measurements according to the type of the bath gas or diluent mixture. The mechanism overpredicts the measured conversion, and thus the intermediate species concentrations, at low temperatures for the mixtures diluted in helium and nitrogen. Furthermore, the mechanism does not predict any difference between the results obtained in N_2 and He dilution. Moreover, the model does not predict the retarding effect of CO_2 on the temperature onset of the dynamic behaviour with respect to the mixture inlet temperatures. However, predictions for the CO_2 diluted system show a better agreement with the measured concentrations, despite an overprediction of formaldehyde for low temperatures.

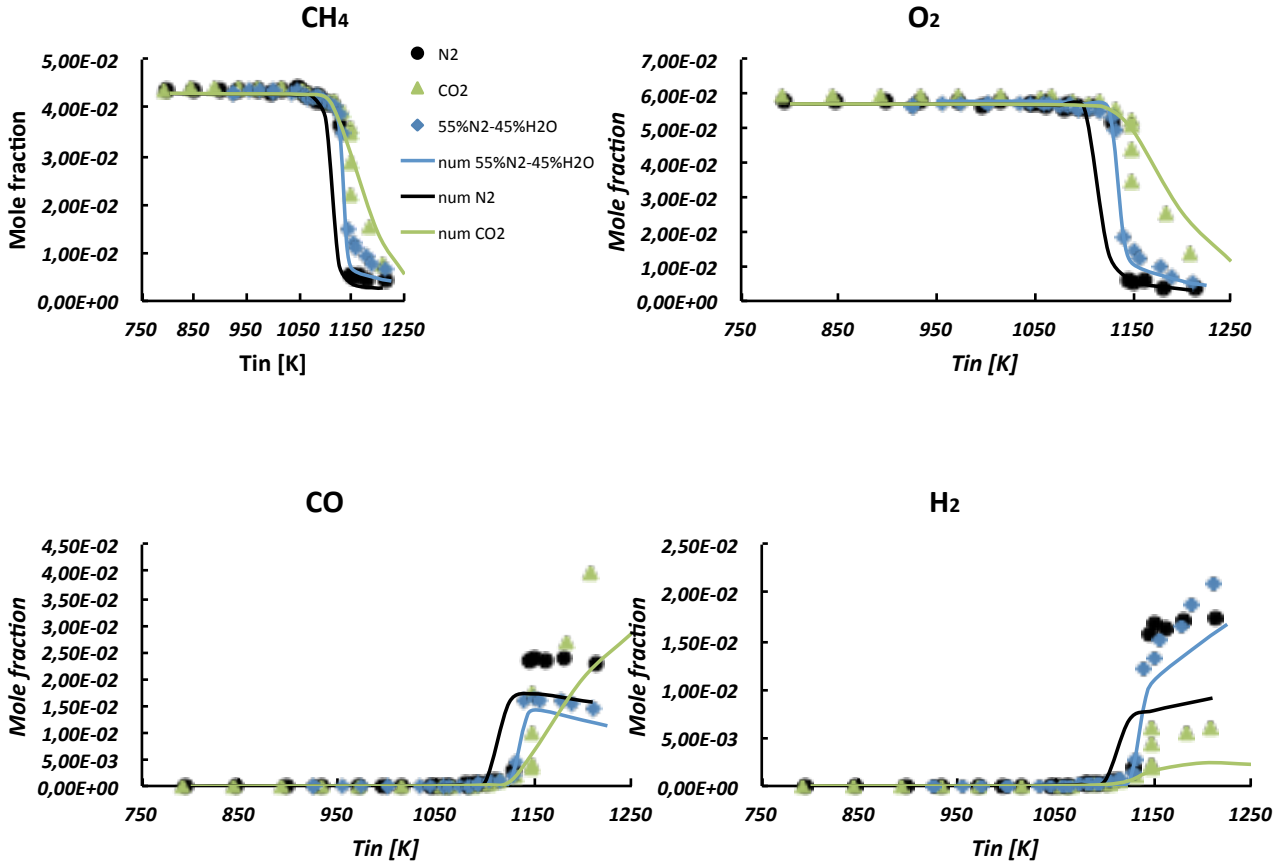

Fig. 4.29 - Experimental (symbols) and numerical (lines) concentration profiles versus inlet temperature. Φ = 1.5, τ = 0.5 s, p = 1.1 atm, d = 90%, N_2 (circle symbols), CO_2 (triangle symbols), N_2-H_2O (square symbols).

The chemical species profiles as a function of inlet temperature of rich CH_4/O_2 mixtures ($\Phi = 1.5$) diluted in N_2, CO_2, or N_2-H_2O at $\tau = 0.5$ s are plotted in Fig. 4.29.
For $\Phi = 1.5$, the experimental onset of the oxidation reactions is identified for $T_{in} > 1065$ K for the N_2-diluted system. Afterwards the conversion abruptly increases and for $T_{in} = 1145$ K the conversion is almost complete. Under rich conditions no stable periodic oscillatory regimes occur, but only damped oscillation in a very narrow inlet temperature range (around 1145 K) have been observed.
CO_2 and H_2O slow down the system reactivity. As matter of fact, oxygen and methane concentrations are higher than the ones obtained for the nitrogen reference case. Similar to the stoichiometric case, the influence of diluent is higher for higher inlet temperatures. For example for $T_{in} = 1210$ K, the CH_4 concentration is 0.42% for the mixture diluted in N_2, 0.64% for the system diluted both in N_2 and H_2O, and 0.75% for the mixture diluted in CO_2, while oxygen content is respectively equal to about 0.39%, 0.51% and 1.35%.
Furthermore, for the CO_2-diluted system, a periodic regime is experimentally detected for $T_{in} > 1185$ K, while for the other mixtures only damped oscillations are detected.
In rich conditions, similar to stoichiometric condition, a quasi-linear increase of the CO concentration with inlet temperature is observed for the CO_2-diluted mixture, while for the other two diluted mixtures a plateau level is reached with CO concentrations of about 2.3% in N_2 and around 1.5% in N_2-H_2O. A similar trend is observed for H_2. In particular for the N_2-H_2O-diluted mixture, H_2 is monotonically produced, while, for the N_2-diluted system and the CO_2-diluted system, it is monotonically produced up to $T_{in} = 1150$ K, then the values remain almost constant and reach a plateau with H_2 concentrations of about 1.7% in N_2 and 0.6% in CO_2.
In the rich case, the numerical predictions of the species concentrations and the experimental results are in good agreement for the three diluent investigated. The CRECK-2014 mechanism correctly reproduces the general trend of species production/consumption as well as it predicts the effect of CO_2 and H_2O at low and high temperatures. Nonetheless, for the N_2-diluted system, the onset of the oxidation reactions occurs for a slightly lower T_{in} with respect to the experimental results and the CO and H_2 concentrations at high temperatures are slightly overestimated for the N_2- and N_2-H_2O-diluted systems. Furthermore, the model properly reproduces the narrow T_{in} range where temperature oscillations are experimentally detected.
Results are now presented in Fig. 4.30 for CH_4/O_2 mixtures diluted in helium, nitrogen, and CO_2, for a rich mixture ($\Phi = 2$), at $\tau = 2$ s.
Under these conditions, the experimental onset of the oxidation reactions is identified for $T_{in} > 1050$ K for the three diluted systems. Afterwards the conversion gradually increases. Under rich conditions no stable periodic oscillatory regimes occur.
The experimental profiles with T_{in} for the mixtures diluted in He or CO_2 are similar to the ones relative to the N_2-diluted mixture. Nonetheless, as observed under stoichiometric conditions, at low temperatures ($T_{in} < 1150$ K) there is a difference between the data obtained in nitrogen and the data obtained in He. This confirms that there may be an impact of nitrogen on the chemical species profiles that reduces with increasing inlet temperature.
Furthermore, Fig. 4.30 shows that, contrary to what observed in the stoichiometric conditions, the difference among the different diluted mixtures is higher for higher temperatures, particularly for the CO_2 that consistently slows down the reactivity.
In particular, at high temperature, the CO_2 effect is again encountered in the CO concentration. In particular, the relative difference of CO concentration between CO_2-diluted system and N_2-diluted system increases with increasing temperature and reaches about 0.4 for $T_{in} = 1225$ K. Furthermore, starting from $T_{in} = 1150$ K, while in N_2- and He-diluted systems the CO concentration increases very slowly with increasing temperature, in CO_2 dilution the CO concentration linearly increases with temperature. The T_{in} value for which this behaviour is observed (1150 K), is the same as in the case of $\tau = 0.5$ s (Fig. 4.29).

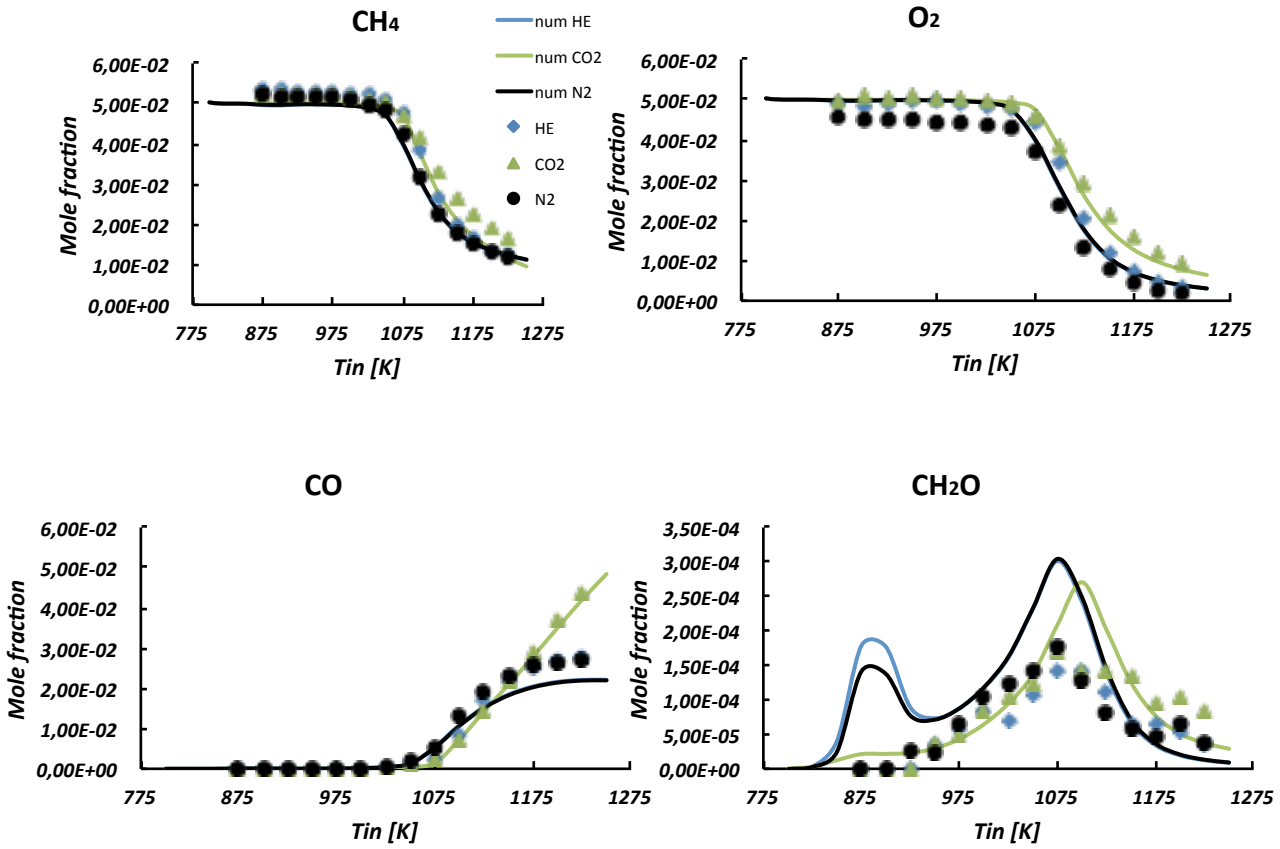

Fig. 4.30 - Experimental (symbols) and numerical (lines) concentration profiles versus inlet temperature. $\Phi = 2$, $\tau = 2$ s, p = 1.05 atm, d = 90%, N_2 (circle symbols), CO_2 (triangle symbols), He (square symbols).

Figure 4.30 also investigates the performance of the CRECK-2014 mechanism to predict species concentrations measurements according to the type of the bath gas or diluent mixture. As observed previously, in rich conditions the CO molar fraction increases linearly with increasing the inlet temperature, for the system diluted in CO_2. Solid lines indicate the computed species concentrations and show a similar linear dependence with CO_2 addition. For rich mixtures, numerical results obtained with the CRECK-2014 mechanism match well with the experimental results for the whole range of temperature and diluents explored, with the exception of an overprediction of formaldehyde for low temperatures in N_2 and He. However, the mechanism does not predict any difference between the results obtained in N_2 and He dilution. Moreover, the model slightly underestimates the CO_2 effect on the CH_4 conversion at high temperatures.

Figure 4. 31 shows the experimental and numerical main species concentration versus T_{in} for fuel lean ($\Phi = 0.5$) methane/oxygen mixtures, at $\tau = 0.5$ s.

For this equivalence ratio, experimental results indicate that the reaction onset occurs for T_{in} equal to about 1050 K for the N_2-diluted system, where periodic oscillations occur. For $T_{in} > 1100$ K methane oxidation process occurs throughout a stationary steady state. For the N_2-H_2O- and CO_2-diluted systems, the reactants profiles are similar to the N_2-diluted system. In particular their concentrations are higher than the ones obtained for the reference system. Therefore also for lean conditions, H_2O and CO_2 decrease the system reactivity.

For the N_2-H_2O mixture, the periodic dynamic behaviour is detected for $T_{in} > 1080$ K, while at $T_{in} = 1150$ K they disappear and the oxidation process occurs thorough a stationary steady state, while for the CO_2-diluted system oscillations occur for 1090 K < T_{in} < 1160 K.

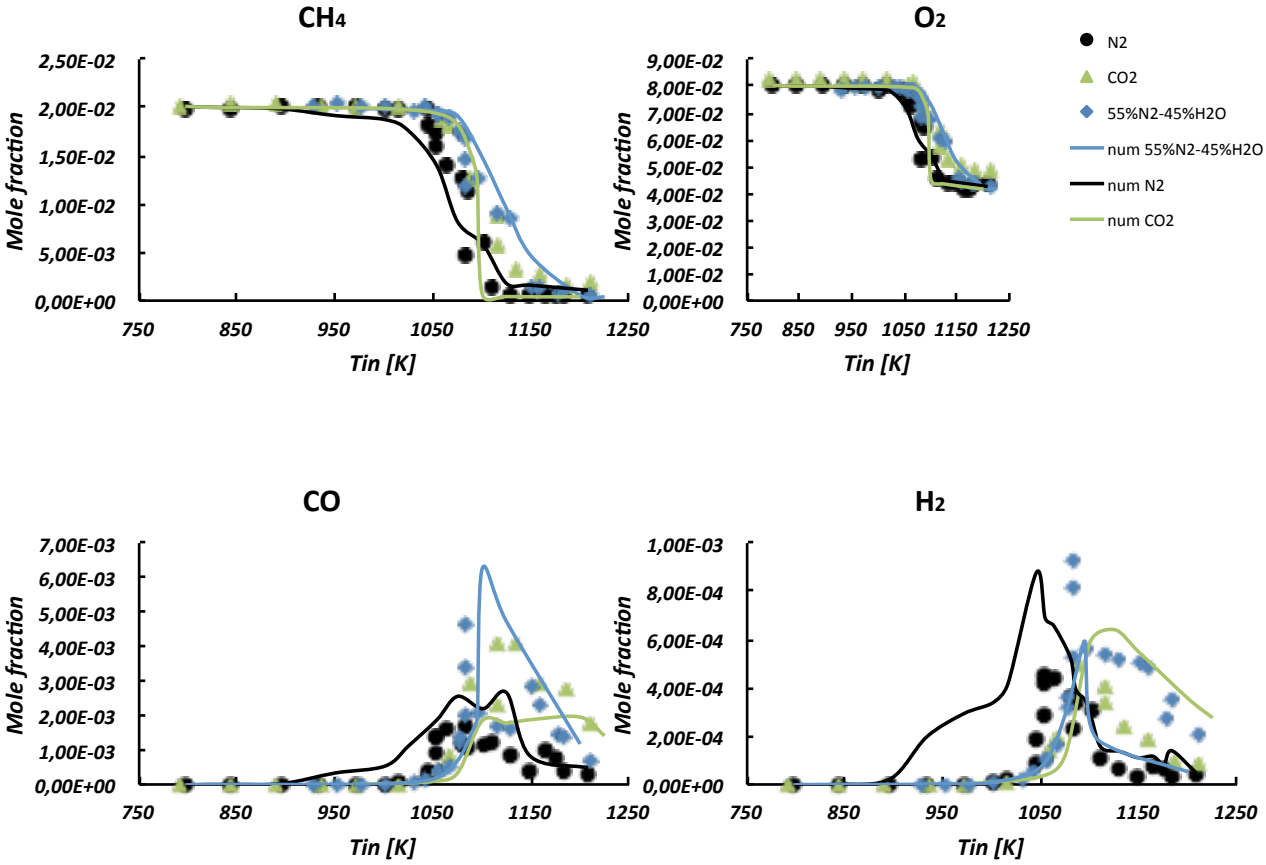

Fig. 4.31 - Experimental (symbols) and numerical (lines) concentration profiles versus inlet temperature. $\Phi = 0.5$, $\tau = 0.5$ s, p = 1.1 atm, d = 90%, N_2 (circle symbols), CO_2 (triangle symbols), N_2-H_2O (square symbols).

Differently from the other investigated equivalence ratios, CO and H_2 profiles reach a maximum value, and subsequently their concentrations diminish for all the mixtures.

In the lean case, the agreement between measured and computed species concentrations is less satisfactory and the difference between the modelling and the measurements is far beyond the experimental uncertainties. In particular the model shifts the onset of reactivity to lower temperatures and does not properly reproduce the T_{in} range where temperature oscillations are experimentally recognized.

Results are now presented in Fig. 4.32 for CH_4/O_2 mixtures diluted in helium, nitrogen, and CO_2, for a lean mixture ($\Phi = 0.5$), at $\tau = 2$ s. The obtained results are similar to that obtained at a residence time of 0.5 s for the same equivalence ratio.

Under these conditions, the experimental onset of the oxidation reactions is identified for $T_{in} > 975$ K for the three diluted systems. Afterwards the conversion gradually increases. Under lean conditions periodic oscillatory regimes occur for $T_{in} > 1000$ K only for the mixture diluted in N_2.

The experimental profiles with T_{in} for the mixtures diluted in He or CO_2 are similar to the ones relative to the N_2-diluted mixture. Nonetheless, as observed under the other equivalence ratios, at low temperatures ($T_{in} < 1075$ K) there is a difference between the data obtained in nitrogen and the data obtained in He.

Furthermore, Fig. 4.32 shows that, similarly to what observed in the stoichiometric condition, the difference among the different diluted mixtures is higher for lower temperatures.

However, at high temperature, the CO_2 effect is again encountered in the CO concentration. In particular, the relative difference of CO concentration between CO_2-diluted system and N_2-diluted system increases with increasing temperature and reaches one order of magnitude for T_{in} = 1175 K.

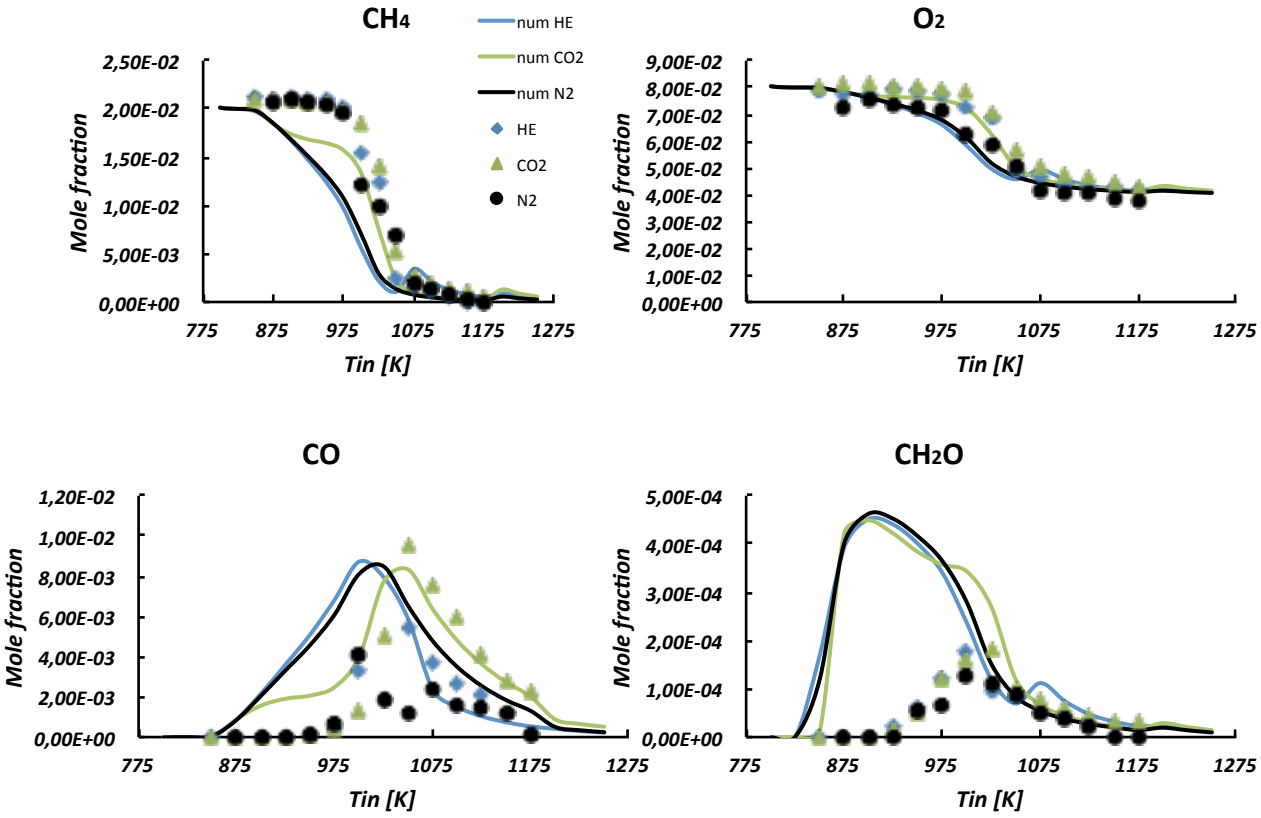

Fig. 4.32 - Experimental (symbols) and numerical (lines) concentration profiles versus inlet temperature. Φ = 0.5, τ = 2 s, p = 1.05 atm, d = 90%, N_2 (circle symbols), CO_2 (triangle symbols), He (square symbols).

Figure 4.32 also investigates the performance of the CRECK-2014 mechanism to predict species concentrations measurements according to the type of the bath gas or diluent mixture. As observed for τ = 0.5 s, in lean conditions the difference between the modelling and the measurements is far beyond the experimental uncertainties. In particular the model shifts the onset of reactivity to lower temperatures and does not properly reproduce the T_{in} range where temperature oscillations are experimentally recognized.

To sum up, the experimental results suggest that the oxidation process onset occurs for lower T_{in} for fuel lean conditions with respect to the stoichiometric and rich cases.

In general CO_2, H_2O and He slow down the reactivity with respect to the N_2-diluted system. Moreover, CO_2 and H_2O, and to a lesser extent He, retard the onset of the oscillatory behaviour with respect to the N_2 system for any equivalence ratio considered in this work. Furthermore, it is worth noting that at high T_{in} the production of CO is higher for the system diluted in CO_2, while the production of H_2 is higher when H_2O dilutes the reactive mixture.

The CRECK-2014 mechanism correctly reproduces the influence of equivalence ratio and diluent. However, trends towards a worse prediction of JSFR experiments by the mechanisms at a lower equivalence ratio can be observed. Disagreement between the experimental data and model predictions is largest in lean conditions and lower inlet temperatures. In contrast to ignition delay

times data, a clear trend towards a decreasing performance with decreasing equivalence ratio can be observed.

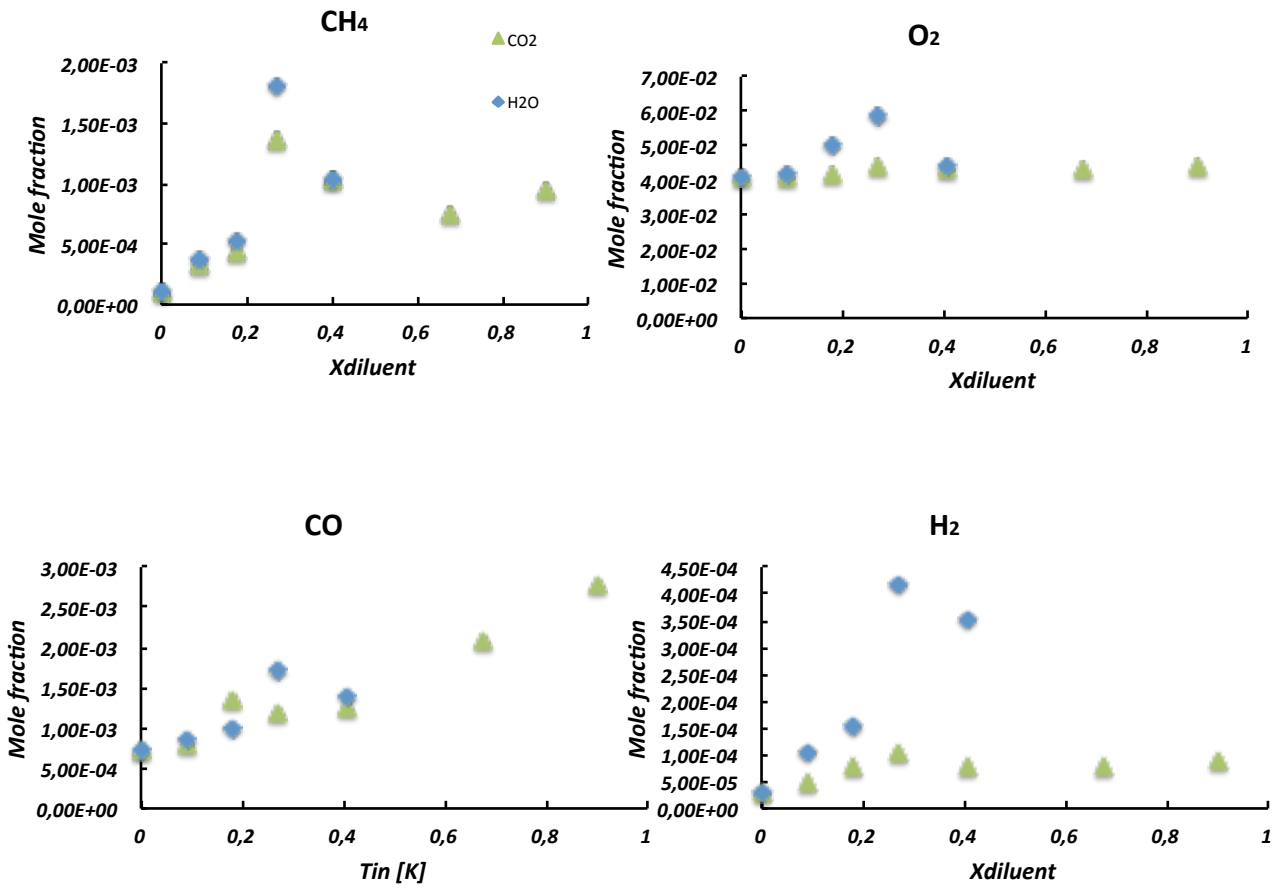

Fig. 4.33 - Experimental concentration profiles versus molar fraction of diluent. $\Phi = 0.5$, $\tau = 0.5$ s, p = 1.1 atm, d = 90%, $T_{in} = 1180$ K, CO_2 (triangle symbols), H_2O (square symbols).

Figure 4.33 shows the experimental evolution of CH_4, CO, H_2, and O_2 concentrations when, starting from a system fully diluted in N_2 at 90%, the CO_2 molar fraction is gradually increased from 0 to 0.9 (therefore up to a system fully diluted in CO_2 at 90%) and the water vapour molar fraction is increased from 0 to 0.405 for a lean mixture ($\Phi = 0.5$) at $T_{in} = 1180$ K, keeping the overall dilution at 90% (the remaining is nitrogen). This inlet condition has been chosen because it allows for a comparison of the different diluents without the presence of oscillatory regimes. However, it has not been possible to make a comparison with the numerical results, since the model predicts dynamic regimes for the N_2 and CO_2 diluted systems for this inlet temperature. It is interesting to observe that the conversion decreases quasi-linearly when the CO_2 and steam molar fractions are increased up to a certain value (X = 0.27). For higher molar fractions the measured values slightly decrease and then reach a plateau. The only exception is found in the CO concentration, which as the other species reach a plateau level, but it starts again to increase for CO_2 molar fraction higher than 0.405. The slope (in absolute value) of the quasi-straight line defined by the experimental data is found to be slightly higher for the H_2O diluted system than one associated with the CO_2 diluted system.

This result, together with those reported so far, suggests that, first of all, CO_2 and H_2O have a significant chemical effect. In fact, any change of a physical property due to the addition of a different species would be proportional to the concentration of that species, and therefore would result in a linear variation in the concentrations of the measured chemical species. Second, water

has a greater impact than CO_2; indeed small percentages of water are sufficient to obtain large variations in the measured chemical species profiles. An explanation of this behaviour will be provided in the next chapter.

4.2.2 Propane mixtures

This set of experiments was performed only in the Napoli JSFR. Experiments were performed at a constant pressure of 1.1 atm, a constant residence time of 0.5 s, over the temperature range 720-1100 K. Three equivalence ratios (Φ = 1.5, 1, 0.5) were considered and mixtures were diluted with N_2 (reference case), CO_2, 50% N_2-50% CO_2, 75% N_2-25% H_2O and 55% N_2-45% H_2O, keeping a fixed overall d of 90%.
The experimental conditions are summarized in Table 4.5.
The results that will be presented in this section, only regarding the influence of CO_2 on propane mixtures in the JSFR, have been published in the following journal paper:
Lubrano Lavadera, M, Sabia, P, Sorrentino, G, Ragucci, R & de Joannon, M 2016, "Experimental study of the effect of CO_2 on propane oxidation in a Jet Stirred Flow Reactor", *Fuel*, vol. 184, pp. 876-888.

Φ	C_3H_8 (vol%)	O_2 (vol%)	N_2 (vol%)	CO_2 (vol%)	H_2O (vol%)	Number of experiments
0.5	0.91	9.09	90	0	0	46
0.5	0.91	9.09	45	45	0	19
0.5	0.91	9.09	0	90	0	19
0.5	0.91	9.09	67.5	0	22.5	25
0.5	0.91	9.09	49.5	0	40.5	23
1	1.67	8.33	90	0	0	49
1	1.67	8.33	45	45	0	21
1	1.67	8.33	0	90	0	23
1	1.67	8.33	67.5	0	22.5	25
1	1.67	8.33	49.5	0	40.5	23
1.5	2.31	7.69	90	0	0	41
1.5	2.31	7.69	45	45	0	18
1.5	2.31	7.69	0	90	0	16
1.5	2.31	7.69	67.5	0	22.5	24
1.5	2.31	7.69	49.5	0	40.5	22

Table 4.5 – Experimental conditions studied in the JSFR for C_3H_8 mixtures. 720 K < T_{in} < 1100 K, P = 1.1 atm, d = 90%, τ = 0.5 s.

Influence of temperature
In order to value the mechanisms performance and to elucidate some peculiar features of the oxidation process of propane under diluted conditions, a preliminary analysis was performed comparing the experimental and numerical temperature increase (ΔT) and C_3H_8 and O_2 conversions as a function of the system initial temperature (T_{in}) for a stoichiometric C_3H_8/O_2 mixture. To perform such an analysis, the results obtained using the mixture completely diluted in N_2 are presented.
Results are reported in Fig. 4.34. Symbols represent experimental results while the predictions are reported with red lines for the CRECK-2014 and green lines for the AramcoMech_1.3-2013. These two mechanisms were found to be the best performing among the tested models.

The ΔT presented results reveal an interesting pattern. At low temperatures (around 800 K), the system starts to react. As the system approaches higher temperatures (around 850 K), in addition to the existing regime, another, slower, regime with a lower temperature increase appears. Therefore, two different well-defined reactor temperatures can be reached under the same inlet conditions.

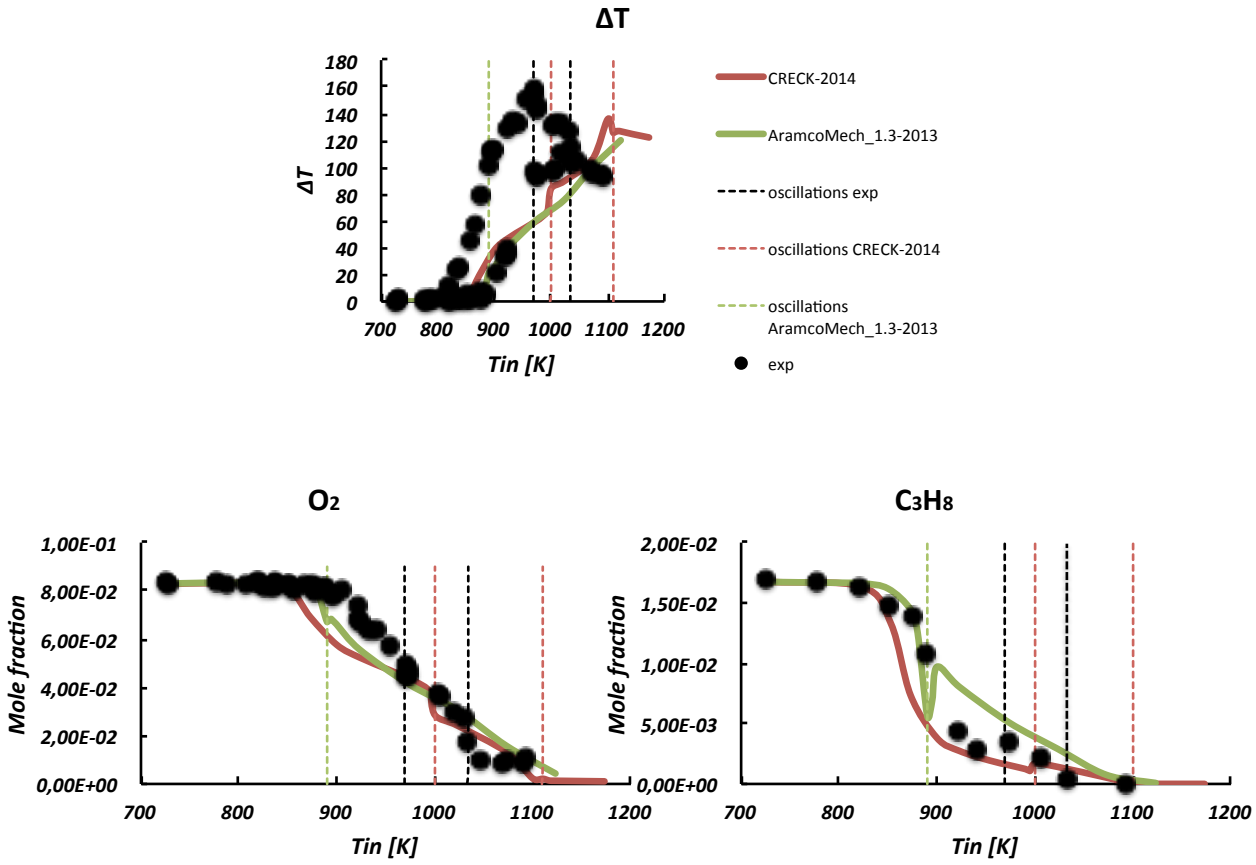

Fig. 4.34 – Experimental (symbols) and numerical (lines) ΔT and concentration profiles versus inlet temperature. Φ = 1, τ = 0.5 s, p = 1.1 atm, d = 90% N_2.

Moreover, both of the steady states are stable an experimental point of view. In fact, the response of the system to an induced temporary displacement in terms of pressure or mixture composition perturbation slightly shifts it from the steady state for a while before it then returns once again to the same steady state. Bistability is an already observed phenomenon for propane oxidation (Bernatosyan & Mantashyan 1986). Immediately after its appearance, the second regime grows increasingly fast, while the first dominant mode becomes slower. This behaviour continues until the two regimes collapse into a single oscillatory regime at T_{in} = 970 K. The reactants concentrations are almost insensitive to the bistability. With regard to the oscillations, is valid all that was said in the case of methane oxidation, since the observed phenomena appear to be very similar. Thus, for this regime, two ΔT are reported in Fig. 4.34. They correspond to the maximum and minimum values detected during the oscillatory behaviour. To better identify this condition in Fig. 4.34, two dashed vertical lines have been included in the diagram, which correspond to the T_{in} range where temperature oscillations were detected. In general, increasing T_{in}, the temperature oscillation amplitude decreases while the frequency increases. Figure 4.34 shows that the propane concentration abruptly decreases for T_{in} > 880 K, and then slowly for T_{in} > 920 K. For T_{in} = 970 K, the system goes throughout the oscillatory behaviour. In such a case, the concentration values are

averaged in time as explained for the methane mixtures. In correspondence of the onset of the oscillatory behaviour, the propane concentration slightly increases with respect to the previous value. Finally, for T_{in} > 1100 K, propane concentration is close to zero.
The O_2 profile is relatively different with respect to the propane one. Actually its concentration diminishes monotonically with T_{in}.
Along with the experimental data, Fig. 4.34 also reports the numerical simulations obtained with two chosen kinetic mechanisms. It should be noted that, by simulating the reactive system with a transient reactor, it is possible to numerically identify oscillatory regimes, but it is not possible to identify multiple solutions.
The CRECK-2014 scheme predicts the onset of the oxidation reactions for T_{in} = 830 K. As matter of fact, for this T_{in} the simulated system temperature starts increasing while reactants concentration diminishes. Afterwards the system temperature increases quickly with T_{in} up to T_{in} = 910 K, then it increases with a minor slope. For T_{in} = 1000 K, the kinetic mechanism predicts the insurgence of temperature oscillations in time that persists up to T_{in} = 1100 K (vertical red dashed lines in the figure). In the case of oscillations, the temperatures reported in Fig. 4.34 are reported as time averaged values considering an oscillation period. Such a choice, as in the case of methane mixtures, comes from the consideration that the numerical temperature oscillation amplitudes are considerably higher than the experimental ones. Thus, for the sake of clearness of the figure just the averaged values are reported. For T_{in} > 1100 K the propane oxidation occurs through a stationary steady state. The numerical working temperatures are slightly higher than the experimental ones at high T_{in}. The kinetic mechanism anticipates the consumption of the reactants with respect to test results. For T_{in} > 1000 K, a good agreement between numerical and experimental data is observable.
The AramcoMech_1.3-2013 mechanism correctly reproduces the onset of the oxidation process considering the reference measurements trend with T_{in}. For T_{in} > 890 K, the simulations predict the insurgence of the dynamic behaviour that persists for all the inlet temperature range considered.
Based on these observations, the CRECK-2014 mechanism was selected to simulate the JSFR propane mixtures experimental data.
Figure 4.35 depicts the experimental and numerical concentrations of some intermediate species as a function of T_{in} for stoichiometric propane/oxygen mixtures diluted at 90% in N_2.
For T_{in} > 940 K, the profiles show a discontinuity with an abrupt decrease of concentration (an increase for the CO_2). With increasing the inlet temperature, the concentrations further increase, or at least reach a plateau level. For higher T_{in}, species concentrations further decrease, with the exception of CO_2 concentration that, of course, increases.
Comparing the experimental data with numerical simulations, it is possible to note that the model is able to reproduce the general trend of species concentration with T_{in}. However, C_2H_2 concentration is relatively overestimated.

Influence of equivalence ratio and diluent: N_2, CO_2, H_2O
The chemical species profiles of C_3H_8/O_2 mixtures of equivalence ratios 1, 0.5, and 1.5 diluted in N_2 and CO_2 with ratios 100/0, 50/50, 0/100 and in N_2 and H_2O with ratios 100/0, 75/25, 55/25 are plotted in Figs. 4.36, 4.37, 4.38, and 4.39. The overall dilution is kept constant at 90%.
In order to elucidate some peculiar features of the propane oxidation process under diluted conditions, for different equivalence ratios and diluents, and to value the mechanisms performance in predicting these features, only the concentrations of some main species as a function of T_{in} are presented. In particular the concentrations of CH_4, O_2, CO and H_2 are shown.
The lower part of Fig. 4.36 depicts the experimental and numerical O_2 concentrations as a function of T_{in} for stoichiometric propane/oxygen mixtures diluted at 90% in N_2, in CO_2 or in N_2 and CO_2 in equimolar fraction (50% N_2-50% CO_2), while the upper part shows the same comparison, but for mixtures diluted at 90% N_2, in 75% N_2 – 25% H_2O or in 55% N_2-45% H_2O.

The overall temperature dependence is quite similar for the six investigated cases. In particular the figure shows that the results for the mixture diluted in 50% N_2-50% CO_2 lie in-between the N_2- and the CO_2-diluted cases, whereas the results for the mixture diluted in 75% N_2-25% H_2O lie in-between the N_2- and 55% N_2-45% H_2O. This was observed in all the analysed operating conditions. Then below, for clarity, the intermediate mixtures will not be shown. However, all the obtained results are stored in the Appendix.

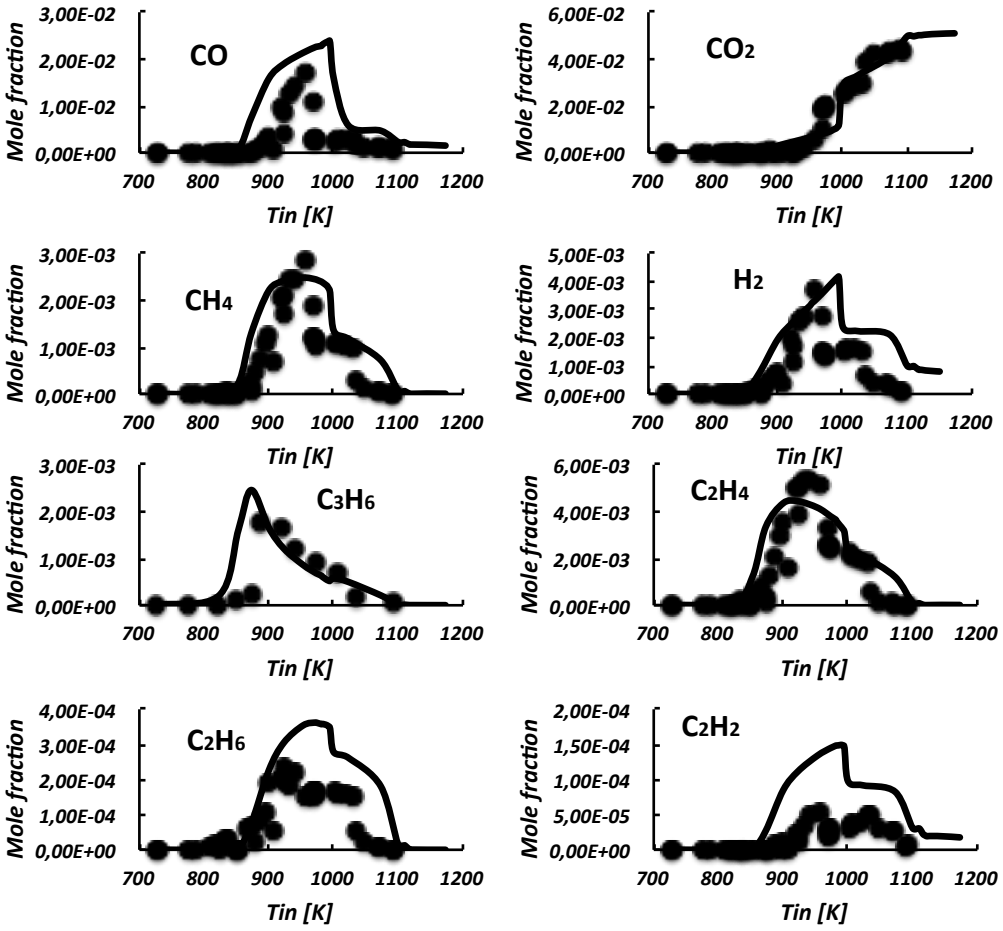

Fig. 4.35 - Experimental (symbols) and numerical (lines) concentration profiles versus inlet temperature. $\Phi = 1$, $\tau = 0.5$ s, p = 1.1 atm, d = 90% N_2.

Fig. 4.37 depicts the experimental and numerical concentrations of some chemical species as a function of T_{in} for stoichiometric propane/oxygen mixtures diluted at 90% in N_2, in CO_2 or in N_2 and H_2O (55% N_2-45% H_2O). Thus the results obtained for the N_2-diluted mixture are the same presented in Figs. 4.34 and 4.35.

As can be seen in Fig. 4.37, the experimental species profiles with T_{in} for the mixture diluted in CO_2 and N_2-H_2O are similar to the ones relative to the N_2-diluted mixture. Nonetheless, Fig. 4.37 shows that the presence of H_2O and, to a lesser extent CO_2, slightly anticipates the reactivity with respect to the N_2-diluted system, in that all chemical species for the CO_2- and the N_2-H_2O-diluted systems start producing at slightly lower T_{in} with respect to the N_2 reference case. Afterwards, there is an inversion point and the effect of CO_2 and H_2O is to slow down the reactivity. This inversion point occurs for T_{in} around 920 K for the CO_2-diluted mixture and T_{in} around 970 K for the N_2-H_2O-diluted mixture. For 1000 K < T_{in} < 1030 K, the periodic dynamic behaviour is also experimentally detected for the system diluted in CO_2, while for the N_2-H_2O diluted system this behaviour is observed for 970 K < T_{in} < 1070 K. Therefore, the dynamic behaviour occurs for

higher T_{in} and for a narrower T_{in} range in the case of mixtures diluted in CO_2 compared to N_2, whereas occurs for the same T_{in} but wider T_{in} range in the case of mixtures diluted in N_2 and H_2O. For higher T_{in}, the species amounts are higher than the ones detected for the reference case, with differences up to one order of magnitude (or higher) for T_{in} = 1100 K. Along with the experimental data, Fig. 4.37 also reports the numerical simulations obtained with the CRECK-2014 mechanism.

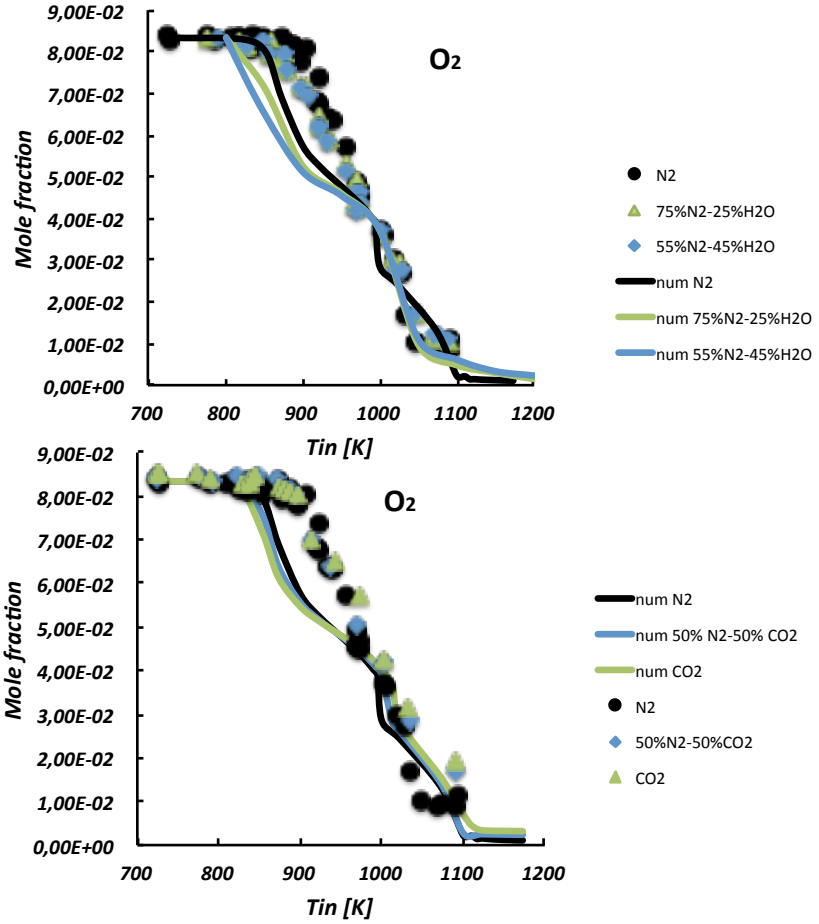

Fig. 4.36 - Experimental (symbols) and numerical (lines) O_2 concentration profiles versus inlet temperature. Φ = 1, τ = 0.5 s, p = 1.1 atm, d = 90% in different bath gases.

For the CO_2- and the N_2-H_2O-diluted systems, the kinetic mechanism predicts the onset of the oxidation reactions for inlet temperatures lower than the one obtained for the N_2-diluted system. Thus the scheme well predicts the anticipating effect of CO_2 and H_2O on the reactivity of the system at low temperatures observed during experimental tests. Furthermore, the model well predicts the inversion point for the system diluted in CO_2, while shifts it to slightly lower temperature respect to the experimental observation for the N_2-H_2O-diluted system. For the CO_2-diluted system and T_{in} = 1010 K, the oxidation process occurs through an oscillatory behaviour, that ends at T_{in} = 1110 K. Thus, the model predicts the retarding effect of the CO_2 on the temperature onset of the dynamic behaviour with respect to the mixture inlet temperatures. For the system diluted in N_2 and H_2O the oscillatory regime is predicted for $1020 < T_{in} < 1200$. Thus, also here the model well predicts the wider T_{in} range in which the oscillations are detected when adding water to the system.
In general, simulations do capture the CO_2 and H_2O effect on the reference species, but overestimate it at low T_{in} whereas underestimate it at high T_{in}.
Figure 4.38 shows the measured chemical species concentrations as a function of T_{in} for fuel rich (Φ = 1.5) propane/oxygen mixtures diluted in N_2, CO_2 and 55% N_2-45% H_2O at 90%.

For Φ = 1.5, the experimental onset of the oxidation reactions is identified for T_{in} > 800 K for the N_2-diluted system. As for the stoichiometric condition, bistability are identified at low temperatures.

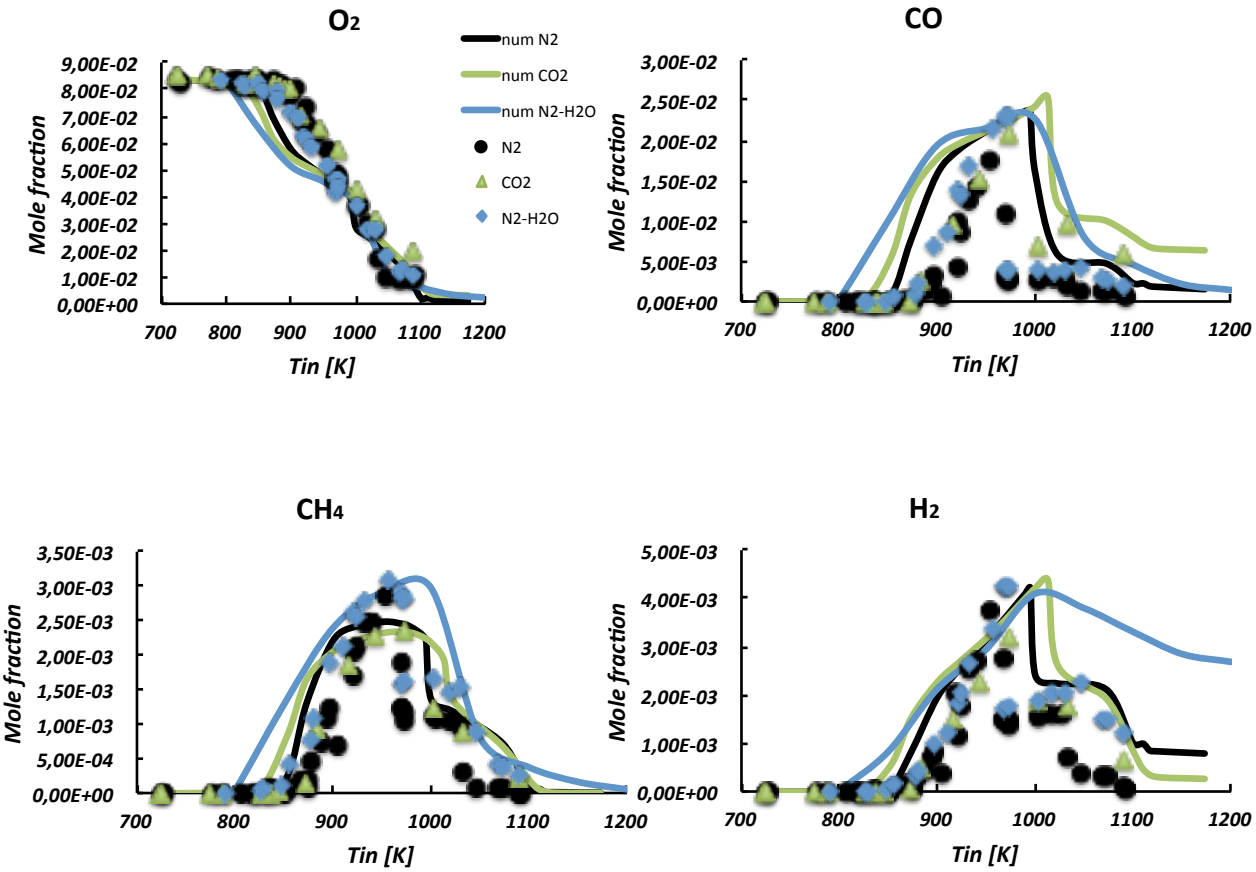

Fig. 4.37 - Experimental (symbols) and numerical (lines) concentration profiles versus inlet temperature. Φ = 1, τ = 0.5 s, p = 1.1 atm, d = 90%, N_2 (circle symbols), CO_2 (triangle symbols), N_2-H_2O (square symbols).

For 970 K < 1050 K, the propane oxidation process occurs throughout a periodic oscillatory behaviour while at T_{in} > 1050 K through a stationary steady state. Reactants are quickly consumed in the range 880 K < T_{in} < 920 K, then with a slower rate during the temperature oscillation range.
At low T_{in}, H_2O, and to a lesser extent CO_2, slightly anticipates the reactivity of the mixture with higher conversion with respect to the N_2-diluted system. At T_{in} > 930 K, the conversion becomes higher for the mixture diluted in N_2. Thus, the inversion point for the fuel rich mixture considered is at T_{in} = 930 K both respect to the CO_2- and to the N_2-H_2O-diluted systems. For T_{in} = 1100 K, the O_2 concentration is 0.52% for the mixture diluted in N_2, 0.73% for the system diluted in both N_2 and H_2O, and 1.53% for the mixture diluted in CO_2.
For the system N_2-H_2O no periodic regime is experimentally detected, while for the CO_2-diluted system the periodic dynamic regime is experimentally observed in the T_{in} range 1040-1100 K. Thus the CO_2 postpones the occurrence of the dynamic behaviour with respect to T_{in}.
CO is formed through the entire inlet temperature range with a lower rate where temperature oscillations occur. At the highest temperature, the CO concentrations are higher for the CO_2-diluted mixtures.
For N_2- and N_2-H_2O-diluted mixtures, H_2 is monotonically produced, while, for the CO_2-diluted system, it is produced monotonically up to T_{in} = 1000 K, then the values remain almost constant and reach a plateau. The H_2 volumetric percentages for the N_2-H_2O-diluted mixture are higher than those observed in the other cases.

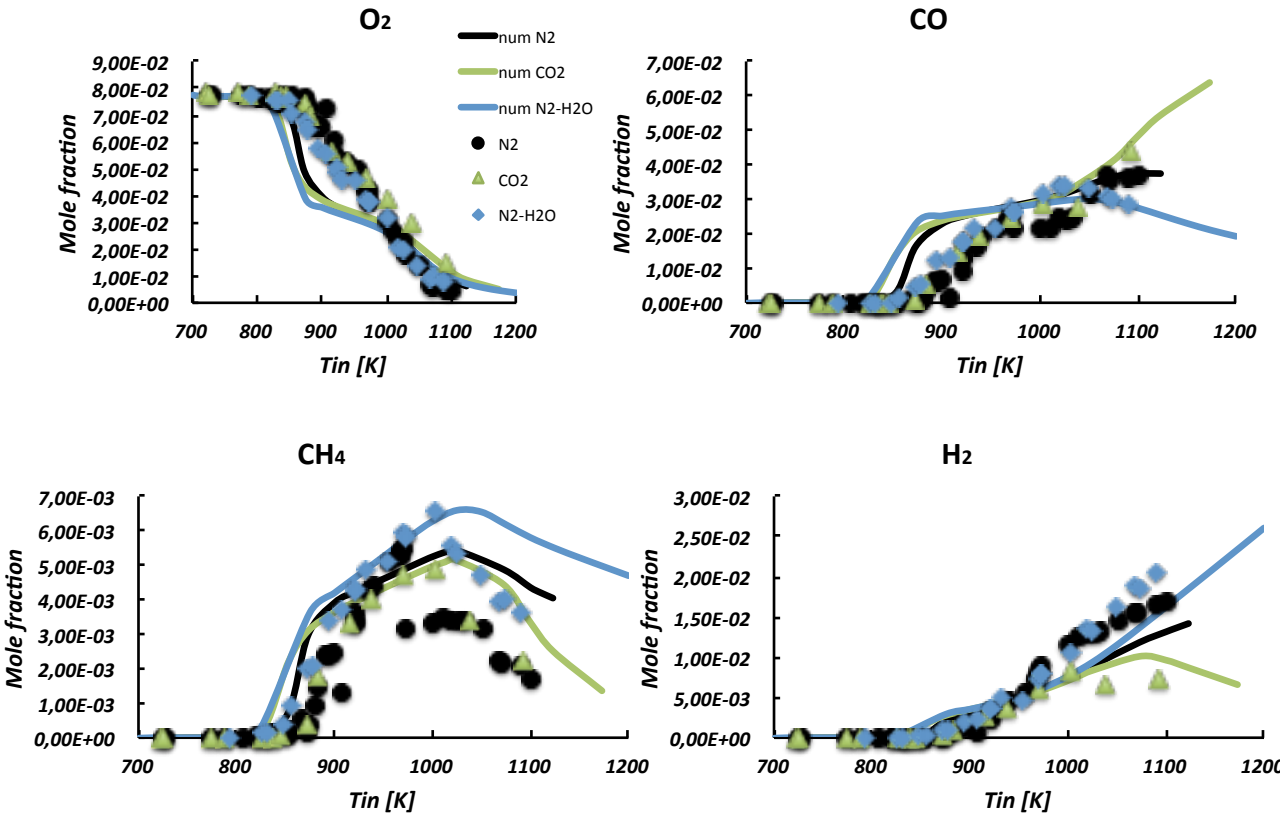

Fig. 4.38 - Experimental (symbols) and numerical (lines) concentration profiles versus inlet temperature. Φ = 1.5, τ = 0.5 s, p = 1.1 atm, d = 90%, N_2 (circle symbols), CO_2 (triangle symbols), N_2-H_2O (square symbols).

CH_4 concentrations reach a maximum, and subsequently they decrease. H_2O, and to a lesser extent CO_2, increases the methane concentration. Furthermore, H_2O and CO_2 shift the maximum value of CH_4 concentration towards higher T_{in}.

The CRECK-2014 mechanism correctly reproduces the general trend of species production/consumption as well as it predicts the effect of CO_2 and H_2O at low and high temperatures. Nonetheless, the onset of the oxidation reactions occurs for a lower T_{in} with respect to the experimental results. The relative difference in species concentration between the N_2-, the CO_2- and the N_2-H_2O-diluted systems is overestimated at low temperatures and well predicted at high ones.

The model does not properly reproduce the T_{in} range where temperature oscillations are experimentally detected. In particular, for the N_2-diluted system, the dynamic behaviour is predicted for 860 K < T_{in} < 890 K, while experimentally it occurs for 970 K < 1050 K. For the CO_2-diluted system, no temperature oscillations were reproduced. However, the mechanism correctly predicts the absence of oscillatory regimes for the mixture with H_2O.

Figure 4.39 shows the experimental and numerical species concentrations versus T_{in} for fuel lean (Φ = 0.5) propane/oxygen mixtures.

For this equivalence ratio, experimental results indicate that the reaction onset occurs for T_{in} equal to about 830 K for the mixture diluted in nitrogen. For this diluted system, the conversion increases abruptly up to T_{in} = 970 K, then periodic temperature oscillations occur. As for the stoichiometric

and rich conditions, bistability are identified at low temperatures. The oxygen concentration diminishes from 9% to 7% at T_{in} = 970 K. For higher T_{in}, it reaches an almost constant value equal to 6%, and then it slightly diminishes for T_{in} = 1100 K.

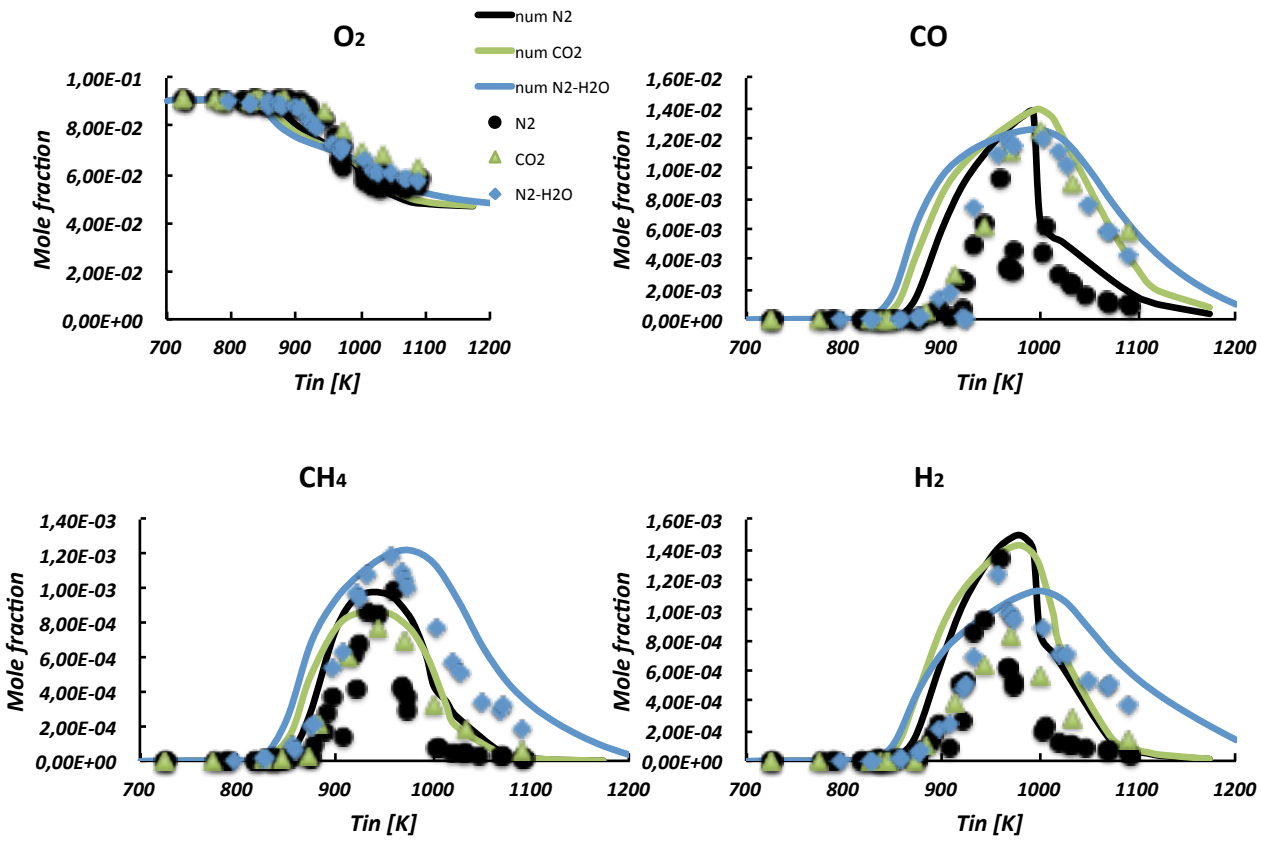

Fig. 4.39 - Experimental (symbols) and numerical (lines) concentration profiles versus inlet temperature. Φ = 0.5, τ = 0.5 s, p = 1.1 atm, d = 90%, N_2 (circle symbols), CO_2 (triangle symbols), N_2-H_2O (square symbols).

For the CO_2- and N_2-H_2O-diluted systems, the concentrations profiles are similar to the N_2-diluted system. In particular for low T_{in}, the conversion is slightly higher than the one obtained for the reference system, while at T_{in} > 900 K for the CO_2 and T_{in} > 970 K for the H_2O (inversion point), it becomes lower. It is interesting to note that for the CO_2- and the N_2-H_2O-diluted mixtures the periodic dynamic behaviour is not detected in the whole investigated temperature range.
All the intermediate species profiles reach a maximum value, and subsequently their concentrations diminish. It is possible to note that also for Φ = 0.5, CO_2 and H_2O accelerate the oxidation process up to T_{in} corresponding to the inversion point, then they decrease the system reactivity.
Also for this case, the model predicts the general trend of the considered measurements along with the effect of CO_2 and H_2O on system reactivity. Under fuel lean condition, the agreement between numerical and experimental species concentration is satisfactory. Nonetheless, the model does not properly reproduce the T_{in} range where oscillations are experimentally recognized.
The experimental results suggest that the oxidation process onset occurs for lower T_{in} for fuel rich conditions with respect to the stoichiometric and the lean cases.
In general, CO_2 and H_2O have a similar effect. They accelerate the reactivity at low temperatures, while slow down it at higher temperatures, compared to N_2-diluted mixtures for any equivalence ratio considered in this work. Also CO_2 and H_2O have an effect on the onset of the oscillatory

behaviour with respect to the N_2 system. Furthermore it is worth noting that at high T_{in} the production of CO is higher for systems diluted in CO_2, while the H_2 concentration is higher for systems diluted in N_2-H_2O.
In particular, under lean conditions, the impact of the CO_2 on C_3H_8 oxidation is less pronounced with respect to stoichiometric and rich conditions. The opposite occurs for H_2O, i.e. the impact is more pronounced in lean conditions with respect to stoichiometric and riche conditions.
The CRECK-2014 mechanism correctly reproduces the dependence of the onset of C_3H_8 oxidation reactions on the mixture equivalence ratio with T_{in}. Actually both the numerical and the experimental results suggest that the oxidation process occurs for lower T_{in} in the case of fuel rich mixtures. Nonetheless, numerical predictions predict the insurgence of oxidation reactions for T_{in} lower with respect to the experimental results for any equivalence ratio considered.
Furthermore, the kinetic model predicts the CO_2 and H_2O effects at low T_{in} and at high T_{in} experimentally identified. The relative differences among reactivities of the N_2-, the CO_2- and the N_2-H_2O-diluted systems are overestimated at low temperatures and underestimated at high ones.

4.2.3 N-pentane mixtures

This set of experiments was performed only in the Nancy JSFR. Experiments were performed at a constant pressure of 1.05 atm, a constant residence time of 2 s, over the temperature range 500-1100 K. Two equivalence ratios (Φ = 2 and 1) were considered and mixtures were diluted with CO_2, keeping a fixed fuel molar fraction of 0.01.
These experiments have mainly been realized in order to understand the CO_2 effect on a fuel with a well-defined cool flame ignition like the n-pentane. This allows understanding the diluent effects also on the low-temperature combustion. For this reason, the experiments conducted by diluting the system in CO_2 are compared with those obtained by Bugler et al. (2016) and Rodriguez et al. (2016) in helium, in the same conditions.
The experimental conditions are summarized in Table 4.6.
Furthermore, the experimental conditions, along with the experimental results, are available upon request.

d (%)	Φ	nC_5H_{12} (vol%)	O_2 (vol%)	CO_2 (vol%)	Number of experiments
91	1	1	8	91	25
95	2	1	4	95	25

Table 4.6 – Experimental conditions studied in the JSFR for nC_5H_{12} mixtures. 500 K < T_{in} < 1100 K. P = 1.05 atm, τ = 2 s.

Influence of diluent: CO_2
In order to understand the CO_2 effect on the n-pentane oxidation under diluted conditions and to value the mechanisms performance, only the stoichiometric mixture is used as a reference case.
Detailed analysis of the influence of temperature and equivalence ratio on n-pentane oxidation can be found in the works of Bugler et al. (2016) and Rodriguez et al. (2016).
The kinetic mechanism used for the simulations is the NUI-Galway-2010, which among the tested mechanism it is the only suitable to simulate C_5 combustion.
About 70 chemical species were detected during the n-pentane experiments. Here, only 4 selected species profiles versus temperature are presented in order to show the effect of CO_2. All species concentrations are available upon request.
Results are reported in Fig. 4.40 that reports the experimental and numerical concentrations of n-pentane, CO, CH_4, and CH_2O as a function of T_{in} for stoichiometric n-pentane/oxygen mixtures

diluted at 91% in He or in CO_2. Symbols represent experimental results while the predictions are reported with lines.

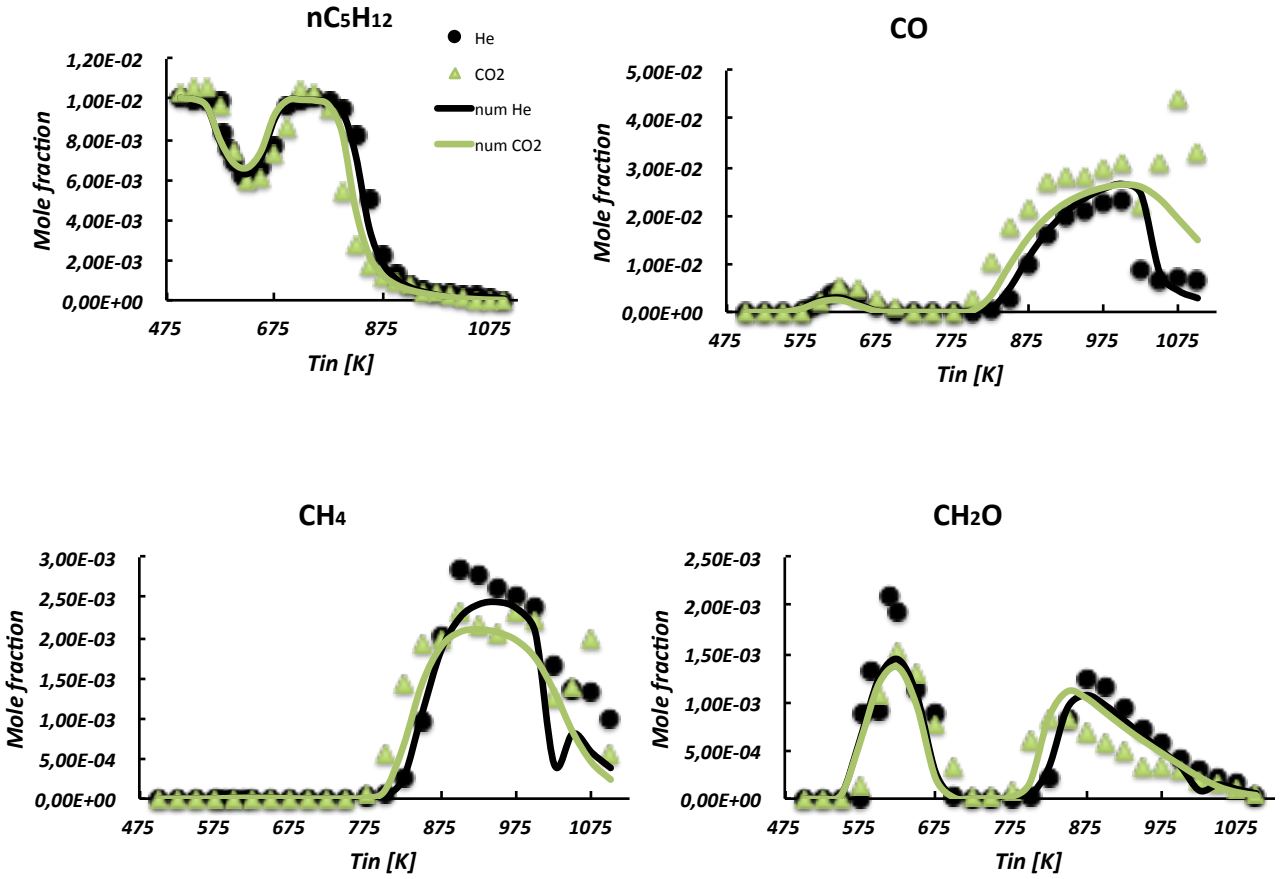

Fig. 4.40 - Experimental (symbols) and numerical (lines) concentration profiles versus inlet temperature. $\Phi = 1$, $\tau = 2$ s, p = 1.05 atm, d = 91%, He (circle symbols), CO_2 (triangle symbols).

As can be seen from Fig. 4.40, the CO and CH_2O concentrations start to form in correspondence of n-pentane consumption, around 570 K. For $T_{in} > 625$ K the profiles show a decrease of conversion. With increasing the inlet temperature, the conversion again increases and also CH_4 is formed. Such a trend is typical of the NTC behaviour described in the chapter 2, which is typical of the low temperature.

The species profiles with T_{in} for the mixture diluted in CO_2 are similar to the ones relative to the He-diluted mixture. Nonetheless, Fig. 4.40 shows that, for $T_{in} > 770$ K, the presence of CO_2 slightly anticipates the reactivity with respect to the He-diluted system, in that all chemical species for the CO_2-diluted system start producing at slightly lower T_{in} with respect to the He reference case.

As in all other cases seen so far, for higher T_{in}, the CO amounts are higher than the ones detected for the reference case, with a relative difference up to 0.8 for $T_{in} = 1100$ K. At low temperature, it seems that there are no differences between the concentrations measured with the two diluents. Thus, CO_2 has an effect on intermediate-temperature chemistry much more profound than that on low-temperature chemistry.

Along with the experimental data, Fig. 4.40 also reports the numerical simulations obtained with the NUI-Galway-2010 mechanism. The agreement is very good in the whole investigated temperature range. For the CO_2-diluted system, the kinetic mechanism well predicts the anticipating effect of CO_2 on the reactivity of the system at intermediate temperatures observed during experimental tests, but underestimate it. Furthermore, for the He-diluted system and $T_{in} > 1050$ K, the simulated oxidation process occurs through an oscillatory behaviour, which is not experimentally detected.

CHAPTER 5 – DISCUSSION AND NUMERICAL ANALYSES

The very rich variety of phenomena that accompany the SECs combustion provides a rigorous foundation against which a kinetic model may be tested qualitatively as well as quantitatively in certain circumstances. The main features are the existence of a NTC-like behaviour for propane mixtures in a certain temperature range, strong and weak ignitions, oscillatory regimes, the form and the location of the ignition boundaries in the temperature-equivalence ratio diagrams, the influence of diluents and/or fuel type on ignition delay times and species concentrations.
Numerical studies form the link between experimental observations and fundamental interpretations. Since several numerical models predict the observed phenomena, these models can help us to gain valuable insights into the nature of the phenomena being explored. Therefore, it would appear valuable to use a detailed model that it is as fundamentally as possible in order to draw reliable conclusions regarding the controlling chemistry.
Therefore, in this chapter it has been attempted to identify the rate-controlling processes to focus attention on what controls the chemistry of the observed phenomena.
In order to facilitate understanding, the main reactions involved in the SECs combustion process are summarized in the Table 5.1.

5.1 NTC-like behaviour

Propane mixtures exhibited peculiar behaviours under diluted operating conditions. First, the reactivity map (Fig. 4.4) showed different oxidation regimes and dynamic behaviours over the analysed ranges of temperature and mixture composition.
A second peculiar behaviour was observed when the analysis of the auto-ignition time showed a change in the slope of ignition curves in the Arrhenius diagram at intermediate temperatures and C/O ratios of 0.15-0.3 ($0.5 < \Phi < 1$). This suggests that the competition among the different ignition regimes is very sensitive to mixture composition (Figs. 4.5 and 4.7).
As noted in the previous chapter, this transition is very similar to the initiation of a cool flame reaction process. While the NTC behaviour at low temperature has been widely investigated and the kinetics responsible of such a behaviour completely identified, in literature there is not a thorough analysis of the phenomenologies observed at intermediate temperatures. Therefore, this part of the study points at the key factors that determine this behaviour of ignition delay times.
For propane mixtures, the ignition delays in a wide temperature range, as well as the change in the effective activation energy observed under high dilution and temperatures below 1100 K are correctly reproduced by the modelling with several mechanisms (at least for mixtures diluted in nitrogen under stoichiometric and lean conditions).
Therefore, in order to understand this phenomenon, simulations were carried out in this case under adiabatic conditions. The absence of heat loss mechanisms from the reactor to the surroundings allows for the evaluation of only the kinetic aspects of the problem, without considering complex interactions between heat exchange mechanisms and chemical reactions. After that, simulations were carried out considering the heat loss processes. This better replicates the experimental combustion processes in the plug flow reactor.
The CRECK-2014 mechanism, one of the more reliable predictors as shown in the previous chapter and as reported in previous works (de Joannon et al. 2005), was selected as the kinetic model for additional numerical simulations in the auto-ignition process. The CRECK-2014 mechanism provides one of the best overall descriptions of the experimental data related to methane, propane and C_1-C_2 mixtures combustion.

Number	Reaction
1	$O_2 + nC_3H_7 \rightarrow HO_2 + C_3H_6$
2	$O_2 + iC_3H_7 \rightarrow HO_2 + C_3H_6$
3	$nC_3H_7 = CH_3 + C_2H_4$
4	$CH_3 + CH_3OO = CH_3O + CH_3O$
5	$CH_3 + HO_2 = CH_3O + OH$
6	$CH_3O + M = CH_2O + H + M$
7	$HO_2 + HO_2 = H_2O_2 + O_2$
8	$H_2O_2 (+M) = OH + OH (+M)$
9	$iC_3H_7 = C_3H_6 + H$
10	$CH_3 + CH_3 + M = C_2H_6 + M$
11	$H + O_2 = OH + O$
12	$H + O_2 + M = HO_2 + M$
13	$CH_3 + OH = CH_3OH$
14	$CH_3 + OH = CH_2(S) + H_2O$
15	$CO_2 + H = CO + OH$
16	$CH_3 + H_2O = CH_4 + OH$
17	$O + H_2O = OH + OH$
18	$H + H_2O = H_2 + OH$
19	$O + H_2 = OH + H$
20	$HCO + M = H + CO + M$
21	$HCO + O_2 = HO_2 + CO$
22	$C_2H_5 \rightarrow C_2H_4 + H$
23	$H + HO_2 = OH + OH$
24	$H + HO_2 = H_2 + O_2$

Table 5.1 – Main reactions involved in the SECs combustion process.

Figure 5.1 reports the numerical auto-ignition time in the Arrhenius diagram for stoichiometric propane mixtures diluted in nitrogen from 80% to 97% (note that the stoichiometric propane/air mixture has a N_2 percentage of approximately 76%). The pressure is atmospheric.

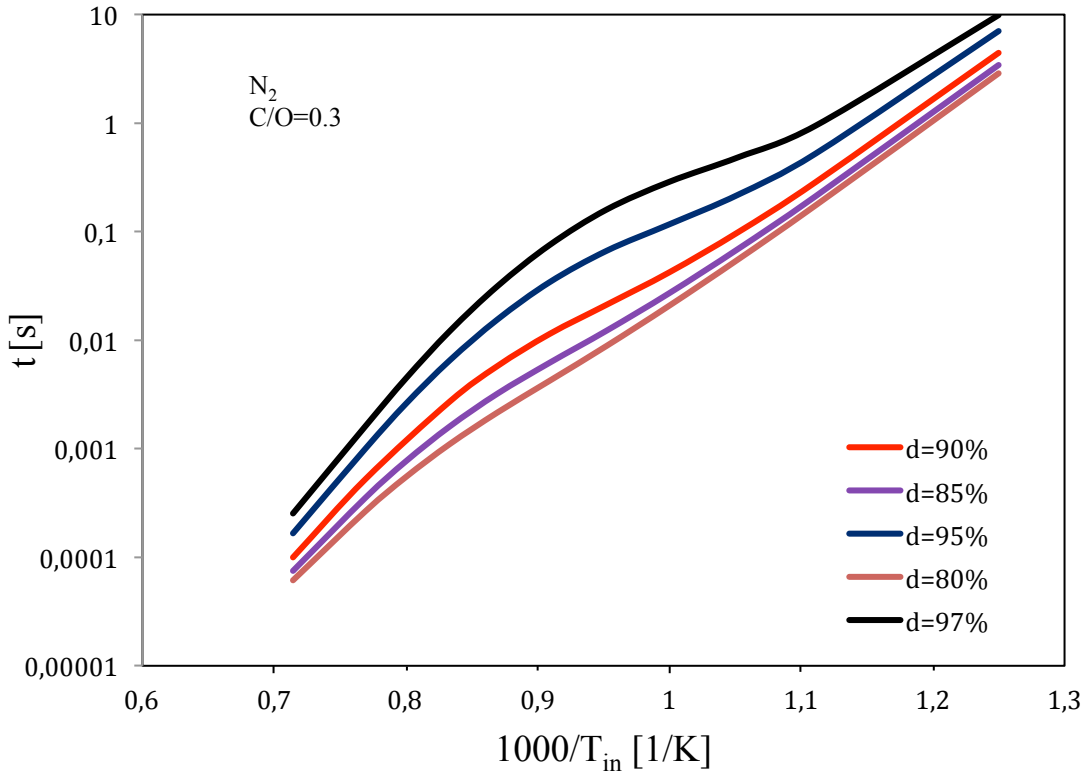

Fig. 5.1 – Auto-ignition delay data for propane stoichiometric mixtures at 1 atm with different dilution levels.

As expected, the auto-ignition delay times increase from a dilution level of 80% to 97%. A change in slope is observed for all dilution values. It is worth noting that it becomes more evident as the nitrogen concentration increases. For instance, at d = 80%, the change in the activation energy of the ignition process is almost unperceivable. Furthermore, the ignition profile inflection point shifts towards lower inlet temperatures with increasing mixture dilutions. Therefore it is possible to say that this observed phenomenon is a direct consequence of the high dilution.

In low-dilution conditions, the ignition process is sustained by high temperature gradients, and a fast chemistry dominates the process evolution. In contrast, for diluted conditions, the reactivity of the system slows down because lower adiabatic flame temperatures make the system more sensitive to the operating conditions and enhances the competition among several pathways, thus permitting the onset of phenomenologies that are generally hidden during conventional combustion processes.

To understand the kinetics behind this behaviour for propane mixtures, numerical analyses were performed. Reaction pathway analysis and sensitivity and rate of production analyses of the main species were carried out and reported for a stoichiometric mixture diluted up to 90% at three different inlet temperatures (T_{in} = 850 K, 1050 K and 1300 K, representing low, intermediate and high temperature conditions, respectively).

The specific selection of the CRECK-2014 mechanism does not alter the generality of this discussion: while elementary reactions in the other kinetic mechanisms have different kinetic parameters, their relative weights are similar, and the main and the ignition controlling reactions are the same.

Figure 5.2 shows the flux diagram at T_{in} = 850 K. The solid line represents the C-species (carbonaceous species), while dashed lines represent the reactions leading to the production of radicals. The reactions reported on the top-right represent the main branching reactions.

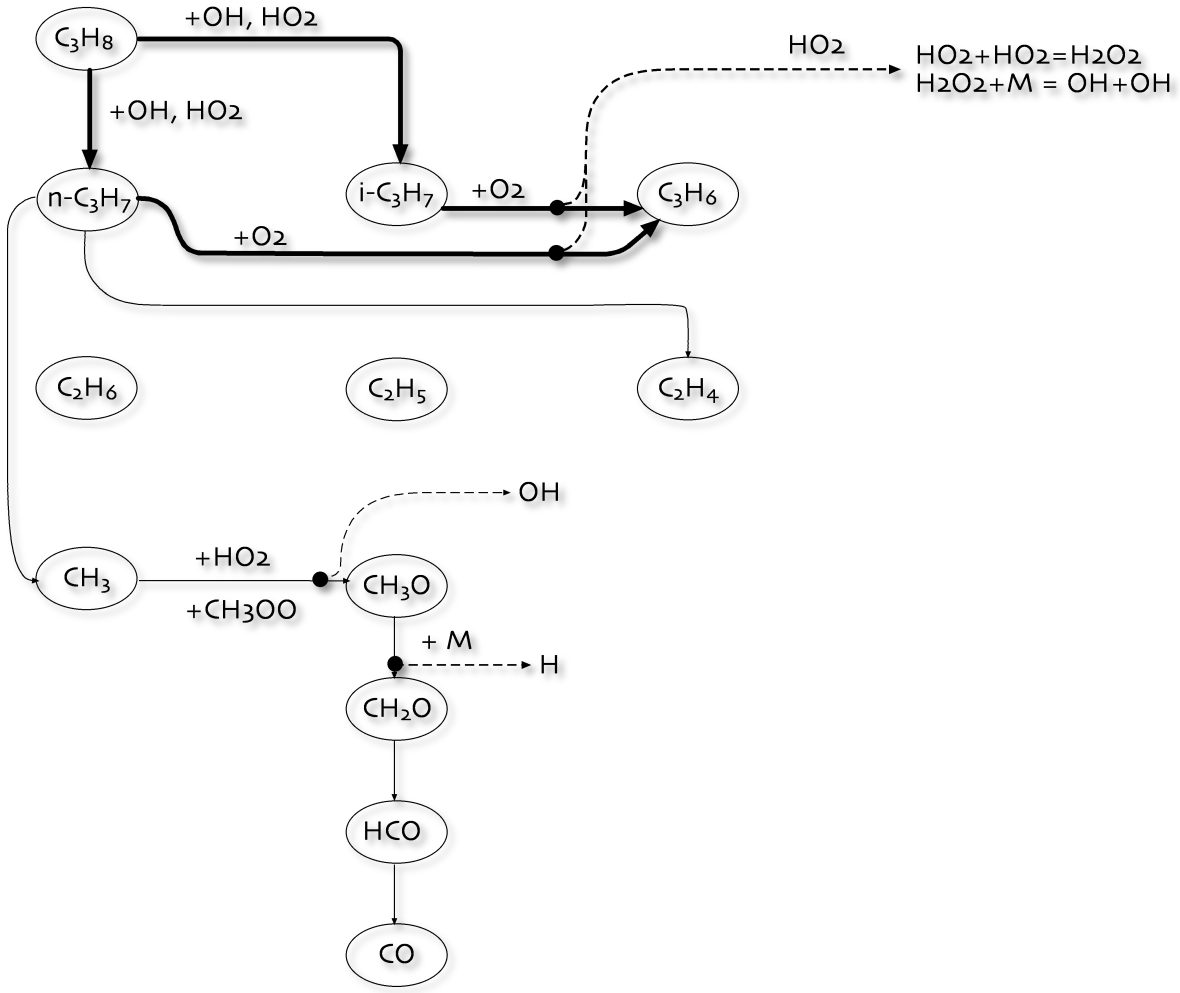

Fig. 5.2 – Flux diagram for a stoichiometric C_3H_8/O_2 mixture diluted in N_2 to 90% with T_{in} = 850 K.

The main reactions involved in the ignition process of propane/oxygen mixtures under diluted operating conditions are summarized in the Table 5.1.
The results suggest that at T_{in} = 850 K, propane is dehydrogenated to iso-propyl and normal-propyl by OH and HO2 radicals. The resultant C_3 radicals mainly undergo dehydrogenation reactions, reacting with molecular oxygen through reactions (1) and (2):

$O_2 + nC_3H_7 \Rightarrow HO_2 + C_3H_6$ (1)

$O_2 + iC_3H_7 \Rightarrow HO_2 + C_3H_6$ (2)

Normal-propyl radicals also decompose to CH_3 and C_2H_4:

$nC_3H_7 = CH_3 + C_2H_4$ (3)

Methyl radicals are oxidized to CH_3O and CH_2O through the following reactions:

$CH_3 + CH_3OO = CH_3O + CH_3O$ (4)

$CH_3 + HO_2 = CH_3O + OH$ (5)

$CH_3O + M = CH_2O + H + M$ (6)

Leading to the production of OH and H radicals. HO_2 radicals, produced by reactions 1 and 2, mainly react through reactions 5 and 7:

$HO_2 + HO_2 = H_2O_2 + O_2$ (7)

$H_2O_2 (+M) = OH + OH (+M)$ (8)

Reaction 8 represents the branching reaction at low temperatures, promoting the formation of OH radicals.
The flux diagram at T_{in} = 1050 K is shown in Fig. 5.3. At this inlet temperature, propane is dehydrogenated to its radicals i-C_3H_7 and n-C_3H_7.

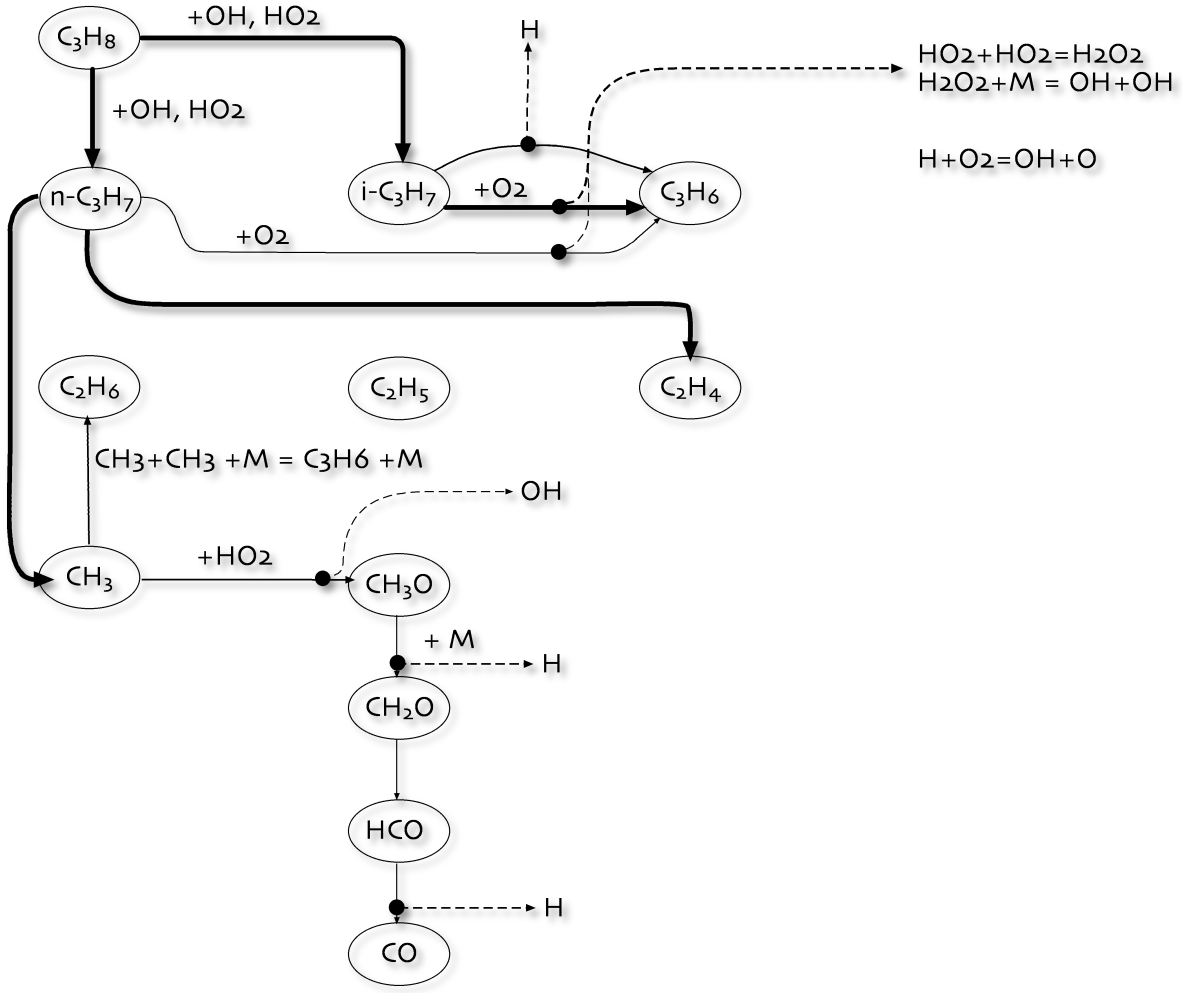

Fig. 5.3 – Flux diagram for a stoichiometric C_3H_8/O_2 mixture diluted in N_2 to 90% with T_{in} = 1050 K.

In this case, i-C_3H_7 can both react with oxygen (leading to the production of HO_2 radicals) and decompose through an equilibrium reaction

$iC_3H_7 = C_3H_6 + H$ (9)

Decomposition leads to the production of H radicals, which mainly reconvert C_3H_6 to i-C_3H_7 at this T_{in}.
However, n-C_3H_7 radicals mainly decompose to methyl radicals and ethylene (reaction 3).
The branching reactions are still related to H_2O_2 formation and decomposition, but the formation of HO_2 radicals is relatively limited with respect to T_{in} = 850 K. At this temperature, n-C_3H_7 does not react with oxygen while i-C_3H_7 decomposition (reaction 9) becomes relevant. In this case, the production of radical species is sustained by the pathway CH_3 => CH_3O => CH_2O => HCO => CO. In particular, methyl radicals are oxidized to CH_3O by HO_2 radicals. For T_{in} > 1000 K, the reaction

$CH_3 + CH_3 + M = C_2H_6 + M$ (10)

plays an important role, promoting recombination and pyrolytic reactions, as described by the sequence C_2H_6 => C_2H_5 => C_2H_4 => C_2H_3. Reaction 10 competes with the oxidation pathways, the rates of which are reduced due to the depleted concentration of HO_2 radicals. This results in decreased production of OH and H radicals. Such an effect, combined with less pronounced

production of HO_2, leads to a relatively lower system reactivity and to changes in the slope of auto-ignition times in the Arrhenius plot diagram.
Figure 5.4 shows the flux diagram at T_{in} = 1300 K. At this inlet temperature, propane is dehydrogenated by OH and H radicals to normal- and iso-propyl species, which then decompose through reaction 3 and 9, respectively. The last reaction boosts the production oh H radicals.

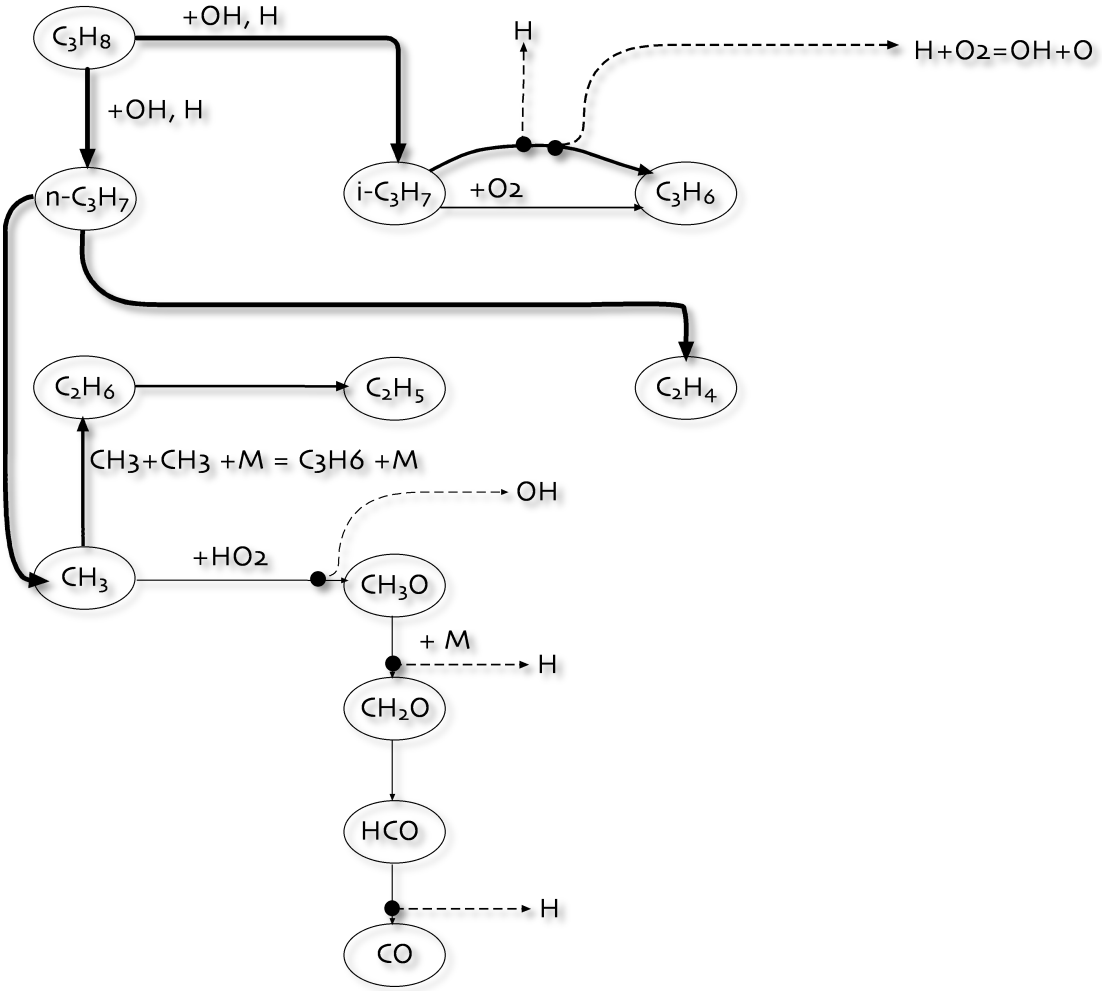

Fig. 5.4 – Flux diagram for a stoichiometric C_3H_8/O_2 mixture diluted in N_2 to 90% with T_{in} = 1300 K.

Propane also thermally decomposes to CH_3 and C_2H_5. Methyl radicals mainly recombine to ethane, thereby feeding the C_2H_6 => C_2H_5 => C_2H_4 => C_2H_3 pathway. The methyl oxidation route is relatively less intense due to the strong rate of the recombination reaction and to the depletion of HO_2 radicals.
The typical high temperature branching reaction
$H + O_2 = OH + O$ (11)
promotes auto-ignition at an inlet temperature of 1300 K.
It significantly increases the reactivity of the system, leading to an increased auto-ignition delay time curve slope in the Arrhenius plot compared with intermediate temperatures.
The kinetics involved in propane auto-ignition as a function of T_{in} can also be deduced from Fig. 5.5. The rate of key reaction is reported as a function of the inlet temperature along with t. In particular, Fig. 5.5a shows the auto-ignition relative to the H_2/O_2 sub-mechanism branching reactions, and Fig. 5.5b shows the auto-ignition relative to the C_1 species.
Figure 5.5a describes the trend of reactions 7, 8 and 11. Furthermore, reaction
$H + O_2 + M = HO_2 + M$ (12)

is included because it competes with reaction 11.

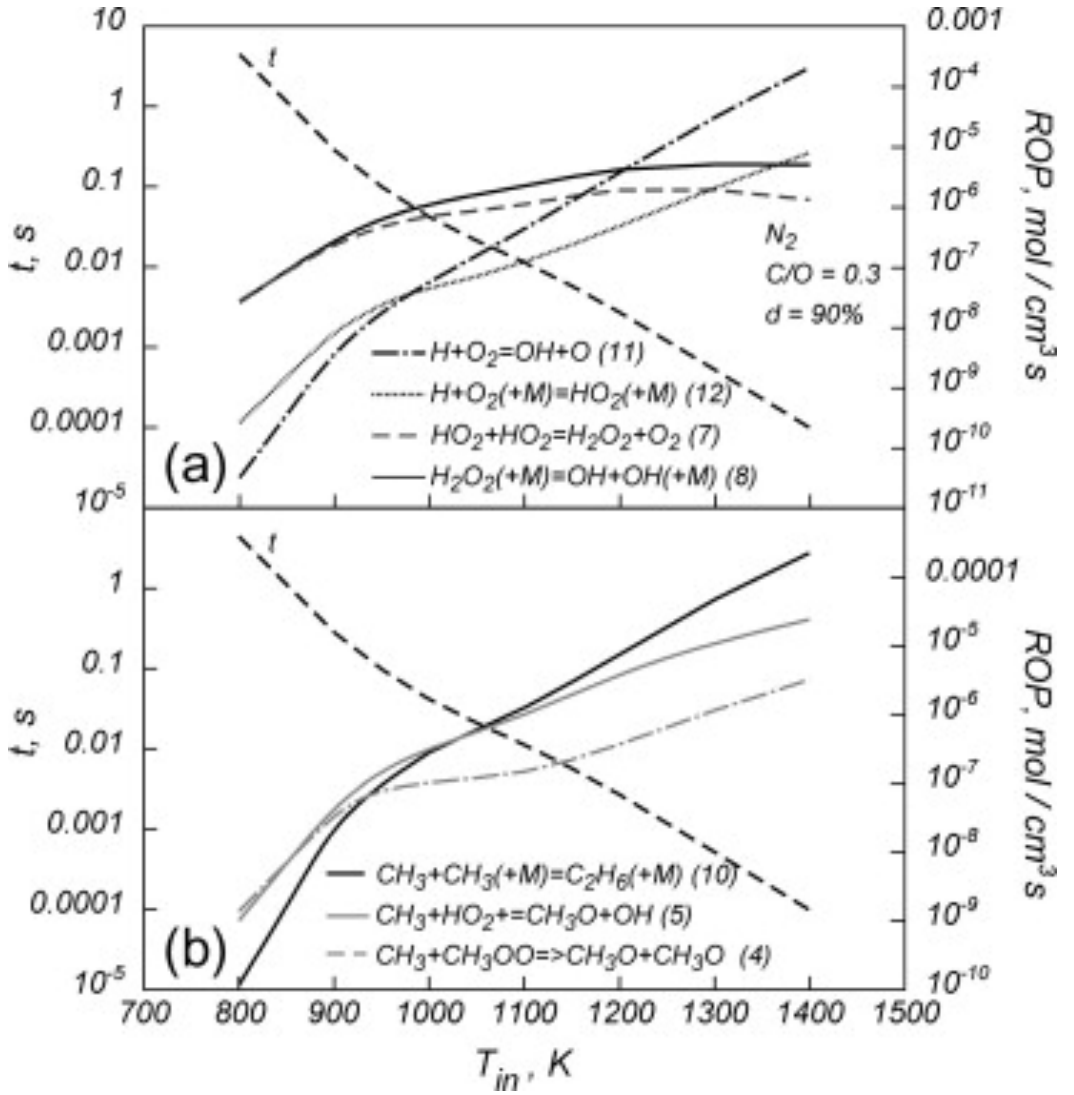

Fig. 5.5 – Rate of production analysis for key reactions for a stoichiometric C_3H_8/O_2 mixture diluted in N_2 to 90%.

It is worth noting that reactions 7 and 8 are the controlling branching mechanisms up to 1200 K. For higher inlet temperatures, reaction 11 is the most important mechanism. Reaction 12 does not act as a controlling step in this temperature range.

Figure 5.5b shows the relative weight of C_1 oxidation and recombination reactions. For $T_{in} < 1100$ K, the C_1 oxidation reactions dominate through reactions 4 and 5. For $T_{in} > 1100$ K, the recombination reaction becomes the most important.

The onset of reaction 10 slows down the mixture reactivity because it stores C and H radicals in the C_2 species, thereby inhibiting the oxidation channel that produces radical species over a temperature range in which the main branching mechanism (reactions 7 and 8) is relatively weak. This mechanism increases auto-ignition delays. At higher temperatures, reaction 11 becomes the dominant branching mechanism, produces a large amount of radicals (thus accelerating the system reactivity), and induces a change in the slope of the ignition time curves.

The rate of production analysis has been extended to stoichiometric mixtures diluted at 95% in N_2 at atmospheric pressure to assess the influence of such a parameter on the controlling kinetics of the auto-ignition times. It has been observed that the reaction rate of the methyl recombination reaction becomes higher than the oxidation one (represented by reaction 5) for $T_{in} = 950$ K. Therefore, because dilution promotes the recombination channel with respect to the oxidation routes for lower

temperatures, the change in slope of the curve of the auto-ignition delay time occurs at lower temperatures with increasing dilution levels. Furthermore, the reaction 11 becomes faster than reaction 8 for T_{in} = 1150 K, widening the range of temperatures for which reaction 8 is the primary branching reaction.
As a direct consequence of the competition among different kinetic route, it is possible to infer that high levels of dilution lead to nearly isothermal conditions that, when associated with strong pre-heating, alter the relative weights of pyrolytic/oxidative routes, promoting the establishment of different regimes. When such competition becomes very sensitive to the operating conditions (i.e., the temperature and the carbon/oxygen mixture feed ratio), dynamic phenomena can emerge.
Such behaviours are not recognizable in conventional systems because the high heat release, associated with standard deflagration or diffusion flames, enhances the shift among the different regimes, thereby promoting the establishment of kinetics typically observed at high temperatures.
In the previous chapter, this behaviour was found to be strongly dependent on the equivalence ratio.
Figure 5.6 shows the numerical auto-ignition delay times in the Arrhenius plot computed for fuel-rich, stoichiometric and fuel-lean conditions identified using C/O = 0.5 (Φ =1.67), C/O = 0.3 (Φ = 1) and C/O = 0.05 (Φ = 0.17), respectively, at inlet temperatures from 800 to 1400 K at atmospheric pressure. The mixtures are diluted at 90% in N_2.

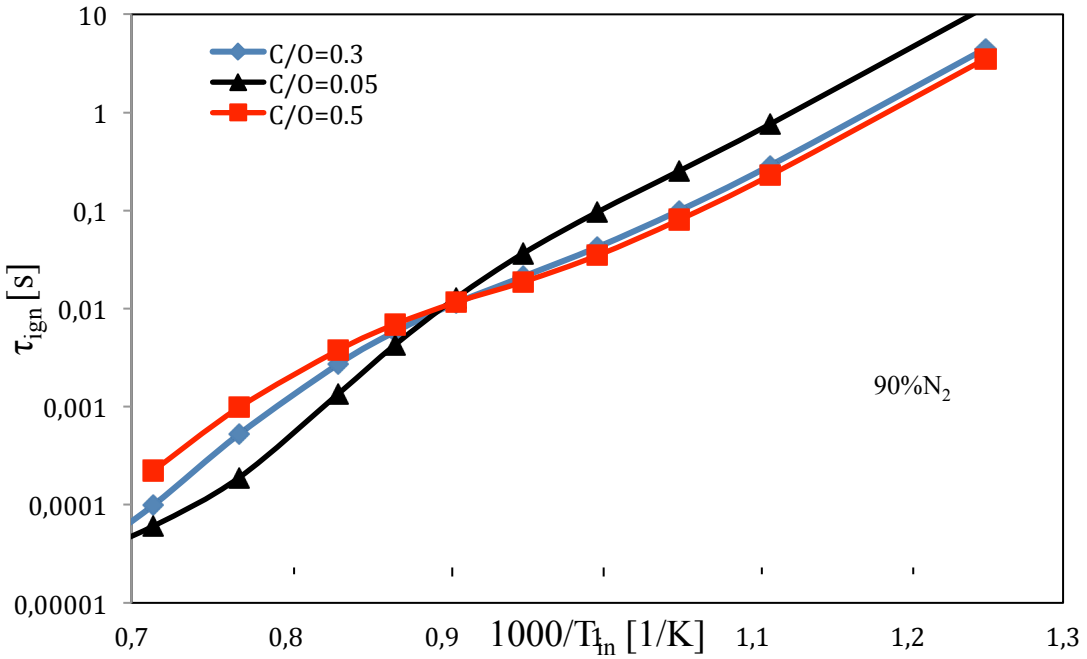

Fig. 5.6 – Auto-ignition delay data for fuel-lean (C/O = 0.05), stoichiometric (C/O = 0.3) and fuel-rich (C/O = 0.5) conditions.

The figure shows that for low inlet temperatures, the auto-ignition delay times decrease from fuel-lean to fuel-rich mixtures.
At temperatures below 1125 K ($1000/T_{in}$ = 0.88), for the fuel-lean mixture, the auto-ignition delay values exhibit a linear dependence on temperature in the Arrhenius plot.
For the fuel stoichiometric and fuel-rich mixtures, there is a change in the slope of the auto-ignition times curves at approximately T_{in} = 950 K. Then, as for $1000/T_{in}$ = 0.8, the slopes of the curves change again, and for high inlet temperatures, fuel-lean mixtures correspond to lower ignition times.
For high temperatures, the fuel-lean mixture exhibits a second change in slope, and thus the auto-ignition data shifts toward the stoichiometric curves.

Therefore, values of t in Fig. 5.6 show a NTC-like behaviour more evident for rich mixtures. Analyses similar to that reported for the stoichiometric mixture have been realized for fuel-rich and fuel-lean conditions (not reported here). These analyses revealed that in lean conditions, the delaying effect induced by reaction 10 is damped by the promotion of reaction 11 due to higher O_2 concentrations, resulting in only a slight change in the auto-ignition delay time curve. Furthermore, the flux diagrams for fuel- lean mixtures have revealed that the competition between oxidation and recombination channels is altered by the promotion of other oxidative routes represented by the following reactions:

$CH_3 + OH = CH_3OH$ (13)

$CH_3 + OH = CH_2(S) + H_2O$ (14).

The onset of such reactions, promoted by the high amount of OH radicals boosted by reaction 11, makes the recombination channel less active, thus lowering its effect on the ignition delay times.

Influence of heat loss

Figure 4.6 in the previous chapter showed that in the region of no dependence of the ignition delay time on temperature, it was experimentally observed a weak ignition phenomenon. In order to understand the influence of heat loss on the observed behaviour, several simulations were performed with different heat exchange coefficients.

Figure 5.7 shows the simulated axial temperature profiles for a stoichiometric propane/oxygen mixture diluted at 90% in nitrogen for various values of the heat transfer coefficient (U), at 1100 K.

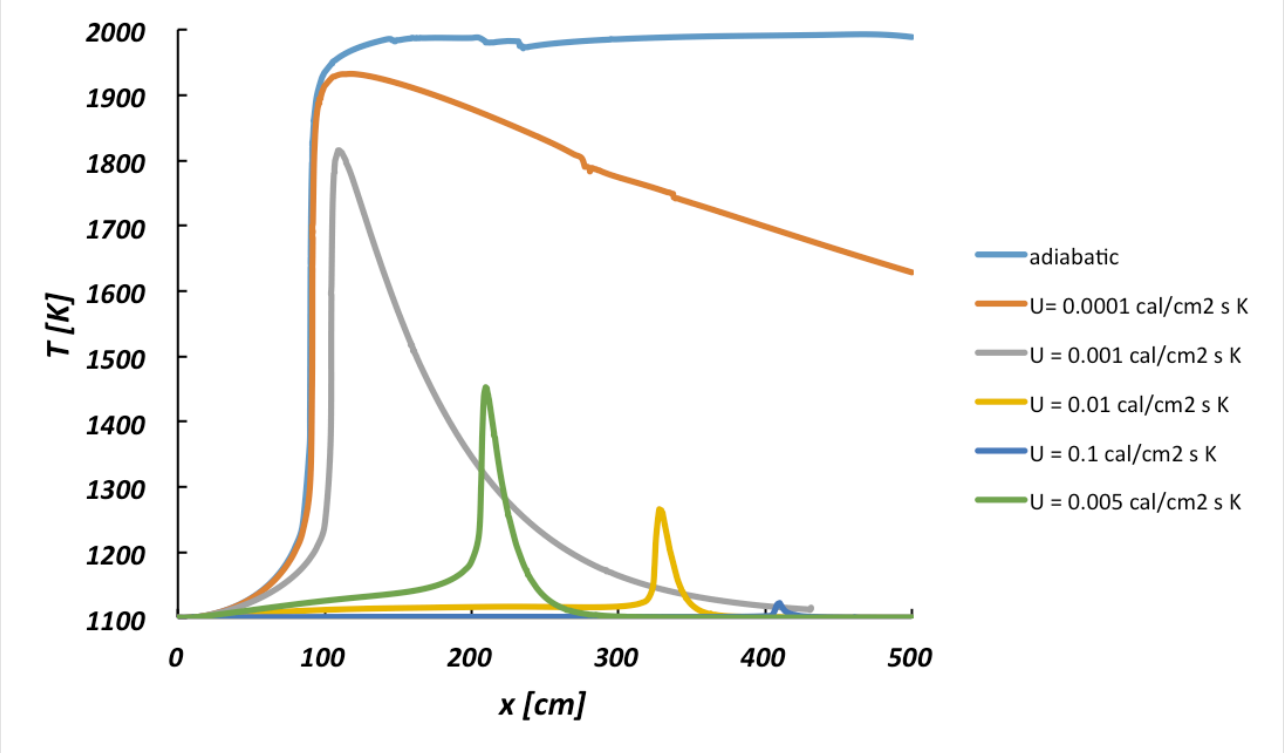

Fig. 5.7 – Numerical temperature profiles for a stoichiometric C_3H_8/O_2 mixture diluted in N_2 at 90% simulated with different values of the global heat exchange coefficient for T_{in} = 1100 K.

From the figure, it can be observed that the temperature profiles strongly depended on U and that the heat loss affected the profiles in two ways. First, the heat loss decreases the maximum temperature. Second, by increasing the global heat exchange coefficient, the temperature history shows a trend similar to a two-stage ignition, where the first stage is weak, as experimentally observed. It should be noted that this effect of the heat loss is predicted only with the ChemKinPRO software, whereas using the OpenSMOKE++ software the heat exchange appears to not influence

the ignition process. However, the trend predicted using the ChemKinPro software is closer to the experimental observation.
After this analysis it has been finally clarified that the observed ignition behaviour for diluted propane mixtures at intermediate temperature is different with respect to two-stage cool flame ignition that occurs at low temperature. First, the kinetics responsible for such a behaviour are different with respect to the kinetics that lead to a cool flame ignition at low temperature. Second, although oscillatory cool flames are an artefact of non-adiabatic conditions, two-stage ignition is a phenomenon that can also be observed in adiabatic systems. On the other hand, the NTC-like ignition behaviour observed in the present experiment has been demonstrated to be due to chemical kinetics, but the correspondent weak ignition is an artefact of non-adiabatic conditions. In fact, in the adiabatic simulation, only one sharp ignition is predicted.
Similarly, Sabia et al. (2013) discussed these behaviours for methane. The authors affirmed that specific combustion regimes occur due to the interaction between the chemistry and heat-transfer mechanisms of the reactor. In conventional confined systems, the flame is stabilized by thermal feedback through wall-to-wall radiation, conduction in the tube wall and convection between the gas stream and the wall. In particular, axial heat conduction provides a thermal feedback mechanism (i.e., heat axial dispersion and conduction in the reactor wall) and can cause instabilities and multiple steady states.
Under diluted operating conditions the heat release and temperature gradients are modest with respect to conventional flames; the pre-heating temperatures, which sustain the oxidation process, promote pyrolytic/recombination reactions; and the high dilution levels decrease the oxidation reaction rates. Both operating conditions lead to slower mixture reactivity with respect to conventional flames. Thus, the interaction between the heat exchanged to the surroundings and the heat produced by fuel oxidation is more dramatic. Such a heat balance leads to the establishment of several combustion regimes that are dependent on system parameters and the mixture composition. The slow transit between kinetic pathways, mainly due to the modest temperature gradients, is a critical point for the establishment of transitional and/or dynamic regimes.
As a matter of fact Choi et al. (2009) showed that for preheated and diluted propane flames, the autoignition behaviour was controlled by the ignition delay time considering heat loss.
At the most fundamental level, ignition occurs when the rates of heat release and/or chain branching are fast relative to the various loss mechanisms. The alkyl radicals tend to react with O_2 to form HO_2 (reactions 1 and 2). The HO_2 reacts with itself to form H_2O_2 (reaction 7), making the sequence essentially chain terminating until the H_2O_2 dissociates to form a pair of OH (reaction 8). Ignition is primarily dependent on the consumption of fuel by radicals, primarily OH, and thus radical production through branching reactions is critical. The H_2O_2 dissociation has high activation energy and is sensitive to heat losses from the reaction zone. Because of the slow rate of H_2O_2 dissociation and the slow rate for these T_{in} of high-temperature radical branching, this intermediate-temperature chemistry tends to progress more slowly toward ignition with a rate that increases strongly with increasing temperature.
At higher temperatures, the rate of the branching reaction 11 becomes faster than chain-terminating reactions, typically reaction 10 and 12, and the overall rates of reaction increase rapidly due to branching. At these temperatures, the chemistry is significantly faster than that of the intermediate-temperature regimes.
A further important point that arises from this analysis is the criterion used to define the delay time.
The ignition delay time usually is observed experimentally when there is a sudden, dramatic change in the thermodynamic state of the system. Although the ignition event is relatively unambiguous, several different diagnostic techniques are used to measure ignition delay in practice, and these methods do not always agree precisely. However, as the systems studied in this work could be characterized by a weak ignition, this can cause some ambiguity as it depends on the sensitivity of the measurement equipment. For some experiments, the ignition delay time cannot be easily identified due to the very low “first-stage” heat release relative to the heat loss to the wall and a

more unequivocal ignition time definition is needed. It is suggested that the criterion used here, accordingly with Abtahizadeh et al. (2012), is a more reliable and accurate method of defining ignition delay time, as the temperature variation with time can be relatively easily monitored experimentally in practical reactive systems.
The present work confirms that the heat exchange must be taken into account in the data processing. Under certain inlet conditions, an adiabatic calculation could give an underestimate of the ignition delay when compared with that under non-adiabatic conditions and any correction to match the experimental measurement without proper allowance for non-adiabaticity thus necessitates some false compensation in kinetic parameters of the reaction scheme.

5.2 Oscillatory periodic behaviour

Oscillatory periodic regimes were identified for all the fuels tested in the present work, both in the TFR and in the JSFR.
Numerical simulations were able to reproduce such behaviour in the PSR. It was not possible to predict oscillations in the PFR because the PFR equations do not include the time as independent variable.
Therefore, in order to determine the rate-limiting reactions in this regime, a reaction flux analysis is performed for radicals generation and destruction reactions for different inlet temperatures. Given that such behaviour was observed for all tested fuels, the analysis is performed using methane as reference fuel, given the simplest kinetics. Once again CRECK-2014 model has been chosen given its strong performance in predicting such phenomenon.

Influence of heat loss
As seen in the chapter 2, in the literature it is reported that these oscillations are thermo-kinetic oscillations and are sensibly influenced by the heat losses. Therefore, preliminary, it is appropriate to analyse the influence of the heat exchange on the involved phenomenon.
Figure 5.8 shows the simulated temporal temperature profiles in a PSR for various values of the heat transfer coefficient (U) for a stoichiometric methane mixture diluted at 90% in nitrogen. From the figure, it can be observed that the temperature profiles strongly depend on U and that the heat loss affects the profiles in two ways. First, the heat loss decreases the maximum temperature. In all cases, it is observed that the temperature increases rapidly around 0.5 s (this time slightly increases by increasing the heat exchange coefficient) until it is close to the adiabatic flame temperature (T_{ad} = 1870 K). However, the peak values are in inverse proportion to the heat loss and are significantly influenced by it. Second, the heat loss leads to both steady and unsteady conditions after the temperature reaches the maximum value. In the case of relatively low values of U (U = 1 and 10 W/m^2 K), the temperature decreases gradually and reaches steady conditions. In contrast, unsteady conditions are observed in the case of high values of U (U = 50, 100 and 1000 W/m^2 K). These unsteady conditions are observed when the temperature decreases below a certain value.
In contrast to what was seen in the case of PFR simulations, in this case it is observed that the predicted influence of heat loss is exactly the same, performing the numerical simulations with the two software ChemKin PRO and OpenSMOKE++.
In addition, it was noted that an oscillatory dynamic regime is also detectable by simulating the reactive system under isothermal conditions (of course in this case only the concentrations of chemical species oscillate and not the temperature). Hence, numerical simulations carried out in order to understand the nature of this phenomenon, have been performed under isothermal conditions, so as to further simplify the combustion process.

Isothermal transient behaviour
First of all, it is worth pointing out that the methane kinetic pathways under the investigated operating conditions, are similar to those discussed in the case of propane combustion, clearly

excluding the reactions involving the C_3 species. Therefore, instead of repeating again the main paths, we will refer to Table 5.1.

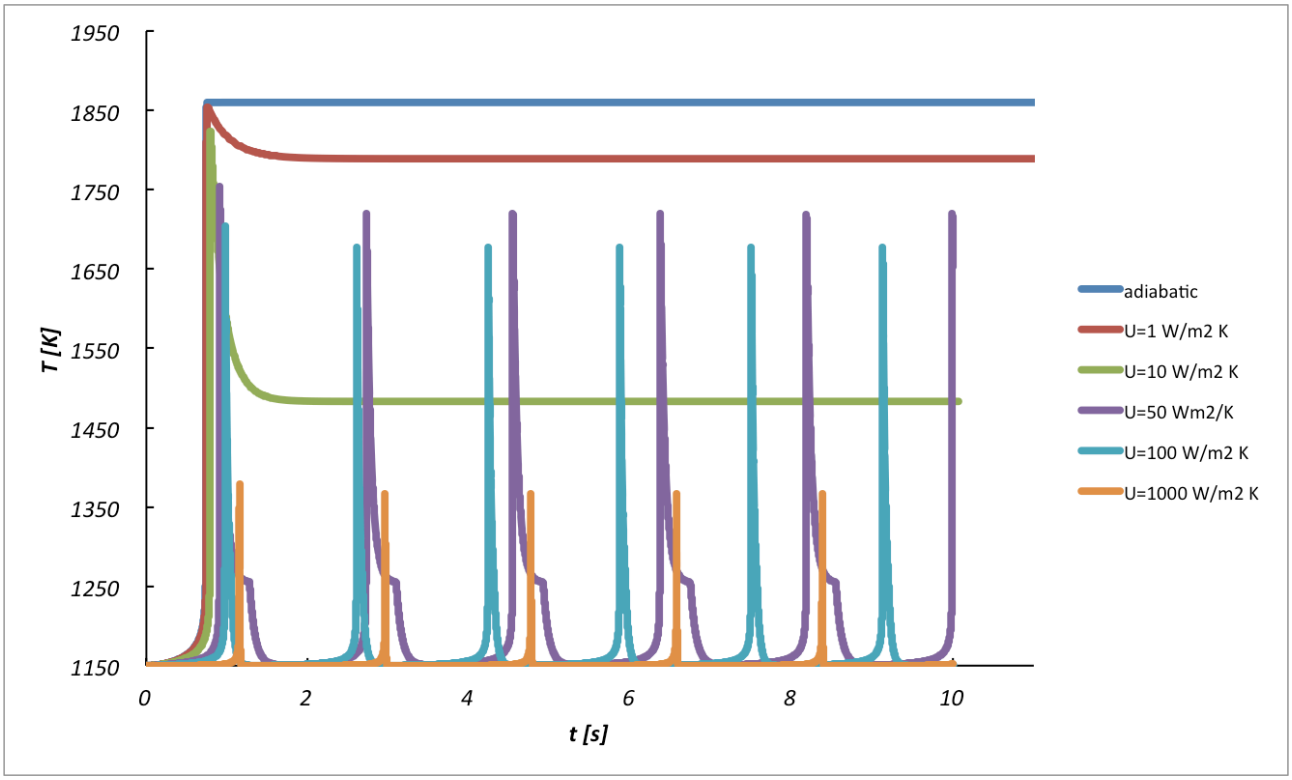

Fig. 5.8 - Numerical temperature profiles for a stoichiometric CH_4/O_2 mixture diluted in N_2 at 90% simulated with different values of the global heat exchange coefficient for T_{in} = 1150 K.

In Fig. 5.9, the rate of the controlling branching and recombination reactions are reported as a function of the inlet temperature.

The vertical dashed lines represent the T_{in} range in which oscillations occur. In order to make the figure clear, for high T_{in}, outside the T_{in} oscillatory range, the rate of reactions are plotted on a secondary axis.

In the investigated temperature range, the combustion kinetics is either dominated by intermediate-temperature chemistry or by high-temperature chemistry, using the CRECK-2014 mechanism.

Intermediate-temperature chemistry is represented by H_2O_2 decomposition (reaction 8) and high-temperature chemistry by reaction 11. The two mechanisms compete leading to the observed behaviour, as shown in Fig. 5.9.

Figure. 5.9 shows that, with increasing temperature, the rates of reaction of intermediate-temperature chemistry (reaction 7 and 8) first exponentially increase and then they reach a plateau as the recombination reaction 12 takes over (around 1100 K). For a certain temperature (around 1120 K), with increasing T_{in}, the rates of reaction of intermediate-temperature chemistry start to decrease. This value of T_{in} represents the critical temperature where a shift from steady to unsteady conditions was observed, as indicated by the vertical dashed line. This temperature is not sufficient to effectively activate the high-temperature branching, which strongly compete with the recombination reaction 12. Indeed the rate of reaction 11 is only two times higher than the rate of reaction 12.

On the other hand, Fig. 5.9 shows that high-temperature chemistry plays an important role in the case of steady conditions, at T_{in} > 1250 K, where the rate of reaction 11 is 3.5 times higher than reaction 12 and the rates of reaction of the intermediate-chemistry are close to zero (in particular the rate of reaction 8 is negative).

As a matter of fact, a certain temperature was required for producing the H radical and activating the high-temperature chemistry. Therefore, a shift from unsteady to steady conditions is observed when the second critical temperature (around 1250 K) is crossed. Temperatures between 1120 K and 1250 K represent the split temperature range between intermediate-and high-temperature chemistries.

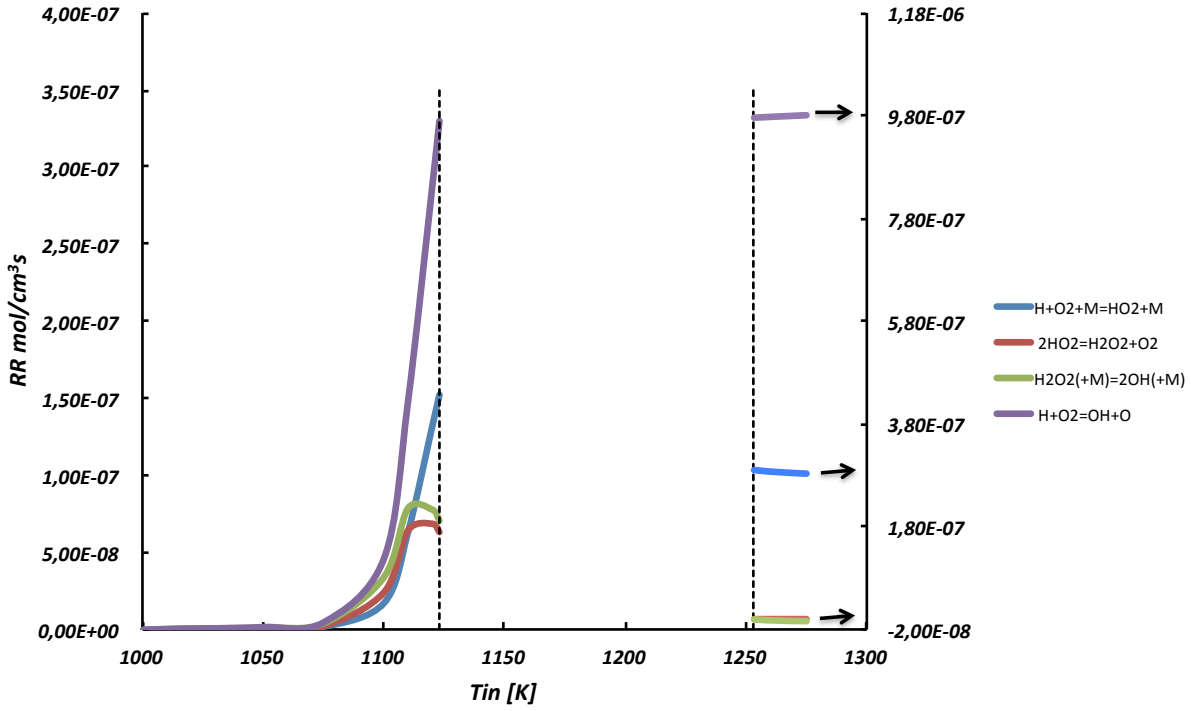

Fig. 5.9 - Rate of reaction analysis for key reactions for a stoichiometric CH_4/O_2 mixture diluted in N_2 to 90%, as a function of T_{in}.

From the results shown in Fig. 5.9, it is clear that active reactions at a temperature below the first critical temperature, namely the HO_2 and H_2O_2 path, play an important role in initiating oscillations. These reactions generate sufficient conversion to activate high-temperature chemistry. In other words, switching between intermediate- and high-temperature chemistries results in oscillations, and these oscillations would not occur without the activation of intermediate-temperature chemistry. In fact, for T_{in} > 1250 K, where steady combustion occurs, ignition bypasses the intermediate-temperature chemistry and starts directly from the high-temperature chemistry.
Figure 5.10 shows the rate of controlling reactions on the top and the net production rate of major radicals down, as a function of time during one cycle of oscillations using the CRECK-2014 mechanism. In the figure also the methane mole fraction is reported on a secondary axis.
In addition to the branching and recombination reactions relating to the hydrogen/oxygen system, also the reactions that show the conversion of CH_3 are a key for understanding the entire mechanism which triggers these oscillations.
From Fig. 5.10 it is implied that CH_3 and HO_2 species are stored (production rate are greater than the consumption rate); the stored species produce active species such as H, O and OH.

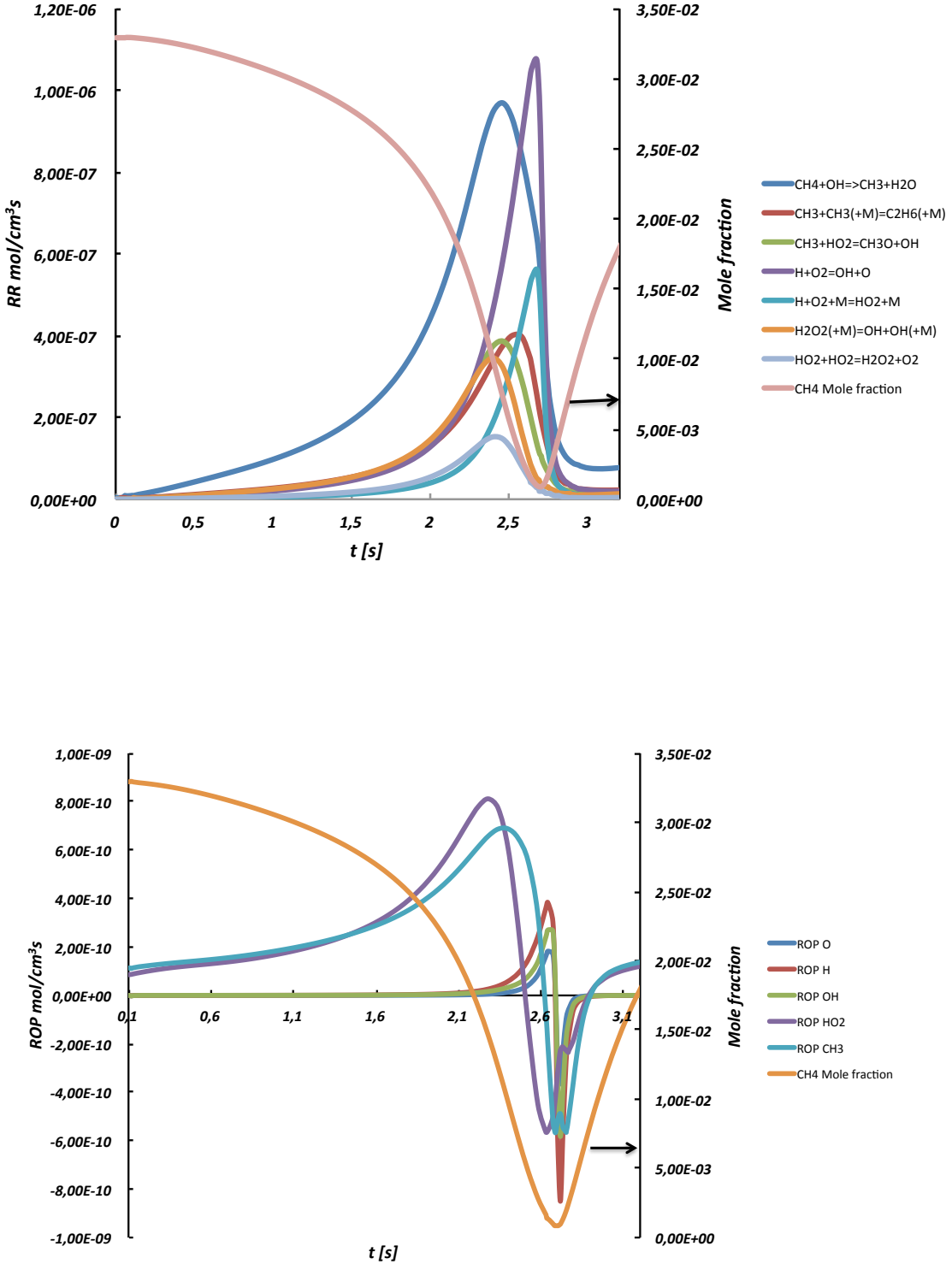

Fig. 5.10 - Rate of reaction analysis for key reactions (top) and rate of production of main radicals (down) for a stoichiometric CH_4/O_2 mixture diluted in N_2 to 90%, as a function of time for one oscillation cycle, at T_{in} = 1125 K.

Meanwhile, methane conversion rapidly increases consuming H, OH and O radicals. In addition, the intermediate-temperature chemistry increases the conversion periodically in two steps. The separation between these two noticeable stages corresponds to a distinct change in the slope of the H, OH and O rate rise. The different exponential rise rates observed between the two stages are mainly due to reactions involving HO_2 radicals. At early times (about 2.3 s), essentially the HO_2 rate is about 50 times higher than OH rate (see the bottom of Fig. 5.10). Even though the rate coefficients for fuel + OH are larger than the rate coefficients for fuel + HO_2, HO_2 nonetheless is responsible for a significant percentage of the total fuel consumption in the first stage through reaction 5 (that produces OH) and through the reaction sequence 7 + 8 (that produces two OH). The HO_2 rate continues to build until reaching a maximum. This just precedes the observed kink in the H, OH and O rate profiles, which indicates the start of the second stage. At this point the rate of HO_2 production decreases significantly and the HO_2 reactions become relatively unimportant (see the top of Fig. 5.10). Under these conditions there are more OH radicals being produced than consumed, thereby propagating the chain branching cycle. In the second stage it can be assumed that HO_2 no longer contributes significantly to the production of radicals.
When the methane conversion is almost complete, the concentrations of intermediates like CO and H_2 are no longer negligible, and any reaction of OH with these products produce CO_2 and H_2O and diverts the active radicals away from the chain branching pathway, thereby reducing the gain of the radical feedback system. The extent to which the growth in radical rates is exponential depends upon the comparative rates of production for radicals versus their loss to other channels. In fact, when these reactions start, it can be seen that all the rates of reaction decrease with the exception of reaction 11 and 12 that continue to increase. At the same time, due to the increase of rate of reaction 12, HO_2 rate again starts to increase. Around 2.7 s the rate of reaction 12, along with the HO_2 rate are the highest and the reaction stops. After the negative peak, the species that remain in the reactor mix with the incoming unburned mixture. However, the amount of radicals is not sufficient to sustain the high conversion and the amount of the remaining CH_4 increases, restarting the next cycle.
This is what happens in isothermal conditions. In non-isothermal conditions it is supposed that the oscillation mechanism in the PSR can be described as follows: the reactor temperature increases until it is close to the adiabatic flame temperature because of autoignition. Then, the temperature decreases because of heat loss even if the fresh mixture is immediately oxidized. When the temperature decreases below the critical temperature (between 1120 K and 1250 K) because of a suitable heat loss, the active reaction path changes from high-to-intermediate-temperature chemistry and the just described mechanism initiates.
In non-isothermal conditions, clearly, it must be also taken into account the competition between the exothermic oxidation and endothermic pyrolytic channels, which forces the reactive system to work in a very narrow temperature range.
As matter of fact, de Joannon et al. (2005) argued that at intermediate temperatures, in the range of 1000-1300 K, and at least for methane, the recombination route is more prevalent and the methyl radical CH_3 recombines to form $C_2H_6 \rightarrow C_2H_5 \rightarrow C_2H_4 \rightarrow C_2H_3 \rightarrow C_2H_2$. As acetylene is a relatively stable species, at temperatures higher than 1200 K, it is argued that it is expected to dramatically reduce the reactivity of the system and to be responsible for the oscillations. The authors also showed that by reducing the activation energy for the recombination reactions the oscillations stopped.
After what has been said in these two paragraphs, it is clear that diluted combustion conditions force the reactive system to work in a temperature range where the competition between oxidation and pyrolysis, branching and recombination, and intermediate- and high-temperature branching is stressed. This competition results in the peculiar observed behaviours that, clearly, strongly depend on temperature, equivalence ratio and diluent.

5.3 CO_2 and H_2O effect

For all the fuels tested in the present work, both in the TFR and in the JSFR, the effect of CO_2 and H_2O has been detected.
Numerical simulations were able to reproduce these effects, although not in all the explored conditions.
Therefore, in this section is presented a numerical analysis in the attempt to unravel the nature of these effects.
It should be pointed out that the experiments also evidenced a difference between the results obtained in nitrogen and the results obtained in helium in the JSFR at low temperatures. However, this difference was not predicted by the kinetic models. Therefore, a numerical analysis on this feature is not possible and we leave it as a question mark for future experimental and theoretical research.

5.3.1 Ignition delay times

Based on the obtained numerical analysis for nitrogen-diluted systems, further simulations were performed to understand the role of CO_2 and H_2O in the propane ignition process. They were extended to a wider range of T_{in} (from 800 K to 1400 K) to highlight the effects of such diluent species on the ignition chemistry at low, intermediate and high temperatures. Figure 5.11 shows the auto-ignition data that were numerically obtained for a stoichiometric mixture that was diluted with the three reference diluents.
In any case, the ignition process presents a complex behaviour. For low temperatures, on the Arrhenius plot, the trend is linear with T_{in}; for intermediate temperatures, the curves present a less pronounced slope, which increases again at high temperatures. As reported above, the change of the auto-ignition process activation energy that passes from low to high inlet temperatures was experimentally recognized in the tubular flow reactor for nitrogen-diluted propane/oxygen mixtures. Figure 5.11 shows that this peculiar behaviour is more evident in case of CO_2 and H_2O mixture dilution.

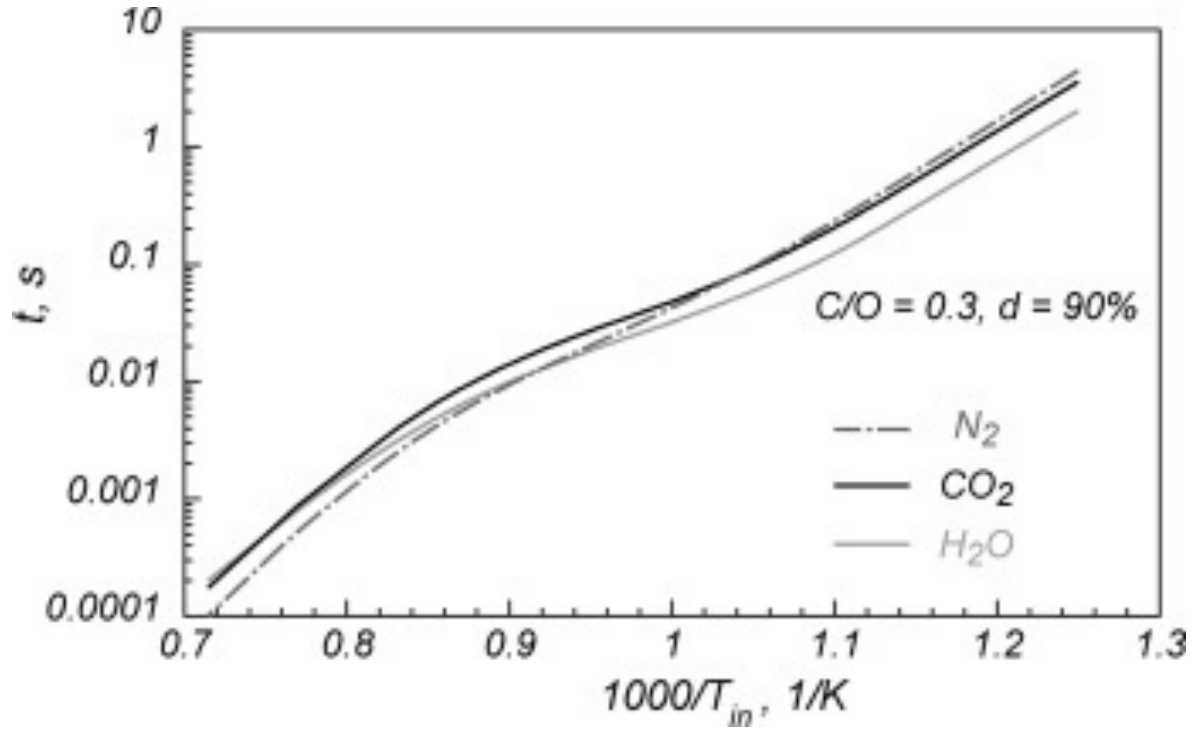

Fig. 5.11 – Comparison among the numerical auto-ignition delay times for the stoichiometric C_3H_8/O_2 mixtures that were diluted to 90% in N_2, CO_2, and H_2O.

For T_{in} < 1000 K, the shortest numerical auto-ignition data are comparable to that of H_2O-diluted system, whereas the longest one is comparable to that of N_2-diluted system. The data of CO_2 dilution lie between and are notably close to the data of N_2. For T_{in} > 1200 K, the situation is reversed, and the N_2-diluted system presents shorter numerical ignition delay than the other two mixtures. In particular, for intermediate temperatures, the CO_2-diluted system has the longest auto-ignition times, whereas for T_{in} > 1300 K, the curves suggest a lower reactivity for the H_2O-diluted system.
The description of the figure suggests that the oxidation paths are significantly modified by the presence of the considered diluent species with complex interactions that depend on T_{in}.
In particular, CO_2 and H_2O have a thermal effect and a chemical effect. The former concerns the greater heat capacity of CO_2 and H_2O with respect to N_2, which decreases the adiabatic flame temperature and alters the kinetic pathways that are promoted by the temperature.
The latter effect concerns the possibility of CO_2 and H_2O interactions with the reaction kinetics. They can:

- directly participate in the elementary reactions as reactants;
- decompose to release/consume radical species;
- participate in termolecular reactions as a third body with third-body efficiencies that are significantly higher than that of N_2.

Furthermore, CO_2 and H_2O are the main products of the combustion process of hydrocarbons; consequently, their high initial concentrations can alter the thermodynamic equilibria of the reactions in which they are involved.

Thermal and chemical effects of CO_2 and H_2O

Further numerical simulations were performed to separate these contributions. In particular, a fictitious species Y with identical molecular structure and thermodynamic properties to either CO_2 or H_2O was defined. This virtual species X does however not appear in the elementary reactions of the kinetic mechanism.
Simulations were performed for both CO_2 and H_2O dilution according to the following steps:
Case (1) diluting the mixtures with Y instead of CO_2 or H_2O to single out the thermal effect from the kinetic effect.
Case (2) diluting the mixtures with Y and setting the third body efficiencies of Y equal to those of CO_2 or H_2O to highlight the effects on the termolecular reactions.
Case (3) diluting the mixtures with the real species CO_2 or H_2O and deleting their third-body efficiencies in the third molecular reactions from the kinetic mechanism to analyse the chemical effect.
Starting from the computed data, the percent variation of the auto-ignition delay times was evaluated case by case with respect to a reference case. In general, negative percent variations indicate that the ignition delay time is accelerated, whereas positive values imply that the process is decelerated.
On the left axis of Fig. 5.12, the percent variations of CO_2 dilution are shown. The dashed-dotted line represents the percent variation of the auto-ignition delay times that were obtained for N_2-diluted mixtures and case (1). It considers the thermal effect of CO_2 with respect to N_2, which varies from 15% to 25% in the entire considered temperature range. With this almost constant thermal contribution, case (1) was chosen as the reference case to evaluate the direct kinetic and third body efficiency effect. Thus, the solid black line is the percent variation between case (2) and case (1) and represents the contribution of the third-body efficiencies of CO_2 to the auto-ignition delay times, whereas the percent variation between case (3) and case (1) represents the chemical effect of these species on the auto-ignition delay time values.
For low temperatures, the main effect is given by termolecular reactions that diminish the auto-ignition times by up to 30% with respect to the Y species. This effect is partially counterbalanced by the thermal effect. At low temperature, the kinetic effect is negligible, which suggests that the

CO_2 contribution as a reactant in bimolecular reactions is negligible. When T_{in} increases, the third-body efficiency effect diminishes, which suggests that the termolecular reactions are less active in the ignition process, which becomes 0 for $1000/T_{in} = 0.98$ and positive for higher temperatures.

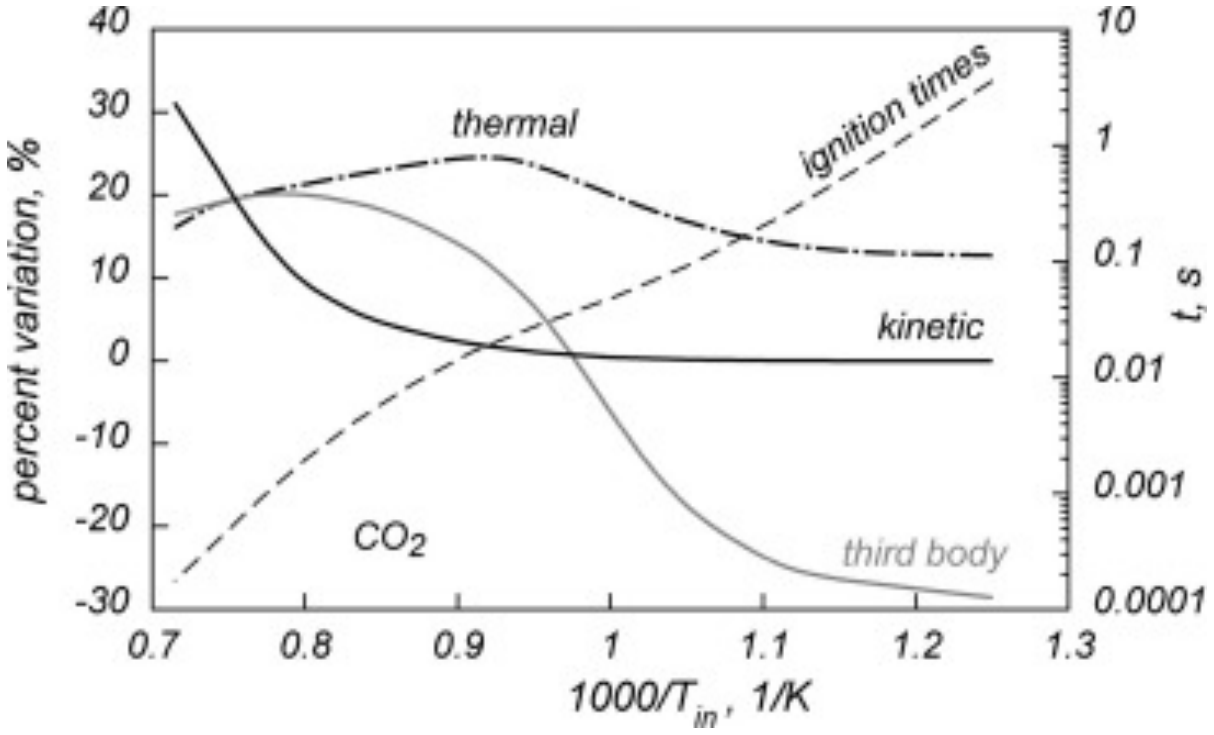

Fig. 5.12 – CO_2 thermal and chemical effects on the auto-ignition delay times.

This trend indicates that in this temperature range, the termolecular reactions inhibit the ignition process.

The kinetic effect becomes important for $1000/T_{in} < 0.8$ with positive values, which determine a delay in the auto-ignition process with respect to the Y case. For high temperatures, it becomes the most important effect.

Similar considerations apply to the H_2O-diluted system. Figure 5.13 shows the third-body efficiency effect and the species direct kinetic effect, and the thermal contribution with respect to N_2 for a stoichiometric propane/oxygen mixture was evaluated as in the previous case.

For the H_2O-diluted system, the thermal effect is less pronounced than that for the CO_2-diluted system because H_2O has a lower heat capacity than CO_2, which slightly decelerates the ignition process with respect to the N_2 case.

At low temperatures, the most effective contribution to alter the auto-ignition process is related to the third-body reactions. They diminish the auto-ignition time values by approximately 60% with respect to the Y species. This contribution diminishes when T_{in} increases, first rapidly for $1.1 < 1000/T_{in} < 0.95$, then slowly up to $1000/T_{in} < 0.8$, where it becomes positive.

The kinetic effect is negligible up to 1.05. At higher temperatures, it becomes slightly negative, which accelerates the oxidation process. Afterwards, it becomes positive and drastically delays the auto-ignition times at high temperatures.

Rate of production analysis

In case of propane mixtures that were diluted in N_2, above it has been thoroughly analysed the propane ignition chemistry to identify the key reactions that control the auto-ignition times using the sensitivity, rate of production analyses and flux diagrams at low, intermediate and high temperatures. Given these kinetic pathways, several numerical analyses were realized to identify the reactions altered by CO_2 and H_2O at the ignition time as a function of system inlet temperature.

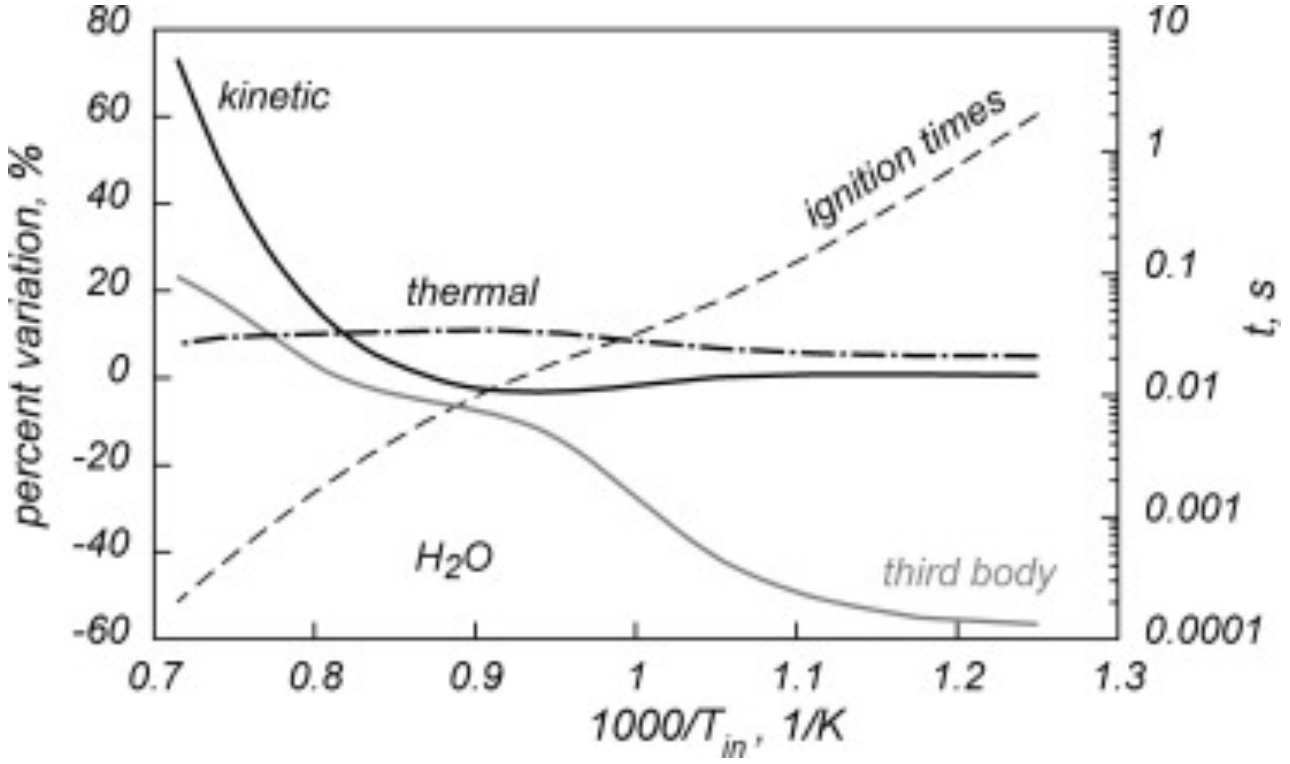

Fig. 5.13 – H_2O thermal and chemical effects on the auto-ignition delay times.

Figure 5.14 shows the Rate of Production (ROP) analysis for a stoichiometric propane/oxygen mixture diluted up to 90% in CO_2. Figure 5.14a is relative to radicals productions, while Fig. 5.14b to CH_3 to consider the competitions between oxidation and recombination route.

At low temperature, CO_2 mainly affects the ignition process accelerating the reaction 8 because it has a higher third molecular efficiency than N_2. Thus the HO_2 radicals, formed by H abstractions from n- and i-propyl radicals by O_2, recombine in H_2O_2 that promotes OH radicals formation by thermal decomposition. As matter of fact, in the CRECK-2014 kinetic scheme, the CO_2 third-body efficiency for this reaction is 2.4, whereas that of N_2 is 1.26.

At intermediate temperatures, CO_2 enhances the methyl recombination reactions because its efficiency is three times higher than that of N_2 and system reactivity slows down. Figure 5.14b shows that for T_{in} > 975 K this channel becomes faster than the methyl oxidation route, represented by the reaction 5 for the considered temperatures.

A proof of this effect is given in Fig. 4.12 by the closeness of the curves of the stoichiometric and rich conditions, for which the recombination reactions have a greater effect. Both curves differ from the lean curve by approximately one order of magnitude. For N_2-diluted mixtures, this effect is less evident (Fig. 4.7).

Figure 5.14a shows that for T_{in} > 1200 K, the reaction 11 becomes dominant with respect to H_2O_2 decomposition and sustains the ignition process. For T_{in} higher than 1300 K, in agreement with Glarborg & Bentzen (2008), the CO_2 decomposition reaction (dashed line) consumes H radicals:

$CO_2 + H = CO + OH$ (15)

At T_{in} = 1400 K it is just 4 times lower than the high temperature branching reaction. Such reaction inhibits the ignition chemistry for two reasons: it is endothermic and competes with the high-temperature branching reactions for H radicals.

The ROP analyses at the ignition times as a function of T_{in}, for a stoichiometric propane/oxygen mixture diluted up to 90% in steam are reported in Fig. 5.15a and b. The former is relative to radicals production while the latter to the CH_3 fate.

At low temperatures, H_2O mainly participates as a third body in the peroxide decomposition reaction because its third-body efficiency is six times higher than that of N_2. Such action reduces the auto-ignition delay times with respect to N_2.

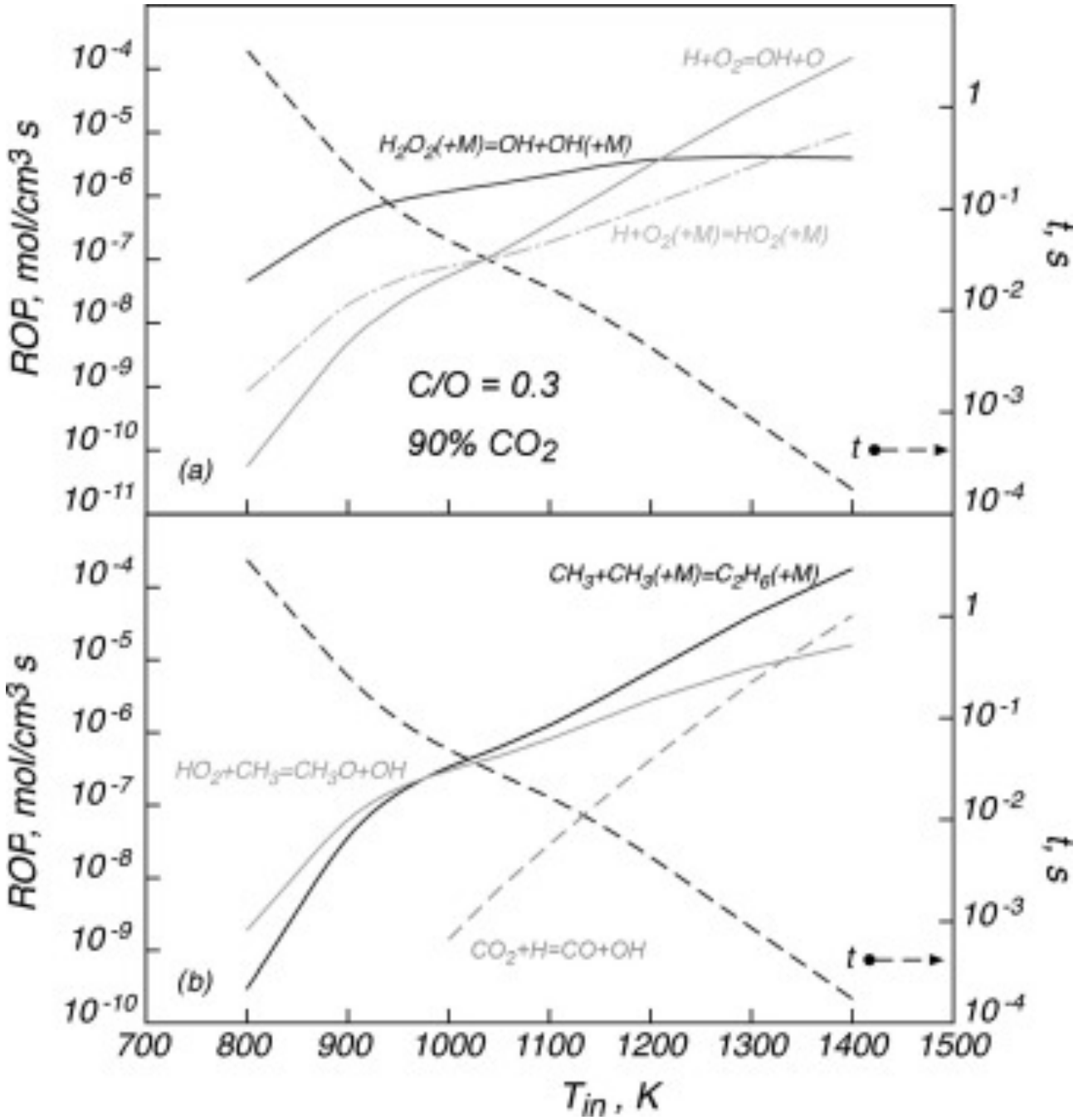

Fig. 5.14 – Rate of production analysis at the ignition time as a function of T_{in} for a stoichiometric C_3H_8/O_2 mixture diluted up to 90% in CO_2 for radicals production/consumption (a) and CH_3 radicals consumption (b).

At intermediate temperatures, H_2O promotes the inhibiting effect of the methyl recombination reactions because its efficiency is five times higher than that of N_2. The ROP analysis (Fig. 5.15b) shows that the methyl recombination reaction overcomes the methyl oxidation through HO_2 species for T_{in} higher than 1000 K.

Simultaneously steam interacts with methyl radicals to convert them to methane and produces OH radicals:

$CH_3 + H_2O = CH_4 + OH$ (16)

Such reaction strongly interacts with the oxidation/recombination-pyrolytic routes of methyl radicals, and for $T_{in} > 1000$ K its reaction rate is comparable to the methyl recombination rate (Fig. 5.15b). Furthermore, this reaction plays an important role also in OH production, as Fig. 5.15a shows, resulting as the fastest reaction in OH production between 1200 and 1350 K.

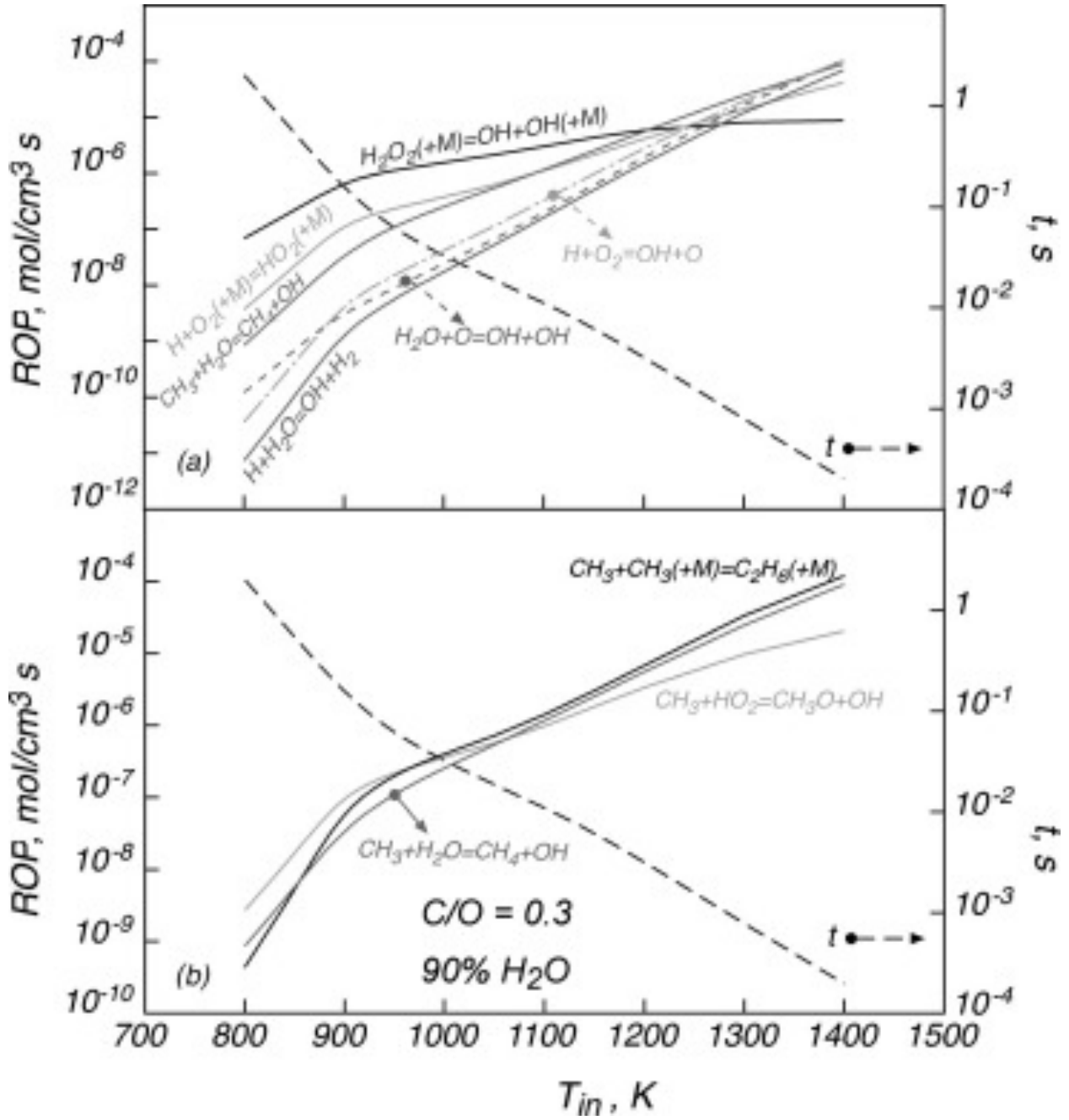

Fig. 5.15 – Rate of production analysis at the ignition time as a function of T_{in} for a stoichiometric C_3H_8/O_2 mixture diluted up to 90% in H_2O for radicals production/consumption (a) and CH_3 radicals consumption (b).

For intermediate temperature, the reaction 12 becomes important because the H_2O third-body efficiency is approximately 15 times higher than that of nitrogen. This reaction assures HO_2 radical to oxidize methyl radicals to CH_3O and feed the oxidation channel with a large production of H radicals from CH_3O and HCO decomposition reactions.

At high temperature reaction 11 becomes faster than reaction 12, and sustain the ignition process.

Numerical analyses suggest that H_2O can also participate in the reactions

$O + H_2O = OH + OH$ (17)

$H + H_2O = H_2 + OH$ (18)

Figure 5.15a shows that the contribution of such reactions to the radical production/consumption is marginal at low-intermediate temperatures, but at high temperatures their reaction rates are comparable with the branching mechanism. They consume O and H radicals that are necessary to sustain the high-temperature branching reactions in the set of reactions 11 and

$O + H_2 = OH + H$ (19)
lowering system reactivity and delaying the ignition process.
The determination of the key reactions in the propane/oxygen mixture oxidation under diluted operative conditions can explain the oxidation regimes that are encountered during the experimental tests and the auto-ignition trend as a function of the inlet temperature and the mixture composition.
In general, as discussed above, for fuel-rich/stoichiometric mixtures and high inlet temperatures, a delicate competition among oxidation, pyrolysis and recombination reactions is established. This condition and the heat exchange to the surroundings determine the onset of dynamic/transient regimes.
At high temperatures, the oxidation/recombination-pyrolytic competition in the presence of CO_2 is altered because this diluent mainly promotes the recombination channel as an effective third-body species and decreases the H radical concentration, which depresses the high-temperature branching mechanism through its decomposition. This effect determines the onset of instabilities in the neighbourhood of the stoichiometric mixture.
For H_2O-diluted mixtures, the oxidation/recombination-pyrolytic balance is altered because of its high efficiency in the third molecular reactions that damp the oxidation routes, which promotes the recombination channel, decreases the high-temperature branching routes (reaction 11) and boosts the productions of HO_2 (reaction 12) radicals. Therefore, when H_2O dilutes the system, a double-competition mechanism establishes, the former is relative to C_1 and C_2 chemistry, the latter occurs between reactions 11 and 12. Although the C_1/C_2 route competition is promoted at high temperatures for fuel-rich mixtures, the latter occurs for lean/ultra-lean mixtures, where H radicals miss. In fact, the behaviour maps that were realized for H_2O- and CO_2- diluted mixtures show that steam promotes instabilities in a wide range of C/O feed ratios.
The analysis of the ignition delay times shows that the data obtained for CO_2-diluted systems are notably sensitive to the mixture composition, which resembles the behaviour of N_2-diluted systems, whereas the H_2O-diluted systems are almost independent. Furthermore, the CO_2 ignition data are similar to the N_2 data for ultra-lean and rich conditions, whereas in H_2O, the strong discrepancy among the data for the three reference systems only reduced for the rich mixtures. These behaviours suggest that CO_2 mainly alter the ignition process for mixtures with composition close to the stoichiometric value, whereas stem delays the ignition process at high temperatures almost independently on mixture composition. The ignition data that were obtained under fuel-rich conditions for the three reference bath gases suggest that the effects of H_2O and CO_2 are less pronounced when the recombination-pyrolytic reactions prevail.
This type of analysis was also carried out in relation to the ignition delay times obtained for pyrolysis gas mixtures. Interestingly, it has been seen that, by varying the fuel type, the reactions influenced by the presence of CO_2 and H_2O are exactly the same as those identified in the case of propane mixtures. In fact, the identified reactions are those of the H_2/O_2 system or those relating to C_1 species, which control the kinetics of any kind of fuel.

5.3.2 Speciation measurements

The thermal and chemical effects of CO_2 and steam addition on the ignition delay times have been discussed previously, based on the comparison between numerical predictions obtained with real and virtual species. It was shown that, for a fixed CO_2 or H_2O molar fraction, the thermal and chemical effects on the ignition delay times vary when the inlet temperature is varied.
Several kinetic analyses were performed with the aim to understand the main oxidation reactions at the stationary conditions for the all the operating conditions considered in the JSFR experiments.
Peculiar attention was devoted to the interference of CO_2 and H_2O on the oxidation kinetics at stationary conditions.
The numerical results confirmed the findings discussed for the ignition delay time, i.e. CO_2 and H_2O alter the oxidation routes of simple fuels in dependence of the temperature and of the

equivalence ratio. In particular for low temperatures, the branching mechanism represented by the reaction 8 is altered in virtue of the higher collisional efficiencies of CO_2 and H_2O with respect to N_2. This is consistent with the experimental ΔT and species trends showed in the previous chapter for propane and n-pentane. It should be pointed out that this effect was not observed experimentally for methane mixtures because methane is a less reactive fuel and thus it starts to react at higher temperature with respect to propane or n-pentane, where the reaction 8 is no longer the main chain-branching pathway.
At high temperatures and mainly for fuel lean conditions, the CO_2 and H_2O effect on the oxidation routes is ascribable to the modification of the reaction 12 because of the higher third body collisional efficiencies of CO_2 and H_2O with respect to N_2.
For all equivalence ratios the relative importance of the methyl recombination reaction 10 is sensibly modified by the presence of CO_2 and H_2O. This is particularly relevant for methane mixtures, where CH_3 results from the H-abstraction from the fuel.
Furthermore, JSFR analyses confirmed the direct chemical effect of CO_2 and H_2O on chemical species at high temperatures. In particular the strong effect of the CO_2 on the CO concentration discussed in the previous chapter was found to be due to the reaction 15, whereas the observed strong effect of H_2O on H_2 concentration was found to be due to reaction 18, confirming the PFR results.
In addition, it should be emphasized that the influence of H_2O on the reaction 16 is very stressed for methane mixtures, since the reverse of reaction 16, as seen before, is the main reaction of methane oxidation.
Until now it has been discussed the effect of diluents as a function of inlet temperature and equivalence ratio on ignition delay times and species concentrations.
In addition, in the previous chapter, it was observed that CO_2 and H_2O have a strong non-linear effect on chemical species when gradually added to nitrogen for a fixed inlet temperature for methane mixtures.
Therefore, the chemical impact of CO_2 and H_2O addition is now examined for different mixtures featuring the same inlet temperature. In particular Fig. 5.16 shows the evolution of the simulated molar fraction of CH_4 and CH_3, OH, H, HO_2, and O radicals when the CO_2 and H_2O percentage is increased from 0 to 100%, for a stoichiometric mixture at T_{in} = 1075 K and d=90%. Therefore in Fig. 5.16, 0% on the abscissa means that the mixture is diluted at 90% in nitrogen, while 100% means that the mixture is diluted at 90% in CO_2 or in H_2O. All the intermediate dilution levels mean mixtures simultaneously diluted in N_2 and CO_2 or N_2 and H_2O in different proportions. T_{in} = 1075 K has been chosen because it represents the onset of reactivity and therefore the combustion temperature is the same for all the mixtures, i.e., $T = T_{in}$. This allows focusing the attention only on the chemical effects, thus excluding the thermal effect. Furthermore, this inlet condition avoids the presence of oscillatory regimes.
Depending on the CO_2 or H_2O molar fraction, the presence of these two molecules leads to changes in the production and in the consumption of stable species and radicals. Note that the trend observed for the CH_4 as a function of diluent percentage reflects to all the other stable species. It is important to note that relatively small quantities of CO_2 and H_2O are required to have significant changes on the chemical species concentrations. The conversion and the total radical pool decrease quasi-linearly when the CO_2 and H_2O molar fractions are increased up to a certain value. Further increasing the CO_2 or H_2O concentration does not lead to proportional changes in the behaviour. In particular the plateau is reached for a CO_2 percentage around 60% and a H_2O percentage around 30%. This may indicate that chemical effects of CO_2 addition are reduced compared to H_2O addition.
Several kinetic analyses were performed with the aim to understand the nature of this phenomenon. The results suggest that this behaviour is attributed to the role of the methyl radical recombination reaction in affecting the chain branching. As a matter of fact, interestingly, the species concentrations behave qualitatively similar to the rate of recombination reaction as a function of the

diluent percentage (Fig. 5.17), indicating that a single rate-controlling process affects both radical growth and reactants consumption.

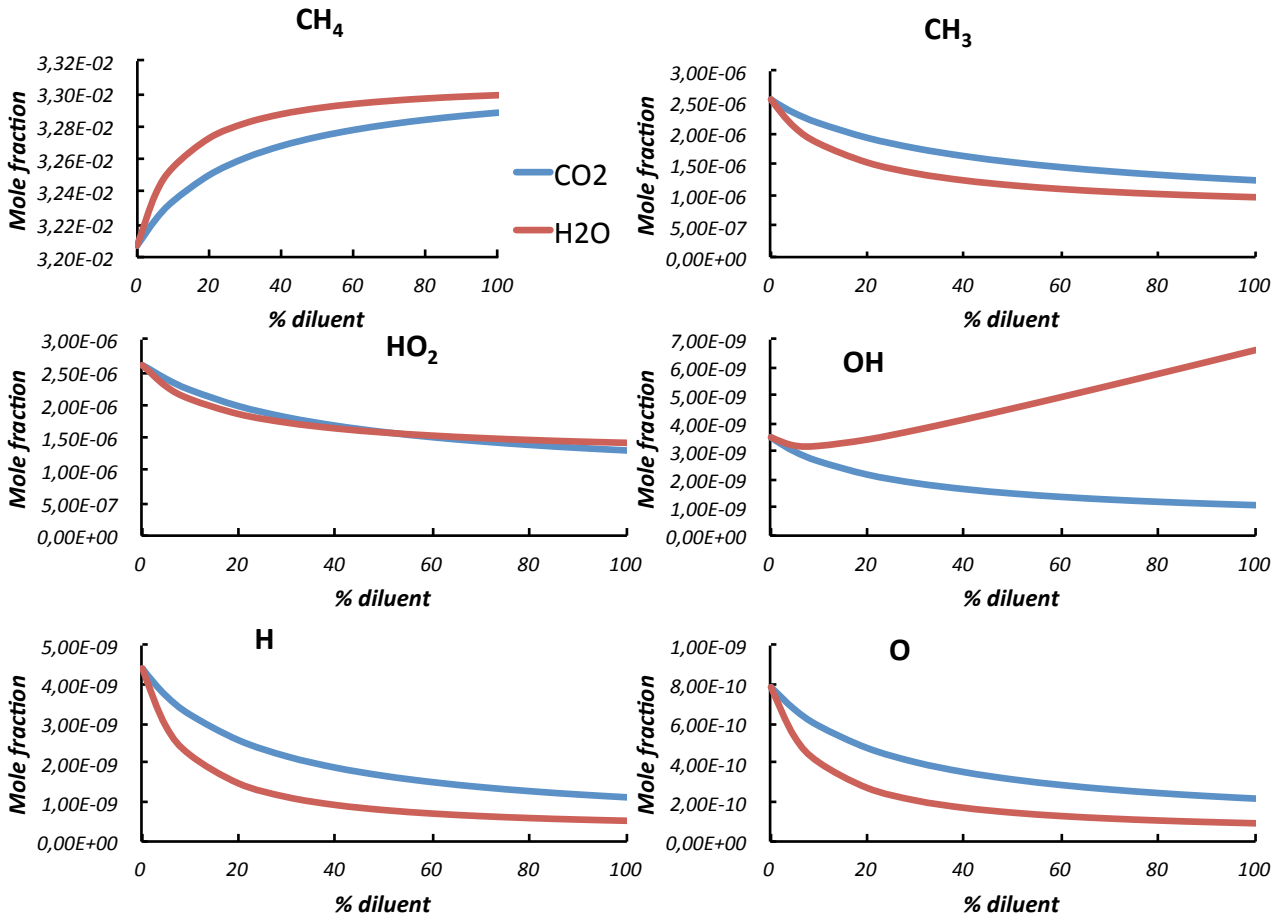

Fig. 5.16 – Simulated concentration profiles versus percentage of diluent. $\Phi = 1$, $\tau = 0.5$ s, p = 1.1 atm, d = 90%, $T_{in} = 1075$ K, CO_2 (blue lines), H_2O (red lines).

This is reasonable because with increasing CO_2 or H_2O content the influence of three-body reaction first increases, then, the low-pressure behaviour switches to high-pressure behaviour in the manner of Lindemann mechanism. Thus the methyl radical recombination reaction is third-order in the nitrogen dilution and second-order in the CO_2 or H_2O dilution.

The increase of CO_2 or H_2O modifies the consumption pathways of CH_4 mainly because the high collisional efficiency of CO_2 and H_2O alters the CH_3 consumption paths through the competing reaction pairs 5 and 10.

Secondarily, the high collisional efficiency of CO_2 and H_2O alters the radicals production paths through the competing reaction pairs

$HCO + M = H + CO + M$ (20)

and

$HCO + O_2 = HO_2 + CO$ (21).

For a mixture fully diluted in CO_2, this molecule reduces values of H, O, OH, CH_3, and HO_2 atom concentrations respectively by about 75%, 72%, 69%, 51%, and 50% compared to the simulations realized with N_2 (Fig. 5.16). The effect of H_2O is more complex. The presence of this molecule reduces H, O, CH_3, and HO_2 atom concentrations respectively by about 88%, 88%, 62%, and 50%. In contrast, the OH concentration is increased by 47% compared to N_2 dilution (Fig. 5.16).

This is due to several reasons. First, with respect to CO_2, water vapour addition also favors O and H radical consumption and OH production in the reaction 17 and 18.

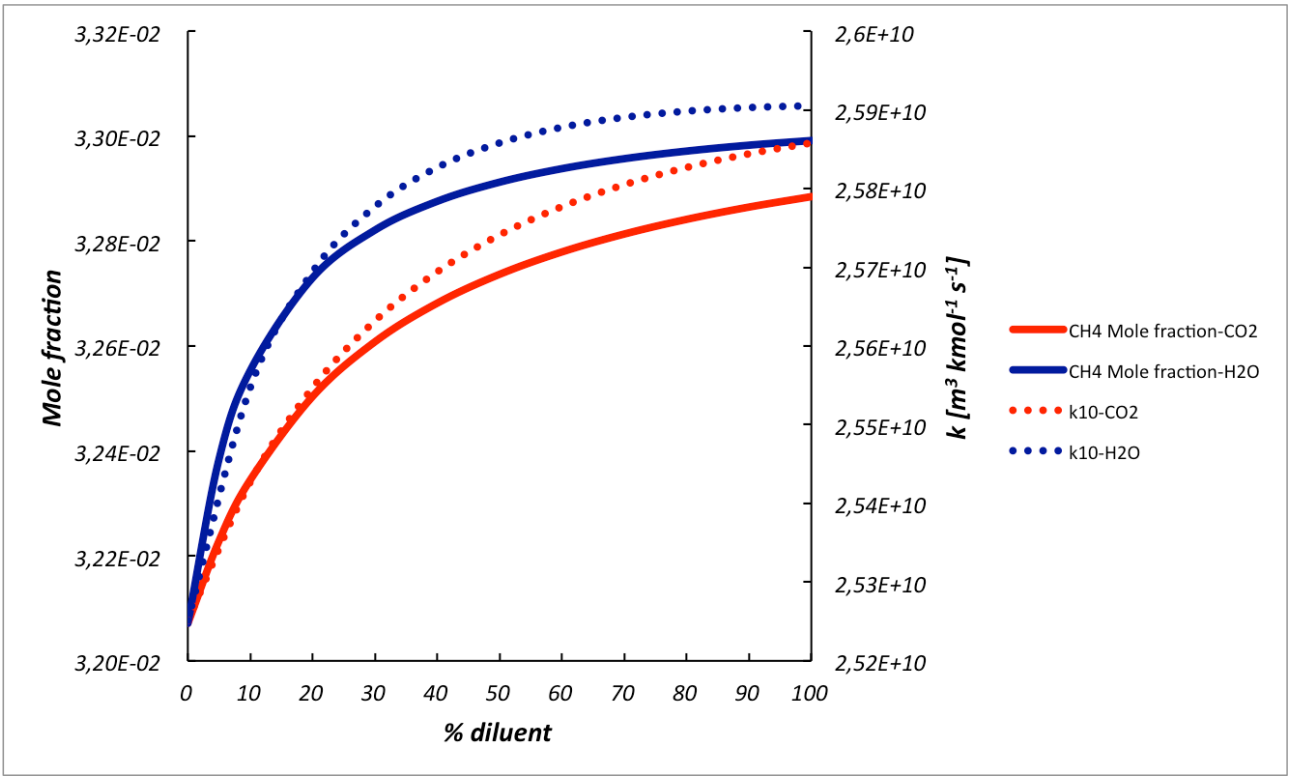

Fig. 5.17 - Simulated methane molar fraction (left axis) and rate of reaction 10 (right axis) versus percentage of diluent. $\Phi = 1$, $\tau = 0.5$ s, p = 1.1 atm, d = 90%, $T_{in} = 1075$ K, CO_2 (blue lines), H_2O (red lines).

Furthermore, while the H_2O is more effective in lowering the concentrations of H, O and CH_3 radicals with respect to CO_2, the percentage reduction of HO_2 radicals reaches the same value reached by the CO_2 dilution. This is due to very high collisional efficiency of H_2O in the H radical recombination reaction 12.

This observation is consistent with the conclusions reported by several authors cited in the chapter 2, who attributed water effect to the high chaperon efficiency in the recombination reaction 12, which competes with the chain-branching reaction 11. Through these mechanisms, HO_2 kinetic pathways become important with water addition, especially at elevated dilution.

In this case it has not been observed a direct chemical effect of CO_2 because the reaction 15 starts to have an effect for higher inlet temperatures.

Given that, as discussed in the chapter 2, most of the studies on the effects of diluents involved very low concentrations of them, the quasi-linear decrease of conversion with increasing CO_2 and steam molar fractions observed for lower CO_2 and H_2O molar fractions have been used in several work to build semi-empirical models, based on one-step overall reactions. De facto, although based on crude assumptions, these models can be used to quickly estimate the combustion properties of CO_2- and/or steam-diluted fuel mixtures. However, as just demonstrated, carefully attention should be paid in the extrapolation of these observations in processes where high concentrations of these species may be present, such as in the case of oxy-fuel combustion. Such an effect would not be captured with a one-step overall reaction. This again highlights the importance of detailed chemistry in modelling such combustion systems.

Finally, the CO_2 effect has been also studied in this work at low-temperature, in the case of n-pentane mixtures.

In the cool flame ignition where low-temperature chemistry dominates, important reaction rates for CO_2 dilution are comparable with that for He dilution, indicating the negligible effect of the CO_2 on low-temperature chemistry. Increasing the inlet temperature, low-temperature chemistry becomes

less important than intermediate-temperature chemistry, where H_2O_2 dissociation reaction is clearly the dominant responsible for OH generation.
Thus, CO_2 has an effect on intermediate-temperature chemistry much more profound than that on low-temperature chemistry.
A reaction mechanism that does not have the appropriate pressure dependence of the rate constants for relevant reactions cannot describe this behaviour.
It is therefore clear that detailed chemical kinetics is needed to explain complex combustion phenomena of this nature.

5.4 Influence of fuel type on combustion characteristics

In this paragraph a comparison of ignition delay times between the various fuels tested in the present work is made.
In particular, the ignition delay results for a lean mixture ($\Phi = 0.3$) of pyrolysis gas are presented in Fig. 5.18 and compared with results for methane and propane pure fuels. In order to show the fuel nature effect on the ignition delay time measurements, the diluent concentration was fixed at 90%.

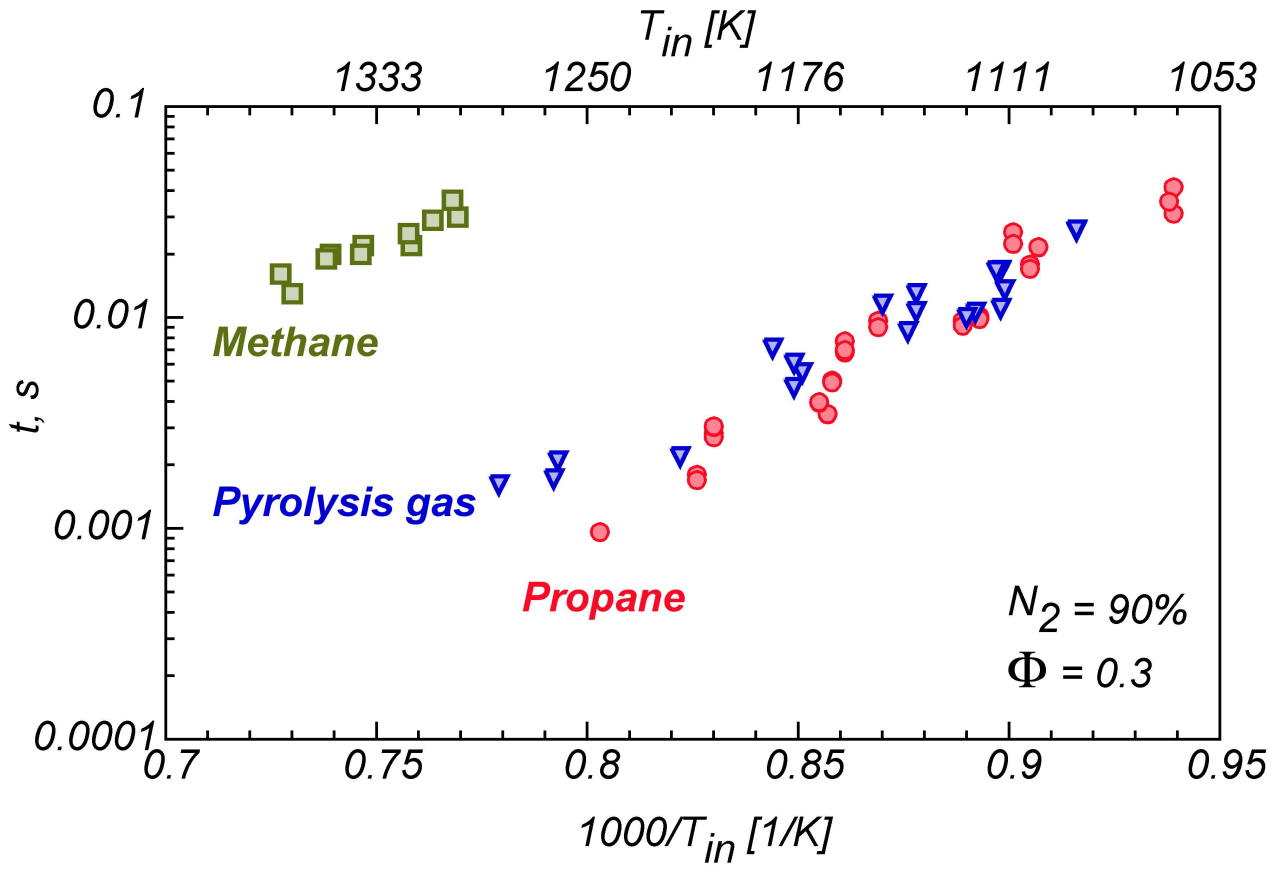

Fig. 5.18 - Experimental ignition delay times (t) at atmospheric pressure for methane, pyrolysis gas, and propane mixtures diluted at 90% in N_2 at $\Phi = 0.9$ (the pyrolysis gas mixture also contains CO_2).

The methane ignition delay times are adapted from the work of Sabia et al. (2013). Under the investigated temperature range, methane and propane represent extremes of reactivity, while the C_1-C_2 hydrocarbons mixture (pyrolysis gas) has intermediate ignition properties due to the presence of C_2 species. In particular, there is no significant difference between the ignition delay times of the C_1-C_2 mixture and pure propane, while the ignition delay of methane is much higher. This is a relevant aspect for potential applications. The used pyrolysis gas has a LHV of 2055 Kcal/Nm^3, compared to the methane LHV of 8555 Kcal/Nm^3 and the propane LHV of 21795 Kcal/Nm^3. In particular, in the first chapter it was said that burning a LCV fuel leads to delayed ignition. Figure

5.18 shows that this is no longer true under diluted conditions and a direct use of a LCV fuel in practical applications is possible, given the compatibility of required characteristic times.
Flux diagrams and rate of production analyses (not reported here) showed that ethane is more reactive than methane because every radical, resulting from H-abstraction from ethane, produces an H atom via reaction
$C_2H_5 \rightarrow C_2H_4 + H$ (22).
Therefore, addition to methane of very small amounts of other hydrocarbons, especially ethane, dramatically increases the ease of igniting methane. Westbrook et al. (2005) clarified that for this simple reason, combustion characteristics of natural gas (which usually consists of more than 90% methane, the remainder being primarily ethane and propane) that involve ignition, are much different than for methane.
It is of interest to note that CO consumption starts after the CH_4 is nearly consumed. Both CH_4 and CO are largely consumed by OH. CH_4 is largely consumed by OH via the reverse of reaction 16 that has a faster rate than the reverse of reaction 15.
Detailed analysis indicates that the OH radical concentration starts increasing only after the CH_4 has been completely consumed. When CO is added, it does not have a chance to be oxidized during the CH_4 oxidation stage, thus behaves like an inert until CH_4 oxidation is completed. Furthermore, the presence of CO_2 and H_2O is very influential because CO_2 shifts the CO conversion reaction to the reactants and the H_2O shifts the CH_4 conversion reaction to the reactants. This emphasizes the critical role of fuel and diluent type on autoignition and should be evaluated for potential applications.

5.5 Implications for kinetic modelling

Given the efforts put in developing of kinetic models to date, our fundamental understanding of combustion processes is significantly improved. The thermochemistry and elementary rate coefficients for many reactions have also been significantly revised during the last few years. Also, there have been tremendous methodological advances for computing the pressure-dependence of rate-coefficients.
However, the observed discrepancies between model predictions and experimental data presented in the previous chapter, and among model predictions themselves, are noteworthy. This suggests that some additional effort should be dedicated to the development of detailed kinetic schemes to correctly describe the ignition and oxidation processes under SECs combustion conditions.
It is clear from the previous sections that mechanisms can differ significantly in their prediction behaviour. In order to improve a chemical model it might be useful to have information about which parts of a mechanism are responsible for a good or bad performance regarding certain type of experiments or a constrained range of experimental conditions. Furthermore, it can be interesting to have an estimate of how the reproduction of some measurements changes if a reaction rate coefficient is tuned to describe another experiment better.
To investigate these relationships, local sensitivity analyses were performed at the conditions of all measurement data. Sensitivity tests form the connection between observables and rate constants. They provide a safe guidance to reliabilities of modelling, opportunities for further research, and rational employment of efforts.
For the calculation of the sensitivity coefficient S, ChemKinPRO and OpenSMOKE++ software were used by varying the pre-exponential Arrhenius parameter A for all reactions one-by-one by means of finite differences. The S values were normalized and then scaled to the range of -1 to +1, where positive S values means that ignition delay time is accelerated.
Reactions are included in forward and backward directions assuming that equilibrium constants are without flaw.
In this section, temperature sensitivity analyses are reported at the ignition time for the C_1C_2 mixtures in the PFR. These represent the set of experiments for which the greater discrepancy between experimental and numerical data was observed.

In particular Figs. 5.19, 5.20 and 5.21 show normalized temperature sensitivities for lean, stoichiometric and rich mixtures, namely Ω = 1.67, 1, 0.7 (see chapter 4 for the Ω definition), throughout the range of temperatures (T_{in} = 900 K, 1050 K and 1300 K), calculated with the Zhukov-2005 mechanism at 1 atm under the conditions of the experiments (remember that the Zhukov-2005 is the mechanism used to simulate the C_1C_2 mixtures experiments in the section 4.1.2).

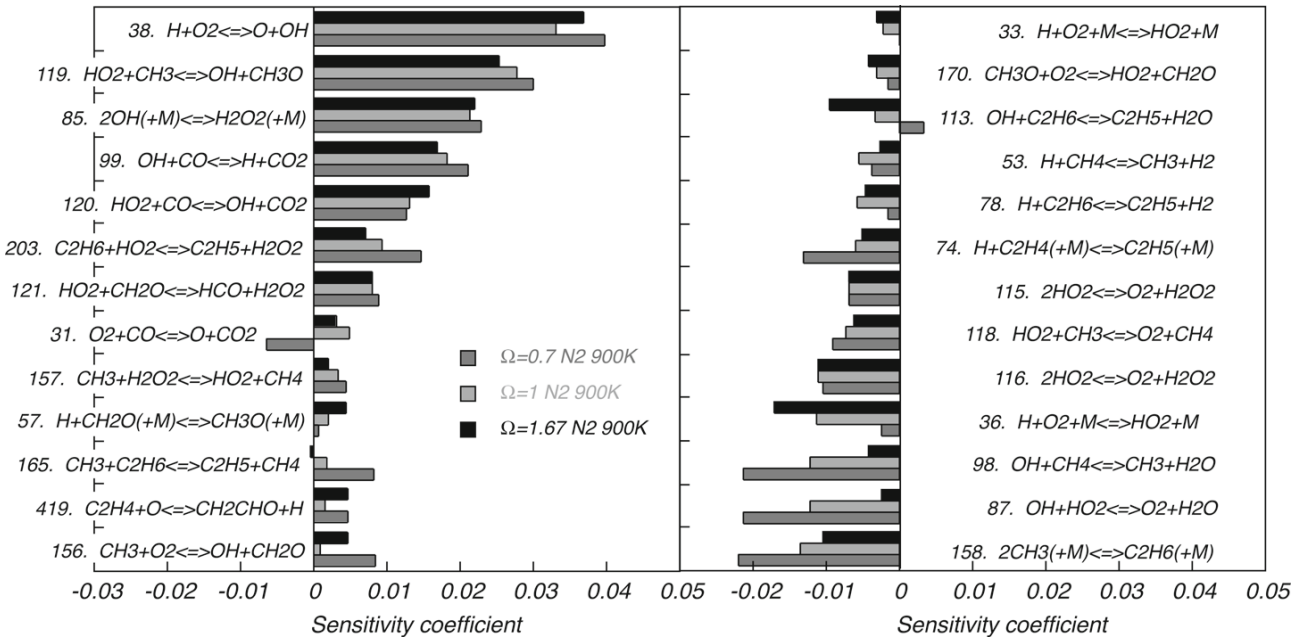

Fig. 5.19- Temperature sensitivity coefficients at the ignition time for the three Ω values considered at T_{in} = 900 K, calculated with the Zhukov-2005 mechanism at 1 atm.

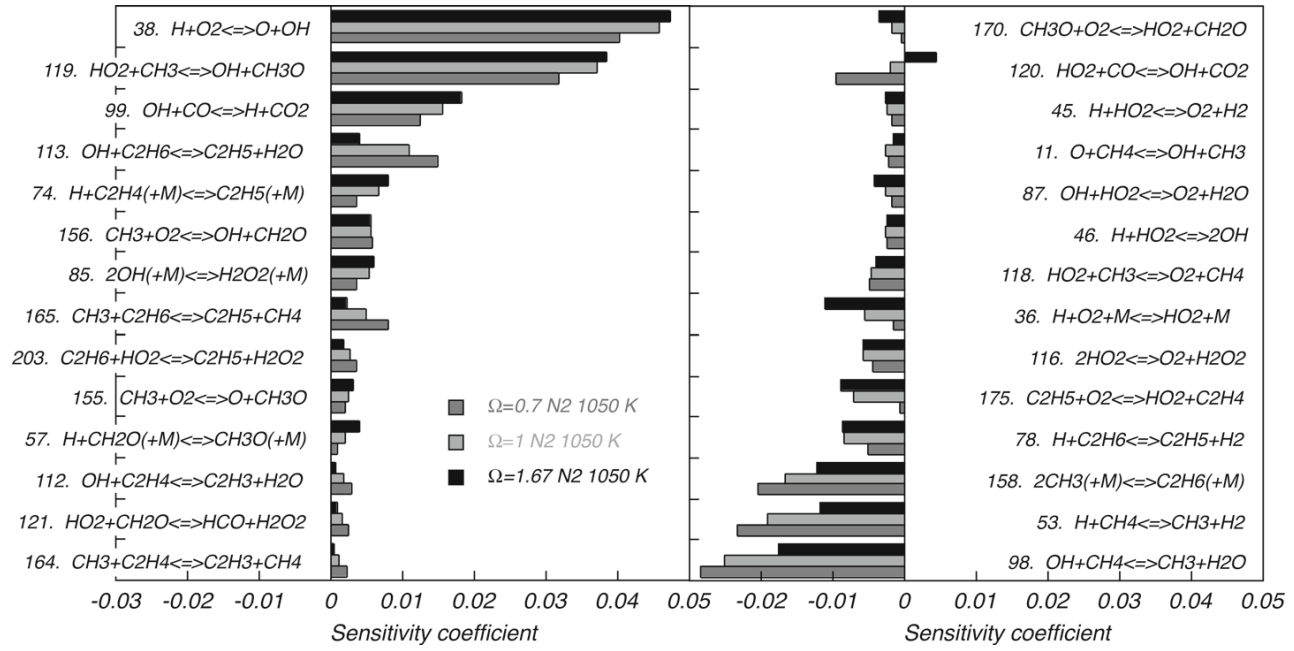

Fig. 5.20- Temperature sensitivity coefficients at the ignition time for the three Ω values considered at T_{in} = 1050 K, calculated with the Zhukov-2005 mechanism at 1 atm.

It is worth emphasizing that the sensitivity coefficients highly depend on the experimental conditions. In other words, different sub-chemistries can be important at various conditions across all types of measurements.

Generally the distributions of sensitivity coefficients are similar for all investigated mechanisms, although minor variations at certain conditions. Hence, the information obtained from the sensitivity analysis of one mechanism can be used at least qualitatively for the improvement of other mechanisms. This statement is valid as long as the predominant reaction pathways are identical in the mechanisms, which is the case. By being able to access and examine a large amount of sensitivity data in connection with the results of the investigation of the performance of a mechanism, it becomes possible for model developers to identify those reactions that have to be revisited in their mechanisms in order to achieve a better agreement with the measured data. A possible further outcome of this investigation can be to identify less well-understood, but still important reactions in the SECs system that require additional theoretical calculations or experimental determinations of the reaction rate coefficients.

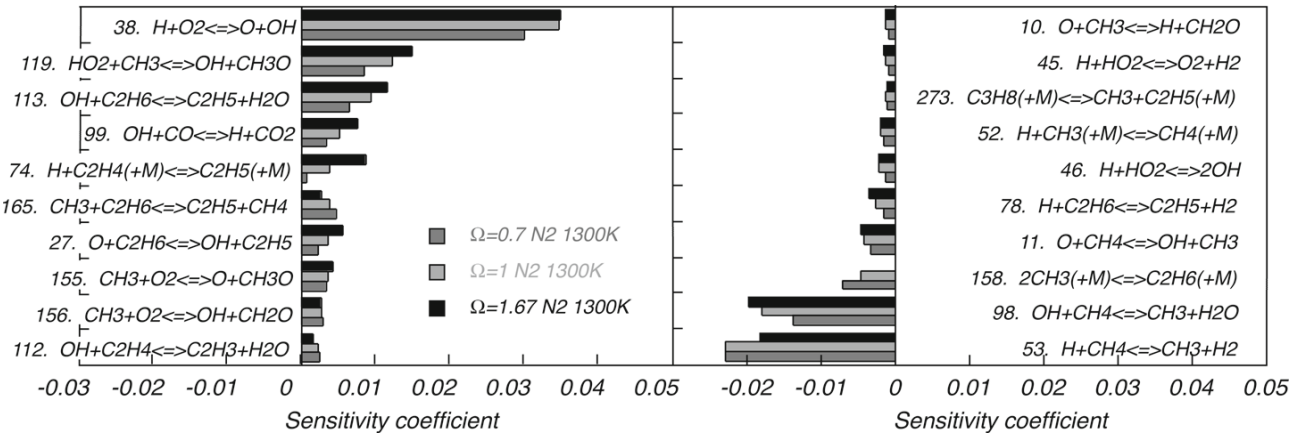

Fig. 5.21- Temperature sensitivity coefficients at the ignition time for the three Ω values considered at T_{in} = 1300 K, calculated with the Zhukov-2005 mechanism at 1 atm.

It should be noted that in Figs. 5.19, 5.20 and 5.21 reactions are identified with a number that corresponds to the one of the original detailed kinetic mechanism. However, in the discussion, for reasons of clarity and consistency with the previous discourse, we will continue to refer to Table 5.1 for the reactions numbering.

For the three Ω values considered, the main reactions are the same, even though the sensitivity coefficients vary with Ω.

Briefly summarizing the results of the sensitivity analysis presented in Figs. 5.19, 5.20 and 5.21 together with those not reported here, one can conclude that, from low (900 K) to high (1300 K) temperatures, calculated C_1-C_2 ignition delay times are mostly sensitive to the rate constant of reactions that give rise to a competition among branching and recombination channels (therefore reactions 11 and 12), intermediate- and high-temperature branching channels (therefore reactions 7+8 and 11), oxidation and recombination channels (mainly reactions 5 and 10).

In fact, ignition delay times are controlled by the ratio of these rate constants with minor impact of other reactions.

In particular, normalized sensitivities of reactions 7+8 are about -0.01 and 0.02 at 900 K and almost linearly approach 0 with temperature increase up to 1300 K. Furthermore, at higher temperatures the role of reaction 12 rapidly vanishes, while other reactions could be important, depending on the mixture stoichiometry. For example, it was found that the reactions

$H + HO_2 = OH + OH$ (23)

and

$H + HO_2 = H_2 + O_2$ (24)

both have negative signs of the sensitivity coefficients for T_{in} = 1050 K and 1300 K.

In addition, among the most sensitive reactions are the CO and CH_4 oxidation (reverse of reaction 15 and 16).

Normalized sensitivities of temperature and species concentrations from 1000 to 1250 K were also calculated in the PSR for the lean, stoichiometric and rich mixture at 1 atm. Similarly to the sensitivity analysis shown in Figs. 5.19-5.21, the just mentioned reactions were found to be the most sensitive.

In agreement with the previous discussion, it is possible to infer that, under the conditions explored in the present work, the ignition and oxidation processes are controlled mainly by the competition among different kinetic pathways, depending on the system temperature and the composition of the mixture.

In terms of ignition delay times, the difference between the experimental and numerical values indicates that the weight of the methyl recombination channel (reaction 10) is numerically underestimated with respect to the oxidation channel (mainly reaction 5). Such a discrepancy depends on the fuel composition. The methyl recombination channel gains relevance, shifting from lean to stoichiometric and rich conditions, so the difference between experimental and numerical data increases. In fact, for fuel lean conditions (i.e., $\Omega = 1.67$), the difference between the experimental and numerical data is less pronounced. As matter of fact, the sensitivity coefficients for the reaction 10 are always higher for rich conditions.

In the case of mixtures diluted with CO_2 and H_2O, the discrepancy between the experimental and numerical data is greater. To highlight the change in the ignition chemistry induced by the dilution with CO_2 and H_2O with respect to N_2, further sensitivity analyses (not reported here) were performed for the three initial temperatures and equivalence ratios considered.

In the case of the system diluted with CO_2, the results showed that at low and intermediate temperatures, the key reactions are the same as the key reactions of the system diluted with N_2, but the third molecular reactions showed higher sensitivity coefficients. In particular, the reaction 10 and 12 showed a higher sensitivity.

Moreover, at higher temperatures ($T_{in} = 1300$ K), the sensitivity with respect to the reverse of reaction 15 becomes negative. In agreement with indications from the literature, such a result suggests that CO_2 decomposes through this reaction.

In case of the dilution in H_2O, at low and intermediate temperatures, the sensitivity analysis showed a relative higher sensitivity coefficient for reactions 8 and 12, implying a higher competition with reaction 11 for H consumption. Reaction 10 still plays an important role because of the relatively high third body efficiency. At $T_{in} = 1300$ K, reaction 11 still competes with reaction 12 for H radical consumption and the H_2O_2 decomposition still plays an important role in the production of OH radicals. Furthermore, the system shows a high negative sensitivity coefficient for the reverse of reaction 18. Water consumes H radicals, producing OH radicals and H_2.

These results indicate important pathways and sensitive reactions that may be different for several diluents, and they can also hint at reaction sequences that may need additional attention, since comparisons of experiments and simulations show discrepancies of more than an order of magnitude.

For the present data, the mechanisms show a wide distribution of the sensitivity coefficients. Therefore, it appears that almost all of the reactions listed in Table 5.1 could potentially contribute to the disagreement between experiments and models or among models, as supported below.

In combustion of small hydrocarbons there is a broad consensus in regard to the necessary reaction pathways underlying the mechanisms. Thus, any inadequacy of the kinetic models essentially rests in their parameter values. Indeed, the lists of the main elementary reactions are very similar among the adopted models, but main differences arise from the kinetic parameters selected, which give rise to the discrepancies observed among predictions by different models.

The temperature and pressure dependence of the rate constants of these reactions was first screened to reveal the reason for the discrepancy.

The final objective is to minimize the prediction uncertainty of the C_1-C_3 models, and to resolve the inconsistency caused by measured quantities at elevated dilution. Particular attention has been paid to the uncertainties of the modelling caused by the uncertainties in the rate constants. The

accumulated errors from each individual rate constant may lead to gross imprecision in numerical prediction.
First, influential model parameters were identified through sensitivity analyses, which rank the influence of pre-exponential factors of the rate coefficients on each prediction against the corresponding experimental target. For each target, the pre-exponential A factors of the reactions that show the largest sensitivities on the prediction were changed in their uncertainty range one by one.
In principle, thermodynamic can also be included in this kind of task, but changing the values of the thermodynamic parameters within their uncertainty ranges usually has a much smaller effect on simulation results than the rate parameters. This is especially true for systems that involve only small molecules, whose physical parameters are known with little uncertainty (Varga et al. 2016).
Then the performance of the modified mechanism was compared to the starting mechanism, where the CRECK-2014 was chosen as the starting mechanism. Figures 5.22 and 5.23 show examples of experimental data sets and simulation results obtained with the modified (C1C3 MOD in the figures) and the starting models (C1C3 in the figures).

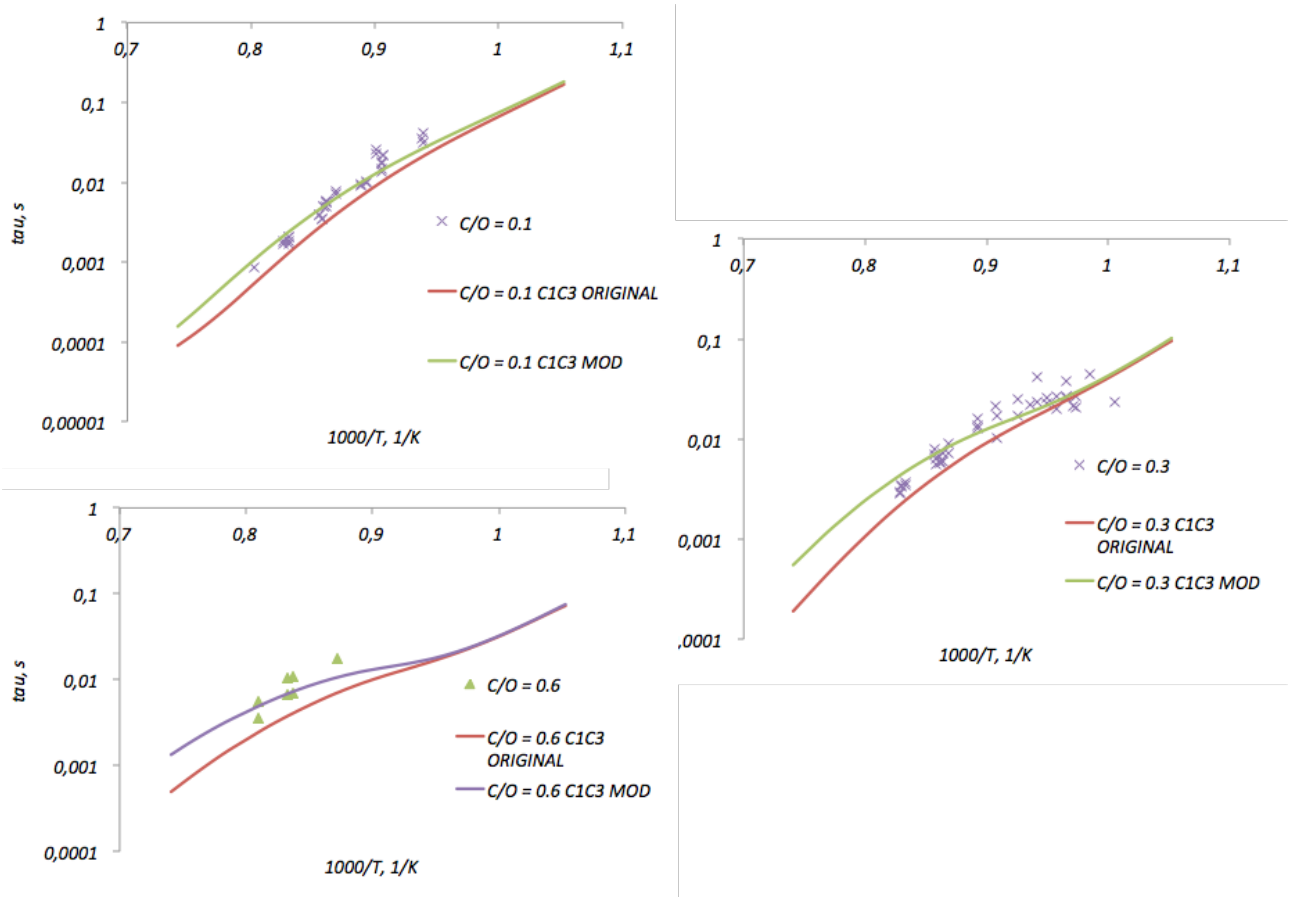

Fig. 5.22 - Experimental (symbols) and numerical (lines) ignition delay times at atmospheric pressure for propane mixtures diluted at 90% in N_2 for C/O = 0.1 (lean), 0.3 (stoichiometric) and 0.6 (rich) as a function of T_{in}. Simulations were obtained with the modified (C1C3 MOD) and the starting (C1C3) models.

Modification of these rate constants improved predictions of ignition delay times and species concentrations, illustrating large uncertainties and potential for improvements in C_1C_3 model predictions at atmospheric pressure.
This strategy was not used to optimize the mechanism, but only to estimate the effect on the prediction interval from the uncertainties of model parameters.

The obtained sensitivity coefficients show which model parameters contribute the most to the uncertainty in the model prediction, and thereby provide guidance to experimental or theoretical research.

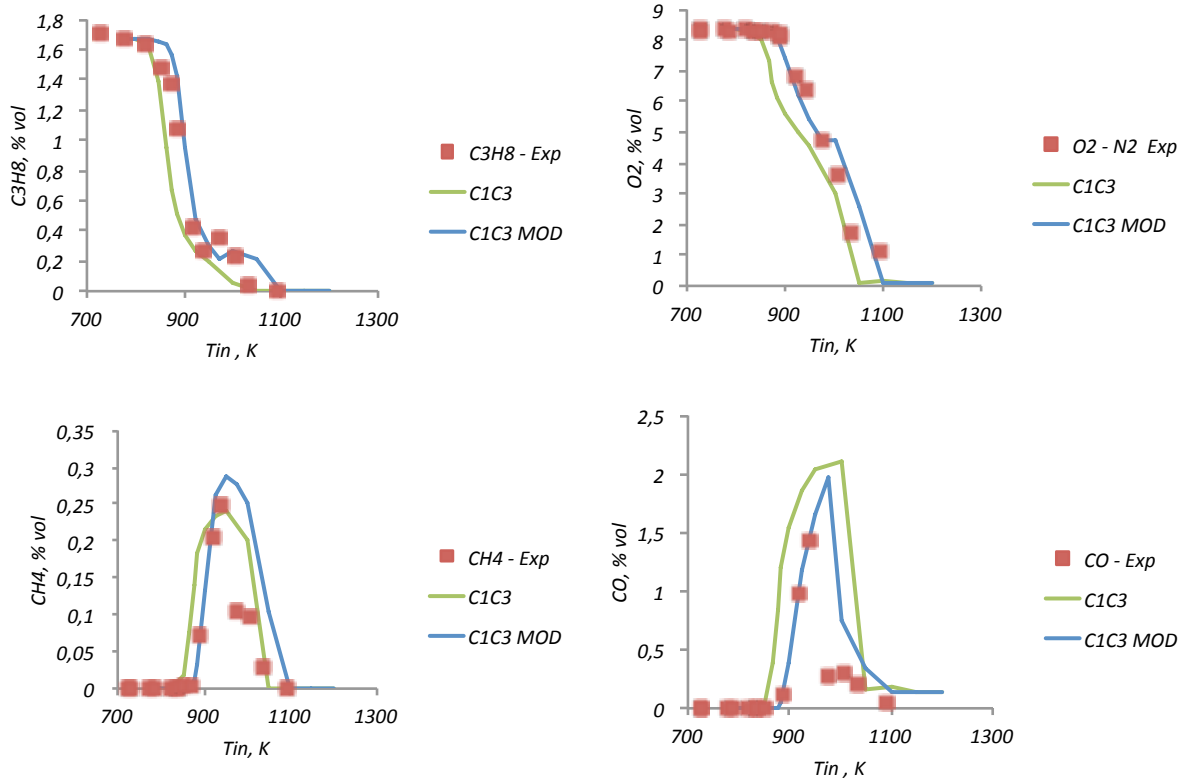

Fig. 5.23 - Experimental (symbols) and numerical (lines) concentrations of stable species at atmospheric pressure for propane mixtures diluted at 90% in N_2 for stoichiometric conditions as a function of T_{in}. Simulations were obtained with the modified (C1C3 MOD) and the starting (C1C3) models.

Sometimes even mechanisms that were comprehensively developed and have similar features could predict qualitatively different results due to the slight change of a single reaction rate constant. As an example, Fig. 4.3 in the previous chapter showed the calculated ignition delay times curves of nitrogen-diluted propane mixtures, obtained by using AramcoMech_1.3-2013 and AramcoMech_2.0-2016 mechanisms, with the latter being an updated version of the former. It is seen that while the 1.3 version predicts the change of the activation energy of ignition delay times at intermediate temperatures, the 2.0 version fails to do so. Thus, by updating an existing mechanism through re-optimization, the rates of some crucial reactions for a particular phenomenon could be inadvertently revised to yield unexpected results.

The reason for some of the bad performances of certain mechanisms is due to lack of validation for certain types of measurements. There is a very substantial foundation to the validation of high temperature chemistry components of comprehensive models. All of this inspires considerable confidence in the understanding of the kinetic foundation of alkane flames and in the kinetic models that describe them. However, although several examples have already been cited, the extent to which comprehensive models for lower temperature oxidation have been tested against experimental chemical measurements is less satisfactory. The rather limited extent to which

comprehensive schemes have been put to a test under low- and intermediate-temperature conditions is a weakness at present.
Most of these mechanisms were assembled based on directly measured or theoretically calculated rate coefficients. However, only a small fraction of the many reactions in these mechanisms have been measured experimentally or computed theoretically. As matter of fact, the number of reactions and species involved is large, and the determination of the rate constants of each of the identified reactions, either experimentally or computationally, is not a trivial task, especially for radical-radical reactions (Lu & Law 2009). In these cases, the best determinations often come from fitting a complex mechanism to experimental data. In fact, many so-called "direct" measurements also involve fitting mechanisms with multiple reactions to experimental data.
Alternatively, most rate coefficients are approximated from rough estimates; this crude approach is particularly true for peroxide chemistry, where the multiplicity of possible isomers and pathways is commonly replaced with a single lumped irreversible pathway and an empirically adjusted rate coefficient.
The difficult of a practical solution lies in the vast dimensionality of the parameter space. Under conditions of an individual experiment, the model responses that correspond to the experimental observations do not depend sensitively on all the parameters. Usually only a small fraction of the parameters shows a significant effect on measured responses. This phenomenon has been termed sparsity and the influential parameters active variables (Frenklach 2007). In this regard, while model parameters have their own uncertainties, usually only representative values are taken in most computational modelling. As such, it is not uncommon to adjust values of the models parameters in order to improve the agreement between the model predictions and measured ignition delay times, burning velocities or concentration profile measurements. These types of experimental data are usually referred to as indirect measurements, since such experimental results are interpretable only by simulations based on a detailed chemical kinetic model (Varga et al. 2016). This practice, however, overlooks the influence of adjusting parameters on predictions against other experiments, and consequently could lead to unreliable kinetic models.
At present, the more general the application (such as across different classes of hydrocarbons or to represent the performance of mixtures of compounds, like SECs can be) the greater will be the empiricism associated with the kinetic parameters. The scope of application of such a model may be severely curtailed by this empiricism and it should be taken into account by subsequent users. This has been widely demonstrated and motivated in the previous chapter.
However, the majority of users of reaction mechanisms are interested in robust, general-purpose mechanisms, which is why the above recommendations are useful from the author's viewpoint. Therefore, in order to improve the model predictive ability, model parameters should be adjusted in a systematic manner on the basis of as many different types of practical systems and as wide a range of conditions as possible. The present work has provided important additions to the experimental database for Smart Energy Carriers atmospheric pressure kinetic model validation.
From this analysis, it was found that the rate parameters of several reactions might need to be studied further. The numerical results here reported give clear indications on the set of reactions to tune to improve the reliability of kinetic mechanisms to properly predict combustion features of small hydrocarbons for non-conventional conditions.
From the comparison of the analyses performed for ignition delays and PSR it appeared that a good candidate for improving the performance of the kinetic models was found to be the reaction mechanism involving oxidation and recombination of CH_3 radicals.
The rate constant of the recombination reaction $CH_3 + CH_3 + M = C_2H_6 + M$ employed in different mechanisms can vary significantly from one model to another. Just to give an example, at 950 K, the rate constant employed by the CRECK-2014 mechanism is 2.3 times lower than that used in the Dagaut-2010 mechanism (note that these two are among the best performing mechanisms). Lower values of this rate constant significantly accelerate the rate of reactants consumption and make the

calculated ignition delays significantly shorter or the PSR species concentrations higher at intermediate-temperature.
On the other hand, the rate constant of the reaction $CH_3 + HO_2 = OH + CH_3O$, which compete with reaction 10, has a relatively high sensitivity and also a large range of uncertainty (Baulch et al. 2005). As opposed to the reaction 10, lower values of this rate constant significantly increase the calculated ignition delay times or decrease the PSR intermediate species concentrations.
Furthermore, many of the most sensitive reactions for the present conditions are highly sensitive reactions in a wide variety of combustion systems.
For example, the reaction mechanism involving chain branching and recombination of H radicals (reactions 11 and 12) along with the mechanism involving the intermediate- and high-temperature branching (reactions 11 and 7+8) are among the most sensitive and important in combustion models. The influence of these crucial reactions on ignition delay times depending on the temperature shown in Figs. 5.19-5.21 is irrefutable. It is notable that the rate constants of these reactions used in different mechanisms can vary significantly.
The intersection of these competitive mechanisms under SECs combustion conditions was found to be the cause of all the peculiar behaviours observed and explained in this thesis. At the same time, the same sub-mechanisms were seen to be the cause of the disagreement between experimental and numerical results and among the numerical predictions themselves.
The mixtures high dilution level implies modest temperature increments with respect to the initial condition, because of the higher mixture heat sink capabilities with respect to conventional systems. This is even more evident in the case of non-adiabatic systems, where heat exchange mechanisms further contain working temperatures. This restricts the reactive system to a narrower temperature window, where branching and recombination channels are more competitive. Since with increasing dilution and decreasing flame temperature recombination reactions are favoured and oxidation process occurs with relatively low reaction rates, flux through recombination and branching channels can become roughly equal. As a result, the sensitivity of the predictions to the rate parameters for those reactions increases dramatically. Under these operating conditions, the effects of the uncertainties of the chemical reaction rates on the kinetic models performance are emphasized and may cause large deviations of experimental evidences from the numerical predictions. On the contrary, at high temperatures, the performance of kinetic models is insured by the promotion of fast high temperature branching reactions, commonly well described in kinetic schemes developed and validated for conventional flame conditions.
The observed discrepancies between numerical and experimental data, and among model predictions themselves, raise for systems diluted in CO_2 and H_2O. The presence of these species ab initio poses several problems. First, the CO_2 and H_2O interaction ab initio on fuel oxidation kinetics process is an aspect not contemplated for traditional systems, where CO_2 and H_2O are present as combustion products in the post-oxidation phase, thus acting only on a sub-set of kinetic reactions that involve few species close to the equilibrium condition. Thus such an aspect has not been thoroughly examined in the validation procedure of detailed kinetic schemes. Given this background, the availability of a reliable experimental database is a crucial point to improve the predictive performance of detailed kinetic schemes.
Second, a critical point for third molecular reactions is the quantification of third body collisional efficiencies. In literature there are sparse data relative to the CO_2 and H_2O collisional efficiencies (Baulch et al. 2005), and in almost all mechanisms available in the literature, such values have been tuned to reproduce the results of indirect measurements. De facto, the kinetic models analysed in this work employ different values for the third body efficiency of CO_2 and H_2O relative to N_2. The sensitivity of the model predictions, which is higher in presence of CO_2 and H_2O, can substantially amplify the effects of this uncertainty in the predictions. Therefore, third body efficiency of CO_2 and H_2O likely requires further attention. Such an aspect should be discussed and addressed by means of a more structured approach.

Until now, we have referred to quantitative uncertainties in the model description due to uncertainties in the model parameters. However, kinetic models may have structural uncertainties, which refer to qualitative uncertainties in the model description due to assumptions/limitations of the model structure itself.
The first limitation refers to the temperature dependence of rate constants. For example, the Arrhenius equation is usually very accurate in a small temperature range. In a wide temperature range many reactions are best represented by a three-parameter rate constant of the form:
$K = AT^n exp(-E/RT)$.
This means that most "elementary reactions" are not elementary at all. This is particularly obvious for complex-forming bimolecular reactions, which generally have the most complicated, multi-channel, intrinsic mechanism such that each reaction would require a lengthy and very specific analysis. As a consequence, attention should be paid to use rate expressions only within the limits for which they have been designed and validated (Miller et al. 2005).
Only by drawing together all known measurements of rate constants for a given reaction over wide ranges of conditions is it possible for the most reliable values for temperature dependences to be deduced.
An example is the chain-branching reaction 11, which is the most sensitive reaction in all the analysed conditions. The rate constant of reaction 11 is considered well known. This is true under conventional combustion conditions. In fact, the ratio of the rate constant used in the CRECK-2014 mechanism and that used in the Baulch et al. (2005) reference database is 1.1 at 1800 K, but it becomes 1.4 at 1000 K. This means that the uncertainty range is not constant as reported in the Baulch et al. (2005) database, but it changes with temperature. This should be taken into account, given the high sensitivity coefficients of this reaction.
Another limitation refers to the pressure dependence of rate constants.
For example, some mechanisms use a different parametrization and third-body collision efficiency factors for the reaction $H + O_2 (+M) = HO_2 (+M)$ depending on the bath gas.
One should note that the method used in the models of representing different fall-off behaviour of particular reactions for different collision partners by writing an individual reaction for each couldn't predict appropriate high-pressure limit behaviour of the mechanism. Each of the expressions reaches the high-pressure limit to be a sum of true high-pressure limit rates. Therefore, only one reaction for the collision partner abundant in the mixture should be kept in the model, especially at high pressures (Konnov 2008). Despite all the experiments in the present work have been realized at atmospheric pressure, it was demonstrated above (see Figs. 5.16 and 5.17) that the high dilution levels, along with the presence of different bath gases with different third body efficiencies, could shift the rate constants of some reactions from the low-pressure limit toward the high-pressure limit (in particular the reaction 10).
Therefore, not only the value of the high-pressure limit rate constant but also the shape of the fall-off curves as a function of [M] would be relevant.
In this regard, Burke et al. (2010) noted that, first there is some variation among values proposed for the center broadening factors, F_c, in pure bath gases. Second, there is a lack of fundamental understanding of the mixing rules for fall-off reactions with bath gases having different broadening factors, which is especially important under the conditions studied in this work where significant concentrations of multiple species were used. The significance of the treatment of fall-off for the present conditions was demonstrated in Figs. 5.16 and 5.17.

CHAPTER 6 – CONCLUSION

The use of advanced combustion technologies (such as MILD, oxy-fuel, LTC, etc.) is among the most promising methods to reduce emission of pollutants. For such technologies, working temperatures are enough low to boost the formation of several classes of pollutants, such as NO_x and soot. To access this temperature range, a significant dilution as well as preheating of reactants is required. Such conditions are usually achieved by a strong recirculation of exhaust gases that simultaneously dilute and pre-heat the fresh reactants. These peculiar operative conditions also imply strong fuel flexibility, thus allowing the use of low calorific values (LCV) energy carriers with high efficiency.

Coupling these innovative combustion technologies with the energy carriers, define the Smart Energy Carriers (SECs). This category includes conventional and novel energetic molecules from alternative or conventional (re)sources, selected on the basis of their best available production and/or utilization technologies. Accordingly, to be considered "smart", an energy carrier and related technologies must be energetically and CO_2 efficient and able to provide the most suitable energy mix to meet the intermittency of renewable energies, to exploit varying and locally diverse sources and to satisfy the requirements for eco-compatibility and sustainability.

An effective use of advanced combustion technologies for SECs requires a thorough analysis of the combustion kinetic characteristics in order to identify optimal operating conditions and control strategies with high efficiency and low pollutant emissions.

As matter of fact, the intersection of low combustion temperatures and highly diluted mixtures with intense pre-heating alters the evolution of the combustion process with respect to traditional flames, thereby affecting the kinetics involved during fuel ignition and oxidation. Furthermore, the high content of diluent species, namely CO_2 and H_2O, deriving either from the presence of diluent in LCV fuels or from the recirculation of flue gases, makes the role of these species relevant in the oxidation chemistry in such a non-standard condition. Such issues are currently largely unexplored.

Therefore, fundamental study is necessary to understand the mechanisms of SECs combustion phenomena. This understanding must rely on validated detailed reaction models established for non-conventional conditions than those conventionally addressed.

As matter of fact, most chemical kinetic models have been validated at higher temperatures and lower dilution. However, these diluted combustion conditions stress a region of parameter space where combustion kinetic characteristics are strongly sensitive to a number of reactions whose rate constants have large uncertainties. Indeed, the higher dilution, lower flame temperatures, and high three-body collisional efficiencies of diluents such as CO_2 and H_2O define a kinetic regime, which is largely controlled by HO_2 and H_2O_2 pathways. Detailed mechanisms for low-temperature combustion are challenging to assemble because significantly more species and reactions must be considered than for high-temperature conditions, and large uncertainties remain regarding reactions and rate coefficients.

Therefore, there is a need of optimal detailed experiments spanning as many different types of practical systems and as wide a range of conditions as possible, in order to assist the development and validation of more reliable chemistry models for SECs combustion, restricting uncertainties for low temperatures and high dilution conditions.

Model reactors are well-established configurations to study chemical reaction pathways in combustion.

The present work experimentally characterized the ignition and oxidation processes of diluted and pre-heated model fuels mixtures (simple hydrocarbons mixed with diluents), at atmospheric pressure, in a Tubular Flow Reactor and a Jet Stirred Flow Reactor under a wide range of operating conditions involving temperatures, mixture compositions and dilution levels. Four reference fuels were studied: CH_4, C_3H_8, n-C_5H_{12}, and a mixture of CO/CH_4/C_2H_4/C_2H_6, while the diluent gases used were He, N_2, CO_2, H_2O. The attention was focused on ignition and oxidation characteristics

and their dependences on the operating parameters, such as temperature, dilution and equivalence ratio.
The influence of these parameters was analysed on ignition delay times, temperature and stable species concentrations profiles. The ignition delays were investigated in a TFR, while the chemical species concentrations were investigated in a JSFR. Kinetic measurements, such as ignition delay and species concentrations, are important targets for the validation and optimization of chemical kinetic mechanisms.
Several main findings can be outlined by the analysis reported here.
The exploitation of the ignition and oxidation processes of fuel mixtures under diluted conditions at intermediate temperatures has led to the identification of different phenomena and combustion regimes as functions of the inlet temperature and mixture composition. The very rich variety of phenomena observed provides a rigorous foundation against which a kinetic model may be tested qualitatively as well as quantitatively.
1) In particular, a peculiar behaviour was observed when the analysis of the **propane mixtures auto-ignition time shows a change in the slope of ignition curves in the Arrhenius diagram at intermediate temperatures and equivalence ratios between 0.5 and 1**, never observed before at atmospheric pressure. For high temperatures (> 1100 K) the experimental results show an Arrhenius type behaviour. This suggests that the competition among the different ignition regimes is very sensitive to mixture composition.
This analysis shows that, under diluted conditions and intermediate temperatures, autoignition is dominated by not only one elementary reaction, like in the conventional high-temperature combustion systems. This complicates the analysis of non-conventional combustion ignition phenomena and focuses kinetic attention on more reactions that control autoignition phenomena.
From a comparison of the present data with the data available in the literature, the behaviour of the current atmospheric data appears closer to the high-pressure data, rather than the other atmospheric pressure data. At the same time, it is also true that the current data are the only ones obtained under highly diluted conditions. This result indicates that highly diluted mixtures are more prone to show a change in slope between low and higher temperatures than undiluted conditions at low pressures. This means that significant errors might occur when low dilution information are extrapolated to higher dilution.
2) Furthermore, **periodic oscillatory behaviours were identified for almost all fuel mixtures tested in the present work, for specific temperature ranges and equivalence ratios, both in the TFR and in the JSFR**. It was observed that this behaviour is conceptually different with respect to two-stage oscillatory cool flame hydrocarbons ignition that occurs at low temperature, and it arises for diluted fuel mixtures at intermediate temperature.
Moreover, the differences detected in relation to the presence of a different diluent atmosphere on fuels ignition and oxidation highlight the importance of this study.
3) As matter of fact, in the experiments realized with different diluents, it was observed that, **compared to pure N_2, the presence of diluents CO_2 or H_2O accelerates the reactivity at intermediate temperatures while slows down it at high temperatures**. Also an accelerating effect of nitrogen compared to helium was observed at intermediate temperature. The relative importance of the effect of diluents on the ignition delay times and on species concentrations also depends upon the equivalence ratio.
Specifically, with regard to ignition delay times, in the case of CO_2 dilution, the difference between N_2 and CO_2 experimental data is less pronounced for ultra-lean and ultra-rich conditions, whereas for steam-diluted mixtures, the difference is less important only for ultra-rich conditions. This aspect suggests that when the recombination/pyrolytic reactions control the ignition process, the effect of H_2O and CO_2 becomes less significant with respect to nitrogen. Furthermore, in the case of CO_2 dilution, the ignition delay data are notably sensitive to the C/O feed ratio, whereas in the case of H_2O dilution, they are almost independent on this parameter.

In addition, the results suggest that the CO_2 and H_2O also have an influence on the C/O-T_{in} plane where oscillatory behaviour occurs.
For methane mixtures in the JSFR, it was observed that the fuel conversion decreases when the CO_2 or water vapour concentration is increased. This decrease is quasi-linear with gradually increasing CO_2 or H_2O molar fraction up to a certain value. Further increasing the CO_2 or H_2O concentration does not lead to proportional changes in the behaviour. This impact is found to be greater in H_2O dilution than in CO_2 dilution.
For n-pentane mixtures, at low temperatures, a homogeneous cool flame process can be observed, where no influence of diluent is found. Therefore, CO_2 and H_2O have an effect on intermediate-temperature chemistry much more marked than that on low-temperature chemistry.
4) Another finding concerns the experiments realized using a pyrolysis gas as reference fuel. These experiments demonstrate the possibility of a **direct use of raw LCV fuels in practical applications**. The ignition delay times reported in this work for pyrolysis gas show that the ignition delay times are compatible with the characteristic times required in real facilities. More specifically, in the present case, the ignition delay times are lower than the methane ignition time reported in the literature under the same conditions of dilution and fuel/oxygen content, due to the presence of the C_2 species.
All these findings are of interest for the development of advanced combustion technologies.
In addition, the measurements were also compared to simulations based on different kinetic mechanisms to verify their validity under diluted combustion conditions. Simulations for comparing the experimental results were performed using 12 recent comprehensive mechanisms available in the literature.
5) Numerical predictions showed that **kinetic models were capable of only partially quantitatively reproducing the observed experimental data**. In addition, large variations, up to two orders of magnitude, can be observed among the model predictions themselves under high dilution and intermediate temperature. Such large discrepancies among the model predictions are surprising given that all were validated against extensive (and frequently the same) data sets.
In particular, the simulations produce significant discrepancies between the experimental and the numerical results when the systems are diluted in H_2O and CO_2. The discrepancy is even more evident when moving from methane to propane and pyrolysis gas.
Comparing the rate coefficients from the 12 mechanisms adopted here, the rate coefficients for some of these reactions can differ significantly, up to differences higher than one order of magnitude. It was shown that at higher dilution a given uncertainty in a rate parameter results in a larger uncertainty in the predictions.
This demonstrates the need for further investigations concerning the ignition and oxidation studies, especially in the intermediate temperature regime at high dilution.
Improving the accuracy of the models would enhance their use in detailed design of combustors for new technologies.
There is clearly rooms for specific improvements. In this perspective, since the studied targets provide a stronger constraint on the model parameters, the wide range of operating conditions studied, in terms of fuel and diluent type, temperatures, equivalence ratios, and dilution levels, made these results a valuable benchmark for validation of detailed kinetic schemes in order to extend their applicability to non-standard conditions. Our study has provided reproducible experimental data in a reference system under non-standard conditions. Comparison of the new obtained experimental and computational results will then enable the re-evaluation and optimization of the current mechanisms.
6) **The key reactions that were identified in this work must be considered** for a further tuning of kinetic schemes, which is needed for a good description of the ignition and oxidation processes under diluted operative conditions.
Furthermore, accurate rate coefficients for these reactions based on detailed theory may help improve the agreement of experiments and simulations to some extent. These reactions typically

have complex temperature and pressure dependencies that cannot be easily resolved through mechanism optimization. Also, there is a lack of fundamental understanding of the mixing rules for fall-off reactions with bath gases having different broadening factors, which is especially important under the conditions studied in this work where significant concentrations of multiple species were used.
Furthermore, the experiments do not only provide data for models validation, but also contain information in itself.
7) It was seen that the experimentally observed phenomena are a direct consequence of the non-conventional operating conditions.
Indeed, in low-dilution conditions, the ignition process is sustained by high temperature gradients, and a fast chemistry dominates the process evolution. In contrast, for diluted conditions the reactivity of the system slows down, making the system more sensitive to the operating conditions and lower adiabatic flame temperatures enhance the competition among several pathways, thus permitting the onset of phenomenologies that are generally hidden during conventional combustion processes.
Specifically, intermediate-temperature chemistry is represented by H_2O_2 decomposition ($HO_2 + HO_2 = H_2O_2 + O_2$ and $H_2O_2 + M = OH + OH + M$) and high-temperature chemistry by reaction $H + O_2 = OH + O$. In the investigated temperature range the two mechanisms compete among them and also both compete with the recombination reaction $H + O_2 + M = HO_2 + M$, leading to the oscillatory behaviours.
Furthermore, the onset of termolecular methyl radical recombination reaction $CH_3 + CH_3 + M = C_2H_6 + M$ at intermediate temperature slows down the mixture reactivity, inhibiting the oxidation channel over a temperature range in which there is a strong competition between intermediate- and high-temperature branching and between branching and recombination, leading to the variation of the slope of ignition delay times in the Arrhenius plot over the intermediate temperature range.
The competition among different kinetic routes is exacerbated by the fact that high levels of dilution lead to nearly isothermal conditions that, when associated with strong pre-heating, alter the relative weights of pyrolytic/oxidative routes, promoting the establishment of different regimes. This competition is very sensitive to the operating conditions (i.e., the temperature and the carbon/oxygen mixture feed ratio).
Such behaviours are not recognizable in conventional systems because the high heat release, associated with standard deflagration or diffusion flames, enhances the shift among the different regimes, thereby promoting the establishment of kinetics typically observed at high temperatures.
Further analyses were performed to understand the main effects on the ignition chemistry of the used diluents. In particular it was observed that, at low temperatures, CO_2 incentivizes intermediate-temperature branching reactions because of its high third-body efficiency that promotes the H_2O_2 decomposition reaction. This effect is partially contrasted by its high heat capacity, which damps the temperature increase. At slightly higher temperatures, CO_2 promotes C_2 chemistry, which inhibits the ignition process. This effect is strengthened at high temperatures ($T_{in} > 1200$ K), where CO_2 decomposes through endothermic reactions ($CO_2 + H = CO + OH$) and competes for H atoms with the high-temperature branching reactions.
In the case of steam dilution, H_2O mainly acts as a third-body species. It boosts the intermediate-temperature branching reactions and decreases the ignition times. At higher temperatures, it inhibits the ignition process depressing the C_1 oxidation channel chemistry and the high-temperature branching reactions, promoting the methyl recombination channel and the reaction $H + O_2 + M = HO_2 + M$, respectively. This effect is strengthened at high temperatures ($T_{in} > 1200$ K), where H_2O decomposes through reactions ($H_2O + H = H_2 + OH$) and competes for H atoms with the high-temperature branching reactions.
In addition, in the case of steam, the double competition between the C_1 and C_2 chemistry, which is established at intermediate temperatures in the neighbourhood of stoichiometric mixtures, and between the H recombination and branching reactions occurred for lean/ultra-lean mixtures, which

makes the system prone to instabilities in a wide range of carbon/oxygen feed ratios with respect to CO_2, as shown in the T_{in}-C/O maps.
Moreover, with increasing CO_2 or H_2O content the influence of three-body methyl radical recombination reaction first increases, then, the low-pressure behaviour switches to high-pressure behaviour in the manner of Lindemann mechanism. Thus the methyl radical recombination reaction is third-order in the nitrogen dilution and second-order in the CO_2 or H_2O dilution.
Finally, it was not possible to understand why the nitrogen accelerates the reactivity at intermediate temperature compared to helium dilution, since none of the used models predicts this effect.
These mechanisms are summarized in the following figure, where the methyl radical oxidation channel is represented as "C_1-Ox", whereas the methyl radical recombination channel is represented as "C_1-Rec".

		Temperature		
		800 K	1000 K	1200 K
N_2	C_1 chemistry	C_1-Ox	C_1-Ox vs C_1-Rec	C_1-Ox
	H_2/O_2	$H_2O_2 + M = 2OH + M$	$H_2O_2 + M = 2OH + M$ vs $H + O_2 = OH + O$ vs $H + O_2 + M = HO_2 + M$	$H + O_2 = OH + O$
CO_2	C_1 chemistry	C_1-Ox	C_1-Ox vs C_1-Rec	C_1-Ox
	H_2/O_2	$H_2O_2 + M = 2OH + M$	$H_2O_2 + M = 2OH + M$ vs $H + O_2 = OH + O$ vs $H + O_2 + M = HO_2 + M$	$H + O_2 = OH + O$ vs $CO_2 + H = CO + OH$
H_2O	C_1 chemistry	C_1-Ox	C_1-Ox vs C_1-Rec	C_1-Ox
	H_2/O_2	$H_2O_2 + M = 2OH + M$	$H_2O_2 + M = 2OH + M$ vs $H + O_2 = OH + O$ vs $H + O_2 + M = HO_2 + M$	$H + O_2 = OH + O$ vs $H_2O + H = H_2 + OH$ vs $H + O_2 + M = HO_2 + M$

In this study, we have confirmed that combinations of properly chosen measurements, together with simulations, can be used to reveal peculiar aspects in detailed combustion chemistry. To assess the potential for low emissions and high efficiency from SECs, reliable combustion models should be available.
There is therefore much more to be done in this line of research. Advances in the future may be anticipated in clarifying combustion characteristics of more complex fuels and fuel mixtures, as well as in analysing the effect of trace species that can be present in exhaust gas (NO_x, SO_x, HC, etc.), some of which are of concern as pollutants. Finally, reduced mechanisms consisting of lower numbers of species and their associated reactions also need to be derived for implementation in large-scale computational simulation. However, they can be developed only after comprehensive detailed mechanisms are first established.
The fidelity of the results will depend on improvements in chemical-kinetic elementary-rate descriptions.

REFERENCES

Abián, M, Giménez-López, J, Bilbao, R & Alzueta, MU 2011, "Effect of different concentration levels of CO_2 and H_2O on the oxidation of CO: experiments and modeling", *Proceedings of the Combustion Institute*, vol. 33, pp. 317-323.

Abtahizadeh, E, van Oijen, J & de Goey, P 2012, "Numerical study of MILD combustion with entrainment of burned gas into oxidizer and/or fuel streams", *Combustion and Flame*, vol. 159, no. 6, pp. 2155-2165.

Agarwal, AK 2007, "Biofuels (alcohols and biodiesel) applications as fuels for internal combustion engines", *Progress in Energy and Combustion Science*, vol. 33, pp. 233-271.

Alekseev, VA, Christensen, M & Konnov, AA 2015, "The effect of temperature on the adiabatic burning velocities of diluted hydrogen flames: a kinetic study using an updated mechanism", *Combustion and Flame*, vol. 159, pp. 151-160.

Anderlhor, JM, Pires da Cruz, A, Bounaceur, R & Battin-Leclerc, F 2010, "Thermal and kinetic impact of CO, CO_2, and H_2O on the postoxidation of IC-engine exhaust gases", *Combustion Science and Technology*, vol. 182, pp. 39-59.

Barbas, M, Costa, M, Vranckx, S & Fernandes, RX 2015, "Experimental and chemical kinetic study of CO and NO formation in oxy-methane premixed laminar flames doped with NH_3", *Combustion and Flame*, vol. 162, pp. 1294-1303.

Basevich, VYa, Borisov, AA, Frolov, SM, Troshin, KYa & Skachkov, GI 2006, "Autoignition of Jet Propulsion Fuel and Its Surrogate: Experiments and Modeling", *Proceedings of the Fifth International Colloquium on Pulsed and Continuous Detonation*, Moskow, Russia.

Battin-Leclerc, F 2008, "Detailed chemical kinetic models for the low-temperature combustion of hydrocarbons with application to gasoline and diesel fuel surrogates", *Progress in Energy and Combustion Science*, vol. 34, no. 4, pp. 440-498.

Baulch, DL, Bowman, CT, Cobos, CJ, Cox, RA, Just, Th, Kerr, JA, Pilling, MJ, Stocker, D, Troe, J, Tsang, W, Walker, RW & Warnatz, J 2005, "Evaluated Kinetic Data for Combustion Modeling: Supplement II", *Journal of Physical and Chemical Reference Data*, vol. 34, no. 3, pp. 757-1397.

Beerer, DJ & McDonell, VG 2011, "An experimental and kinetic study of alkane autoignition at high pressures and intermediate temperatures", *Proceedings of the Combustion Institute*, vol. 33, pp. 301-307.

Benson, SW 1981, "The kinetics and thermochemistry of chemical oxidation with application to combustion and flames", *Progress in Energy and Combustion Science*, vol. 7, no. 2, pp. 125-134.

Bergthorson, JM, Goroshin, S, Soo, MJ, Julien, P, Palecka, J, Frost, DL & Jarvis, DJ 2015, "Direct combustion of recyclable metal fuels for zero-carbon heat and power", *Applied Energy*, vol. 160, pp. 368-382.

Bernatosyan, SG & Mantashyan, AA 1986, "Bistability in the oscillating oxidation of propane and the effects of weak perturbations", *Combustion, Explosion and Shock Waves*, vol. 22, no. 3, pp. 337-340.

Brokaw, R & Jackson, J 1955, "Effect of Temperature, Pressure and Composition on Ignition Delays for Propane Flames", *Fifth Symposium (International) on Combustion*, Reinhold, New York.

Bugler, J, Rodriguez, A, Herbinet, O, Batin-Leclerc, F, Togbé, C, Dayma, G, Dagaut, P & Curran, HJ 2016, "An experimental and modelling study of n-pentane oxidation in two jet-stirred reactors: The importance of pressure-dependent kinetics and new reaction pathways", *Proceedings of the Combustion Institute*, In Press.

Buhre, BJP, Elliot, LK, Sheng, CD, Gupta, RP & Wall, TF 2005, "Oxy-fuel combustion technology for coal-fired power generation", *Progress in Energy and Combustion Science*, vol. 31, no. 4, pp. 283-307.

Burcat, A, Scheller, K & Lifshitz, A 1971, "Shock-tube investigation of comparative ignition delay times for C_1-C_5 alkanes", *Combustion and Flame*, vol. 16, no. 1, pp. 29-33.

Burke, MP, Chaos, M, Dryer, FL & Ju, Y 2010, "Negative pressure dependence of mass burning rates of H_2/CO/O_2/diluent flames at low flame temperatures", *Combustion and Flame*, vol. 157, pp. 618-631.

Burke, MP, Goldsmith, CF, Klippenstein, SJ, Welz, O, Huang, H, Antonov, IO, Savee, JD, Osborn, DL, Zádor, J, Taatjes, CA & Sheps, L 2015, "Multiscale Informatics for Low-Temperature Propane Oxidation: Further Complexities in Studies of Complex Reactions", *The Journal of Physical Chemistry*, vol. 119, pp. 7095-7115.

Cadman, P, Thomas, GO & Butler, P 2000, "The auto-ignition of propane at intermediate temperatures and high pressures", *Physical Chemistry Chemical Physics*, vol. 2, pp. 5411-5419.

Cancino, LR, Fikri, M, Oliveira, AAM & Schulz, C 2001, "Ignition delay times of ethanol-containing multi-component gasoline surrogates: Shock-tube experiments and detailed modeling", *Fuel*, vol. 90, pp. 1238-1244.

Caprio, V, Insola, A & Lignola, PG 1981, "Isobutane cool flames in a CSTR: The behaviour dependence on temperature and residence time", *Combustion and Flame*, vol. 43, pp. 23-33.

Cavaliere, A & de Joannon, M 2004, "Mild Combustion", *Progress in Energy and Combustion Science*, vol. 30, pp. 329-366.

Chang, CJ, Thompson, AL & Winship, RD 1958, "Ignition delay of propane in air between 725-880°C under isothermal conditions", *Symposium (International) on Combustion*, vol. 7, no. 1, pp. 431-435.

Chaos, M & Dryer, F 2010, "Chemical-kinetic modeling of ignition delay: Considerations in interpreting shock tube data" *International Journal of Chemical Kinetics*, vol. 42, no. 3, pp. 143-150.

CHEMKIN-PRO 15131, Reaction Design: San Diego, 2013.

Choi, BC, Kim, KN & Chung, SH 2009, "Autoignited laminar lifted flames of propane in coflow jets with tribrachial edge and mild combustion", *Combustion and Flame*, vol. 156, pp. 396-404.

Christo, FC & Dally, BB 2005, "Modeling turbulent reacting jets issuing into a hot and diluted coflow", *Combustion and Flame*, vol. 142, pp. 117-129.

Colorado, AF, Herrera, BA & Amell, AA 2010, "Performance of a Flameless combustion furnace using biogas and natural gas", *Bioresource Technology*, vol. 101, no. 7, pp. 2443-2449.

Cowell, LH & Lefebvre, A 1986, "Influence of Pressure on Auto-ignition Characteristics of Gaseous Hydrocarbon-air Mixtures", *SAE Technical Paper 860068*, pp. 1-11.

Cuoci, A, Frassoldati, A, Faravelli, T & Ranzi, E 2015, "OpenSMOKE++: An object-oriented framework for the numerical modelling of reactive systems with detailed kinetic mechanisms", *Computer Physics Communications*, vol. 192, pp. 237-264.

D'Anna, A, Mercogliano, R, Barbella, R & Ciajolo, A 1992, "Low Temperature Oxidation Chemistry of iso-Octane under High Pressure Conditions", *Combustion Science and Technology*, vol. 83, no. 4-6, pp. 217-232.

Dagaut, P, Cathonnet, M, Rouan, JP, Foulatier, R, Quilgars, A, Boettner, JC, Gaillard, F & James, H 1986, "A jet-stirred reactor for kinetic studies of homogeneous gas-phase reactions at pressures up to ten atmospheres (≈1 MPa)", *Journal of Physics E: Scientific Instruments*, vol. 19, no. 3, pp. 207-209.

Dally, BB, Karpetis, AN & Barlow, RS 2002, "Structure of turbulent non-premixed jet flames in a diluted hot coflow", *Proceedings of the Combustion Institute*, vol. 29, no. 1, pp. 1147-1154.

Dally, BB, Riesmeier, E & Peters, N 2004, "Effect of fuel mixture on moderate and intense low oxygen dilution combustion", *Combustion and Flame*, vol. 137, pp. 418-431.

Dally, BB & Peters, N 2007, "Heat Loss-Induced Oscillation of Methane and Ethylene in a Perfectly Stirred Reactor", paper presented to the 6th Asia-Pacific Conference on Combustion, Nagoya, Japan, 20-23 May.

David, R & Matras, D 1975, "Règles de construction et d'extrapolation des réacteurs auto-agités par jets gazeux", *The Canadian Journal of Chemical Engineering*, vol. 53, pp. 297-300.

de Joannon, M, Cavaliere, A, Donnarumma, R & Ragucci, R 2002, "Dependence of autoignition delay on oxygen concentration in mild combustion of high molecular weight paraffin", *Proceedings of the Combustion Institute*, vol. 29, no. 1, pp. 1139-1146.

de Joannon, M, Cavaliere, A, Faravelli, T, Ranzi, E, Sabia, P & Tregrossi, A 2005, "Analysis of process parameters for steady operations in methane mild combustion technology", *Proceedings of the Combustion Institute*, vol. 30, no. 2, pp. 2605-2612.

de Joannon, M, Matarazzo, A, Sabia, P & Cavaliere, A 2007, "Mild combustion in Homogeneous Charge Diffusion Ignition (HCDI) regime", *Proceedings of the Combustion Institute*, vol. 31, no. 2, pp. 3409-3416.

de Joannon, M, Sabia, P, Sorrentino, G & Cavaliere, A 2009, "Numerical study of mild combustion in hot diluted diffusion ignition (HDDI) regime", *Proceedings of the Combustion Institute*, vol. 32, pp. 3147-3154.

de Joannon, M, Sorrentino, G & Cavaliere, A 2012, "MILD combustion in diffusion-controlled regimes of Hot Diluted Fuel", *Combustion and Flame*, vol. 159, pp. 1832-1839.

de Joannon, M, "SMARTCAT: Chemistry of Smart Energy Carriers and Technologies", *Memorandum of understanding for the implementation of a European Concerted Research Action designated as COST Action CM1404* 2014, http://www.cost.eu/fileadmin/domain_files/CMST/Action_CM1404/mou/CM1404-e.pdf.

de Joannon, M, Sabia P, Sorrentino, G, Bozza, P & Ragucci, R 2016, "Small size burner combustion stabilization by means of strong cyclonic recirculation", *Proceedings of the Combustion Institute*, In Press.

Di, H, He, X, Zhang, P, Wang, Z, Wooldrige, MS, Law, CK, Wang, C, Shuai, S & Wang, J 2014, "Effects of buffer gas composition on low temperature ignition of iso-octane and n-heptane", *Combustion and Flame*, vol. 161, pp. 2531-2538.

Di Blasi, C 2009, "Combustion and gasification rates of lignocellulosic chars", *Progress in Energy and Combustion Science*, vol. 35, pp. 121-140.

Effuggi, A, Gelosa, D, Derudi, M & Rota, R 2008, "Mild Combustion of Methane-Derived Fuel Mixtures: Natural Gas and Biogas", *Combustion Science and Technology*, vol. 180, no. 3, pp. 481-493.

Fieweger, K, Blumenthal, R & Adomeit, G 1997, "Self-Ignition of S.I. Engine Model Fuels: A Shock Tube Investigation at High Pressure", *Combustion and Flame*, vol. 109, pp. 599-619.

Freeman, G & Lefebvre, AH 1984, "Spontaneous ignition characteristics of gaseous hydrocarbon-air mixtures", *Combustion and Flame*, vol. 58, no. 2, pp. 153-162.

Frenklach, M 2007, "Transforming data into knowledge-Process Informatics for combustion chemistry", *Proceedings of the Combustion Institute*, vol. 31, pp. 125-140.

Gallagher, SM, Curran, HJ, Metcalfe, WK, Healy, D, Simmie, JM & Bourque, G 2008, "A rapid compression machine study of the oxidation of propane in the negative temperature coefficient regime", *Combustion and Flame*, vol. 153, pp. 316-333.

Galletti, C, Parente, A & Tognotti, L 2007, "Numerical and experimental investigation of a mild combustion burner", *Combustion and Flame*, vol. 151, pp. 649-664.

Giménez-López, J, Millera, A, Bilbao, R & Alzueta, MU 2010, "HCN oxidation in an O_2/CO_2 atmosphere: an experimental and kinetic modelling study", *Combustion and Flame*, vol. 157, pp. 267-276.

Glarborg, P & Bentzen, LLB 2008, "Chemical effects of a high CO_2 concentration in oxy-fuel combustion of methane", *Energy & Fuels*, vol. 22, pp. 291-296.

Gonzalo-Tirado, C & Jiménez, S 2015, "Detailed analysis of the CO oxidation chemistry around a coal char particle under conventional and oxy-fuel combustion conditions", *Combustion and Flame*, vol. 162, pp. 478-485.

Griffiths, JF & Scott, SK 1987, "Thermokinetic interactions: Fundamentals of spontaneous ignition and cool flames", *Progress in Energy and Combustion Science*, vol. 13, no. 3, pp. 161-197.

Griffiths, JF 1995, "Reduced kinetic models and their application to practical combustion systems", *Progress in Energy and Combustion Science*, vol. 21, pp. 25-107.

Gupta, KK, Rehman & Sarviya, RM 2010, "Bio-fuels for gas turbine: A review", *Renewable and Sustainable Energy Reviews*, vol. 14, pp. 2946-2955.

Healy, D, Kalitan, DM, Aul, CJ, Petersen, EL, Bourque, G & Curran, HJ 2010, "Oxidation of C1-C5 Alkane Quinternary Natural Gas Mixtures at High Pressures", *Energy and Fuels*, vol. 24, no. 3, pp. 1521-1528.

Herbinet, O, Marquaire, P-M, Battin-Leclerc, F & Fournet, R 2007, "Thermal decomposition of n-dodecane: Experiments and kinetic modeling", *Journal of analytical and applied pyrolysis*, vol. 78, no. 2, pp. 419-429.

Herbinet, O & Dayma, G 2013, "Jet-Stirred Reactors", in Battin-Leclerc, F, Simmie, JM & Blurock, E (eds.), *Cleaner Combustion: Developing Detailed Chemical Kinetic Models*, Springer, Green Energy and Technology, pp. 183-210.

Herzler, J, Jerig, L & Roth, P 2004, "Shock-tube study of the ignition of propane at intermediate temperatures and high pressures", *Combustion Science and Technology*, vol. 176, no. 10, pp. 1627-1637.

Heufer, KA, Fernandes, RX, Olivier, H, Beeckmann, J, Röhl, O & Peters, N 2011, "Shock tube investigations of ignition delays of n-buthanol at elevated pressures between 770 and 1250 K", *Proceedings of the Combustion Institute*, vol. 33, pp. 359-366.

Holton, MM, Gokulakrishnan, PP, Klassen, MS, Roby, RJ & Jackson, GS 2010, "Autoignition Delay Time Measurements of Methane, Ethane, and Propane Pure Fuels and Methane-Based Fuel Blends", *Journal of Engineering for Gas Turbines and Power*, vol. 132, no. 9, pp. 091502-091502-9.

Horning, DC 2001, "A study of the high-temperature autoignition and thermal decomposition of hydrocarbons", *Report No. TSD-135 2001*, High-Temperature Gasdynamics Laboratory Department of Mechanical Engineering Stanford University, Stanford.

Hosseini, SE & Wahid, MA 2013, "Biogas utilization: Experimental investigation on biogas flameless combustion in lab-scale furnace", *Energy Conversion and Management*, vol. 74, pp. 426-432.

Ihme, M 2012, "On the role of turbulence and compositional fluctuations in rapid compression machines: Autoignition of syngas mixtures", *Combustion and Flame*, vol. 159, pp. 1592-1604.

Jacobs, TJ & Assanis, DN 2007, "The attainment of premixed compression ignition low-temperature combustion in a compression ignition direct injection engine", *Proceedings of the Combustion Institute*, vol. 31, no. 2, pp. 2913-2920.

Kohse-Höinghaus, K & Brockhinke, A 2009, "Experimental and Numerical Methods for Studying the Flame Structure", *Combustion, Explosion, and Shock Waves*, vol. 45, no. 4, pp. 349-364.

Konnov, AA 2008, "Remaining uncertainties in the kinetic mechanism of hydrogen combustion", *Combustion and Flame*, vol. 152, pp. 507-528.

Konnov, AA 2009, "Implementation of the NCN pathway of prompt-NO formation in the detailed reaction mechanism", *Combustion and Flame*, vol. 156, no. 11, pp. 2093-2105.

Kreith, F & Bohn, MS 2001, *Principles of Heat Transfer*, 6th edn, Brooks/Cole, Pacific Grove, USA.

Lamoroux, J, Ihme, M, Fiorina, B & Gicquel, O 2014, "Tabulated chemistry approach for diluted combustion regimes with internal recirculation and heat losses", *Combustion and Flame*, vol. 161, pp. 2120-2136.

Le Cong, T, Bedjanian, E & Dagaut, P 2010, "Oxidation of Ethylene and Propene in the Presence of CO_2 and H_2O: Experimental and Detailed Kinetic Modeling Study", *Combustion Science And Technology*, vol. 182, no. 4-6, pp. 333-349.

Levenspiel, O 1958 *Chemical Reaction Engineering*, John Wiley and Sons, Inc., New York.

Lezberg, EA 1957, "Preliminary Investigation of Propane Combustion in a 3-Inch-Diameter Duct at Inlet-Air Temperatures of 1400 to 1600 F", *Technical Note 4028*, National Advisory Committee for Aeronautics.

Liu, F, Guo, H, Smallwood, GJ & Gülder, OL 2001, "The chemical effects of carbon dioxide as an additive in an ethylene diffusion flame: implications for soot and NO_x formation", *Combustion and Flame*, vol. 125, pp. 778-787.

Liu, F, Guo, H & Smallwood, GJ 2003, "The chemical effect of CO_2 replacement of N_2 in air on the burning velocity of CH_4 and H_2 premixed flames", *Combustion and Flame*, vol. 133, pp. 495-497.

Liu, H & Okazaki, K 2003, "Simultaneous easy CO_2 recovery and drastic reduction of SO_x and NO_x in O_2/CO_2 coal combustion with heat recirculation", *Fuel*, vol. 82, pp. 1427-1436.

Liu, Y, Chen, S, Yang, B, Liu, K & Zheng, C 2015, "First and second thermodynamic-law comparison of biogas MILD oxy-fuel combustion moderated by CO_2 or H_2O", *Energy Conversion and Management*, vol. 106, pp. 625-634.

Lu, T & Law, CK 2009, "Toward accommodating realistic fuel chemistry in large-scale computations", *Progress in Energy and Combustion Science*, vol. 35, pp. 192-215.

Marinov, NM, Pitz, WJ, Westbrook, CK, Hori, M & Matsunaga, N 1998, "An Experimental and Kinetic Calculation of the Promotion Effect of Hydrocarbons on the NO-NO_2 Conversion in a Flow Reactor", *Proceedings of the Combustion Institute*, vol. 27, pp. 389-396.

Matras, D & Villermaux, J 1973, "Un réacteur continu parfaitement agité par jets gazeux pour l'étude cinétique de reactions chimiques rapides", *Chemical Engineering Science*, vol. 28, no. 1, pp. 129-137.

Mazas, AN, Fiorina, B, Lacoste, DA & Schuller, T 2011, "Effects of water vapour addition on the laminar burning velocity of oxygen-enriched methane flames", *Combustion and Flame*, vol. 158, pp. 2428-2440.

Mendiara, T & Glarborg, P 2009, "Reburn chemistry in oxy-fuel combustion of methane", *Energy & Fuels*, vol. 23, pp. 3565-3572.

Mendiara, T & Glarborg, P 2009, "Ammonia chemistry in oxy-fuel combustion of methane", *Combustion and Flame*, vol. 156, pp. 1937-1949.

Merchant, SS, Goldsmith, CF, Vandeputte, AG, Burke, MP, Klippenstein, SJ & Green, WH 2015, "Understanding low-temperature first-stage ignition delay: Propane", *Combustion and Flame*, vol. 162, no.10, pp. 3658-3673.

Metcalfe, WK, Burke, SM, Ahmed, SS & Curran, HJ 2013, "A Hierarchical and Comparative Kinetic Modeling Study of C1-C2 Hydrocarbon and Oxygenated Fuels", *International Journal of Chemical Kinetics*, vol. 45, no. 10, pp. 638-675.

Miller, JA, Pilling, MJ & Troe, J 2005, "Unravelling combustion mechanisms through a quantitative understanding of elementary reactions", *Proceedings of the Combustion Institute*, vol. 30, pp. 43-88.

Minamoto, Y, Swaminathan, N, Cant, SR & Leung, T 2014, "Morphological and statistical features of reaction zones in MILD and premixed combustion", *Combustion and Flame*, vol. 161, pp. 2801-2814.

Mueller, CL, Musculus, MPB, Pitz, WJ & Westbrook, CK 2003, "The Oxygen Ratio: A Fuel-Independent Measure of Mixture Stoichiometry", https://e-reports-ext.llnl.gov/pdf/303708.pdf.

Natarajan, J, Lieuwen, T & Seitzman, J 2007, "Laminar flame speeds of H_2/CO mixtures: effect of CO_2 dilution, preheat temperature, and pressure", *Combustion and Flame*, vol. 151, pp. 104-119.

Natarajan, J, Lieuwen, T & Seitzman, J 2008, "Laminar flame speeds and strain sensitivities of mixtures of $H_2/O_2/N_2$ at elevated preheat temperatures", *Journal of Engineering for Gas Turbines and Power*, vol. 130, no. 6, pp. 061502-061502-8.

Natarajan, J, Kochar, Y, Lieuwen, T & Seitzman, J 2009, "Pressure and preheat dependence of laminar flame speeds of $H_2/CO/CO_2/O_2$/He mixtures", *Proceedings of the Combustion Institute*, vol. 32, pp. 1261-1268.

Olm, C, Zsély, IGy, Pálvölgyi, R, Varga, T, Nagy, T, Curran, HJ & Turányi, T 2014, "Comparison of the performance of several recent hydrogen combustion mechanisms", *Combustion and Flame*, vol. 161, pp. 2219-2234.

Parente, A, Galletti, C & Tognotti, L 2008, "Effect of the combustion model and kinetic mechanism on the MILD combustion in an industrial burner fed with hydrogen enriched fuels", *International Journal of Hydrogen Energy*, vol. 33, no. 24, pp. 7553-7564.

Penyazkov, OG, Ragotner, KA, Dean, AJ & Varatharajan, B 2005, "Autoignition of propane-air mixtures behind reflected shock waves", *Proceedings of the Combustion Institute*, vol. 30, no. 2, pp. 1941-1947.

Peschke, WT & Spadaccini, LJ 1985, *Determination of Autoignition and Flame Speed Characteristics of Coal Gases Having Medium Heating Values*, Research Project No. 2357-1, Report No. AP-4291.

Plessing, T, Peters, N & Wünning, JG 1998, "Laseroptical investigation of highly preheated combustion with strong exhaust gas recirculation", *Symposium (International) on Combustion*, vol. 27, no. 2, pp. 3197-3204.

Prathap, C, Anjan Ray & Ravi, MR 2012, "Effects of dilution with carbon dioxide on the laminar burning velocity and flame stability of H_2-CO mixtures at atmospheric condition", *Combustion and Flame*, vol. 159, pp. 482-492.

Qiao, L, Gu, Y, Dahm, WJA, Oran, ES & Faeth, GM 2007, "A study of the effects of diluents on near-limit H_2-air flames in microgravity at normal reduced pressures", *Combustion and Flame*, vol. 151, pp. 196-208.

Qiao, L, Gan, Y, Nishiie, T, Dahm, WJA & Oran, ES 2010, "Extinction of premixed methane/air flames in microgravity by diluents: effects of radiation and Lewis number", *Combustion and Flame*, vol. 157, pp. 1446-1455.

Ranzi, E, Frassoldati, A, Grana, R, Cuoci, A, Faravelli, T, Kelley, AP & Law, CK 2012, "Hierarchical and comparative kinetic modeling of laminar flame speeds of hydrocarbon and oxygenated fuels", *Progress in Energy and Combustion Science*, vol. 38, no. 4, pp. 468-501.

Ranzi, E, Cavallotti, C, Cuoci, A, Frassoldati, A, Pelucchi, M & Faravelli, T 2014, "New reaction classes in the kinetic modeling of low temperature oxidation of n-alkanes", *Combustion and Flame*, vol. 162, no. 5, pp. 1679-1691.

Ratna Kishore, V, Ravi, MR & Anjan Ray 2011, "Adiabatic burning velocity and cellular flame characteristics of H_2-CO-CO_2-air mixtures", *Combustion and Flame*, vol. 158, pp. 2149-2164.

Ren, J-Y, Qin, W, Egolfopoulos, FN, Mak, H & Tsotsis, TT 2001, "Methane reforming and its potential effect on the efficiency and pollutant emissions of lean methane-air combustion", *Chemical Engineering Science*, vol. 56, pp. 1541-1549.

Richards, GA, McMillian, MM, Gemmen, RS, Rogers, WA & Cully, SR 2001, "Issues for low-emission, fuel-flexible power systems", *Progress in Energy and Combustion Science*, vol. 27, pp. 141-169.

Rodriguez, A, Herbinet, O, Wang, Z, Qi, F, Fittschen, C, Westmoreland, PR, Battin-Leclerc, F 2016, "Measuring hydroperoxide chain-branching agents during n-pentane low-temperature oxidation", *Proceedings of the Combustion Institute*, In Press.

Sabia, P 2006, "*Experimental and Numerical Studies of Mild Combustion processes in Model Reactors*", PhD Thesis, Università degli Studi di Napoli Federico II, http://www.fedoa.unina.it/view/people/Sabia_Pino.html.

Sabia, P, de Joannon, M, Fierro, S, Tregrossi, A & Cavaliere, A 2007, "Hydrogen-enriched methane mild combustion in a well stirred reactor", *Experimental Thermal and Fluid Science*, vol. 31, no. 5, pp. 469-475.

Sabia, P, de Joannon, M, Picarelli, A & Ragucci, R 2013, "Methane auto-ignition delay times and oxidation regimes in MILD combustion at atmospheric pressure", *Combustion and Flame*, vol. 160, no. 1, pp. 47-55.

Santner, J, Dryer, FL & Ju, Y 2013, "The effects of water dilution on hydrogen, syngas, and ethylene flames at elevated pressure", *Proceedings of the Combustion Institute*, vol. 34, pp. 719-726.

Sarathy, SM, Oβwald, P, Hansen, N & Kohse-Höinghaus, K 2014 "Alcohol combustion chemistry", *Progress in Energy and Combustion Science*, vol. 44, pp. 40-102.

Schönborn, A, Sayad, P, Konnov, AA & Klingmann, J 2013, "Visualisation of propane autoignition in a turbulent flow reactor using OH* chemiluminescence imaging", *Combustion and Flame*, vol. 160, pp. 1033-1043.

Sims, REH, Mabee, W, Saddler, JN & Taylor, M 2010, "An overview of second generation biofuel technologies", *Bioresource Technology*, vol. 101, pp. 1570-1580.

Smith, GP, Golden, DM, Frenklach, M, Moriarty, NW, Eiteneer, B, Goldenberg, M, Bowman, CT, Hanson, R, Song, S, Gardiner, WC, Lissianski, JrV, Qin, Z, *GRI-Mech3.0*, http://www.me.berkeley.edu/gri_mech/.

Struckmeier, U, Lucassen, A, Hansen, N, Wada, T, Peters, N & Kohse-Höinghaus, K 2010, "Demonstration of a burner for the investigation of partially premixed low-temperature flames", *Combustion and Flame*, vol. 157, pp. 1966-1975.

Togbé, C, Tran, L-S, Liu, D, Felsmann, D, Oβwald, P, Glaude, P-A, Sirjean, B, Fournet, R, Battin-Leclerc, F & Kohse-Höinghaus, K 2014, "Combustion chemistry and flame structure of furan group biofuels using molecular-beam mass spectrometry and gas chromatography – Part III: 2,5-Dimethylfuran", *Combustion and Flame*, vol. 161, no. 3, pp. 780-797.

Toporov, D, Bocian, P, Heil, P, Kellermann, A, Stadler, H, Tschunko, S, Förster, M & Kneer, R 2008, "Detailed investigation of a pulverized fuel swirl flame in CO_2/O_2 atmosphere", *Combustion and Flame*, vol. 155, pp. 605-618.

Tsuji, H, Gupta, AK, Hasegawa, T, Katsuki, M, Kishimoto, K & Morita, M 2002, *High Temperature Air Combustion: From Energy Conservation to Pollution Reduction*, CRC Press.

Varga, T, Olm, C, Nagy, T, Zsély, I, Valkó, É, Pálvölgyi, R, Curran, HJ & Turányi, T 2016, "Development of a Joint Hydrogen and Syngas Combustion Mechanism Based on an Optimization Approach", *International Journal of Chemical Kinetics*, vol. 48, no. 8, pp. 407-422.

Wada, T, Paczko, G & Peters, N 2009, "Numerical Investigations of Highly Diluted Lean CH4/Air Oscillations at Low Temperatures", paper presented to the European Combustion Meeting.

Wang, H, You, X, Joshi, AV, Davis, SG, Laskin, A, Egolfopoulos, F & Law, CK 2007, *USC Mech Version II. High-Temperature Combustion Reaction Model of H2/CO/C1-C4 Compounds*, http://ignis.usc.edu/USC_Mech_II.htm.

Watanabe, H, Yamamoto, J & Okazaki, K 2011, "NO_x formation and reduction mechanisms in staged O_2/CO_2 combustion", *Combustion and Flame*, vol. 158, pp. 1255-1263.

Watanabe, H, Arai, F & Okazaki, K 2013, "Role of CO_2 in the CH_4 oxidation and H_2 formation during fuel-rich combustion in O_2/CO_2 environments", *Combustion and Flame*, vol. 160, pp. 2375-2385.

Westbrook, CK & Dryer, FL 1984, "Chemical kinetic modeling of hydrocarbon combustion", *Progress in Energy and Combustion Science*, vol.10, no. 1, pp. 1-57.

Westbrook, CK 2000, "Chemical kinetics of hydrocarbon ignition in practical combustion systems", *Proceedings of the Combustion Institute*, vol. 28, pp. 1563-1577.

Westbrook, CK, Mizobuchi, Y, Poinsot, TJ, Smith, PJ & Warnatz, J 2005, "Computational combustion", *Proceedings of the Combustion Institute*, vol. 30, pp. 125-157.

World Energy Council 2012, *World Energy Trilemma: Time to get real – the case for sustainable energy policy*.

Wu, H & Ihme, M 2014, "Effects of flow-field and mixture inhomogeneities on the ignition dynamics in continuous flow reactors", *Combustion and Flame*, vol. 161, no. 9, pp. 2317-2326.

Wünning, JA & Wünning, JG 1997, "Flameless oxidation to reduce thermal NO formation", *Progress in Energy and Combustion Science*, vol. 23, pp. 81-94.

Yao, M, Zheng, Z & Liu, H 2009, "Progress and recent trends in homogeneous charge compression ignition (HCCI) engines", *Progress in Energy and Combustion Science*, vol. 35, no. 5, pp. 398-437.

Zhang, W, Chen, Z & Kong, W 2012, "Effects of diluents on the ignition of premixed H_2/air mixtures", *Combustion and Flame*, vol. 159, pp. 151-160.

Zhang, P, Ji, W, He, T, He, X, Wang, Z, Yang, B & Law, CK 2016, "First-stage ignition delay in the negative temperature coefficient behaviour: Experiment and simulation", *Combustion and Flame*, vol. 167, pp. 14-23.

Zhou, C-W, Li, Y, O'Connor, E, Somers, KP, Thion, S, Keesee, C, Mathieu, O, Petersen, EL, DeVerter, TA, Oehlschlaeger, MA, Kukkadapu, G, Sung, C-J, Alrefae, M, Khaled, F, Farooq, A, Dirrenberger, P, Glaude, P-A, Battin-Leclerc, F, Santner, J, Ju, Y, Held, T, Haas, FM, Dryer, FL & Curran, HJ 2016, "A comprehensive experimental and modelling study of isobutene oxidation", *Combustion and Flame*, vol. 167, pp. 353-379.

Zhukov, VP, Sechenov, VA & Starikovskii, AYu, "Autoignition of a Lean Propane-Air Mixture at High Pressures", *Kinetics and Catalysis*, vol. 46, no. 3, pp. 319-327.

Zornek, T, Monz, T & Aigner, M 2015, "Performance analysis of the micro gas turbine Turbec T100 with a new FLOX-combustion system for low calorific fuels", *Applied Energy*, vol. 159, pp. 276-284.

Appendix

PFR Results

Propane mixtures

Pressure [atm]	Equivalence ratio	C_3H_8 [vol %]	O_2 [vol %]	N_2 [vol %]	Residence time [s]	Inlet temperature [K]	Ignition delay time [s]
1	0.083	0.16	9.84	90	0.029	1128	0.0067
1	0.092	0.18	9.82	90	0.036	1075	0.023
					0.029	1084	0.014
1	0.1	0.20	9.80	90	0.048	875	-
					0.041	1070	0.032
					0.036	1075	0.024
					0.029	1083	0.014
					0.036	1100	0.0077
					0.036	1105	0.015
					0.029	1115	0.010
					0.036	1117	0.007
					0.036	1120	0.013
					0.036	1120	0.013
					0.029	1120	0.0073
					0.029	1120	0.0074
					0.024	1120	0.0077
					0.021	1125	0.0061
					0.036	1151	0.0049
					0.036	1159	0.0079
					0.036	1159	0.0080
					0.029	1163	0.0055
					0.036	1166	0.0042
					0.024	1167	0.0024
					0.029	1170	0.0029
					0.024	1170	0.0037
					0.029	1205	0.0018
					0.024	1205	0.0016
					0.021	1211	0.00098
					0.024	1250	0.00067
1	0.11	0.21	9.79	90	0.036	1071	0.027
1	0.12	0.23	9.77	90	0.048	940	-
					0.048	985	-
					0.048	985	-
					0.048	997	-
					0.048	1000	-
					0.048	1005	-
					0.048	1015	-
					0.048	1015	-
					0.048	1027	-
					0.048	1030	-
					0.048	1045	-

					0.048	1065	-
					0.041	1070	0.037
					0.036	1071	0.030
					0.029	1083	0.017
					0.029	1083	0.017
					0.036	1100	0.013
					0.036	1100	0.013
					0.036	1105	0.016
					0.029	1115	0.011
					0.036	1120	0.013
					0.036	1120	0.013
					0.024	1120	0.0082
					0.029	1125	0.0097
					0.029	1125	0.0096
					0.021	1125	0.0068
					0.036	1159	0.0031
					0.036	1159	0.0042
					0.024	1161	0.0038
					0.024	1161	0.0038
					0.029	1163	0.0037
					0.029	1163	0.0037
					0.036	1166	0.0043
					0.024	1167	0.0024
					0.029	1170	0.0030
					0.029	1205	0.0010
					0.024	1205	0.00088
					0.021	1211	0.00090
					0.024	1250	0.00048
1	0.17	0.32	9.68	90	0.048	875	-
					0.048	891	-
					0.048	940	-
					0.048	960	-
					0.048	985	-
					0.048	985	-
					0.048	997	-
					0.048	1000	-
					0.048	1015	-
					0.048	1015	-
					0.048	1027	-
					0.048	1030	-
					0.048	1045	-
					0.048	1065	-
					0.041	1069	-
					0.048	1071	0.043
					0.036	1071	-
					0.036	1076	0.032
					0.048	1080	0.026
					0.048	1080	0.026
					0.029	1082	-
					0.029	1083	0.026
					0.048	1095	0.019

					0.036	1100	0.012
					0.036	1100	0.012
					0.048	1103	0.026
					0.048	1105	0.021
					0.048	1105	0.021
					0.036	1105	0.018
					0.029	1115	0.013
					0.036	1117	0.012
					0.036	1120	0.013
					0.036	1120	0.013
					0.024	1120	0.010
					0.029	1125	0.010
					0.029	1125	0.010
					0.021	1125	0.0081
					0.036	1151	0.0076
					0.036	1157	0.0063
					0.036	1157	0.0063
					0.024	1161	0.0054
					0.024	1161	0.0052
					0.029	1163	0.0051
					0.029	1163	0.0047
					0.036	1166	0.0046
					0.024	1167	0.0028
					0.029	1170	0.0034
					0.029	1170	0.0034
					0.029	1205	0.0016
					0.024	1205	0.0017
					0.021	1211	0.0014
					0.024	1245	0.00072
1	0.25	0.48	9.52	90	0.048	875	-
					0.048	940	-
					0.048	955	-
					0.048	985	-
					0.048	985	-
					0.048	997	-
					0.048	1000	-
					0.048	1005	-
					0.048	1015	-
					0.048	1015	-
					0.048	1027	-
					0.048	1030	-
					0.036	1035	-
					0.048	1045	-
					0.036	1058	-
					0.048	1065	-
					0.041	1069	-
					0.036	1071	-
					0.029	1081	-
					0.048	1103	0.030
					0.048	1103	0.031
					0.036	1105	0.027

					0.036	1105	0.027
					0.029	1110	0.022
					0.029	1110	0.022
					0.036	1120	0.012
					0.036	1120	0.012
					0.024	1120	0.020
					0.024	1120	0.020
					0.029	1125	0.010
					0.029	1125	0.010
					0.021	1125	0.019
					0.021	1125	0.018
					0.036	1151	0.0066
					0.036	1157	0.0057
					0.036	1157	0.0052
					0.029	1161	0.0055
					0.029	1161	0.0056
					0.024	1161	0.0059
					0.024	1161	0.0058
					0.036	1166	0.0053
					0.036	1166	0.0054
					0.024	1167	0.0035
					0.029	1170	0.0041
					0.029	1170	0.0040
					0.029	1205	0.0029
					0.029	1205	0.0028
					0.024	1205	0.0030
					0.021	1211	0.0022
					0.024	1245	0.00097
1	0.33	0.62	9.38	90	0.048	875	-
					0.048	891	-
					0.048	935	-
					0.048	955	-
					0.048	955	-
					0.048	985	-
					0.048	985	-
					0.048	995	-
					0.036	996	-
					0.048	997	-
					0.048	1000	-
					0.048	1005	-
					0.029	1008	-
					0.036	1009	-
					0.036	1012	-
					0.048	1015	-
					0.048	1015	-
					0.024	1019	-
					0.036	1026	-
					0.048	1030	-
					0.048	1065	0.031
					0.048	1065	0.042
					0.041	1066	0.036

					0.036	1071	-
					0.029	1081	-
					0.048	1103	0.022
					0.048	1103	0.022
					0.048	1105	0.015
					0.048	1105	0.014
					0.036	1105	0.018
					0.036	1105	0.017
					0.029	1110	0.025
					0.029	1110	0.022
					0.024	1117	-
					0.036	1120	0.010
					0.036	1120	0.0099
					0.029	1125	0.0096
					0.029	1125	0.0092
					0.036	1151	0.0077
					0.036	1151	0.0070
					0.029	1161	0.0057
					0.029	1161	0.0057
					0.024	1161	0.0058
					0.024	1161	0.0050
					0.036	1166	0.0050
					0.036	1166	0.0049
					0.024	1167	0.0035
					0.024	1167	0.0035
					0.029	1170	0.0039
					0.029	1170	0.0040
					0.029	1205	0.0020
					0.029	1205	0.0021
					0.024	1205	0.0018
					0.024	1205	0.0017
					0.021	1211	0.0018
					0.021	1211	0.0017
					0.024	1245	0.00086
1	0.4	0.74	9.26	90	0.048	985	-
					0.036	996	-
					0.048	997	-
					0.036	1010	-
					0.048	1015	0.042
1	0.43	0.80	9.20	90	0.048	985	-
					0.036	996	-
					0.048	997	-
					0.036	1010	-
1	0.5	0.91	9.09	90	0.048	985	0.024
					0.048	985	0.023
					0.041	990	0.020
					0.048	997	0.032
					0.048	997	0.024
					0.048	999	0.023
					0.048	999	0.022
					0.048	1000	0.021

0.048	1000	0.020
0.048	1005	0.023
0.048	1005	0.022
0.041	1005	0.020
0.041	1005	0.019
0.036	1010	0.024
0.048	1015	0.021
0.048	1015	0.019
0.041	1020	0.018
0.041	1020	0.016
0.036	1026	0.017
0.036	1026	0.016
0.048	1030	0.021
0.048	1030	0.019
0.032	1031	0.019
0.041	1035	0.018
0.041	1035	0.017
0.036	1035	0.017
0.036	1035	0.016
0.032	1041	0.016
0.032	1041	0.016
0.048	1065	0.020
0.048	1065	0.019
0.041	1066	0.015
0.041	1066	0.016
0.036	1070	0.016
0.036	1070	0.014
0.029	1076	0.014
0.029	1076	0.017
0.048	1103	0.020
0.048	1103	0.018
0.036	1105	0.015
0.036	1105	0.016
0.029	1110	0.014
0.029	1110	0.013
0.036	1120	0.0076
0.036	1120	0.0075
0.029	1125	0.0086
0.029	1125	0.0074
0.036	1151	0.0056
0.036	1151	0.0058
0.029	1157	0.0043
0.029	1157	0.0045
0.036	1160	0.0046
0.036	1160	0.0045
0.024	1161	0.0044
0.024	1161	0.0040
0.029	1166	0.0039
0.029	1166	0.0039
0.024	1167	0.0035
0.024	1167	0.0035

					0.029	1205	0.0028
					0.029	1205	0.0029
					0.024	1205	0.0031
					0.024	1205	0.0030
					0.021	1211	0.0023
					0.021	1211	0.0024
					0.024	1245	0.0018
					0.024	1245	0.0017
1	0.67	1.18	8.82	90	0.048	875	-
					0.048	935	-
					0.048	955	-
					0.048	980	0.024
					0.048	980	0.022
					0.048	985	0.019
					0.048	985	0.016
					0.041	990	0.020
					0.048	995	0.022
					0.048	997	0.022
					0.036	997	0.033
					0.048	1000	0.018
					0.048	1000	0.021
					0.048	1005	0.022
					0.048	1005	0.022
					0.041	1005	0.020
					0.041	1005	0.018
					0.036	1005	0.033
					0.036	1010	0.018
					0.037	1012	0.022
					0.048	1015	0.021
					0.048	1015	0.018
					0.041	1020	0.018
					0.041	1020	0.019
					0.036	1022	0.021
					0.036	1026	0.024
					0.036	1026	0.016
					0.048	1030	0.017
					0.048	1030	0.021
					0.041	1035	0.018
					0.041	1035	0.015
					0.036	1035	0.017
					0.036	1035	0.016
					0.032	1041	0.015
					0.048	1063	0.021
					0.048	1063	0.018
					0.041	1066	0.018
					0.041	1066	0.016
					0.036	1071	0.016
					0.036	1071	0.015
					0.029	1076	0.014
					0.048	1080	0.013
					0.048	1080	0.016

					0.048	1103	0.014
					0.048	1103	0.018
					0.036	1105	0.013
					0.036	1105	0.014
					0.029	1110	0.014
					0.036	1120	0.0079
					0.036	1120	0.0076
					0.029	1120	0.0098
					0.029	1120	0.0088
					0.036	1151	0.0058
					0.036	1151	0.0055
					0.029	1157	0.0044
					0.029	1157	0.0045
					0.036	1160	0.0047
					0.036	1160	0.0045
					0.024	1161	0.0057
					0.024	1161	0.0052
					0.029	1166	0.0040
					0.029	1166	0.0040
					0.024	1167	0.0037
					0.024	1167	0.0036
					0.029	1205	0.0026
					0.029	1205	0.0026
					0.024	1205	0.0021
					0.024	1205	0.0021
					0.021	1206	0.0019
					0.021	1206	0.0014
					0.024	1245	0.0010
					0.024	1245	0.00094
1	0.83	1.43	8.57	90	0.048	985	0.023
					0.048	1000	0.021
					0.041	1005	0.020
					0.048	1015	0.020
					0.041	1020	0.027
					0.048	1030	0.022
					0.048	1030	0.018
					0.041	1035	0.020
					0.041	1035	0.019
					0.036	1035	0.017
					0.048	1063	0.022
					0.048	1063	0.021
					0.041	1066	0.020
					0.041	1066	0.018
					0.036	1071	0.017
					0.048	1103	0.016
					0.048	1103	0.014
					0.036	1105	0.014
					0.036	1120	0.012
					0.036	1120	0.008
					0.029	1120	0.013
					0.029	1120	0.012

					0.036	1151	0.0064
					0.036	1151	0.0059
					0.029	1157	0.0058
					0.029	1157	0.0050
					0.036	1160	0.0051
					0.036	1160	0.0052
					0.024	1161	0.0063
					0.024	1161	0.0053
					0.029	1166	0.0046
					0.029	1166	0.0043
					0.024	1167	0.0054
					0.024	1167	0.0048
					0.029	1205	0.0030
					0.029	1205	0.0029
					0.024	1205	0.0033
					0.024	1205	0.0033
					0.021	1206	0.0032
					0.021	1206	0.0031
					0.024	1245	0.0021
					0.024	1245	0.0020
1	1	1.67	8.33	90	0.048	870	-
					0.048	891	-
					0.048	935	-
					0.048	955	-
					0.048	980	-
					0.048	985	-
					0.036	992	-
					0.036	992	-
					0.048	995	0.024
					0.036	1005	-
					0.029	1005	-
					0.036	1012	-
					0.048	1015	0.044
					0.024	1015	-
					0.036	1023	-
					0.048	1027	0.021
					0.048	1027	0.026
					0.048	1030	0.022
					0.041	1035	0.037
					0.036	1035	0.027
					0.036	1035	0.025
					0.029	1035	-
					0.048	1045	0.020
					0.048	1045	0.027
					0.036	1053	0.026
					0.036	1053	0.023
					0.029	1062	0.023
					0.048	1063	0.042
					0.026	1068	0.022
					0.024	1069	-
					0.029	1076	-

					0.048	1080	0.017
					0.048	1080	0.025
					0.048	1100	0.017
					0.048	1100	0.010
					0.048	1103	0.022
					0.036	1120	0.016
					0.036	1120	0.013
					0.029	1120	0.014
					0.036	1151	0.0072
					0.036	1151	0.0089
					0.029	1157	0.0059
					0.029	1157	0.0072
					0.036	1160	0.0060
					0.036	1160	0.0057
					0.029	1166	0.0064
					0.029	1166	0.0055
					0.024	1167	0.0071
					0.024	1167	0.0080
					0.029	1200	0.0036
					0.029	1200	0.0035
					0.024	1205	0.0034
					0.024	1205	0.0033
					0.021	1206	0.0028
					0.021	1206	0.0030
					0.024	1241	0.0014
					0.024	1241	0.0013
1	1.25	2.00	8.00	90	0.048	985	-
1	1.33	2.11	7.89	90	0.048	870	-
					0.048	935	-
					0.048	955	-
					0.048	980	-
					0.048	985	-
					0.036	988	-
					0.048	995	-
					0.029	1003	-
					0.048	1005	-
					0.036	1005	-
					0.036	1012	-
					0.048	1015	-
					0.036	1021	-
					0.048	1030	-
					0.036	1035	-
					0.036	1053	-
					0.048	1058	-
					0.041	1065	-
					0.036	1069	-
					0.029	1076	-
					0.048	1100	0.044
					0.048	1100	0.021
					0.036	1105	-
					0.048	1149	0.0091

					0.048	1149	0.0099
					0.036	1160	0.010
					0.036	1160	0.0090
					0.029	1166	0.0088
					0.029	1200	0.0057
					0.029	1200	0.0065
					0.024	1200	0.0064
					0.024	1200	0.0061
					0.021	1206	0.0058
					0.021	1206	0.0044
					0.024	1241	0.0030
					0.024	1241	0.0024
1	1.67	2.50	7.50	90	0.048	887	-
					0.048	955	-
					0.048	985	-
					0.048	1027	-
					0.048	1045	-
					0.048	1080	-
					0.048	1100	-
					0.048	1102	-
					0.036	1149	-
					0.048	1150	0.041
					0.048	1150	0.040
					0.036	1150	-
					0.036	1160	-
					0.029	1165	-
					0.024	1167	-
1	2	2.86	7.14	90	0.048	985	-
					0.048	995	-
					0.048	1005	-
					0.048	1015	-
					0.048	1027	-
					0.048	1045	-
					0.048	1080	-
					0.048	1100	-
					0.048	1147	-
					0.029	1195	0.011
					0.024	1200	0.010
					0.024	1235	0.0036
1	2.67	3.48	6.52	90	0.048	870	-
					0.048	935	-
					0.048	955	-
					0.048	975	-
					0.048	985	-
					0.048	995	-
					0.048	995	-
					0.048	1005	-
					0.048	1015	-
					0.048	1015	-
					0.048	1027	-
					0.048	1030	-

					0.048	1045	-
					0.048	1058	-
					0.048	1080	-
					0.048	1100	-
					0.048	1150	-
					0.048	1150	-
					0.029	1195	0.0098
					0.024	1235	0.0065
1	3.33	4.00	6.00	90	0.048	870	-
					0.048	887	-
					0.048	935	-
					0.048	955	-
					0.048	955	-
					0.048	975	-
					0.048	985	-
					0.048	985	-
					0.048	995	-
					0.048	995	-
					0.048	1005	-
					0.024	1011	-
					0.048	1015	-
					0.048	1015	-
					0.048	1029	-
					0.048	1030	-
					0.048	1045	-
					0.048	1058	-
					0.048	1080	-
					0.048	1100	-
					0.048	1150	-
					0.029	1195	-
					0.024	1200	-
					0.024	1235	0.018
1	0.2	0.19	4.81	95	0.036	1116	-
1	0.25	0.24	4.76	95	0.048	1116	-
					0.048	1118	-
1	0.27	0.25	4.75	95	0.048	1168	0.021
					0.048	1168	0.021
1	0.33	0.31	4.69	95	0.048	1025	-
					0.048	1040	-
					0.048	1075	-
					0.048	1112	-
					0.048	1118	-
					0.048	1161	0.035
					0.048	1161	0.035
					0.048	1168	0.019
					0.048	1168	0.019
					0.029	1211	0.010
					0.029	1211	0.011
					0.024	1245	0.0066
					0.024	1245	0.0056
1	0.5	0.45	4.55	95	0.048	1161	0.043

					0.048	1161	0.043
					0.036	1170	0.021
					0.036	1170	0.022
					0.029	1211	0.012
					0.029	1211	0.011
1	0.67	0.59	4.41	95	0.048	1025	-
					0.048	1040	-
					0.048	1075	-
					0.048	1112	-
					0.048	1118	-
					0.048	1162	-
					0.048	1171	0.028
					0.048	1171	0.030
					0.029	1211	0.015
					0.029	1211	0.014
					0.024	1245	0.010
					0.024	1245	0.0087
1	0.83	0.71	4.29	95	0.048	1118	-
					0.048	1168	0.027
					0.048	1168	0.042
1	1	0.83	4.17	95	0.048	1025	-
					0.048	1040	-
					0.048	1075	-
					0.048	1112	-
					0.048	1120	-
					0.048	1162	-
					0.048	1169	-
					0.029	1211	0.017
					0.029	1211	0.018
					0.024	1245	0.011
					0.024	1245	0.011
1	1.33	1.05	3.95	95	0.048	1025	-
					0.048	1035	-
					0.048	1070	-
					0.048	1162	-
					0.048	1210	0.023
					0.048	1210	0.023
					0.048	1245	0.021
					0.048	1245	0.021
1	1.67	1.25	3.75	95	0.048	1210	0.044
					0.048	1210	0.043
1	2	1.43	3.57	95	0.048	1025	-
					0.048	1035	-
					0.048	1070	-
					0.048	1210	-
					0.048	1245	0.036
					0.048	1245	0.036
1	2.67	1.74	3.26	95	0.048	1025	-
					0.048	1035	-
					0.048	1070	-
					0.048	1245	0.042

					0.048	1245	0.041
1	3.33	2.00	3.00	95	0.048	1025	-
					0.048	1035	-
					0.048	1070	-
					0.048	1245	0.043
1	0.5	0.27	2.73	97	0.048	1210	0.032
					0.048	1210	0.033
					0.048	1245	0.021
					0.048	1245	0.021
1	0.67	0.35	2.65	97	0.048	1164	-
					0.048	1210	0.035
					0.048	1210	0.035
					0.048	1245	0.023
					0.048	1245	0.023
1	0.83	0.43	2.57	97	0.048	1210	0.040
					0.048	1210	0.041
					0.048	1245	0.023
					0.048	1245	0.024
1	1	0.50	2.50	97	0.048	1210	0.041
					0.048	1210	0.044
					0.048	1245	0.026
					0.048	1245	0.025
1	1.33	0.63	2.37	97	0.048	1211	-
					0.048	1245	0.035
					0.048	1245	0.037
1	2	0.86	2.14	97	0.048	1245	-

Pressure [atm]	Equivalence ratio	C_3H_8 [vol %]	O_2 [vol %]	CO_2 [vol %]	Residence time [s]	Inlet temperature [K]	Ignition delay time [s]
1	0.12	0.23	9.77	90	0.048	1080	-
					0.041	1096	0.034
					0.036	1103	0.028
					0.029	1110	0.024
					0.036	1124	0.016
					0.036	1130	0.014
					0.036	1166	0.0049
					0.029	1167	0.0048
					0.024	1170	0.0042
					0.036	1175	0.0045
					0.029	1181	0.0032
					0.024	1189	0.0025
					0.036	1211	0.0016
					0.029	1215	0.0014
					0.024	1220	0.0012
					0.024	1247	0.00053
					0.021	1250	0.00043
1	0.13	0.26	9.74	90	0.048	1005	-
					0.048	1010	-
					0.048	1020	-
					0.048	1029	-

					0.048	1034	-
					0.048	1037	-
					0.048	1049	-
					0.048	1065	-
					0.036	1090	-
					0.048	1091	0.035
					0.041	1096	0.030
					0.036	1103	0.026
					0.048	1109	0.023
					0.029	1110	0.021
					0.036	1122	0.016
					0.036	1124	0.016
					0.029	1133	0.011
					0.041	1134	0.0091
					0.024	1142	0.0081
					0.041	1157	0.0049
					0.048	1166	0.0041
1	0.17	0.32	9.68	90	0.048	900	-
					0.048	1005	-
					0.048	1010	-
					0.048	1020	-
					0.048	1029	-
					0.048	1033	-
					0.048	1037	-
					0.048	1049	-
					0.048	1065	-
					0.048	1080	-
					0.036	1090	-
					0.048	1091	0.033
					0.041	1096	0.028
					0.036	1130	0.016
					0.041	1157	0.0079
					0.032	1163	0.0046
					0.036	1166	0.0058
					0.029	1167	0.0058
					0.024	1170	0.0055
					0.036	1211	0.0018
					0.029	1215	0.0017
					0.024	1220	0.0016
					0.024	1247	0.0012
					0.021	1250	0.00098
1	0.25	0.48	9.52	90	0.048	900	-
					0.048	1000	-
					0.048	1005	-
					0.048	1010	-
					0.048	1020	-
					0.048	1029	-
					0.048	1033	-
					0.048	1049	-
					0.048	1075	-
					0.048	1091	0.042

					0.041	1096	0.040
					0.048	1109	0.031
					0.029	1110	0.027
					0.036	1120	0.021
					0.036	1125	0.020
					0.029	1131	0.015
					0.041	1133	0.014
					0.024	1140	0.011
					0.048	1166	0.0071
					0.036	1166	0.0066
					0.029	1168	0.0066
					0.024	1170	0.0064
					0.036	1175	0.0049
					0.029	1181	0.0043
					0.024	1188	0.0033
					0.036	1208	0.0026
					0.029	1215	0.0022
					0.024	1217	0.0018
					0.024	1247	0.00081
					0.021	1248	0.00076
1	0.33	0.63	9.38	90	0.048	900	-
					0.048	1005	-
					0.048	1010	-
					0.048	1019	-
					0.048	1028	-
					0.048	1030	-
					0.048	1033	-
					0.048	1047	-
					0.048	1063	-
					0.048	1075	-
					0.048	1090	-
					0.048	1107	0.032
					0.048	1109	0.037
					0.036	1115	0.026
					0.036	1120	0.030
					0.036	1125	0.028
					0.029	1127	0.022
					0.041	1133	0.019
					0.024	1138	0.016
					0.041	1157	0.010
					0.048	1166	0.0092
					0.036	1166	0.0088
					0.024	1166	0.0081
					0.029	1168	0.0080
					0.036	1170	0.0079
					0.029	1181	0.0062
					0.024	1188	0.0051
					0.036	1208	0.0039
					0.029	1214	0.0034
					0.024	1217	0.0029
					0.024	1247	0.0017

1	0.5	0.91	9.09	90	0.048	1109	-
					0.036	1120	-
					0.036	1125	-
					0.029	1128	-
					0.024	1138	-
1	0.67	1.18	8.82	90	0.048	900	-
					0.048	1005	-
					0.048	1010	-
					0.048	1019	-
					0.048	1025	-
					0.048	1030	-
					0.048	1033	-
					0.048	1047	-
					0.048	1063	-
					0.048	1075	-
					0.048	1090	-
					0.048	1109	-
					0.036	1125	-
					0.048	1166	0.018
					0.048	1166	0.018
					0.036	1166	0.021
					0.024	1166	0.020
					0.029	1168	0.019
					0.036	1170	0.015
					0.029	1176	0.010
					0.024	1182	0.0085
					0.036	1206	0.0054
					0.029	1214	0.0051
					0.024	1217	0.0045
					0.024	1245	0.0026
1	1	1.67	8.33	90	0.048	896	-
					0.048	1005	-
					0.048	1010	-
					0.048	1015	-
					0.048	1025	-
					0.048	1030	-
					0.048	1032	-
					0.048	1045	-
					0.048	1061	-
					0.048	1075	-
					0.048	1090	-
					0.048	1109	-
					0.048	1149	0.042
					0.048	1156	0.035
					0.048	1166	0.025
					0.048	1166	0.025
					0.036	1166	0.031
					0.029	1166	0.026
					0.024	1165	-
					0.036	1170	0.022
					0.036	1170	0.022

					0.029	1176	0.021
					0.029	1176	0.021
					0.024	1182	0.018
					0.024	1182	0.018
					0.036	1203	0.011
					0.029	1211	0.0091
					0.029	1211	0.0089
					0.024	1214	0.0080
					0.024	1242	0.0045
1	1.33	2.11	7.89	90	0.048	896	-
					0.048	1005	-
					0.048	1005	-
					0.048	1015	-
					0.048	1024	-
					0.048	1030	-
					0.048	1032	-
					0.048	1045	-
					0.048	1061	-
					0.048	1070	-
					0.048	1109	-
					0.036	1165	-
					0.029	1165	-
					0.024	1165	-
					0.048	1166	0.036
					0.036	1170	0.030
					0.029	1176	0.026
					0.024	1182	-
					0.036	1203	0.016
					0.029	1206	0.013
					0.024	1214	0.012
					0.024	1239	0.0065
1	1.67	2.50	7.50	90	0.048	1165	0.041
					0.036	1170	-
					0.029	1182	-
1	2	2.86	7.14	90	0.048	896	-
					0.048	1005	-
					0.048	1005	-
					0.048	1015	-
					0.048	1022	-
					0.048	1030	-
					0.048	1032	-
					0.048	1043	-
					0.048	1060	-
					0.048	1070	-
					0.048	1166	0.044
					0.036	1170	-
					0.029	1182	-
					0.036	1203	0.021
					0.029	1206	0.018
					0.024	1211	0.015
					0.024	1239	0.0091

1	2.67	3.48	6.52	90	0.048	896	-
					0.048	1005	-
					0.048	1005	-
					0.048	1015	-
					0.048	1020	-
					0.048	1030	-
					0.048	1030	-
					0.048	1041	-
					0.048	1060	-
					0.048	1070	-
					0.036	1200	0.030
					0.029	1206	0.026
					0.024	1210	-
					0.024	1234	0.011
1	3.33	4.00	6.00	90	0.048	896	-
					0.048	1005	-
					0.048	1005	-
					0.048	1015	-
					0.048	1020	-
					0.048	1030	-
					0.048	1030	-
					0.048	1041	-
					0.048	1059	-
					0.048	1070	-
					0.036	1201	-
					0.029	1206	-
					0.024	1210	-
					0.024	1237	0.018
1	0.27	0.25	4.75	95	0.048	1159	0.040
1	0.33	0.31	4.69	95	0.048	1159	0.043
					0.048	1159	0.042
					0.048	1177	0.024
					0.048	1201	0.025
					0.048	1247	0.017
1	0.5	0.45	4.55	95	0.048	1159	-
1	0.67	0.59	4.41	95	0.048	1160	-
					0.048	1178	0.037
					0.048	1178	0.037
					0.048	1201	0.031
					0.048	1247	0.020
1	1	0.83	4.17	95	0.048	1180	-
					0.048	1201	0.037
					0.048	1247	0.022
1	1.33	1.05	3.95	95	0.048	1208	0.041
					0.048	1208	0.041
					0.048	1246	0.027
					0.048	1246	0.027
1	1.67	1.25	3.75	95	0.048	1203	-
1	2	1.43	3.57	95	0.048	1246	0.035
1	2.67	1.74	3.26	95	0.048	1246	-
1	3.33	2.00	3.00	95	0.048	1247	-

1	0.5	0.27	2.73	97	0.048	1202	0.041
					0.048	1202	0.041
					0.048	1247	0.026
1	0.67	0.35	2.65	97	0.048	1202	-
					0.048	1247	0.028
					0.048	1247	0.029
1	1	0.50	2.50	97	0.048	1202	-
					0.048	1247	0.035
					0.048	1247	0.035
1	1.33	0.63	2.37	97	0.048	1202	-
					0.048	1247	-
					0.048	1247	-
1	2	0.86	2.14	97	0.048	1246	-

Pressure [atm]	Equivalence ratio	C_3H_8 [vol %]	O_2 [vol %]	H_2O [vol %]	Residence time [s]	Inlet temperature [K]	Ignition delay time [s]
1	0.12	0.26	9.74	90	0.048	910	-
					0.048	980	-
					0.048	1000	-
					0.048	1015	-
					0.048	1035	-
					0.048	1065	-
					0.048	1093	-
					0.048	1105	-
					0.048	1125	-
					0.048	1150	0.041
					0.048	1185	0.041
1	0.13	0.26	9.74	90	0.036	1176	0.024
1	0.17	0.32	9.68	90	0.048	910	-
					0.048	980	-
					0.048	1000	-
					0.048	1015	-
					0.048	1035	-
					0.048	1065	-
					0.048	1093	-
					0.048	1105	-
					0.048	1125	0.042
					0.048	1149	0.036
					0.036	1176	0.020
					0.048	1185	0.024
					0.036	1232	0.017
					0.029	1235	0.013
1	0.25	0.48	9.52	90	0.048	910	-
					0.048	980	-
					0.048	1000	-
					0.048	1015	-
					0.048	1035	-
					0.048	1065	-
					0.048	1093	-
					0.048	1105	0.043
					0.048	1125	0.036

					0.048	1125	0.036
					0.048	1149	0.028
					0.036	1176	0.017
					0.048	1185	0.023
					0.036	1232	0.015
					0.029	1235	0.010
1	0.33	0.63	9.38	90	0.048	910	-
					0.048	980	-
					0.048	1000	-
					0.048	1015	-
					0.048	1035	-
					0.048	1065	-
					0.048	1091	-
					0.048	1105	0.044
					0.048	1120	0.038
					0.048	1120	0.038
					0.048	1149	0.028
					0.048	1149	0.028
					0.036	1176	0.017
					0.048	1181	0.024
					0.048	1181	0.024
					0.036	1232	0.012
					0.029	1235	0.010
1	0.67	1.17	8.82	90	0.048	910	-
					0.048	980	-
					0.048	1000	-
					0.048	1015	-
					0.048	1035	-
					0.048	1065	-
					0.048	1090	-
					0.048	1105	-
					0.048	1120	0.041
					0.048	1120	0.042
					0.048	1149	0.032
					0.048	1149	0.032
					0.036	1176	0.019
					0.048	1181	0.023
					0.048	1181	0.023
					0.036	1230	0.012
					0.029	1233	0.011
1	1	1.67	8.33	90	0.048	905	-
					0.048	980	-
					0.048	1000	-
					0.048	1020	-
					0.048	1035	-
					0.048	1065	-
					0.048	1090	-
					0.048	1105	-
					0.048	1120	-
					0.048	1149	0.037
					0.048	1149	0.036

					0.048	1181	0.026
					0.048	1181	0.027
					0.036	1181	0.023
					0.036	1230	0.014
					0.029	1233	0.011
1	1.33	2.11	7.89	90	0.048	905	-
					0.048	980	-
					0.048	1000	-
					0.048	1010	-
					0.048	1035	-
					0.048	1060	-
					0.048	1090	-
					0.048	1105	-
					0.048	1120	-
					0.048	1149	0.042
					0.036	1176	0.026
					0.036	1176	0.026
					0.048	1181	0.031
					0.048	1181	0.029
					0.029	1229	0.013
					0.029	1229	0.014
					0.036	1230	0.016
					0.036	1230	0.016
1	2	2.86	7.14	90	0.048	905	-
					0.048	980	-
					0.048	1000	-
					0.048	1010	-
					0.048	1035	-
					0.048	1060	-
					0.048	1090	-
					0.048	1105	-
					0.048	1120	-
					0.048	1147	-
					0.036	1176	0.030
					0.029	1176	0.030
					0.048	1181	0.040
					0.048	1181	0.037
					0.036	1230	0.018
					0.036	1230	0.020
					0.029	1230	0.019
1	2.67	3.48	6.52	90	0.048	905	-
					0.048	980	-
					0.048	1000	-
					0.048	1010	-
					0.048	1035	-
					0.048	1060	-
					0.048	1085	-
					0.048	1105	-
					0.048	1120	-
					0.048	1147	-
					0.048	1181	0.043

					0.048	1181	0.043
					0.036	1181	-
					0.029	1181	0.021
					0.036	1230	0.024
1	3.33	4.00	6.00	90	0.048	905	-
					0.048	980	-
					0.048	1000	-
					0.048	1010	-
					0.048	1035	-
					0.048	1060	-
					0.048	1085	-
					0.048	1105	-
					0.048	1120	-
					0.048	1147	-
					0.048	1180	-
					0.036	1180	-
					0.029	1229	0.022
					0.036	1230	0.027
					0.036	1230	0.026

C_1-C_2 mixtures

Pressure [atm]	Ω	Pyrolysis gas [vol %]	O_2 [vol %]	N_2 [vol %]	Residence time [s]	Inlet temperature [K]	Ignition delay time [s]
1	0.7	15.63	4.06	80.31	0.048	1016	-
					0.048	1055	-
					0.048	1075	-
					0.048	1112	-
1	0.8	14.39	4.53	81.08	0.048	1016	-
					0.048	1055	-
					0.048	1075	-
					0.048	1112	-
					0.024	1255	0.018
					0.024	1255	0.018
1	0.9	13.33	4.93	81.73	0.048	1115	-
					0.036	1164	-
					0.029	1164	-
					0.029	1205	0.019
					0.029	1205	0.019
1	0.95	12.86	5.11	82.03	0.048	1143	-
					0.036	1176	-
1	1	12.42	5.28	82.30	0.048	986	-
					0.048	1010	-
					0.048	1016	-
					0.048	1040	-
					0.048	1055	-
					0.048	1076	-
					0.048	1080	-
					0.048	1095	-
					0.048	1112	-
					0.048	1115	-
					0.036	1130	-

					0.048	1131	-
					0.048	1142	-
					0.048	1143	-
					0.036	1167	0.026
					0.029	1175	-
					0.036	1178	0.021
					0.029	1206	0.016
					0.021	1256	0.011
					0.024	1258	0.011
					0.021	1282	0.0086
1	1.25	10.61	5.97	83.42	0.036	1133	0.027
					0.048	1145	0.030
					0.036	1170	0.018
					0.024	1170	0.015
					0.036	1179	0.015
					0.029	1211	0.010
					0.021	1258	0.0071
					0.024	1263	0.0074
					0.021	1285	0.0056
1	1.5	9.26	6.48	84.26	0.048	1105	0.034
					0.048	1105	0.034
					0.048	1111	0.031
					0.036	1111	0.030
					0.048	1134	0.024
					0.036	1134	0.020
					0.024	1134	0.016
					0.029	1135	0.018
					0.048	1145	0.023
					0.036	1171	0.013
					0.029	1171	0.012
					0.024	1171	0.011
					0.024	1171	0.010
					0.036	1179	0.014
					0.029	1212	0.0075
					0.024	1261	0.0053
					0.021	1261	0.0052
					0.021	1287	0.0042
1	1.67	9.26	6.48	84.26	0.048	986	-
					0.048	1010	-
					0.048	1016	-
					0.048	1040	-
					0.048	1055	-
					0.048	1076	-
					0.048	1100	-
					0.048	1107	0.029
					0.036	1114	0.021
					0.029	1114	0.021
					0.048	1115	0.025
					0.024	1134	0.014
					0.048	1135	0.021
					0.036	1135	0.015

					0.029	1138	0.015
					0.036	1140	0.021
					0.048	1147	0.020
					0.029	1172	0.010
					0.036	1174	0.0094
					0.024	1174	0.0088
					0.024	1174	0.0088
					0.036	1181	0.012
					0.029	1214	0.0065
					0.018	1256	0.0045
					0.015	1256	0.0040
					0.016	1258	0.0042
					0.024	1259	0.0047
					0.021	1261	0.0042
					0.018	1282	0.0036
					0.016	1284	0.0035
					0.015	1284	0.0034
					0.021	1285	0.0034
1	2	7.20	7.38	85.42	0.048	1080	-
					0.048	1089	0.036
					0.048	1092	0.036
					0.048	1110	0.024
					0.032	1117	0.016
					0.029	1117	0.016
					0.036	1119	0.017
					0.024	1119	0.014
					0.048	1136	0.017
					0.048	1148	0.016
					0.036	1182	0.010
1	2.5	6.13	7.67	86.20	0.048	1092	0.028
					0.048	1148	0.014
					0.036	1182	0.0083
1	3	5.25	8.01	86.75	0.048	1091	0.026
					0.048	1114	0.017
					0.036	1119	0.012
					0.033	1119	0.011
1	3.33	4.79	8.18	87.03	0.048	986	-
					0.048	1010	-
					0.048	1016	-
					0.048	1040	-
					0.048	1055	-
					0.048	1076	-
					0.048	1080	-
					0.048	1092	0.026
					0.048	1092	0.026
					0.036	1112	0.014
					0.048	1114	0.017
					0.029	1114	0.011
					0.048	1115	0.017
					0.024	1116	0.0092
					0.021	1117	0.0079

					0.018	1120	0.0068
					0.032	1121	0.011
					0.036	1124	0.010
					0.016	1124	0.0061
					0.048	1139	0.013
					0.036	1139	0.011
					0.029	1142	0.0086
					0.048	1149	0.012
					0.029	1175	0.0055
					0.036	1178	0.0061
					0.024	1178	0.0047
					0.036	1185	0.0072
					0.029	1217	0.0022
					0.024	1261	0.0021
					0.021	1263	0.0017
					0.021	1284	0.0016
1	5	3.33	8.74	87.94	0.048	986	-
					0.048	1010	-
					0.048	1016	-
					0.048	1040	-
					0.048	1055	-
					0.048	1076	-
					0.048	1080	-
					0.048	1093	0.025
					0.048	1094	0.024
					0.036	1112	0.013
					0.048	1116	0.014
					0.048	1140	0.012
					0.036	1142	0.010
					0.029	1142	0.0079
					0.048	1149	0.012
					0.029	1176	0.0048
					0.036	1178	0.0053
					0.024	1178	0.0042
					0.036	1183	0.0068
					0.036	1218	0.0013
					0.024	1261	0.0016
					0.021	1263	0.0011
					0.021	1285	0.0015
1	7	2.44	9.07	88.49	0.048	986	-
					0.048	1010	-
					0.048	1016	-
					0.048	1040	-
					0.048	1055	-
					0.048	1076	-
					0.048	1080	-
					0.048	1092	0.030
					0.048	1119	0.017
					0.036	1139	0.012
					0.048	1142	0.016
					0.029	1142	0.0095

					0.048	1149	0.015
					0.036	1178	0.0085
					0.029	1178	0.0066
					0.024	1178	0.0055
					0.036	1183	0.0088
					0.029	1218	0.0028
					0.021	1261	0.0019
					0.024	1263	0.0024
					0.021	1285	0.0021
1	10	1.74	9.34	88.92	0.048	986	-
					0.048	1010	-
					0.048	1016	-
					0.048	1040	-
					0.048	1055	-
					0.048	1076	-
					0.048	1080	-
					0.048	1100	-
					0.048	1112	-
					0.048	1119	0.023
					0.036	1138	0.015
					0.029	1140	0.013
					0.048	1142	0.019
					0.048	1149	0.021
					0.029	1175	0.0097
					0.024	1175	0.0081
					0.036	1178	0.013
					0.036	1182	0.013
					0.029	1217	0.0096
					0.021	1285	0.0073
1	0.8	7.19	2.27	90.54	0.036	1279	-
1	0.9	6.67	2.47	90.87	0.029	1263	0.022
					0.029	1263	0.022
					0.036	1264	0.024
					0.036	1264	0.024
					0.029	1290	0.018
					0.029	1290	0.018
1	1	6.21	2.64	91.15	0.036	1264	0.019
					0.036	1264	0.019
					0.029	1264	0.018
					0.029	1264	0.018
					0.029	1290	0.013
					0.029	1290	0.014
1	1.25	5.31	2.98	91.71	0.029	1264	0.011
					0.029	1264	0.011
					0.036	1266	0.011
					0.029	1292	0.0086
1	1.5	4.63	3.24	92.13	0.029	1264	0.0078
					0.036	1266	0.0083
					0.029	1292	0.0063
1	1.67	4.26	3.38	92.36	0.029	1264	0.0065
					0.036	1266	0.0071

					0.029	1292	0.0052
1	3.33	2.40	4.09	93.51	0.036	1266	0.0035
					0.029	1266	0.0032
					0.029	1290	0.0024
1	5	1.66	4.37	93.97	0.036	1279	-
					0.029	1279	-
					0.029	1311	-
1	7	1.22	4.54	94.24	0.036	1279	-
1	10	0.87	4.67	94.46	0.036	1279	-
1	0.9	4.00	1.48	94.52	0.048	1278	0.036
					0.048	1278	0.035
					0.048	1310	0.027
					0.048	1310	0.027
1	1	3.73	1.58	94.69	0.048	1278	0.027
					0.048	1278	0.028
					0.048	1310	0.021
					0.048	1310	0.021
1	1.25	3.18	1.79	95.03	0.048	1278	0.017
					0.048	1278	0.017
					0.048	1310	0.015
					0.048	1310	0.014
1	1.5	2.78	1.94	95.28	0.048	1278	0.014
					0.048	1278	0.015
					0.048	1310	0.015
					0.048	1310	0.015
1	1.67	2.56	2.03	95.41	0.048	1278	0.015
					0.048	1310	0.016
					0.048	1310	0.016
1	2	2.21	2.16	95.63	0.048	1278	0.017
					0.048	1310	0.019
1	3.33	1.44	2.45	96.11	0.048	1278	-
					0.048	1310	-
1	5	1.00	2.62	96.38	0.048	1278	-
					0.048	1310	-

Pressure [atm]	Ω	Pyrolysis gas [vol %]	O_2 [vol %]	Added CO_2 [vol %]	Residence time [s]	Inlet temperature [K]	Ignition delay time [s]
1	0.75	14.98	4.31	80.71	0.024	1255	-
1	0.8	14.39	4.53	81.08	0.024	1256	0.018
1	0.9	13.33	4.93	81.73	0.048	1111	-
					0.024	1256	0.014
					0.021	1256	0.013
					0.029	1259	0.022
					0.029	1259	0.022
1	0.95	12.86	5.11	82.03	0.036	1202	-
1	1	12.42	5.28	82.30	0.048	1111	-
					0.036	1202	-
					0.021	1256	0.010
					0.024	1258	0.010
					0.029	1259	0.018
					0.021	1287	0.011

1	1.25	10.61	5.97	83.42	0.036	1186	0.025
					0.021	1259	0.0070
					0.029	1261	0.011
					0.024	1261	0.0073
					0.021	1289	0.0074
1	1.5	9.26	6.48	84.26	0.036	1186	0.019
					0.021	1258	0.0053
					0.029	1261	0.0088
					0.024	1261	0.0056
					0.021	1290	0.0055
1	1.67	8.52	6.76	84.72	0.048	1125	-
					0.048	1142	0.026
					0.036	1144	0.022
					0.036	1187	0.016
					0.029	1222	0.0085
					0.024	1261	0.0052
					0.021	1263	0.0046
					0.029	1264	0.0076
					0.021	1290	0.0048
1	2	7.20	7.38	85.42	0.048	1111	-
					0.048	1125	-
					0.048	1142	0.023
					0.036	1145	0.018
					0.036	1188	0.013
					0.029	1189	0.011
					0.024	1190	0.0098
					0.024	1263	0.0043
					0.021	1263	0.0038
					0.029	1264	0.0063
					0.021	1290	0.0039
1	2.5	6.13	7.67	86.20	0.048	1125	-
					0.048	1143	0.020
					0.036	1147	0.015
					0.036	1189	0.012
					0.024	1263	0.0035
					0.021	1263	0.0029
					0.029	1264	0.0052
					0.021	1290	0.0030
1	3	5.25	8.01	86.75	0.048	1125	-
					0.048	1144	0.019
					0.036	1148	0.015
					0.029	1149	0.012
					0.024	1153	0.0093
					0.021	1157	0.0079
					0.018	1161	0.0073
					0.018	1259	0.0026
					0.021	1261	0.0025
					0.016	1261	0.0025
					0.024	1263	0.0028
					0.015	1263	0.0021
					0.029	1264	0.0052

					0.021	1289	0.0034
1	3.33	4.79	8.18	87.03	0.048	1111	-
					0.048	1125	-
					0.048	1144	0.019
					0.036	1145	0.015
					0.036	1188	0.012
					0.029	1225	0.0055
					0.021	1259	0.0030
					0.029	1264	0.0053
					0.024	1264	0.0043
					0.021	1289	0.0033
1	4	4.07	8.45	87.47	0.048	1142	-
					0.048	1144	0.024
					0.036	1148	0.018
1	5	3.33	8.74	87.94	0.048	1111	-
					0.048	1125	-
					0.048	1142	-
					0.048	1145	0.032
					0.036	1170	-
					0.036	1188	0.015
					0.029	1225	0.0075
					0.021	1259	0.0038
					0.029	1264	0.0093
					0.024	1264	0.0062
					0.021	1289	0.0052
1	7	2.44	9.07	88.49	0.048	1111	-
					0.036	1202	-
					0.024	1263	0.010
					0.021	1267	0.0052
					0.021	1287	0.0078
1	10	1.74	9.34	88.92	0.048	1111	-
					0.036	1202	-
					0.029	1282	-
					0.021	1309	-
1	1	6.21	2.64	91.15	0.048	1175	-
					0.048	1202	-
1	1.67	4.26	3.38	92.36	0.048	1175	-
					0.048	1202	-
1	2	3.69	3.60	92.71	0.048	1202	-
1	3.33	2.40	4.09	93.51	0.048	1175	-
					0.048	1202	-
1	5	1.66	4.37	93.97	0.048	1175	-
					0.048	1202	-
1	7	1.22	4.54	94.24	0.048	1175	-
					0.048	1202	-
1	10	0.87	4.67	94.46	0.048	1175	-
					0.048	1202	-

Pressure [atm]	Ω	Pyrolysis gas [vol %]	O_2 [vol %]	H_2O [vol %]	Residence time [s]	Inlet temperature [K]	Ignition delay time [s]
1	0.8	14.39	4.53	81.08	0.048	1135	-

					0.048	1220	-
					0.048	1256	0.038
					0.029	1282	0.023
1	0.9	13.33	4.93	81.73	0.048	1119	-
					0.048	1135	-
					0.048	1170	-
					0.048	1220	-
					0.048	1241	-
					0.048	1256	0.031
					0.048	1256	0.031
					0.036	1256	0.025
					0.029	1258	-
					0.029	1284	0.022
1	1	12.42	5.28	82.30	0.048	1119	-
					0.048	1135	-
					0.048	1170	-
					0.048	1220	-
					0.048	1241	-
					0.048	1258	0.028
					0.036	1258	0.021
					0.029	1284	0.018
					0.029	1284	0.018
1	1.25	10.61	5.97	83.42	0.048	1202	-
					0.048	1218	0.036
					0.048	1218	0.036
					0.048	1258	0.022
					0.036	1258	0.021
					0.029	1259	0.020
					0.029	1285	0.013
1	1.5	9.26	6.48	84.26	0.048	1202	0.038
					0.048	1220	0.034
					0.048	1259	0.019
					0.036	1259	0.018
					0.029	1261	0.016
					0.029	1285	0.012
1	1.67	8.52	6.76	84.72	0.048	1119	-
					0.048	1135	-
					0.048	1170	-
					0.048	1220	0.031
					0.048	1259	0.018
					0.036	1259	0.017
					0.029	1261	0.016
					0.029	1287	0.012
1	2	7.20	7.38	85.42	0.048	1119	-
					0.048	1135	-
					0.048	1170	-
					0.048	1202	0.037
					0.048	1220	0.035
					0.048	1220	0.034
					0.048	1259	0.019
					0.036	1259	0.016

					0.029	1263	0.014
					0.029	1287	0.011
1	2.25	6.70	7.45	85.85	0.048	1202	0.038
1	2.5	6.13	7.67	86.20	0.048	1119	-
					0.048	1135	-
					0.048	1170	-
					0.048	1202	-
					0.048	1203	0.038
					0.048	1221	0.035
					0.048	1259	0.019
					0.036	1261	0.015
					0.029	1263	0.014
					0.029	1287	0.010
1	3	5.25	8.01	86.75	0.048	1202	-
					0.048	1203	0.039
					0.048	1221	0.036
					0.048	1259	0.021
					0.036	1261	0.016
					0.029	1263	0.014
					0.029	1289	0.011
1	3.33	4.79	8.18	87.03	0.048	1119	-
					0.048	1135	-
					0.048	1170	-
					0.048	1202	-
					0.048	1220	-
					0.048	1221	0.037
					0.048	1261	0.022
					0.036	1261	0.017
					0.029	1263	0.014
					0.029	1289	0.011
1	5	3.33	8.74	87.94	0.048	1119	-
					0.048	1135	-
					0.048	1170	-
					0.048	1202	-
					0.048	1241	-
					0.048	1261	0.036
					0.036	1261	0.023
					0.029	1263	0.019
					0.029	1290	0.013
1	7	2.44	9.07	88.49	0.048	1119	-
					0.048	1135	-
					0.048	1170	-
					0.048	1202	-
					0.048	1220	-
					0.048	1241	-
					0.048	1280	-
					0.029	1282	-
					0.036	1284	-
					0.029	1289	0.016
1	10	1.74	9.34	88.92	0.048	1119	-
					0.048	1135	-

0.048	1170	-
0.048	1202	-
0.048	1220	-
0.048	1241	-
0.048	1280	-
0.029	1311	-